



UNIVERSITY OF
LIVERPOOL

Epigenetic mechanisms involved in the cellular response to DNA damage processed by Base Excision Repair

Thesis submitted in accordance with the requirements of the
University of Liverpool for the degree of Doctor in Philosophy by

Laura Gail Bennett

November 2017

Abstract

Chromatin remodelling is required for access to occluded sequences of DNA by proteins involved in important biological processes, including DNA replication and transcription. There is an increasing amount of evidence for chromatin remodelling during DNA repair, although this has been mostly focused towards DNA double strand break and nucleotide excision repair. At this time there is little evidence for chromatin remodelling in base excision repair (BER). BER is a highly conserved DNA repair pathway which processes spontaneous endogenous DNA base damages generated by oxidative metabolism, but also those induced by exogenous agents (eg. ionising radiation), to maintain genome stability. The mechanism in which the BER repairs damaged bases has been extensively studied and the repair proteins involved are well known. However in terms of chromatin, BER is poorly understood. It is thought that chromatin remodelling occurs due to accumulating evidence indicating that certain BER enzymes are significantly less efficient at acting on sterically occluded sites and near the nucleosome dyad axis. At this time the mechanisms and enzymes involved to facilitate BER are unknown. Therefore, the study presented in this thesis aimed to identify specific histone modification enzymes and/or chromatin remodellers that are involved in the processing of DNA base damage during BER.

A method to generate two mononucleosome substrates with a site specific synthetic AP site (tetrahydrofuran; THF) was used to measure recombinant AP endonuclease 1 (APE1) activity alone, and APE1 in HeLa whole cell extract (WCE) that contained chromatin modifiers. The substrates contained either a THF rotationally positioned in the mononucleosome so the DNA backbone was facing outwards (THF-OUT) so accessible to APE1, or facing inwards (THF-IN) towards the histone octamer and so sterically occluded to APE1. I discovered that the THF-OUT substrate was efficiently processed by recombinant APE1 alone and by APE1 in HeLa WCE. In contrast, recombinant APE1 activity was significantly impeded by THF-IN, but which was efficiently processed by APE1 in HeLa WCE in the presence of factors supporting ubiquitination. This suggested the presence of a chromatin modifier, predictably E3 ubiquitin ligase(s) present in WCE that was increasing THF-IN accessibility to APE1. A sequential chromatography approach was utilised to purify these novel activities from HeLa WCE, and I identified three separate activities capable of stimulating APE1 activity towards the THF-IN mononucleosome. Y-box protein 3 (YBX3) and HECT Domain E3 Ubiquitin Protein Ligase 1 (HECTD1) were identified by mass spectrometry analysis of active fractions and their presence aligned with the APE1 stimulatory activity profile of the THF-IN substrate. Depletion of these proteins using siRNA in HeLa cells decreased cell survival following ionising radiation, and delayed DNA damage repair in both HeLa cells and in normal lung fibroblasts. Together

these results suggest that HECTD1 and YBX3 are strong candidates required to facilitate BER through histone ubiquitination and/or chromatin remodelling, and provide new mechanistic information on the process of BER in cellular chromatin.

Acknowledgements

This PhD thesis becomes reality with the kind support and help of many individuals. I would like to gratefully acknowledge various people who have been instrumental in the completion of this thesis. I would like to acknowledge the University of Liverpool for funding this project.

First and foremost, I would like to thank my supervisor, Dr Jason Parson for his encouragement, expertise, motivation and patience during this project, and for instilling confidence in myself and my work. I am very grateful for the valuable comments and proofreading of this thesis.

I have been very lucky to have been part of a research team with helpful and supportive members who have helped me survive and kept me (moderately) sane. I would particularly like to thank Dr Katie Nickson, Dr Matthew Edmonds, Dr Rachel Carter and Sarah Williams for their advice and encouragement. I am also grateful to all other members of the group and other teams in the North West Cancer Research Centre.

Finally, I must express my very profound gratitude to my long-suffering parents, my sister, pets and friends for providing me with unfailing support and continuous encouragement throughout my years of study, research and writing of this thesis. This accomplishment would not have been possible without them.

Table of Contents

Abstract	i
Acknowledgements	iii
Table of Contents	iv
List of Tables	xvii
Abbreviations	xviii
 CHAPTER I	 1
INTRODUCTION	1
1.1 Genome Stability and Instability	1
1.1.1 Deoxyribose Nucleic acid	2
1.1.2 DNA Damage	5
1.1.3 Endogenous DNA damage	6
1.1.3.1 Hydrolysis	6
1.1.3.2 Oxidation	7
1.1.3.3 Errors from DNA Processing	8
1.1.4 Exogenous damage	8
1.1.4.1 UV	8
1.1.4.2 Ionising Radiation	9
1.1.4.3 Alkylation	9
1.1.5 Common types of DNA damage	10
1.1.5.1 Double strand breaks	10
1.1.5.2 Single strand breaks	11
1.1.5.3 AP sites	12
1.1.5.4 8-oxoG	13
1.1.5.5 Thymine Glycol	14
1.2 DNA Repair	15
1.2.1 Double strand break repair	15

1.2.1.1 Homologous Recombination	16
1.2.1.2 Non-homologous end-joining.....	17
1.2.2 Nucleotide excision repair	19
1.2.2.1 GG-NER Recognition	20
1.2.2.2 TC-NER Recognition	20
1.2.2.3 Incision, excision, gap filling and ligation.....	21
1.2.3 Base excision repair.....	22
1.2.3.1 Base Removal	23
1.2.3.2 AP Site Incision.....	25
1.2.3.3 PARP1 and single strand break repair	26
1.2.3.4 End Processing.....	27
1.2.3.5 Gap Filling.....	28
1.2.3.6 Nick Sealing.....	29
1.2.3.7 Base excision repair and Cancer.....	29
1.3 Chromatin Formation and Dynamics	31
1.3.1 Overview of chromatin Structure and Dynamics.....	31
1.3.1.1 Nucleosome structure.....	34
1.3.1.2 Histone Variants	35
1.3.1.3 Nucleosome stability and alternative structures	35
1.3.1.4 Chromatin Secondary Structure	36
1.3.1.5 Chromatin Tertiary Structures	36
1.3.1.6 Regulation of Chromatin Structure	37
1.3.2 Post Translational Modifications (PTMs) of Histones	37
1.3.2.1 Phosphorylation of Histones.....	38
1.3.2.2 Acetylation of Histones	39
1.3.2.3 Methylation of Histones	40
1.3.2.4 Ubiquitination	40
1.3.2.4.1 Ubiquitination pathway	41
1.3.2.4.2 Ubiquitination of Histones.....	42
1.3.2.5 Poly(ADP-ribosyl)ation of Histones	43
1.3.3 Histone Chaperones	44

1.3.4 ATP – dependent chromatin remodelling complexes	44
1.3.5 Chromatin Dynamics in DNA repair	45
1.3.5.1 Histone Modifications.....	46
1.3.5.1.1 Histone Phosphorylation	46
1.3.5.1.2 Histone Acetylation.....	46
1.3.5.1.3 Histone Ubiquitination	48
1.3.5.1.4 Histone methylation.....	48
1.3.5.1.5 Histone Poly(ADP-ribosyl)ation	49
1.3.5.1.6 Histone Modifications in BER	50
1.3.5.2 Chromatin Remodelling	50
1.4 BER in Chromatin	52
1.4.1 Mononucleosome Substrates	52
1.4.2 Analysing BER in vitro utilising Mononucleosome Substrates	54
1.4.2.1 Activity of DNA glycosylases on nucleosomes.....	54
1.4.2.2 Activity of APE1 on nucleosomes.....	56
1.4.2.3 Activity of Pol β on nucleosomes.....	57
1.4.2.4 Activity of Lig III α -XRCC1	57
1.4.2.5 APE1 activity using nuclear extracts in single and clustered DNA damage site	57
1.4.3 Chromatin Remodelling factors.....	58
1.5 Aims	60
CHAPTER II.....	61
MATERIALS AND METHODS	61
2.1 Materials.....	61
2.1.1 601 nucleosome positioning sequence.....	61
2.1.2 Oligonucleotides.....	62
2.1.2.1 Oligonucleotides for preparation of THF containing DNA	62
2.1.3 Antibodies	67
2.1.4 Tissue culture reagents.....	68
2.2 Transformation of competent cells.....	69
2.2.1 Purifying DNA from bacterial cultures	69

2.3 Polyacrylamide gel electrophoresis (PAGE)	69
2.4 Denaturing PAGE	70
2.5 Sodium dodecyl sulphate polyacrylamide gel electrophoresis (SDS-PAGE) and Western blotting	70
2.5.1 SDS-PAGE	70
2.5.3 Western Blots	71
2.6 HeLa whole cell extract preparation	71
2.6.1 Protein Concentration	72
2.7 Preparation of purified APE1	72
2.7.1 Overexpression of his-tagged APE1	72
2.7.2 Purification of his-tagged APE1	72
2.8 Immunodepletion of proteins	73
2.9 Tissue Culture	73
2.9.1 Defrosting cells	73
2.9.2 Sub Culturing	74
2.9.3 Harvesting Cells	74
2.10 Preparation site-specific THF containing DNA	74
2.10.1 Amplification of 601 nucleosome positioning sequence	74
2.10.2 Restriction digests of the 601 nucleosome positioning sequence	75
2.10.3 DNA Purification from gel pieces	76
2.10.4 Preparation of duplex oligonucleotide	76
2.10.5 Sequential ligation of restriction digest products	76
2.11 Expression and purification of Recombinant histones	77
2.11.1 Recombinant Histone Expression	77
2.11.2 Inclusion body preparation	78
2.11.3 Recombinant Histone Purification by gel filtration chromatography	78
2.11.4 Recombinant Histone Purification by FPLC ion-exchange chromatography	79
2.11.5 Refolding of the Histone Octamer	80
2.12 Analysing APE1 activity in mononucleosomal and free DNA	80
2.12.1 Nucleosome Reconstitution	81
2.12.2 Preparation of Free DNA	81
2.12.3 In Vitro BER Repair Assay and DNA extraction	82

2.13 HeLa Cell Fractionation.....	82
2.13.1 Preparation of HeLa Whole cell extract for Phosphocellulose Chromatography	83
2.13.2 Phosphocellulose Chromatography	83
2.13.4 Ion exchange chromatography (MonoQ)	83
2.13.5 Gel filtration	84
2.13.6 Final Ion exchange (MonoQ) chromatography	84
2.14 Seeding cells for RNA interference	84
2.14.1 Seeding cells for preparation of WCE	84
2.15 Reverse Transcription and Real-time PCR	85
2.16 Clonogenic survival assay	86
2.17 Alkaline COMET assay	86
 CHAPTER III	 88
RESULTS I	88
Generation of the Mononucleosome Containing Site Specific Damage	88
3.1 Introduction	88
3.2.1 Amplification of 601 nucleosome positioning sequence	90
3.2.2 Restriction digest of the 601 nucleosome positioning sequence	92
3.2.3 Sequential ligation of restriction digest products	94
3.3 Expression and purification of recombinant histones for histone octamer preparation	94
3.3.1 Recombinant Histone Purification by gel filtration chromatography	96
3.3.2 Recombinant histone purification by Ion-exchange chromatography	96
3.3.4 Refolding of the Histone Octamer	103
3.4 Generation of mononucleosomes containing site-specific DNA damage	104
3.4.1 Optimising Nucleosome reconstitution	105
3.4.2 Generation of the THF site facing outwards and inwards mononucleosomes	107
3.5 Summary	108

CHAPTER IV	110
RESULTS II.....	110
BER in vitro assays using mononucleosomal DNA containing site-specific DNA damage in different orientations to examine difference in APE1 activity	110
4.1 Introduction	110
4.2 BER in vitro assays using free and mononucleosomal DNA containing site- specific DNA damage; THF-OUT and THF-IN.....	111
4.2.1 Optimising gel conditions for denaturing (7 M urea) PAGE.....	113
4.2.2 BER in vitro assays using free THF-OUT and THF-IN DNA	113
4.2.3 Quantifying APE1 concentration in HeLa WCE.....	117
4.2.4 BER in vitro assays using THF-OUT and THF-IN mononucleosome substrates	117
4.3 BER in vitro assays using HeLa WCE in the presence of ubiquitin and other factors.....	120
4.3.1 BER in vitro time course assays using HeLa WCE and ubiquitin with THF-IN and THF-OUT	120
4.3.2 BER in vitro time course assays using HeLa whole cell extract and Ubiquitin with THF-IN free DNA.....	122
4.3.3 BER in vitro time course assays analysing different conditions using HeLa WCE with THF-IN mononucleosome.....	124
4.3.4 BER in vitro time course assays using both HeLa WCE and purified APE1 in the presence of ubiquitin, E1/E2s and NAD using THF-IN mononucleosome substrate	126
4.3.5 BER in vitro assays with HeLa WCE and purified APE1 in the presence of supplementary ubiquitin, E1/E2 enzymes and NAD using THF-OUT and THF-IN mononucleosome substrates.....	128
4.4 Analysing structural changes in the THF-IN mononucleosome following BER in vitro assay in the presence of additional factors.....	130
4.4.1 Modifications and structural changes the THF-IN mononucleosome following BER in vitro assay in the presence of ubiquitin	130
4.4.2 Structural changes the THF-IN mononucleosome following BER in vitro assay in the presence of ubiquitin, E1/E2s and NAD	132
4.5 Summary.....	133

CHAPTER V	136
RESULTS III.....	136
Identification of histone modification/chromatin remodelling factors that stimulate APE1 activity towards the THF-IN mononucleosome substrate	136
5.1 Introduction	136
5.2 A candidate approach to discover the possible E3 ubiquitin ligase responsible for ubiquitinating histones.....	137
5.2.1 Analysing the efficiency of the knockdown for each E3 ubiquitin ligase in HeLa cells	139
5.2.3 BER in vitro assay time course with E3 ubiquitin ligase knockdown HeLa WCE with THF-IN mononucleosome.....	140
5.3 Fractionation of HeLa WCE to identify novel activities that stimulate APE1 activity towards the THF site in THF-IN mononucleosome substrate.....	144
5.3.1 Phosphocellulose chromatography of HeLa WCE	144
5.3.1.1 Immunodepletion of APE1 in HeLa WCE, PC150 and PC1000	145
5.3.1.2 BER in vitro assays to analyse APE1 stimulation in PC150 and PC1000	145
5.3.2 Ion exchange chromatography of the PC150 fraction of HeLa WCE	148
5.3.2.1 Identifying novel activities for stimulation of APE1 activity from ion exchange chromatography of PC150.....	148
5.3.2.2 Analysing fractions for residual APE1 incision activity	149
5.3.3 Further fractionation of the three activities and identifying candidate proteins that stimulate APE1 activity	151
5.3.3.1.1 Gel filtration chromatography of activity 1	151
5.3.3.1.2 Ion exchange chromatography of activity 1.....	152
5.3.3.1.3 Mass spectrometry of fraction 16 from ion exchange chromatography of activity 1.....	155
5.3.3.1.4 Alignment of CHIP and HECTD1 with the APE1 stimulatory activity from each of the chromatography steps for activity 1	156
5.3.3.1.4.1 Ion exchange chromatography alignment of the activity 1 profile to CHIP and HECTD1	156
5.3.3.1.4.2 Gel filtration chromatography alignment of the activity 1 profile to HECTD1	156

5.3.3.1.4.3 Final ion exchange chromatography alignment of the activity 1 profile to HECTD1	158
5.3.3.1.4.4 Analysing ubiquitination dependence of activity 1	158
5.3.3.1.4.5 The effect of HECTD1 immunodepletion from fraction 16 of activity 1	159
5.3.3.2.1 Gel filtration chromatography of activity 2	162
5.3.3.2.2 Ion exchange chromatography of activity 2.....	162
5.3.3.2.3 Mass spectrometry of fraction 21 from ion exchange chromatography of activity 2.....	162
5.3.3.2.4 Alignment of MULE and DDB1 with the activity from each of the chromatography steps for activity 2.....	166
5.3.3.2.4.1 Ion exchange chromatography alignment of the activity 2 profile to MULE and DDB1	166
5.3.3.2.4.2 Gel filtration chromatography alignment of the activity 2 profile to MULE and DDB1	166
5.3.3.2.4.3 Final ion exchange chromatography alignment of the activity 2 profile to MULE and DDB1	167
5.3.3.3.4.4 Analysing ubiquitination dependence of activity 2	169
5.3.3.3.1 Gel filtration chromatography of activity 3	171
5.3.3.3.2 Ion exchange chromatography of activity 3.....	171
5.3.3.3.3 Mass spectrometry of fraction 29 from ion exchange chromatography of activity 3.....	174
5.3.3.3.4.1 Ion exchange chromatography alignment of the activity 3 profile to YBX1 and YBX3.....	175
5.3.3.3.4.2 Gel filtration chromatography alignment of the activity 3 profile to YBX1 and YBX3.....	175
5.3.3.3.4.3 Final ion exchange chromatography alignment of the activity 3 profile to YBX1 and YBX3	175
5.3.3.3.4.4 Analysing ubiquitination dependence of activity 3	176
5.4 Analysing IR-induced DNA damage repair kinetics and cell survival following siRNA knockdown of candidate proteins	179
5.4.1 Knockdown of HECTD1, YBX1 and YBX3 in HeLa cells	179
5.4.2 Analysing IR-induced cell survival after YBX1, YBX3 and HECTD1 knockdown	179

5.4.4 Analysing IR-induced cellular DNA damage repair kinetics following knockdown of YBX1, YBX3 and HECTD1	182
5.5 Summary.....	185

CHAPTER VI

DISCUSSION	188
6.1 Overview	188
6.2 Mononucleosomes as substrates for BER	190
6.3 APE1 in HeLa WCE can efficiently incise THF-IN	191
6.4 HECTD1 and YBX3 are possible candidates for chromatin modelling activity to facilitate BER.....	194
6.5 Future Work.....	197
6.6 Concluding remarks	199
References	200
Appendix I	216
Appendix II	225
Appendix III	239

List of Figures

CHAPTER I

Page Number

Figure 1:	The chemical structure of the four nitrogenous bases and an example of nucleotide structure	3
Figure 2:	Base pairing and the DNA double helix	5
Figure 3:	DNA Double Strand Break	11
Figure 4:	DNA Single Strand Break	12
Figure 5:	Apurinic/apyrimidinic site in DNA	13
Figure 6:	Molecular Structure of 8-Oxoguanine	13
Figure 7:	Molecular Structure of Thymine Glycol	14
Figure 8:	Homologous Recombination	17
Figure 9:	Non-homologous end joining pathway	19
Figure 10:	Nucleotide excision Repair	21
Figure 11:	The Base Excision Repair Pathway	23
Figure 12:	The Primary, Secondary and Tertiary Structure that form Chromatin	33
Figure 13:	The Nucleosome Core Particle	34
Figure 14:	Histone post translational modifications	38
Figure 15:	ATP-dependent chromatin remodelling families	45
Figure 16:	Comparing the Widom 601 Sequence with α -satellite DNA Nucleosome Core	53
Figure 17:	Uracil Rotational Orientation and Translational Position effect on the Activity of Glycosylase UDG1 and APE1	56

CHAPTER II

Figure 18:	Double strand 256bp DNA sequence for the 601 nucleosome positioning sequence	61
Figure 19:	Restriction Digest cut sites and 17bp oligonucleotide insert	62

CHAPTER III

Figure 20:	Positions of THF sites in the crystal structure of the nucleosome core particle containing the Widom 601 nucleosome	89
-------------------	---	----

Figure 21:	Schematic diagram showing the formation of the THF containing DNA and nucleosome	91
Figure 22:	DNA Substrate Preparation containing a site specific THF site	93
Figure 23:	Steps of the purification process of histones and refolding of the histone octamer	95
Figure 24:	Purification of recombinant histones H2A and H2B by gel filtration chromatography	97
Figure 25:	Purification of recombinant histones H3 and H4 by gel filtration chromatography	98
Figure 26:	Purification of recombinant histones H2A and H2B by ion-exchange chromatography	99
Figure 27:	Purification of recombinant histones H3 and H4 by ion-exchange chromatography	100
Figure 28:	Purification of Histone H4	102
Figure 29:	Refolding of the histone octamer	104
Figure 30:	Generation of a Mononucleosome containing unlabelled DNA comparing agarose gel conditions and DNA:histone octamer ratio	106
Figure 31:	Generation of a Mononucleosome containing an THF	107

CHAPTER IV

Figure 32:	DNA sequence for THF-OUT and THF-IN before and after incision of APE1	112
Figure 33:	Optimising gel condition for BER <i>in vitro</i> assays using AP-O free DNA and purified APE1	115
Figure 34:	<i>In vitro</i> BER assays using Free DNA Substrates containing an AP site for either THF-OUT (orange) or THF-IN (blue)	116
Figure 35:	Quantifying APE1 concentration in HeLa WCE	117
Figure 36:	<i>In vitro</i> BER assays using mononucleosome substrates containing an THF-OUT (orange) or THF-IN (blue)	119
Figure 37:	<i>In vitro</i> BER assays time course using THF-IN and THF-OUT mononucleosomes with HeLa WCE plus and minus ubiquitin	121
Figure 38:	<i>In vitro</i> BER assays time course using free THF-IN DNA substrate HeLa WCE plus and minus ubiquitin	123
Figure 39:	<i>In vitro</i> BER assays time course using THF-IN mononucleosome substrate with HeLa WCE or purified APE1 in the presence of ubiquitin, NAD and E1/E2 enzymes	127
Figure 40:	<i>In vitro</i> BER assays using mononucleosome substrates containing an THF-OUT (orange) or THF-IN (blue) with factors added to support ubiquitination and poly(ADP-ribosyl)ation	129

Figure 41:	Analysing structural changes and modifications of THF-IN mononucleosome substrate	131
Figure 42:	Analysing major structural changes in the THF-IN mononucleosome substrate with HeLa WCE in the presence of ubiquitin, NAD and E1/E2s	132

CHAPTER V

Figure 43:	Percentage knockdown for each siRNA candidate E3 Ligases	139
Figure 44:	The effect of candidate siRNA E3 ubiquitin ligase knockdowns titrations on the BER <i>in vitro</i> assay with THF-IN mononucleosome	142
Figure 45:	The effect of candidate siRNA E3 ubiquitin ligase knockdowns on the BER <i>in vitro</i> assay using a time course with THF-IN mononucleosome	143
Figure 46:	Analyses of APE1 stimulation by WCE, PC150 and PC1000 fractions	147
Figure 47:	Mono Q chromatography of HeLa PC150	150
Figure 48:	Gel filtration chromatography of activity 1	153
Figure 49:	Ion exchange chromatography of activity 1	154
Figure 50:	Alignment of candidate proteins to the activity profiles of activity 1 for each of the sequential chromatography stages	159
Figure 51:	Analysing the ubiquitination dependence of activity 1	160
Figure 52:	HECTD1 immunodepletion from fraction 16 from the final ion exchange chromatography	161
Figure 53:	Gel filtration chromatography of activity 2	163
Figure 54:	Ion exchange chromatography of activity 2	164
Figure 55:	Alignment of candidate proteins to the activity profiles of activity 2 for each of the sequential chromatography stages	168
Figure 56:	Analysing the ubiquitination dependence of activity 2	170
Figure 57:	Gel filtration chromatography of activity 3	172
Figure 58:	Ion exchange chromatography of activity 3	173
Figure 59:	Alignment of YBX1 and YBX3 to the activity profiles of activity 3 for each of the sequential chromatography stages	177
Figure 60:	Analysing the ubiquitination dependence of activity 3	178
Figure 61:	Knockdown of HECTD1, YBX1 and YBX3 in HeLa cells	180
Figure 62:	The effect of YBX1, YBX3 and HECTD1 on cellular sensitivity to IR	181

Figure 63:	Analysing ionising radiation-induced DNA damage repair kinetics following siRNA knockdown of YBX1, YBX3 and HECTD1 in HeLa cells	183
Figure 64:	Analysing IR-induced DNA damage repair kinetics following siRNA knockdown of YBX1, YBX3 and HECTD1 in normal lung fibroblasts	184

List of Tables

CHAPTER I

Page Number

Table 1	Human DNA Glycosylases	25
----------------	------------------------	----

CHAPTER II

Table 2	Fluorescently 5' tagged primers for THF containing site DNA preparation	63
Table 3	Oligonucleotide sequences with a THF (1) which is either outwards or inwards facing after nucleosome DNA reconstitution	63
Table 4	Real-time primer sequences for target gene	64
Table 5	siRNA pool sequences for knockdowns	65-66
Table 6	Primary Antibodies	67
Table 7	Secondary antibodies	68
Table 8	Histone molecular weights and molar extinction	80

CHAPTER IV

Table 9	BER <i>in vitro</i> time course assays analysing different conditions using HeLa WCE with THF-IN Mononucleosome	125
----------------	---	-----

CHAPTER V

Table 10	Candidate E3 Ligases for stimulation of THF-IN incision	138
Table 11	Mass Spectrometry results for activity 1	155
Table 12	Mass Spectrometry results for activity 2	165
Table 13	Mass Spectrometry results for activity 3	174

Abbreviations

6-4PPs	6-4 pyrimidine-pyrimidone photoproducts
8-oxoG	8-oxoguanine
A	Adenine
A	Alanine
APE1	AP endonuclease 1
AP-Sites	apurinic/apyrimidinic site
Asf1	Nucleosome assembly protein 1
ATM	Ataxia telangiectasia mutated
ATP	Adenosine triphosphate
ATPases	Adenosine triphosphatases
ATR	ATM and Rad 3-related
BER	Base Excision Repair
BRCA1	Breast cancer gene 1
BRCA2	Breast cancer gene 2
C	Cytosine
CBP	CREB-binding protein
CDKs	Cyclin-dependent kinases
CENT2	Centrin 2
CHD	Chromodomain helicase DNA binding
CHIP	Hsc-70-interacting protein
CoA	Acetyl cofactor A
CPDs	Cyclobutane pyrimidine dimers
CUL1	Cullin 1
CUL4a	Cullin 4a
DDB1	DNA damage binding protein 1
DDR	DNA damage response
DMEM	Dulbecco's modified eagle's medium
DNA	Deoxyribose nucleic acid
DNA-PKcs	DNA-dependent protein kinase catalytic subunit
DZIP3	DAZ Interacting Zinc Finger Protein 3
ERK	Extracellular signal-regulated kinase
FACT	Facilities chromatin transcription
FRET	Fluorescence resonance energy transfer
G	Guanine
G	Glycine
GG-NER	Global genome NER

H	Histidine
HATs	Histone acetyl transferases
HDACs	Histone deacetylases
HECTD1	HECT Domain E3 Ubiquitin Protein Ligase 1
HEPES	Hydroxyethyl piperazineethanesulfonic acid
HhH	Helix-hairpin-helix
HMTases	Histone methyltransferases
HP1	Heterochromatin protein 1
HR	Homologous Recombination
I	Isoleucine
ING1	Inhibitor of growth 1
INO80	Inositol requiring 80
IRIF	Ionising radiation-induced foci
ISWI	Imitation switch
JAMM	JAB1/MPN/Mov34 metalloenzyme
K	Lysine
Lig	Ligase
LSD1	Lysine-specific demethylase 1
M	Methionine
MDC1	Mediator of DNA damage checkpoint protein 1
Mdm2	Mouse double minute 2 homolog
MeCP2	Methyl-CpG-binding protein 2
MEK1	Mammalian protein kinase 1
MENT	Myeloid, erythroid nuclear termination stage specific protein
MMS	Methanesulfonate
MOF	Males absent on the first
MSL2	Male-specific lethal-2
MULE	Mcl-1 ubiquitin ligase E3
MWCO	Molecular weight cut off
N	Nitrogen
NAD	Nicotinamide adenine dinucleotide
Nap1	Nucleosome assembly protein 1
NASP	Nuclear autoantigenic sperm protein
NEIL	Endonuclease VIII-like 1
NEM	<i>N</i> -Ethylmaleimide
NHEJ	Nonhomologous end-joining
O	Oxygen
OUT	The Ovarian tumor
PAGE	Polyacrylamide gel electrophoresis
PARP	Poly [ADP-ribose] polymerase 1

PBS	Phosphate-buffered saline
PcG	Polycomb Proteins
PCR	Polymerase chain reaction
PI-3	Phosphate-buffered saline
PMSF	Phenylmethylsulfonyl fluoride
PNKP	Polynucleotide kinase 3'-phosphatase
PRC1/2	Polycomb repressive complex 1 and 2
PRCs	Polycomb repressive complexes
PTMs	Post translational modifications
PVDF	Immobilon-FL polyvinylidene difluoride
R	Arginine
RNF	Ring finger protein
RNF168	Ring finger protein 168
RNF2	Ring finger protein 2
RNF20	Ring finger protein 20
RNF8	Ring finger protein 8
RNS	Reactive nitrogen oxygen species
ROC	Regulator of cullins
ROS	Reactive oxygen species
RSC	Remodels structure of chromatin
RT	Real-time
S	Serine
SAM	S-adenosylmethionine
SDS-PAGE	Sulphate polyacrylamide gel electrophoresis
SiRNA	Small interfering mRNA
SSB	Single strand breaks
SW1/SNF	Switching defective/sucrose nonfermenting
T	Thymine
T	Threonine
TC-NER	Transcription-coupled NER
TDP1	Tyrosyl-DNA phosphodiesterase 1
TEMED	<i>N,N,N,N</i> -Tetramethylethylenediamine
TFIIH	Transcription initiation factor IIH
Tg	Thymine glycol
TGS	Tris-glycine
THF	Tetrahydrofuran
THF-IN	THF with DNA backbone facing inwards
THF-OUT	THF with DNA backbone facing outwards
TOP1	DNA topoisomerase 1
U	Uracil

UBR2	Ubiquitin protein ligase E3 component N-recognin 2
UCH	Ubiquitin c-terminal hydrolases
UNGs	Uracil DNA glycosylase
USP/UBP	Ubiquitin specific protease
USP7	Ubiquitin specific protease 7
UV	Ultraviolet light
UVSSA	UV stimulated scaffold protein A
WCE	Whole cell extract
XP	Xeroderma pigmentosum
XRCC1	X-ray repair cross-complementing protein 1
Y	Tyrosine
YBX1	Y-Box protein 1
YBX3	Y-Box protein 2
γ-H2AX	Phosphorylated H2AX

CHAPTER I

INTRODUCTION

1.1 Genome Stability and Instability

The cell is a basic biological, functional and structural building block of most living organisms. Most organisms are single cells but others including ourselves are arranged of extensive multicellular systems comprising of specialised groups of cells that have their own functions but all communicate through elaborate systems. There more than 10^{13} cells in the human body which all originated from one cell. The whole organism is the result of countless cell divisions from the original single cell which acts as a carrier of genetic information that creates a species. Cells contain the machinery needed and have the ability to use materials from the environment to build a copy of the image of itself and genetic information.

Genetic information in all living cells in earth is stored in the form of double stranded molecules called deoxyribose nucleic acid (DNA). In human cells identical copies of DNA, genome, are distributed between 23 pairs of chromosomes. Double stranded DNA is a linear unbranched polymer made up of four types of monomers; adenine (A), cytosine (C), guanine (G) and thymine (T). These monomers are strung together to form a long sequence that encodes for the genetic information. Their specific order in DNA forms a code vital to the purpose of DNA. A gene is a region of DNA that encodes for a particular protein, the sequence of DNA encodes sequences of proteins. Humans have around 20-25,000 genes, although this only represent 3% of the human genome. 20 different types of amino acid are used to build proteins, which type and order of the amino acid sequence is determined by the DNA sequence. Three DNA bases (codon) encodes for a specific amino acid within a protein sequence. The relationship of DNA sequence to the protein sequence is called the genetic code. Protein molecules are made up of long chains of amino acids. Each individual type of protein contains its own unique amino acid sequence. Proteins have a vast array of functions including cell mobility and shape, enzymes need to produce energy and inter/intra cellular signals.

The DNA sequence can be altered during copying of genetic information, storage and random errors occurring chemically (for example from normal cellular metabolism) and by radiation from the environment. Damage to DNA can, in some instances, have no significant alteration on the cell. However, some however can lead to a change in the sequence of amino

acids in protein that may cause an alteration on the proteins structure, function (loss or gain of function) and regulation which can have a damaging effect on an organism. To maintain genome stability required for an organism's survival it is important that these damage to DNA are repaired before they can have an effect on the whole organism. The significance of DNA repair in cells is apparent from the large collection of DNA enzymes that are in cells. Mutations in DNA the majority of the time are effectively repaired by DNA repair proteins, however when damage is not repaired it can lead to disease. Cancer, neurogenerative disorders and ageing are key examples of diseases that are predominantly caused by mutations in DNA. Extensive DNA damage (genomic instability) is a marker of almost all cancer cells. Cancer occurs when DNA errors are not repaired properly through DNA repair proteins being mutated, inaccuracies in repair, or whether there has been a huge increase in DNA damage overwhelming DNA repair proteins. This leads to abnormal cellular proliferation and survival due to key proteins in these pathways being defective due to mutations in the genes encoding for them or their regulators. Currently chemotherapy and radiotherapy are the key treatments for cancer. These work by causing extensive DNA damage in cancer cells, overwhelming the ability of the cell to repair DNA and so causing cell death. As cancer will affect 1:3 people in their lifetimes there is a need to understand more about basic cellular process to identify key drivers in the onset and progression of cancers, so these can be targeted for cancer treatment. As DNA damage is a hallmark of cancer and used as a frontline treatment it is an important area of research for treatment and development of cancers.

1.1.1 Deoxyribose Nucleic acid

DNA is a fundamental feature across all living organisms. The three dimensional structure of DNA was discovered to be a molecule comprising of two linear polynucleotide chains made up by four different nucleotides. These two polynucleotide chains were found to be held together by hydrogen bonds between corresponding nucleotide pairs (1). DNA has a fixed backbone that is composed of repeating pentose sugar-phosphate components. Each pentose sugar, 2'deoxyribose is connected by two 5'phosphate groups via a phosphodiester bond on the 3'hydroxyl residue on the sugar. 2'Deoxyribose sugars are attached to a base, there are four possible nitrogenous bases A, T, G, C (Figure 1A). A single unit of the DNA polymer is formed when one of this bases is linked to the pentose sugar by a covalent glycosidic bond forming a 2'deoxyribonucleoside, this is linked via the 5' position of the pentose sugar to one or more phosphates to become a 2'deoxyribonucleotide (figure 1B). The 2'deoxyribose molecules are orientated in the same position so each of the DNA polymers are polar, consequently the ends of the phosphate backbone are easily discernible; 5' phosphate on one end and 3'hydroxyl on the other, the bonding between these only occurs in the 5' to 3' direction. The double helix occurs because of the structural and chemical

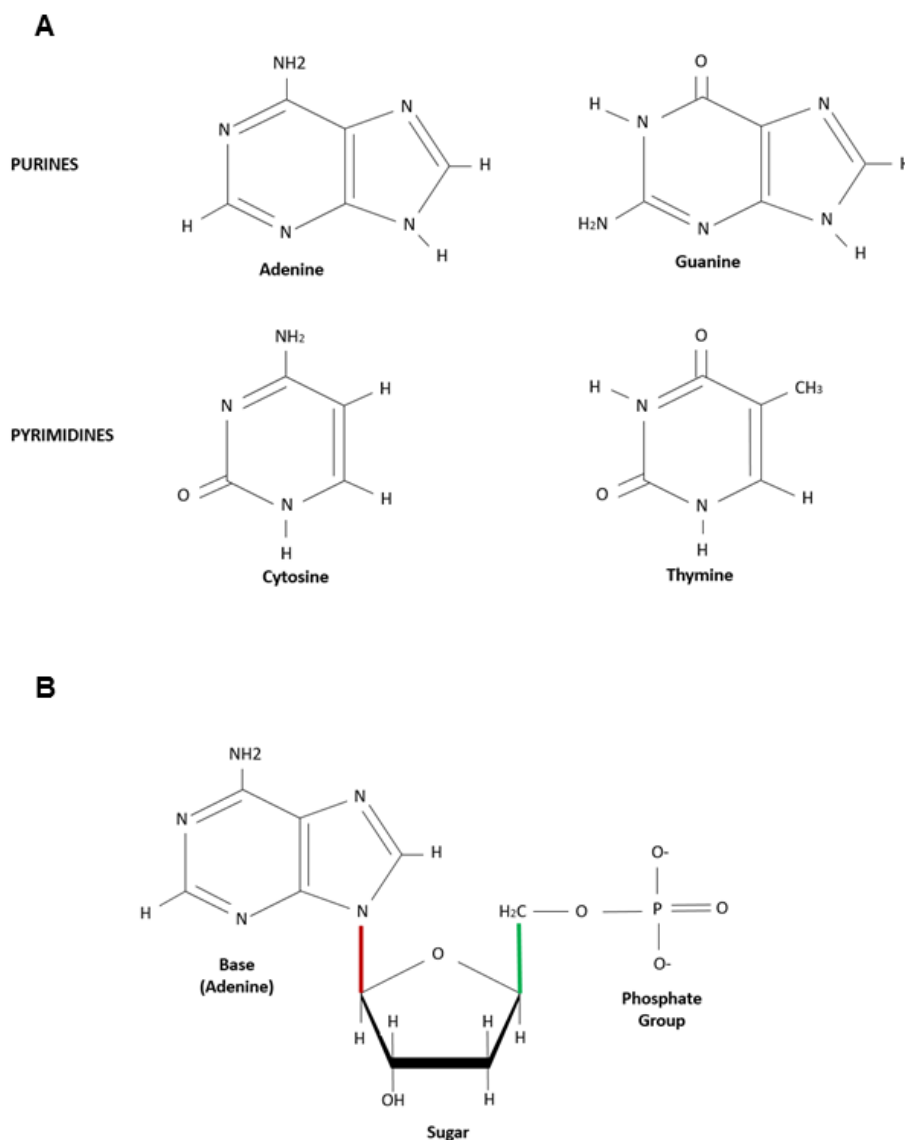


Figure 1: The chemical structure of the four nitrogenous bases and an example of nucleotide structure. (A) The chemical structure of the four main DNA nitrogenous bases, the two pyrimidines; C and T, which are composed of a single ring, and the two purines; A and G which are composed of 2 fused ring. (B) The nucleotide molecular structure using adenine as an example. When a base is attached to a deoxyribose sugar via a glycosidic bond (red bond) a nucleoside molecule is formed and which attached to a phosphate group by a phosphodiester bond (green bond) and together form the nucleotide.

features of the polynucleotide chains. All bases lie within the DNA helix due to the hydrogen bonds holding the two polymers together and the pentose sugar-phosphate backbone on the outside. A purine, a bulky two-ring base (A and G), is matched with a pyrimidine, a single ring base (T and C). A to T and G to C will only pair together due to the structure of bases and because of the structure of the DNA backbone. These wind around to form the DNA double helix with 10 bases for every 360° turn. Due to the necessity of base pairing each of the two pairs of DNA polymers are complementary to one another, but run antiparallel to one another as the polarity of the two strands is opposite and intertwined to form the DNA double helix (figure 2). The hydrogen bonds that hold the base pair together are much weaker than covalent bonds (such as the C-C or C-N that compose the structures of the bases). These weak bonds are essential in biochemical systems, in that they are weak enough to be broken apart in systems (like transcription to produce RNA from which mRNA is produced by translation the messenger molecule that encodes for protein), but still robust enough to stabilise the double helix. The stacking of bases on top of each other provided stability to the DNA helix. This is achieved by the hydrophobic effect from the hydrophobic bases which group in the centre, away from neighbouring water. The polar surfaces however; the DNA backbone which is negatively charged is strongly hydrophilic. The stacking of bases on top of each other because of this hydrophobic effect attracts bases to one another through van der Waals forces, although these forces are weak in the double helix a large proportion of atoms are attracted by this force and so the net effect is considerable. Though this rigidity in the construction of DNA the storage and protection of genetic information allows its preservation of hereditary information.

DNA in cells must be packaged into a small volume so it can be fit in the cell's nucleus. This is achieved by specialised proteins that fold and package DNA in increasingly complex levels of organisation that fold nuclear DNA into a series of loops and coils bound to specific proteins to form chromatin. This tight organisation of DNA limits the access of proteins involved in DNA transcription, replication and repair to DNA. To allow access of these proteins to the target DNA sequences loosening of DNA and its protein contacts is required, this occurs by specific proteins and epigenetic changes. Arranging DNA into these regulated structures also stops DNA becoming an unmanageable jumble and provides protection of DNA from damage for the cellular environment by reducing its surface area. Section 3 provides a more in depth discussion of chromatin formation and regulation.

Figure from (2), Figure 4

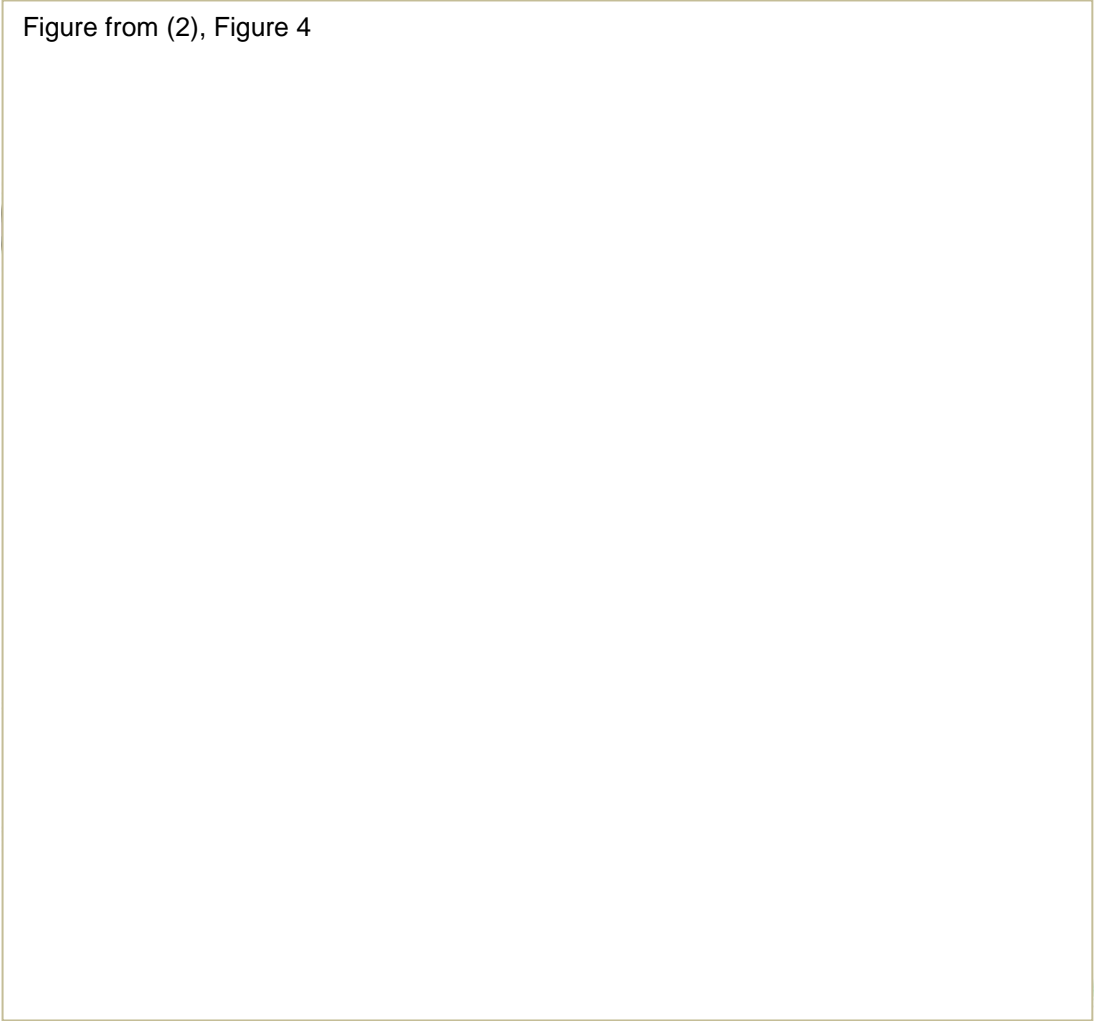


Figure 2; Base pairing and the DNA double helix. Image was taken from L. A. Pray (2). Image shows the molecular structure of DNA and a basic version of the DNA helix is shown on the left. The two grey lines running anti parallel are the DNA sugar-phosphate backbone which twisted to form the DNA helix and the base pairs in the middle. On opposite ends of the DNA backbone there are a 5' phosphate and 3'hydroxyl group. The zoomed in picture describes the molecular structure and bonds which make up DNA, the phosphate, sugar and base to form the nucleotide are clearly shown. The two bases G and C are held together by three hydrogen bonds and T and A are held by two, the hydrogen bonds are marked as dotted red lines.

1.1.2 DNA Damage

The structure of DNA makes it well suited to preserve the genetic information it contains. The double helix and bases compacted into the centre provides a degree of protection from biochemical attacks by guarding the possibly reactive assemblies e.g. the amine side chains of bases which are very susceptible to attack. Under normal physiological settings the N-

linked glycosidic bonds that attach the four bases to the backbone of DNA and phosphodiester bonds that make up this backbone are both quite stable. However, DNA despite the clever design is frequently broken or chemically modified by endogenous sources such as normal metabolism and exogenous sources from environmental factors (3, 4). Damage to DNA can block transcription and replication leading to apoptosis or necrosis, and causes genome instability which can lead to cancer, ageing and neurodegeneration if not repaired, examples will be discussed next. To maintain genome stability cells have developed various DNA repair pathways that repair different lesions (5, 6).

1.1.3 Endogenous DNA damage

The majority of DNA damaged occurs through intrinsic agents of endogenous origin, particularly from water and oxygen from the cell environment (7). DNA damage from endogenous sources causes approximately 20,000 lesions per cell per day. The simplest form of endogenous damage to DNA is hydrolysis, this occurs to the N-glycosidic bond that links the DNA base to the 2'-deoxyribose sugar when produce an array of damages to DNA (4). Reactive molecules that are produced in normal cell metabolism can also damage DNA, reactive oxygen species (ROS) are produced this way and constantly cause damage to DNA (8). Damages can also incur due to errors in normal DNA processing, including misincorporation bases during DNA replication.

1.1.3.1 Hydrolysis

DNA bases are particularly susceptible to hydrolysis. The N-glycosidic bond is extremely vulnerable to acid-catalysed hydrolysis and apurination. Loss of bases to produce apurinic/apyrimidinic site (AP-sites) are the result of spontaneous hydrolysis, alkylation-induced hydrolysis, but also during base excision repair (BER). These occur at an approximate rate of 10,000 per cell per day (4, 9). G and A (purines) are released from DNA at comparable proportions; however T and C (apyrimidinic) are released at a 5% lower rate (4). At these AP-sites β -elimination occurs within a few days and causes cleavage of the DNA as it is weakened (10). Typically AP site causes base pair substitutions, the most common being AP site \rightarrow T, however they may cause a frameshift of the DNA sequence both of which could cause a alternation in the protein they encode for (11).

Hydrolytic deamination of DNA bases containing exocyclic amino groups (NH_2) is another common reaction concerning hydrolysis. The loss of the amino group in adenine, cytosine, guanine and 5'-methylcytosine occur randomly and spontaneously and causes the conversion to hypoxanthine, uracil and thymine respectively (7, 12). C and its homologue are the main

targets for deamination (4). C to uracil is the most common event and occurs at an approximate rate of 100-500 uracil residues per cell per day (7). The deamination of purines occurs at a much lower rate for example adenine being deaminated to hypoxanthine occurs at only a 2-3% the rate of which cytosine does (13). The GT base pair formed from the hydrolysis of 5'methylcytosine is repaired slowly (mismatch repair), as a result these account for one third of single base mutations that cause inherited disease and is seen commonly mutated in the p53 gene of many different cancers (14).

1.1.3.2 Oxidation

Cells are exposed to reactive oxygen during normal cellular aerobic metabolism and this provides a large source of damage to the cells genome (4). The most prevalent of these reactive molecules are ROS, these are oxygen containing molecules that contain a radical making them highly reactive to biomolecules. Oxidative stress is caused by the discrepancy in the formation and degradation of ROS, in favour of the formation of ROS. Free radicals have a single electron in their orbit, it is this which makes free radicals more reactive (8). Examples of oxygen radicals include superoxide, hydroxyl, peroxy and alkoxy and the non-radicals ozone, singlet oxygen and hydrogen peroxide which are either oxidising or are easily changed into radicals (15, 16). ROS are produced constantly in a normal cell as a consequence of cellular metabolism and play critical roles in signal transduction, oxidative metabolism and killing ingested microorganisms. Although most of the oxygen during oxidative metabolism in mitochondria is converted to water up to 2% is converted to ROS (6). Most excess ROS is neutralised by superoxide dismutases, glutathione peroxidases and catalases, however remaining ROS can damage proteins and DNA. ROS is capable of producing over 100 oxidative damages to DNA including DNA adducts (e.g. base modification), deoxyribose modifications, single/double stranded breaks and DNA crosslinks (17). ROS can contribute to the initiation of cancer by causing structural alterations in DNA (such as AP-sites and single strand breaks (SSBs)), as they are small molecules that are able to gain access to nucleosomal DNA (11). DNA bases, especially G (because of its low redox potential) are highly susceptible to oxidation by ROS. The cells response to oxidative damage is DNA repair, cell cycle arrest or apoptosis. If these mutations are not reversed then they can contribute to tumorigenesis (15, 16). 8-oxoguanine (8-oxoG) is an example of DNA oxidative damage, and is used as a marker of oxidative damage in biological systems (18). Reactive nitrogen oxygen species (RNS) particularly nitric oxide produce similar array of oxidative adducts in DNA as ROS (19). Alkylation is another example of reactive molecules produced endogenously and primarily react with oxygen and nitrogen atoms on bases. Examples of alkylating agents are the methyl donor S-adenosylmethionine (SAM), methyl radicals produced from lipid peroxidation and nitrosated amines (7, 20)

1.1.3.3 Errors from DNA Processing

DNA damage can occur through errors resulting from physiological DNA processing. These resulting damages such as DNA mis-matches, deletions and insertions are very occasionally introduced into DNA. Replicative and translesion synthesis polymerases have a base disincorporation rate overall of one for every billion base pair copied (9). Polymerase (Pol) β involved in the BER DNA repair pathway has an overall approximate error efficiency of 5×10^{-4} , the backup polymerase Pol λ in BER has been shown to have a overall error rate 160 fold higher than Pol β (21, 22). Another source of DNA damage for replication is the wrong incorporation of oxidised nucleotide like dUTP and 8-oxo-dGTP by Y family DNA polymerases encouraging mutagenesis and facilitating translesion DNA synthesis (23). Failed topoisomerase activity (such as topoisomerase II) can cause what is normally a transient enzyme-DNA to a permanent double strand break (DSB). This can lead to chromosome translocations (such as in mixed lineage leukaemia) and other DNA abnormalities (24). DNA repair processes may also introduce errors into DNA. For example the repair of double strand breaks can be done via two pathways. Non-homologous end joining is an error-prone pathway that causes changes in the sequence near the double strand break. Homologous recombination was thought to be an error free process however recent evidence has shown that it can be highly mutagenic causing translocations and chromosome rearrangements, particularly when large amount of DNA need to be synthesised (25).

1.1.4 Exogenous damage

Exogenous damage to DNA is from environmental sources which can be physical or chemical. Ultraviolet light (UV) damage is an example of a physical stress from the sun. Ionising radiation is another physical agent which occurs both naturally occurring (cosmic radiation) and artificially (medical x-rays). Chemical compounds are able to intercalate or covalently bind to DNA in numerous ways, examples of chemical compounds are air pollutants (diesel and industrial fumes), dietary carcinogens and chemotherapeutic drugs (26, 27).

1.1.4.1 UV

The stratospheric ozone layer that shields earth from hazardous solar radiation is constantly undergoing depletion due to atmospheric pollutants. Subsequently there is an increase in earth's exposure to solar radiation. Solar radiation is a toxic agent to genomic DNA, the spectrum of sunlight contains two maxima in the UV spectrum that have mutagenesis potential, this is due to DNA bases absorbing UVB photons. UVA is also mutagenic however to a smaller degree than UVB due to DNA not being a chromophore for UVA. UV is one of the

most damaging exogenous carcinogens that can interact with DNA (26, 28, 29). UV radiation provides DNA with enough energy to excite the molecular bonds within to cause covalent modifications between pyrimidine nucleotides. Namely cyclobutane pyrimidine (CPD) dimers and pyrimidine photoproducts (6-4) both possess an atypical covalent bond between pyrimidines and account for 75% and 25% respectively of UV induced damage (26, 30). In solar radiation the most energetic form is UVB radiation causes direct absorption of UVB photons by DNA nucleotides by primarily pyrimidine thymine, cytosine and 5-methylcytosine, however it has been shown that purines are also to absorb photons to a lesser degree. Both of these DNA lesions distort the DNA helix by causing a bend of 7 for CPDs and pyrimidine photoproducts (6-4) 44° interfering with DNA transcription and replication which can cause misreading of the genetic information (30).

1.1.4.2 Ionising Radiation

Ionising radiation originates from natural sources such as cosmic and gamma radiation and artificial sources for example medical X-rays and radiotherapy. Ionising radiation has both positive and negative impacts in that may lead to modifications in normal tissues but decreases the survival of tumour cells. Ionising radiation causes damages to DNA leading to cell death if not repaired. The effect of ionising radiation specifically to bases which is accountable to 30-40% of lesions and the free radicals generated from this 60 – 70% (31, 32). The most harmful of the DNA lesions produced is DSBs which if not repair can cause apoptosis. If they are not repaired correctly genomic rearrangement can take place causing genomic instability and so increased mutagenesis. Ionising radiation can also cause damage indirectly by the production of ROS through the hydrolysis of water to form hydroxyl radicals (33). ROS through ionising radiation produces around 850 pyrimidine lesions such as Tg, 450 purine lesions for example oxo-7, 8-dihydro-2'-deoxyguanosine, 1000 SSB and 20 – 40 double strand break (DSB) per cell (34).

1.1.4.3 Alkylation

Alkylating agents are a groups of molecules that transfer an array of alkyl group from one molecule to another, modifying the molecules structure and so disrupting its function, they are genotoxic and mutagenic. Agents causing alkylation are unavoidable due to the abundance in the environment from water, food and constituents in the air and pollutants from sources such as industrial and diesel fumes. Despite their adverse effects to health alkylating agents are used systemically as cytostatic drugs in cancer patients with the aim of killing cancer cells by inducing an overwhelming amount of DNA damage (35, 36).

Alkylating agents cause DNA damage by reacting with ring nitrogen's (N) and extra cyclic oxygen (O) in the DNA nucleotide bases causing a broad range of covalent adducts. They can comprise genome integrity promoting mutagenesis and cause cell death by blocking DNA replication (cytotoxic). Depending on the number of reactive sites on the agent, its specific reactivity, the type of the alkyl group and DNA substrate the damages can range from the addition of modest methyl groups to intricate alkyl add-ons (35, 36). There are two types of alkylating agents based on number of reactive sites; monofunctional (one chemical moiety) and bifunctional (two chemical moieties) the latter being able to form interstrand crosslinks. Based on the specific reactivity of the agent there are S_N2 alkylating agents which target nitrogen rings and S_N1 which alter both the nitrogen rings and the extra cyclic oxygen. N7-methyl guanine is a primary methylation adduct due to the reactivity of N7 in guanine by monofunctional alkylating agents and is noted in 60-80% of all alkylation lesions in DNA. This lesion although not mutagenic is susceptible to depurination to a AP-site which is mutagenic. N3-methyladenine can also be formed by this agent at a rate of 10-20% of methyl adducts (36). This lesion is significantly cytotoxic as it blocks DNA polymerases inhibiting DNA synthesis (37). S_N1 type alkylating agents are highly reactive to the O6 position in guanine resulting in a lesion called O6-methylguanine. This lesion is produced at a much lower rate than N-alkyl groups but is important as it is prone to mismatch with thymine during DNA replication causing mutagenic and cytotoxic effects (36). Methyl methanesulfonate and temozolomide are example of monofunctional alkylating agents used to treat cancer by causing alkylation of DNA bases. Bifunctional alkylating agents including nitrogen mustards, platinum compounds and mitomycin C cause DNA damage by causing intra/interstrand crosslinks (38).

1.1.5 Common types of DNA damage

The genome of cell is under constant attack from DNA damaging agents comprising genetic stability. These insults can arise from normal cellular processes (endogenous) such as the cells normal metabolism and from the environment (exogenous). Many of the lesions that caused by these insults result in structural damage to DNA and can modify or disrupt vital cellular processes. Common types of DNA damage are as follows DSB, single strand breaks (SSB), AP sites, thymine glycol (Tg) and 8-oxoG.

1.1.5.1 Double strand breaks

DSB are one of the most dangerous types of DNA damage. They result from exogenous agent including ionising radiation and chemotherapy drugs, and endogenously from reactive oxygen species (ROS) from the cells environment. Another major form of endogenous damage is when DNA replication forks come across DNA lesions causing fork collapse (39, 40). They

occur when the phosphodiester bond on complementary strands in the DNA helix are simultaneously broken at sites that are suitably close to each other (within 0-20 base pairs) so that the hydrogen bonds of the other bases and chromatin structure can keep the DNA strands juxtaposed figure 3 (40, 41). This causes the double stranded DNA to become prone to dissociation from one another making DNA repair more difficult. DSB are highly cytotoxic and mutagenic if it inactivates a vital gene and can cause chromosomal translocations. The two key DNA repair pathways that process this type of lesion are homologous recombination (HR) and nonhomologous end-joining (NHEJ) (39, 40).

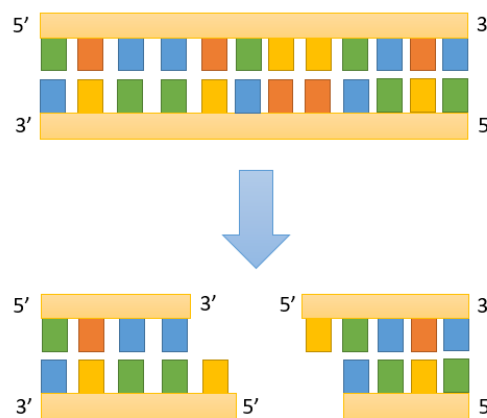


Figure 3: DNA Double Strand Break. Schematic diagram shows the formation of DNA DSB with DNA bases coded in colour and the phosphodiester back shown in light orange. The phosphodiester backbone is broken at opposing sites in DNA but are kept juxtaposed due to their close proximity.

1.1.5.2 Single strand breaks

SSBs can result from endogenous agents such as ROS and abortive enzyme activity (such as DNA topoisomerase 1 (TOP1), and exogenous sources such as ionising radiation. SSBs are formed when the phosphodiester bond is broken causing usually loss of a nucleotide and damage to either or both the 5' and 3' at the SSB site (figure 4). If these are not repaired this can lead to genome instability and cell survival. If not repaired a DNA replication forks can collapse leaving the site prone to forming a DSB, stall RNA polymerases during transcription and cause excessive protein poly(ADP-ribose) polymerase 1 (PARP1) activation. SSBs are also a intermediate in BER after incision of the AP-site (42).

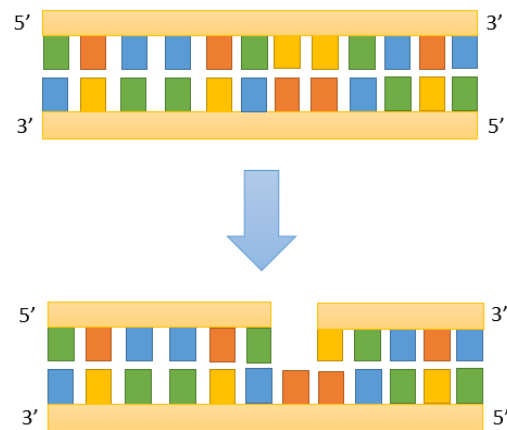


Figure 4: DNA Single Strand Break. Schematic diagram shows the formation of DNA SSB with bases coded for in colour and the DNA backbone in orange. A single strand break is formed in one side of the DNA backbone which commonly also causes the loss of the base and damage to the 3' and 5' ends of DNA.

1.1.5.3 AP sites

AP sites are one of the most common types of DNA damage and are estimated to occur at 10,000 per cell per day, a lesion is classed as a AP-site when there is neither a purine or pyrimidine base (43). AP-site are formed by spontaneous, alkylation induced hydrolysis of the N-glycosylic bond in nucleotides (figure 5). AP-site are also formed as an intermediate in BER by glycosylases when removing a damaged base such as 8-oxoG and Tg. AP site are dangerous to cells as they can cause mutations and they can block DNA replication and transcription. AP-sites are processed and repaired by the BER pathway (44).

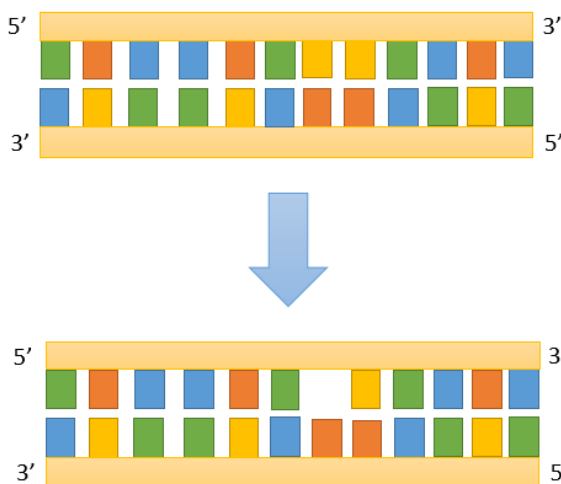


Figure 5: Apurinic/aprimidinic site in DNA. Schematic diagram shows an AP site in DNA with the colours showing the bases and DNA backbone in orange. A AP site is a location in DNA where there is no purine or pyrimidine base resulting from DNA damage and intermediates in DNA repair.

1.1.5.4 8-oxoG

8-oxoG is a common nucleotide modification in cells following oxidative stress from the cells environment or ionizing radiation and is used as a marker for oxidative stress (figure 6). It is a major source of mutagenesis caused by hydroxyl radicals which add a hydroxyl group to the base (4, 8). This lesion is found at higher amounts in animals that have a higher basal metabolism due to the increase in ROS production from normal metabolism. The presence of this lesion causes GC→TA transitions and if not repaired contributes to disease (45). 8-oxoG has been found to be increased in premature ageing, neurogenerative disease and cancer (8, 45).

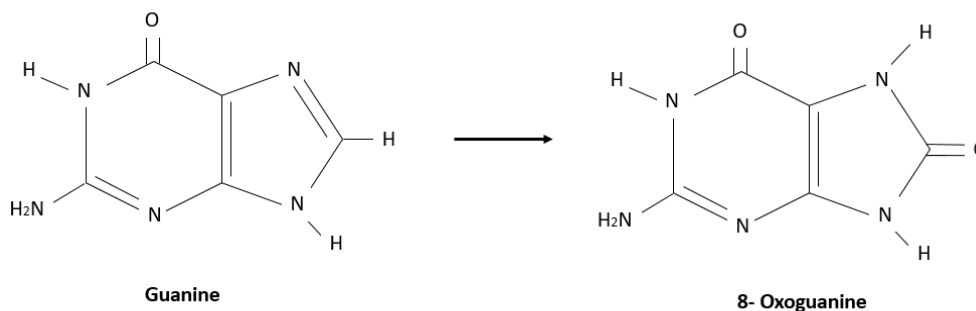


Figure 6: Molecular of Structure of 8-Oxoguanine. The molecular structure of G (left) and 8-oxoG (right) are shown. 8-oxoG is a major product of oxidation damage and the difference is found on the N8 where oxygen has been added.

1.1.5.5 Thymine Glycol

Thymine is the most prone to oxidation from sources such as oxidation stress and ionising radiation and Tg being the most stable product of thymine oxidation (figure 7). Tg can also form after hydrolytic deamination of 5-methylcytosine glycol which is unstable. It has been estimated that 400 Tg lesions occur per cell per day and is used as a marker for oxidative stress. Tg lesions can block DNA polymerases in replication and repair which is cytotoxic. Tg is not particularly mutagenic as it base pairs with adenine the majority of the time with only 0.3% T → C mutations arising as a result (46).

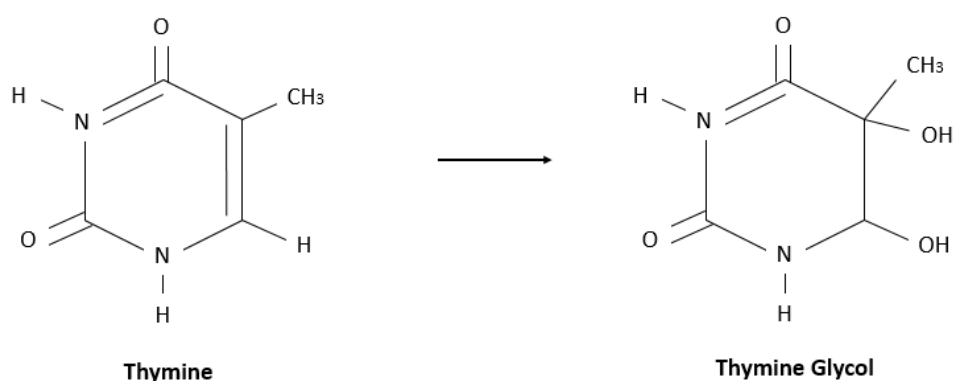


Figure 7; Molecular Structure of Thymine Glycol. The molecular structure of T (left) and Tg (right) are shown. Tg is a product of oxidative damage and difference lays on the N5 and N6 where oxidation is shown.

1.2 DNA Repair

Maintaining the genomic integrity of an organism is vital for survival, consequently a high fidelity systems are required for both DNA replication and for repairing the numerous lesions that occur every day to DNA. Damage that occurs to DNA in a cell can occur from heat, normal cellular metabolism, radiation from the environment. Damage to DNA can be as modest as a mispaired base or more complex, including chemical cross links or breaks in one or both of the phosphodiester backbones. The majority of spontaneous damage to DNA is temporary due to their instant rectification by a set of biological process which are mutually called DNA repair. There can be serious implications if these lesions are not repaired including cell death or transformation, blockage to DNA replication systems, or changes to the DNA sequence that might be passed onto upcoming generations and are therefore implicated in the development of several human diseases, including premature ageing, neurodegenerative diseases and cancer. There are range of DNA repair processes that have evolved to recognise and repair specific types of damage to restore DNA to its undamaged state. DSB repair, BER and nucleotide excision repair (NER) are the three major DNA repair pathways that are described below.

1.2.1 Double strand break repair

DSB are one of the most cytotoxic forms of DNA damage caused endogenously from cellular metabolism (ROS) and exogenously from ionising radiation for example. The repair of DSBs it imperative for the cells survival, if left unrepaired they can prompt apoptosis, genome rearrangement and initiate carcinogenesis (47, 48). Conversely DSBs are essential intermediates which can be beneficial for an organism when controlled in processes that require genome rearrangements, such as immune system development and genetic diversity in meiosis (47). To neutralise the harmful effects of DSBs two types of DSB repair pathways have been identified; non homologous end joining (NHEJ) and homologous recombination (HR). NHEJ is the simplest mechanism to repair DSBs and encompasses direct ligation of the broken ends of DNA using restricted or no sequence homology to re-join DNA ends and as a consequence is error prone. For HR the undamaged homologous sequence from the sister chromatid is required to act as a template to repair the two damaged strands ensuring accurate repair of the DSB. The choice of pathway is dependent on the structure of the broken DNA ends and what cell cycle phase the cell is in (47, 48). NHEJ is the predominant choice of repair pathway in humans due to the DSB substrate that is generated (ends in close proximity) and because it can be used at any point in the cell cycle. HR is only active during or just after DNA replication when the cell is in S and early G2 phases, as the sister chromatid is close to serve as a template, it is also able to bind to single strand DNA overhangs which NHEJ can inadequately accomplish (48).

1.2.1.1 Homologous Recombination

HR repairs DSBs by using genetic information from the sister chromatid or homologous chromosome, needing sequence homology to accurately repair constituents. HR is a major repair pathway for DSBs in prokaryotes and lower eukaryotes and functions infrequently in cells of higher eukaryotes (which use NHEJ predominantly) (49). HRs ability to maintain genome stability is demonstrated by the BRCA2 gene which is a tumour suppressor, and dysfunctional/mutated BRCA2 causes damaged DNA to not be repaired properly (50). HR events are complex and based on research in different organisms and biological circumstances and there are various models for precisely how it takes place (40).

A key step in HR is the introduction of a 3' single stranded DNA tails. The nucleolytic resection of DNA DSB acts as a control point for which DSB repair pathway and initiates HR. The effectiveness of this resection depends on the MRN complex of RAD50, MRE11 and NBS1. Following binding of the MRN complex to DSBs the MRE11 subunit initiates single strand end resection with the aid of CtIP to produce 3' DNA single stranded DNA overhangs. Both of the 3' single stranded DNA tails from DSB resection provide a substrate for RAD51 filaments (49). The 3' single stranded DNA tails are then coated in RPA protein which has a higher affinity for single strand DNA than RAD51. RPA stimulates HR by neutralising the secondary structure in single stranded DNA (50). RAD51 loading facilitated by breast cancer gene 1 (BRCA1) and breast cancer gene 2 (BRCA2). BRCA2-PALB2 complex recruits and interacts with RAD51 affecting its nuclear localisation and binding properties and allow RAD51 to arrange foci at DNA damage sites. BRCA1 is thought to assist in chromatin remodelling and so facilitating HR by making DSB more accessible (40). RAD51 then binds to 3' single stranded DNA overhangs to produce RAD51 filaments. HR is catalysed by the RAD51 protein. RAD52 which is activated by the binding of the p34 subunit of RPA is thought to modulate RAD51 actions through its interacting region and RAD52 action to induce (51). The RAD51 nucleoprotein filament interacts with an undamaged homologous duplex and catalyses strand exchange events in which one of the 3' single stranded DNA tails invaded the intact DNA duplex and generates a D loop structure by displacing one of the strands, RPA also binds to this strand of the D loop (40, 49, 50). The 3' ends then facilitates DNA synthesis using the undamaged DNA as template, the 3' end of the damage DNA molecule is extended by DNA polymerase I leading to the generation of two Holiday junctions (DNA crossovers). After migration along the DNA (branch migration) extending or shrinking the region of the heteroduplexed DNA the Holiday junctions are resolved by cleaving the crossed or non-crossed DNA strands by a resolvase and then ligated by DNA ligase I (40, 49). The HR pathway is summarised in figure 8.

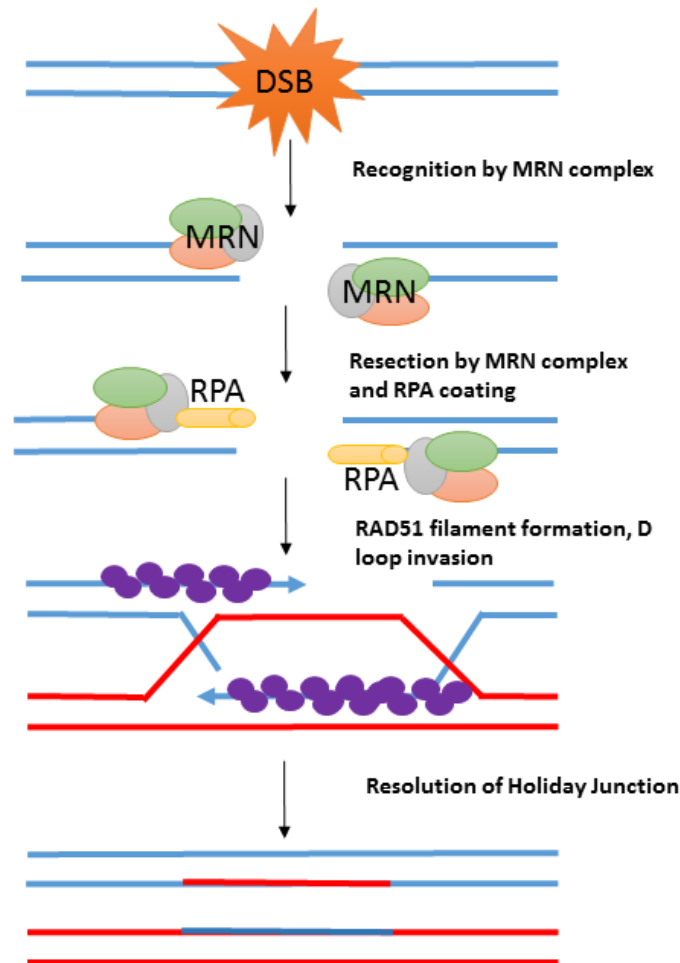


Figure 8: Homologous Recombination. Homologous recombination pathway. DSBs are recognised by the MRN complex which resects DNA to form 3' single strand overhangs which are coated by RPA. RPA is replaced by RAD51 and the RAD51 filament invades the sister chromatid to use a template for repair so form a D loop and then a holiday junction. After synthesis the holiday junctions are resolved, based on (40).

1.2.1.2 Non-homologous end-joining

NHEJ is a vital DNA repair pathway for the repair of DSB in eukaryotic cells. NHEJ repairs damages to DSBs in DNA caused from exogenous and endogenous sources. DSBs are also created deliberately in class switch recombination and V(D)J recombination for the development of B cells and T cells of which NHEJ plays an essential role. NHEJ does not need a homologous template for repair and can process DSB at any point in the cell cycle. It processes two termini of any type in a broken DNA molecule so they can be directly ligated. Consequently, this can lead to a loss of nucleotides and so comprise genomic integrity. The mechanism of NHEJ is broken down into several steps; the recognition and capture of the

broken end of DNA, bridging of the molecular ends to bring them back together and the religation of the broken DNA ends (52).

The initial step of NHEJ is the recognition and binding of the Ku heterodimer to the DSB. The heterodimer is made up of two proteins, Ku70 and Ku80 in a non-sequence dependent manner. Ku functions by creating an open ring structure that DNA is threaded onto. When Ku is bound to DNA it acts as a scaffold for the assembly of the other NHEJ proteins and attracts the DNA-dependent protein kinase catalytic subunit (DNA-PKcs) to the DSB forming DNA-PK holoenzyme (40, 53). DNA-PKcs is a member of the phosphatidylinositol-3 (PI-3) kinase-like kinases. The C-terminal domains of this kinase form a crown structure with the N-terminus of the protein to produce a pincer structure which modulates its ability to bind to DNA (52). Once bound, DNA-PKcs demonstrates serine / threonine kinase activity and its likely substrate involved in NHEJ is XRCC4 which it phosphorylates and facilitates NHEJ. It has been suggested that DNA-PKcs also helps to bridge the two broken DNA ends, preventing them from becoming degraded and helping to relax chromatin to enhance NHEJ efficiency (40). Ku directly recruits XRCC4-DNA ligase IV complex to the DNA and facilitates its loading onto DNA to stimulate DNA end ligation (40, 52). Figure 9 shows a simplified diagram of NHEJ.

The identity of the DNA polymerases that might be involved NHEJ at the moment is not clear (40). It has been proposed that when necessary (depending on the complexity of the DNA break being ligated) filling in the gaps in DNA is achieved by X-family of polymerases, including polymerases μ and γ . Pol μ can polymerase across a discontinuous template strand when in the presence of Ku and XRCC4/DNA ligase IV (52). The MRE11-RAD50-NBS1 complex is thought to play a role in NHEJ; the complex has exonuclease, endonuclease and DNA unwinding activity primarily when the broken DNA end require processing before ligation. There are also suggested candidates for this activity such MRE11 alone or other nucleases such as Artemis (40).

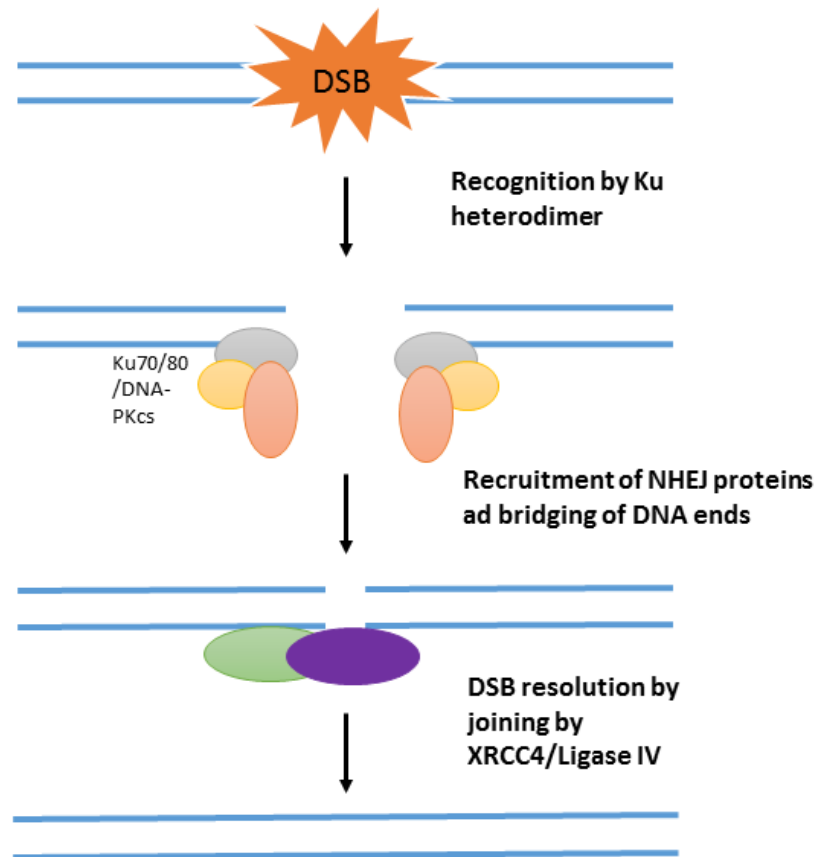


Figure 9: Non-homologous end joining pathway. Double strand breaks are recognised by Ku70 and Ku80 heterodimer and form a ring structure which is threaded onto DNA. Ku70/80 attracts DNA-PKcs to bridge the ends and phosphorylates XRCC4 to facilitate NHEJ. Ku recruits XRCC4-DNA ligase IV complex to DNA to stimulate DNA end ligation, based on (40).

1.2.2 Nucleotide excision repair

NER is the major DNA repair mechanism for bulky helix-distorting DNA lesions that occur through UV radiation, environmental mutagens and some chemotherapy drugs. NER can repair a large spectrum of DNA damages including 6-4 pyrimidine-pyrimidone photoproducts (6-4PPs), cyclobutane pyrimidine dimers (CPDs) which are formed from UV radiation, many bulky adducts, intrastrand cross links by drugs like cisplatin and cyclopurines generated from ROS (54, 55). There are two forms of DNA damage detection by NER; global genome NER (GG-NER) and transcription-coupled NER (TC-NER). GG-NER as the name suggests repairs the global genome with varying efficiencies and TC-NER indirectly detects lesions through its ability to detect the blockage of transcription elongation such as CPDs which are poorly recognised by GG-NER but interfere with transcription elongation (54, 56). Defective GG-NER can promote carcinogenesis, alternatively defective TC-NER can lead to a range of diseases,

including xeroderma pigmentosum (XP) an extreme sensitivity to sunlight and serious premature ageing such as Cockayne syndrome (54).

1.2.2.1 GG-NER Recognition

The initial step in NER is the recognition of lesions. In GG-NER the whole genome is surveyed for helix distortions or structural changes which are recognised by XPC. XPC is stabilised upon binding with the assistance of RAD23B and centrin 2 (CENT2) (54, 56). XPC is able to bind to a range of bulky lesions. This is due to the ability of XPC to bind to the undamaged strand of DNA opposite the lesion which is distorted in structure displaying a more single stranded DNA character due to the thermodynamic destabilisation by the lesion. RAD23B dissociates from XPC upon binding to DNA suggesting it aids in the stability of XPC and the delivery of XPC to damaged sites. CENT2 stimulates NER activity, the exact role of the protein however remains unknown (55). Certain lesions such as CPD are weak substrates for XPC due to the DNA helix only being mildly destabilised. To repair these types of lesions the ultraviolet radiation DNA damage binding protein (UV-DDB) complex is employed. The complex comprises of DDB1 and DDB2 which are part of the Cullin (CUL)4-regulator of cullins (ROC) ubiquitin ligase complex which ubiquitinates DDB2, XPC (increasing its affinity to DNA damage) and histones which are required for efficient NER. Histone removal allows XPC recognition to occur. DDB2 binds to these lesions to distort lesions into its binding pocket to create single stranded DNA to facilitate XPC binding. Binding of XPC recruits the transcription initiation factor IIH (TFIIH) complex to the lesion by direct interaction with XPC-RAD23B (54-56).

1.2.2.2 TC-NER Recognition

The TC-NER indirectly recognises DNA lesions through the blocking of transcription elongation. The initial step in TC-NER is the stalled RNA polymerase II (RNAPII) which causes the recruitment of Cockayne syndrome protein B (CSB) and Cockayne syndrome WD repeat protein A (CSA). CSB binds to RNAPII when blocked by a lesion and wraps the DNA around itself, translocating RNAPII, figure 10 (54-56). CSB can then recruit the CSA complex, core NER factors (excluding UV-DDB and XPC) and several TC-NER specific factors, and p300 to blocked sites. CSB also recruits UV stimulated scaffold protein A (UVSSA) and its partner ubiquitin specific processing protease 7 (USP7) which bind to RNAPII after arrest. USP7 then deubiquitinates CSB for stabilisation and together UVSSA and USP7 prevent the degradation of CSB (54). TFIIH which is a transcription elongation factor is required for the recovery of RNA synthesis after DNA damaged and is recruited by CSA. The next steps of repair are achieved by XPE and the XPC complex in GG-NER pathway (56).

Figure from (47), Figure 2a

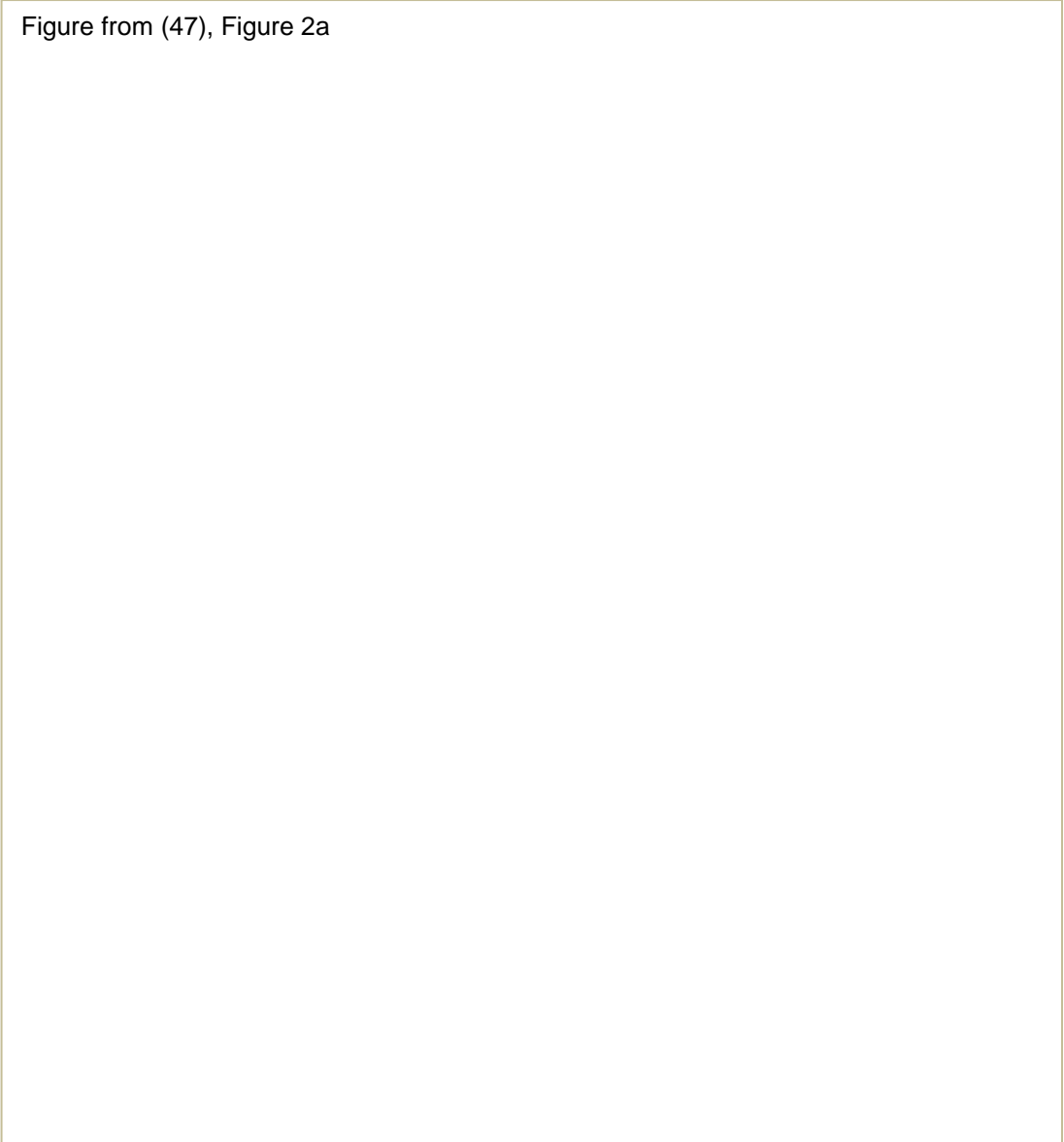


Figure 10: Nucleotide excision Repair. Diagram showing recognition by GG- NER (Left arm) and TC-NER (right arm) recognition. Recognition occurs by the XPC/HHR23B (RAD23B homolog) in GG-NER or RNA polymerase, CSA and CSB proteins in TC-NER. DNA is opened around the lesion by RPA, XPA and the helicase subunits of TFIIH, XPB/XPD allows incision of DNA to take place either side of the lesion by ERCC1/XPF and XPG removing the damage and the gap is then filled by DNA synthesis, image from (57).

1.2.2.3 Incision, excision, gap filling and ligation

The TC and GG recognition sub pathways of NER unite at the point that the TFIIH complex is recruited to the damaged site (figure 10) of 10 proteins, two of these are bidirectional adenosine triphosphatases (ATPases)/helicases called XPB and XPD which

unwind the DNA to allow for open DNA conformation around the lesion. The ATPase activity of XPD is used for the recruitment of the TFIIH complex to the DNA damage site. XPD is critical for the 5'-3' unwinding of DNA to create a 20 – 30 nucleotide bubble (54, 56). There are other constituents of TFIIH also contribute to NER these include, p8, p52 which simulate XPD and p44 which then stimulates XPD. Once the pre-incision complex is assembled around the lesion XPD, RPA and XPG are employed for their dual (5'-3') strand incision of the lesion. XPD binds to the DNA by the 5' end and recruits ERCC1-XPF which has endonuclease activity and RPA protects the single stranded DNA on the opposite side to lesion from degradation. XPG interact with TFIIH for structural support and its endonuclease activity is triggered once ERCC1-XPF has been recruited (54-56). The lesion excision is catalysed by XPG and ERCC1-XPF which leaves a single stranded gap of 22-30 nucleotides. The DNA replication complex Pol $\delta/\epsilon/\kappa$ – PCNA-RFC-RPA is recruited by XPD to synthesis a patch of DNA to replace the damaged excised strand. XRCC1-DNA ligase III α complex is the employed to seal the gap in DNA to leave (usually) a repaired strand of DNA (54, 56).

1.2.3 Base excision repair

Around 10,000 DNA base lesions are thought to occur in every cell per day from endogenous (particularly ROS) and exogenous sources. These types of small base damages are commonly the result from oxidation, hydrolysis, methylation or deamination (4). These can lead to DNA base damages including AP sites, alkylated and oxidative base (e.g. 8-oxoG and Tg), SSB and misincorporated bases. The BER pathway is a highly conserved DNA repair process and is essential to repair the majority of spontaneous endogenous DNA damages to maintain genome integrity. These type of lesions to DNA can cause alteration of the specific base pairing in DNA causing genomic instability, promoting diseases such as cancer, premature ageing and neurodegenerative disorders. The steps and enzymes involved in BER are well defined and can be divided into five distinct steps; 1. Recognition and removal of the damaged/misincorporated base, 2. AP site incision, 3. Removal of sugar moiety 4. Gap filling with the correct undamaged nucleotide, 5. Sealing of the remaining nick. Once BER has been initiated repair can take place either by short patch repair or long patch repair figure 11. A single nucleotide gap is generated and filled during short patch repair and in long patch a gap of 2 to 10bp is created and filled. Short patch repair is the dominant pathway in BER, long patch is used after AP-site incision if the 5' end of the damage site DNA is resistant to end processing (58, 59).

Figure from (59), Figure 1

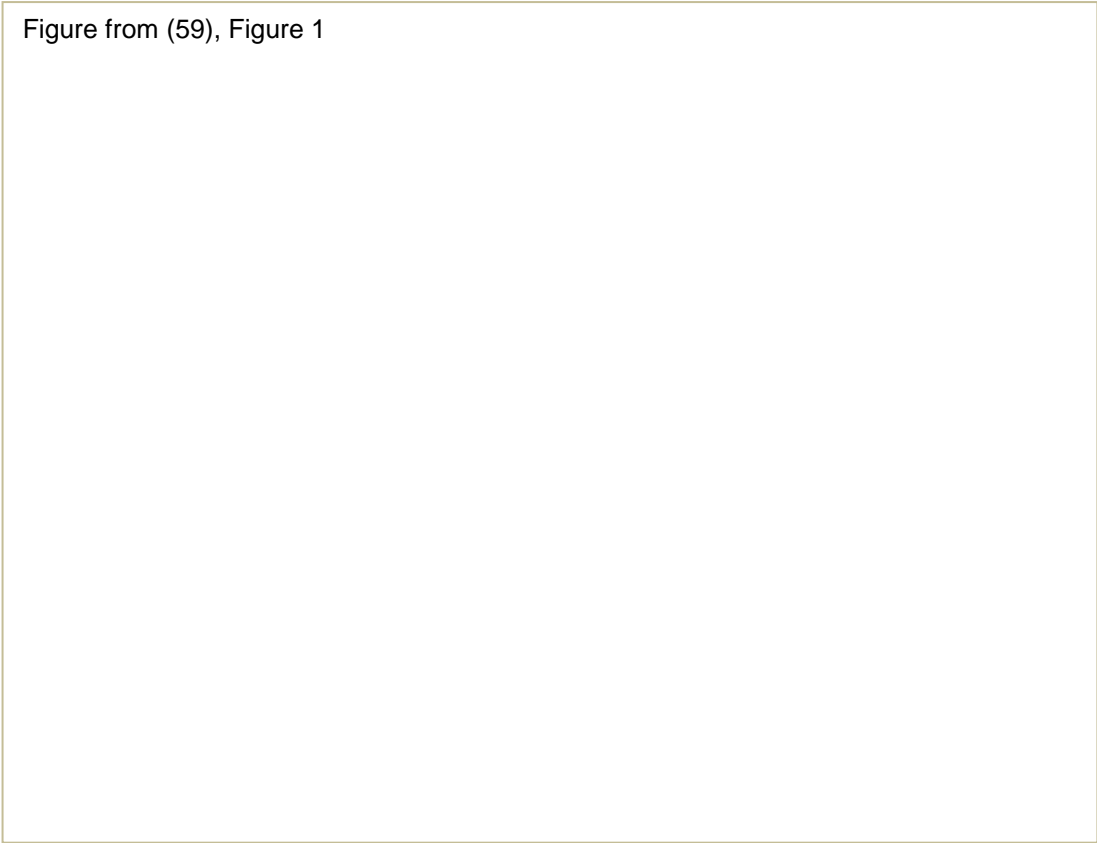


Figure 11: The Base Excision Repair Pathway. Figure depicting the schematic pathway of BER was taken from Parsons and Dianov (59). A DNA-specific glycosylase recognises and removes the damaged base to produce an AP site which is then incised by APE1 leaving a blocking 5'-deoxyribose phosphate residue. Following the left path of short patch repair at this point Pol β removes this blocking residue through its lyse activity and fills the gap with the correct base, XRCC1-LigIII α then seals the nick. If there are non-conventional DNA ends after APE1 incision which are resistant to Pol β activity, then BER goes through to long patch repair as shown on the right. Pol δ/ϵ then synthesises from 2 to 8 bases in the repair gap to form a 5'-flap which is removed by FEN1 which is facilitated by PCNA, Lig I then seals the remaining nick.

1.2.3.1 Base Removal

The first enzymatic step in BER is conducted by a specific DNA glycosylase which are responsible for the search of DNA lesions and catalysis of the cleavage of the N-glycosidic bond between the damaged base and 2'deoxyribose forming a AP-site, an activity universal to all classes of DNA glycosylases. It has been suggested that glycosylases seek out lesions by sliding and distributive interactions by gently pinching DNA in a bidirectional and random manner (60). Upon damage recognition the glycosylase bends DNA so the damaged base is rotated around the phosphodiester backbone axis to 180° at the damage site to produce a broadened and flattened minor groove, promoting the damaged base to flip

out from the double helix into the binding site of the DNA glycosylase for surveying and protein-substrate complex formation. This interaction is stabilised by specific amino acids in the DNA glycosylase and DNA (58, 61, 62). This mechanism is known 'base flipping' common in all glycosylases and is required as the active site of glycosylases can only interact with extrahelical bases (58). There are 11 distinct DNA glycosylases which recognise particular types of base damage or DNA lesions which can be divided into four structural families; uracil DNA glycosylases (UNGs), helix-hairpin-helix (HhH) glycosylases, endonuclease VIII-like (NEIL) glycosylases and methylpurine DNA glycosylases, table 1 summaries the human DNA glycosylases (62). DNA glycosylases are classified as either monofunctional or bifunctional dependent on their catalytic mechanism and AP lyse strand incision ability, see table 1.

Monofunctional glycosylases have glycosylase activity only (table 1), and so removes the damaged base by cleaving the N-glycosidic bond to create an AP-site which is then processed by APE1. They do this by utilising a water molecule to act as a nucleophile to assault the C aromatic ring of the damaged base which promotes its release and so create a AP-site, which is the same as AP-site created from depurination or depyrimidination by ROS (58).

Bifunctional glycosylases have both glycosylase and β -lyase or β , δ -lyase activity (table 1 for examples). They are able to remove the damaged base and incise the AP-site to create a single strand break. These types of DNA glycosylases have an amine moiety active site which acts as a nucleophile to remove the damaged base. The AP-site is then incised by the glycosylase between the 3' phosphodiester linkage to AP-site to create single strand break with a blocking irregular residue at the 3' of the single nucleotide gap. These irregular residues can either be phosphor- α,β -unsaturated aldehyde (created through β -elimination) or a phosphate group produced by two sequential elimination stages, β , δ -elimination. These 3' blocking residues need to be further processed by specific enzymes AP endonuclease 1 (APE1) and polynucleotide kinase 3'-phosphatase (PNKP) respectively to become an acceptable DNA substrate for Pol β (58, 60, 61).

Glycosylase	Mono (M) / bi (B) functional	AP Lyase activity	Damaged base type
UNG	M	No	Deaminated base
TDG	M	No	Deaminated base
SMUG1	M	No	Deaminated base
MBD4	M	No	Deaminated base
AAG/MPG	M	No	Alkylated base
MYH	M	Yes (β) / No	Oxidised base
OGG1	M/B	Yes (β)	Oxidised base
NTH1	B	Yes (β)	Oxidised base
NEIL1	B	Yes (β , δ)	Oxidised base
NEIL2	B	Yes (β , δ)	Oxidised base
NEIL3	M/B	Yes (β , δ)	Oxidised base

Table 1: Human DNA Glycosylases. List of the human DNA glycosylases their mono or bi-functional activity, AP lyase activity and damaged base type, based on tables in (58, 61).

1.2.3.2 AP Site Incision

Once the damaged base has been removed by a DNA glycosylase, APE1 incises the DNA backbone 5'- to the AP site to produce a single strand break with a 3'- hydroxyl group (59). APE1 is the primary AP endonuclease in mammalian cells contributing to approximately 95% total AP site incision (63). APE1 incises the DNA phosphodiester bond through a catalysed

acid-base reaction which is promoted through the binding of a magnesium ion (Mg^{2+}) which stabilises the increasing charge on the oxygen atom in the phosphate group and positioning them for nucleophilic attack from aspartate-activated hydroxyl radical (44, 64). There are many amino acid interactions that take place that allow APE1 activity and selectivity towards AP-sites. When APE1 is bound to DNA it bends the DNA to approximately 35° and the helical axis kinked to roughly 5\AA . APE1 causes this kinking by residues from four loops and one α helix, at the 5'- end of the AP site arginine (R) 73, alanine (A) 74 and Lysine (K) 78 interact with DNA phosphate on the opposite strand, and tyrosine (Y) 128 and glycine (G) 127 cross and widened the minor groove forcing the AP site into the active site of APE1. The catalysis of APE1 is facilitated through Asparagine (N) 283- histidine (H) 309 and water (44). The amino acid pair N283-H309 form a hydrogen bond which has been suggested to facilitate the H residue to act as a base and accept a proton from water which helps to protonation of N210 to generate a hydroxyl nucleophile (44, 64, 65). The 3'- phosphate group of the AP site forms a hydrogen with R177 which penetrates the major groove for stabilisation and so slows APE1 dissociation from incised DNA. The observation that mutant R177A increased APE1 activity by 25%, it was concluded that enzymes in the BER pathway have evolved so rather than having maximum activity and so produces many toxic intermediates, the enzymes remain associated with intermediate to facilitate the next protein in the pathway (64). The cellular levels and activity of APE1 are closely regulated with the level of other downstream BER proteins to avoid the production of toxic single strand breaks which can cause blockage of DNA replication forks causing collapse and so producing even more toxic DSBs (59). The enzyme also processes the 3'- to 5'- exonuclease activity which has been postulated to serve as a proofreading mechanism during the synthesis step of BER, removing mismatches or damaged nucleotides (66).

1.2.3.3 PARP1 and single strand break repair

Following APE1 incision of the AP site it has shown that PARP1 binds to incised AP sites due to its high affinity to DNA single strand breaks. PARP1 is considered to be fundamental in BER in acute DNA damage (67, 68). PARP1 has been shown to control repair capacity through binding to extensive single strand breaks, regulating the access of other repair proteins (Pol β and X-ray repair cross-complementing protein 1 (XRCC1) - DNA lig III α) when they are at adequate levels (68). Single strand break repair is considered a sub-pathway of BER. Single strand breaks are recognised by PARP1, a nick sensor and repaired by later stage BER proteins; Pol β , Lig III α , and XRCC1. PARP1 recruits XRCC1 to single strand breaks and together they stabilise the single strand break whilst the DNA ends are processed so gap filling synthesis and nick ligation can take place (42, 69). Single strand breaks often hold unconventional DNA ends that cannot be processed for complete repair and so need to be processed before repair can take place. Single strand breaks can be generated directly through ROS or ionising radiation or indirectly e.g. BER intermediates. DNA single strand

breaks with modified 5'- and/or 3'- ends are often produced from endogenous sources such as oxidative metabolism (ROS), exogenous agents (eg. IR) or indirectly through processes such as BER intermediates. These types of single strand breaks can have 3'- phosphate or phosphoglycolate ends (oxidised 1' and 4' C respectively). Unconventional 3'- residues can also result from abortive DNA TOP1 activity which forms single strand breaks and briefly remains attached to the 3'- end, however in the presence of DNA lesions it can remain attached to the 3'- end. These ends block DNA polymerases and need to be processed before DNA repair can take place (42, 70). APE1 and PNKP, as mentioned previously, remove some of these unconventional 3'- ends. PNKP has been shown to interact with XRCC1, Pol β and Lig III α , and furthermore promotes recruitment of XRCC1-Lig III α complex to single strand breaks (70). PNKP is responsible for processing 5' end of the blocked TOP1 intermediate single strand breaks by its 5' kinase activity (42). Tyrosyl-DNA phosphodiesterase 1 (TDP1) can also process 3'- phosphoglycolate ends however at much lesser extent than APE1 (71). Aprataxin which interacts with XRCC1 has been found to be associated with abortive DNA ligation intermediates by releasing the 5'- adenylate groups to complete repair (70).

1.2.3.4 End Processing

There are a variety of nonconventional 5'- or 3'- blocking residues from the results of bifunctional glycosylases, strand break intermediates, APE1, ionising radiation or ROS. These residues hinder the extension by DNA polymerases and nick ligation in downstream BER processes and must be processed to allow for efficient repair. Examples of these blocking residues are 5'-deoxyribosephosphate, 3'-phosphate, 3'-phosphoglycolate and 3'-phosphor- α,β -unsaturated aldehyde residues (72). Pol β is primarily involved in the removal of 5'- deoxyribosephosphate through its dRP lyase activity to produce the required 5'-phosphate needed to for nick sealing. DNA Pol λ and ι also have this lyase activity and can remove this type of blocking residue (73, 74).

APE1 also has 3'-phosphodiesterase activity and very weak 3'-phosphatase ability to remove 3'- blocking moieties such as those produced by bifunctional glycosylases (phosphor- α , β -unsaturated aldehydes) and 3'-phosphoglycolate, ROS from normal cellular metabolism and IR to produce a 3'-hydroxyl group (59). Blocking 3'-phosphate groups are mostly processed by PNKP as APE1 phosphatase activity is very weak. PNKP is bifunctional as it has both a 5'- kinase and 3'-phosphatase domain. It is able to hydrolyse the 3' phosphate group to produce a 3' hydroxyl terminus and it's 5'-kinase activity prepares the nick for ligation by phosphorylation of the 5'- hydroxyl to 5'- phosphate (75).

1.2.3.5 Gap Filling

To fill the gap during BER cells use polymerases to initiate repair synthesis to insert the correct nucleotide, they require at 3'-hydroxyl terminus and an undamaged template so the correct nucleotide can be added. Replicative polymerases harbour 3'- to 5'-exonuclease activity which is used for proofreading and can remove the incorrect or damaged nucleotide straight after phosphodiester bond formation (76). In BER there are considered to be four polymerases that act in different sub-pathways, DNA Pol β , δ , ϵ and λ . Pol β is the primary polymerase in short patch BER to add the correct nucleotide, however it lacks 3'- to 5'-endonuclease activity. Pol β is a small 39 kDa protein with 2 domains, an 8 kDa amino-terminal domain for dRp lyase and DNA binding activity and a 31 kDa C-terminal domain for DNA polymerisation. It also contains subdomains (thumb, fingers and palm) which facilitate catalysis (77, 78). Pol β is recruited to the gap site by interaction with APE1, PARP1 or XRCC1 to a DNA single strand break (79, 80). Pol β requires a bend of 90° in the single strand DNA template at the gap site by its 31 kDa domain and stabilised by its 8 kDa domain is needed for Pol β function and may increase nucleotide selectivity in DNA repair (78). Pol β also plays a role in long patch BER by incorporating the first nucleotide into the gap and so starting this subpathway of BER (77). Pol λ can act as a back-up polymerase for Pol β in some circumstances, and has been suggested to be activated in Pol β deficient mouse embryonic fibroblast extracts, however it is significantly less efficient at binding to nicked DNA (81).

The choice between either short patch or long patch BER can be determined by the type of originating lesion. When Pol β cannot remove the 5'-deoxyribose as the moiety is reduced or oxidised, such as the C1' oxidised AP site lesion 2-deoxyribonolactone, as they are resistant to Pol β lyase activity and must be processed by long patch BER which Pol β initiates by adding the first nucleotide (82, 83). The cellular adenosine triphosphate (ATP) concentration after 5'-deoxyribose removal can also in part determine whether to proceed to long patch or short patch BER. When ATP concentration is high the repair pathway is more probable to go straight to short patch repair so ligation by DNA Lig III α . However when the ATP concentration is low long patch repair is more commonly seen as ligation is unfavourable (84). Long patch BER integrates 2-8 bp during the synthesis step conducted by Pol δ and Pol ϵ with PCNA. These two polymerases use strand displacement to synthesise a short nucleotide sequence at the 5'-DNA termini creating a flap intermediate. The displaced newly synthesised strand is then removed by FEN1 with PCNA to create a DNA substrate which can then be ligated (59, 85). Uncommonly, Pol η , Pol ι and Pol κ which are error prone translesion DNA polymerases, can be used in BER to fill the gap leading to the formation of a Schiff base complex with the 5'-deoxyribose moiety which is a blocking residue and prevents nucleotide incorporation (72, 86).

1.2.3.6 Nick Sealing

The concluding step in BER is to seal the remaining nick to complete repair. Ligases catalyses a phosphodiester bond between the 3'-hydroxyl and 5'-phosphate groups, by using energy from phosphoanhydride hydrolysis using ATP or nicotinamide adenine dinucleotide (NAD⁺) (87). Long patch BER is completed by Lig I and short patch BER is completed by predominantly LigIII α with its scaffolding protein XRCC1, catalyzing the nick sealing of the DNA backbone (59, 88, 89). XRCC1 is required for the stability of DNA Lig III α and forms a stable complex as seen in XRCC1 deficient cells which have reduced levels of DNA Lig III α causing a deficiency in repair of single strand breaks and increased sensitivity to DNA modifying agents (69, 90, 91). Pol β has been suggested to enhance the recruitment of DNA Lig III α -XRCC1 complex through an interaction with XRCC1, indeed the presence of this complex has been shown to increase the activity of Pol β and overall repair which indicates that the interaction between Pol β and XRCC1-Lig III α is an essential for proficient repair conclusion (92-94).

1.2.3.7 Base excision repair and Cancer

BER is a critical pathway for the preservation of genome integrity, which is achieved through the processing of DNA base damage and the coordination of each step by the balance of the enzymatic activities, both of which are vital for genome integrity and complete repair (95). It has long been recognised that defects in DNA repair and consequently increased genome instability are linked to cancer susceptibility. An example of this is the oxidative lesion 8-oxoG that BER processes has been found in tumour DNA and urine from patients with an array of malignancies (5). Currently there is increasing evidence which suggests that cancer cells typically either display defects in a DNA repair process (at least one pathway) or have increased expression of DNA lesions that are caused by a mutant endogenous source (96). In humans DNA repair pathways play a pivotal role in the protection from cancer, this is emphasised through the accumulating evidence for the predisposition towards hereditary cancers by germ-line mutations in DNA repair genes (97). In BER the connection between defective repair and cancer risk is known through the germ-line line biallelic mutation in the *MUTYH* gene that encodes for a DNA glycosylase MYH that is involved in the repair of oxidative lesion (5, 97). This mutation causes a predisposition to a rare hereditary form of colorectal cancer (97). In the normal human population there are above 100 germ-line single nucleotide polymorphisms in numerous BER proteins including DNA glycosylases, APE1, XRCC1 and Pol β that are anticipated to change the amino acid sequence of the protein (98). Somatic variants (single nucleotide polymorphisms) of BER proteins are also found in sporadic cancers, the majority of which are heterozygous suggesting either a dominant phenotype or as BER is highly coordinated small alterations could cause genome instability. Variants of these proteins cause aberrant BER which if joined with continuous DNA damage over time

could produce a mutant phenotype (97, 98). Variants of Pol β are found in approximately 30% of tumours which are not in the germ-line (97-99). Somatic mutations of Pol β have been found in a number of cancers including gastric, colorectal, prostate, lung, bladder, breast, and oesophageal (100). The majority of the somatic mutations observed are point mutants and these mutations may only slightly modify the folding of Pol β causing an aberrant phenotype (98). It has been suggested that Pol β variants may cause mutations during the gap filling step in BER reducing its fidelity such as the K289 methionine (M) and Isoleucine (I)260M variants and so increasing genomic instability. In both cases this can lead to DNA repair synthesis errors as the fidelity of BER is dependent on the polymerisation stage, this may cause imbalances in BER that can lead to a mutator phenotype (5, 77, 99).

There is also accumulating evidence for frequent BER enzymes misregulation in various cancers. There are a number of cases of glycosylase overexpression in cancer cells which has been suggested to lead to drug resistance (96). Down regulation of OGG1 has been implicated in cancer, for example Head and neck squamous cell carcinomas and overexpressed in various other cancers (101). PARP1 also has been found to be over expressed in some cancer including colon adenoma and carcinoma. APE1 is overexpressed in ovarian cancer which promotes the cancer progression (102). High XRCC1 expression in head and neck squamous carcinoma is an indicator of poor survival (103). Recently Pol β has been found to be overexpressed at mRNA and protein levels in a third of tumour types examined in a study, particularly in the ovary, prostate and uterus (104). This highlights the possibility of potentially targeting these proteins for cancer therapy.

1.3 Chromatin Formation and Dynamics

Nearly all DNA in a cell is contained within the nucleus. The double helices of all 46 chromosomes in human cells if laid out in a line would be approximately 2 meters long. To fit this amount of DNA in an around 6µm diameter nucleus, the DNA must be packaged tightly in a co-ordinated structure. This is called chromatin which is generated from an array of loops and coils by specialised proteins. Despite this compaction of DNA, chromatin is arranged and regulated in a way to still make it accessible to protein for biological processes such as DNA transcription, replication and repair. In eukaryotes proteins that bind to DNA to shape chromosomes are defined as two classifications; histones and non-histone chromosomal proteins and together form chromatin. The nucleosome, which is a protein-DNA complex, represents the rudimentary form of chromosome packing and from nucleosome arrays, with sequences of DNA linking each nucleosome. These are further compacted one on top of the other to condense DNA further to form a chromatin fibre. Chromatin not only compacts DNA into a small volume it also serves to protect DNA from damage, control gene expression and strengthen DNA to allow for mitosis or meiosis when entering anaphase. Tightly packed chromatin is termed heterochromatin and encompasses a small number of genes that are (the majority of the time) turned off by this compaction. A gene that is frequently expressed is typically located in euchromatin which is situated in a relaxed area of chromatin. Nucleosomes and chromatin are dynamic, relaxing of the DNA-proteins contacts are required for biological processes so proteins can access the DNA sequence to accommodate the needs of the cell.

1.3.1 Overview of chromatin Structure and Dynamics

In human cells nucleosomes are comprised of two copies of the four core histone proteins H3, H4, H2A and H2B forming a histone octamer, which 147bp genomic DNA is wrapped around to form the nucleosome core particle and are further processed into densely packed chromatin (figure 12). The nucleosome is a fundamental component of chromatin and formed with newly replicated or repaired DNA. This is initiated with the wrapping of DNA around the H3-H4 tetramer and followed by the inclusion of two H2A-H2B dimers that help with the organisation of the outer wraps of the nucleosomal DNA. Positively charged residues in the histone core interact with the phosphate backbone of DNA in the minor groove at regular 10bp intervals on each adjacent pseudo two fold axis of symmetry called the dyad axis, (figure 13) (16, 105). This provides 14 relatively weak histone-DNA interactions, however all together provide positional stability in the nucleosome. Nucleosomes are connected by short segments of DNA (linker DNA) and form linear 10nm beads-on-a-string like structures termed nucleosome arrays which are packed together to form secondary structure of the 30nm chromatin fibre and other more highly ordered tertiary structures (figure 13; (105, 106)). The

N-terminal tails of histones contain K residues that protrude out from the nucleosome which can be modified through epigenetic post-translational modifications (PTMs); phosphorylation, ubiquitination, acetylation, methylation, SUMOylation and PARylation by a multitude of different specific enzymes with different biological outcomes and over 100 have been identified. This varies chromatin composition and can recruit specific chromatin complexes that are able to alter chromatin function (106, 107). Histone variants which have differences in their amino acid sequence also regulate chromatin organisation, these variants differ in expression throughout the cell cycle and localisation in chromatin and are escorted in and out of chromatin by specific histone chaperones. Mostly, histone variants have been identified for H2A and H3, the histone variants are highly conserved between species suggesting that they accomplish function that cannot be by their non-variant counterparts which has been shown with H2A.Z in processes such as transcription (107). Chromatin arrangement is also controlled by ATP-dependent chromatin remodelling complexes, these are large multi-subunit complexes built around a catalytic ATPase domain. Chromatin-remodelling complexes and PTMs can alter the interaction between nucleosomes and recruit chromatin-binding proteins (106). The packaging of DNA into chromatin limits access to DNA for transcription, replication and repair, a change in the structure is required to allow factors that facilitate these activities to bind. This is thought to occur through PTMs of histone N-terminal tails or the recruitment of chromatin remodelling complexes causing chromatin condensation (108).

Figure from (106), Figure 1

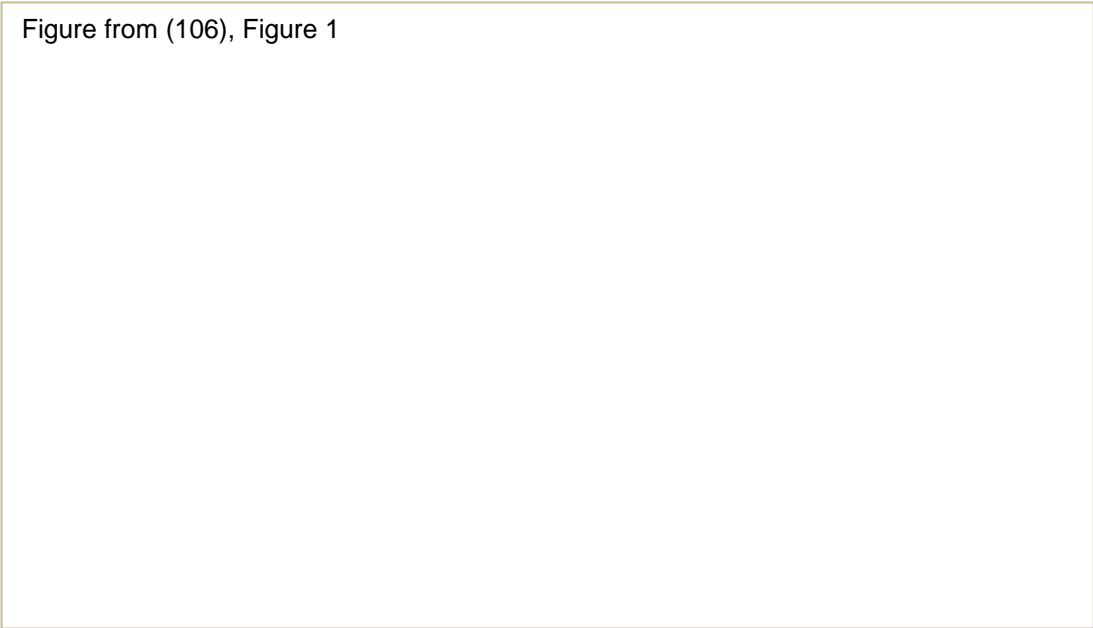


Figure 12; The Primary, Secondary and Tertiary Structure that form Chromatin. Image taken from K.Luger *et al* (106). The primary structure of chromatin is shown at the top which is a nucleosome array containing canonical histones (light blue and yellow) and histone variants (green, purple and light blue) and all these types of histones vary in the number and type of post-translational modifications they endure. Nucleosome – nucleosome interaction form chromatin fibres (bottom left) and fibre-fibre (bottom right), the secondary and tertiary structures of chromatin respectively. The chromatin fibre on both levels of folding is dependent on the primary structure of chromatin (PTMs and histone variants). The secondary and tertiary structure of chromatin is stabilised by architectural protein (orange triangle). These three states are transitional, indicated to by the arrows by chromatin remodelling factors, histone exchange and PTMs.

Figure from (109), Figure 1

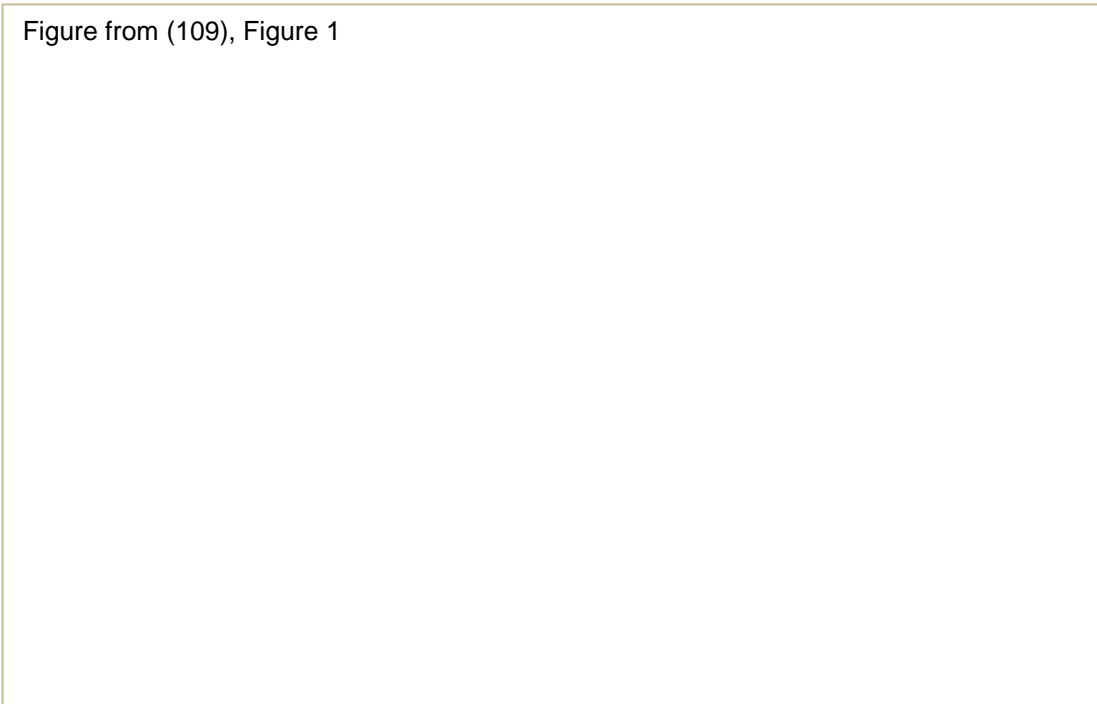


Figure 13; The Nucleosome Core Particle. Image taken from Luger *et al* (109) detailing the first structure of the nucleosome with detailed interactions of DNA and histones to near atomic level. Ribbon colour brown and turquoise from the backbone of 147bp DNA and the 8 histones which make up the histone octamer; green H4, blue H3, yellow H2A and red H2B. Image shows the view down the DNA super helix and vertical to it in the right image. The 2-fold axis of symmetry (dyad axis) is associated vertically with DNA at the top in each image.

1.3.1.1 Nucleosome structure

Each of the canonical histones H2A, H2B, H3 and H4 (major type histones) are highly positively charged have structural similarities, they share a structural domain called the histone fold that comprises on 3 α helices; $\alpha 1$, $\alpha 2$ and $\alpha 3$, which are divided using 2 loops; L1 and L2. This domain is required for the heterodimerisation. Each of these form a motif which is termed a 'handshake' leading to the two loops coming close together which are essential for histone to DNA interaction. The 4 helix bundle then allows for dimerization of the histone pairs. In H3 the α -helices allow for the H3-H4 histone pair to come together which forms (H3 and H4)₂ tetramers, the central tetrameric axis of the histone octamer (109). A similar 4 helix bundle is formed with H2B and H4 with both copies and so forms the ordered histone octamer. H3 – H4 in the octamer are very stable whereas H2A – H2B can be removed or exchange more easily (110, 111). The 147bp DNA then forms a tight left handed superhelix approximately 1.65 times around the histone octamer to form the nucleosome, (Figure 13, (109)). This histone octamer is stabilised by numerous protein, electrostatic interactions and hydrogen bonds between DNA and the histone proteins. Interactions with DNA and histones

are predominately in the structured areas the nucleosome, the histone tails which stretch away from DNA are more involved in interaction with other nucleosomes and are the site of most PTMs (112-116).

1.3.1.2 Histone Variants

Histone protein variants are encoded by genes distinct from their major type equivalent. Variant histones are exchanged into nucleosomes by DNA replication independent pathways through ATP chromatin remodelling, PTMs and histone chaperones, and are expressed at all phases in the cell cycle contrasting to the major type histones. Variants for H2A and H3 are the most common and are very conserved which suggests they are needed for certain functions that the major histone type cannot achieve (114, 117).

The variant histone H3.3 has a five amino acid difference to its major type, however this does not have a significant effect on the nucleosome structure (118). These amino acids are involved in the localisation of histone H3.3 by histone chaperones that bind to them (113, 119). H3.3 contains areas of DNA for gene promoters, enhancers and gene bodies (120, 121). Exchange of H3.3 has been suggested to expose these areas transiently to allow transcription factors to bind and function (122). Exchange of H3.3 with gene bodies is linked to an increase in transcription suggesting that this exchange is regulated by Pol II and other associated factors (123).

H2A.Z is highly conserved between species and is expressed with H2A, its major type, in all organisms. H2A.Z has numerous amino acid variations but has little effect on the overall structure of the nucleosome (124). There are minor structural changes to the nucleosome which alters its stability by affecting the interactions between the H2A.Z – H2B dimers due to the steric interference of the L1 loops laying at opposed ends of the dyad axis and (H3 – H4)₂ (125). This instability of the nucleosome helps with transcription initiation, DNA repair and chromosomal domain segregation and this variant is usually found in promotor regions (126).

1.3.1.3 Nucleosome stability and alternative structures

Chemical alterations of nucleosome components can affect the overall stability of a nucleosome through disrupting protein – protein and protein – DNA interactions but without altering the structure (127). Thermal denaturation of the nucleosome with nuclease accessibility and electron microscopy investigation have revealed that DNA that is towards the edges of the nucleosome are more susceptible to dissociation from the histone octamer than DNA in the histone core (128). The use of restriction enzyme analysis on incision target sites of nucleosomal DNA found that these enzymes could partially cleave DNA in proportion with

the distance of the target site and dyad axis i.e. target sites further away were cleaved at higher rates than ones closer to the dyad axis. It was thought that DNA on the nucleosome edge experiences spontaneous unwrapping and rewinding, this was also seen *in vivo* by DNA footprinting and transcription studies and allows the binding of transcription factors (129, 130). Fluorescence resonance energy transfer (FRET) have shown that DNA unwrapping occur a number of times a second and can last for approximately 25mS (131). Spontaneous unwrapping and wrapping of nucleosomal DNA has associations on the regulation of nuclear processes and it explains how some associated proteins can access and so bind to DNA. Rates of unwrapping are influenced by DNA sequence and histone variation, for instance the PTM acetylation of H3 lysine (Lys) 56 causes an increase rate of site exposure (132). The compaction of DNA into chromatin fibres only exhibits small changes in the DNA exposure rates proposing that nucleosomes in chromatin experience transient breathing (133).

1.3.1.4 Chromatin Secondary Structure

Nucleosomes are attached through linker DNA, H1 binds to this linker DNA and the nucleosome dyad stabilises the nucleosome to form high order structures such as nucleosome arrays. Nucleosome arrays are compacted to form a three – dimensional higher order structure which has been suggested to be facilitated by H1 (134). The secondary structure of chromatin is defined as structures from folding a single nucleosome array to form a defined fibre; 30nm fibre. The structure of the 30nm fibre is still yet to be resolved and there are at the moment two possible models; solenoid and zigzag organisation of nucleosomes on the basis of *in vivo* models. In the one start solenoid model neighbouring nucleosomes are intact by linker DNA and follow a superhelical orientation with the bending of linker DNA. Two start zig zag model involves two rows of nucleosomes connected by straight linker DNA with the alternative nucleosome with straight linker DNA (135).

1.3.1.5 Chromatin Tertiary Structures

It has long been regarded that coiling of the 30nm chromatin fibre into increasing higher orders of chromatin compacted and at each stage of compaction dependent on the folding and coiling of chromatin in the previous step to form chromosomes. The formation and existence of the 30nm chromatin fibre has been questioned however recently. It has been suggested that chromosomes are formed in a much less step wise manner and the idea that a chromosome may be similar to a molten globule state as a result of compacted and irregular coiling folding of nucleosome arrays (106). Other chromatin organising and compacting proteins are thought to play in role in chromatin compaction such as polycomb repressive complex 1 and 2 (PRC1/2) and myoid, erythroid nuclear termination stage specific protein (MENT), PARP1, methyl-CpG-binding protein 2 (MeCP2) heterochromatin protein 1 (HP1) (106, 135).

1.3.1.6 Regulation of Chromatin Structure

Nucleosomes regulate DNA accessibility to proteins by causing an obstruction so the strength and positioning DNA and nucleosome interfaces affect the access to sequences. Histones are dynamic and are regulated to either stimulate or suppress biological processes such as DNA transcription, replication and repair. Chromatin compaction is regulated by the cell cycle through development and external signals. For example in mitosis, chromatin condensation occurs, when cells enter interphase chromosomes separate irregularly so that some areas remain condensed and others relaxed. Factors that target histone octamer-DNA interactions are enzymes that modify histones covalently through PTMs, or use ATP to alter nucleosome interactions. These are called ATP chromatin remodelling complexes which are recruited by PTMs on histones (108).

1.3.2 Post Translational Modifications (PTMs) of Histones

PTMs are covalent modifications of a protein which occur during or after protein synthesis. They occur on amino acid side chains or at the C or N terminus of the protein and widen their chemical functionality by the addition of groups such as phosphate, amide, methyl or ubiquitin moieties (136). Over 100 PTMs on histones have been described and common modifications are shown in figure 14 shows common examples (137). For example phosphorylation, ubiquitination, acetylation and methylation occur predominantly on the N-terminal tails and are essential in the regulation of chromatin structure and are essential in a wide array of cellular processes including regulating transcription, DNA repair, recombination through meiosis and DNA replication scheduling in mitosis (108, 137). A number of PTMs have been reported to occur within the histone core, including 10 - 20 histone modifications that occur between the DNA – Histone octamer interface (137). PTMs alter gene expression without changing the DNA sequence so are frequently called epigenetic changes although they are not sustained over the cell cycle (138). PTMs effect the stability of the nucleosome by changing the chemical interactions in the nucleosome or with an adjacent nucleosome changing the compaction of chromatin; opening or closing of chromatin (139). PTMs can also regulate biological processes, for example during transcription, PTMs can act as scaffolds or binding sites so other proteins can bind and can also prevent the binding of proteins to DNA (137, 140, 141). These PTMs of histones can also regulate chromatin by the recruitment of ATP dependent chromatin remodelling complexes (142).

Figure from (143), Figure 2

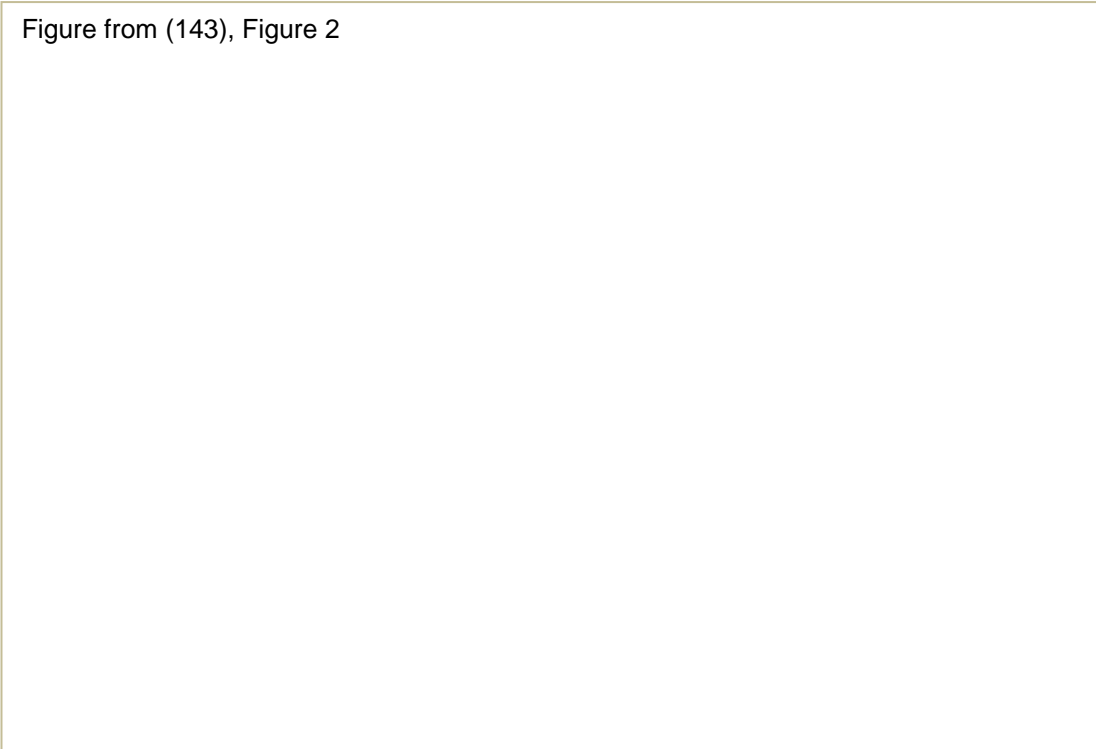


Figure 14: Histone post translational modifications. Common patterns of histone modifications in normal and cancer cells. The majority are located on the N-terminal tails, but there are also some located in the C-terminal region. Histones undergo a range of PTMs (Ac, acetylation; Me, methylation; P, phosphorylation; Ub, ubiquitination) which contribute to global and local chromatin condensation or decondensation. Figure has been modified slightly from (143).

1.3.2.1 Phosphorylation of Histones

Protein phosphorylation is a type of PTM which is the most commonly used for signal transduction in all basic cellular processes. This particular PTM has been related chromatin structure and function and play a vital part in transcription, apoptosis, DNA repair, chromosome condensation (108). Protein kinases utilise ATP to catalyse the addition of a γ -phosphate group using to specific amino acids (usually Serine (S), Threonine (T) and Y in eukaryotes) in a protein. There are in total 518 kinases that make up approximately 1.7% of the genome, one of the principal families of genes and it has been estimated that 30% of proteins in cells are modified in this way and there around 700,000 sites of possible phosphorylation. Kinases are very variable in the number of sites in which they can phosphorylate, an example of this is mammalian protein kinase 1 (MEK1) that probably only acts on four sites (two in extracellular signal-regulated kinase (ERK) 1 and two in ERK2) in contrast to cyclin-dependent kinases (CDKs) which act on hundreds (144). Protein phosphatases act by removing phosphate groups, therefore allowing flexible and versatile

regulation of protein phosphorylation. There are approximately 200 protein phosphatases which are broadly separated into three main families; 40 serine/ threonine, 100 tyrosine and 50 dual-specificity phosphatases (144).

Histone phosphorylation is highly dynamic and is involved in chromatin function and structure, through (in the majority of cases) modification of S and T amino acids on histone tails. This modification on amino acids causes a substantial negative charge on the histone which is thought to alter chromatin structure (142). The majority of phosphorylation events occur on the N-terminal tails of histone to alter chromatin structure and function, some do occur on the C-terminal of certain histones for example phosphorylation of a H4H74 which also causes changes in chromatin structures (108, 142). Phosphorylation in the core of the nucleosomes also occur such as a H3Y41 (108). H3Y118 phosphorylation at the nucleosome dyad has been shown to destabilise the nucleosome altering chromatin structure using mononucleosome substrates and has been implicated in DNA transcription and repair (137). The action of phosphatases on histones is less well known, but it can be assumed that due to vast amount of phosphorylation events that happen there has to be high amount of phosphatases to reverse this activity. At mitosis the PP1 phosphatase acts antagonistically in relation to Aurora B kinases that induces genome wide H3S10 and H3S28 phosphorylation (142).

1.3.2.2 Acetylation of Histones

Histone acetylation involves the transfer of negatively charged acetyl group on to a ϵ -amino group of lysine residue in all core histones. This process is regulated by two opposing families of proteins; histone acetyl transferases (HATs) and histone deacetylases (HDACs). HATs catalyse the addition of acetyl group by utilising acetyl cofactor A (CoA) as a cofactor. This in turn neutralises the positive charge on lysine residues as the acetyl group is negatively charged which is thought to weaken the electrostatic interactions between the histone octamer – DNA and so relaxes the chromatin to allow for processes such as transcription (142, 145). An example of this is acetylation of lysines are H3K115 and H3K122 in the nucleosome dyad was found to reduce histone octamer interactions using mononucleosome substrates which may facilitate nucleosome repositioning and de/assembly (146). There is an increasing amount of evidence of HATs in DNA repair and replication which also require an open chromatin structure to operate (147). There are two primary families of HATs; type B which acetylate free histones in the cytoplasm such as those synthesised on H4K5 and H4K12 which is required for the deposition of histones, and type A which are much more varied. Type A is split into three groups; GNAT, MYST and CBP/p300 and can acetylate various sites on histone N-terminal tails (predominantly) and histone core (142). As well as the relaxing chromatin acetylation of histones can also be recognised by a number of proteins that contain a bromodomain which stabilises the interaction with acetylated histones, which occur in many transcription coactivators and SW1/SNF chromatin remodelling factors (108).

1.3.2.3 Methylation of Histones

Covalent methylation of histones largely occurs on the side chains of amino acids L and R, particularly through the transfer of a methyl group from a S-Adenosyl methionine (SAM) to histones H3 and H4. Methylation of histones does not change the charge of histones like its other PTM counterparts, phosphorylation and acetylation (108, 148). Lysine residues in histones are methylated on the ϵ -nitrogen by a lysine specific SET domain (130 – 140 amino acid motif) lysine histone methyltransferases (HMTases) involved in the methylation of K4, 9, 27 and 36 in H3 and 20 in H4 or non-SET lysine histone methyltransferases which will methylate H3K79 (148). Arginine methyltransferases methylate arginine residues 2, 17 and 26 in H3 and 3 in H4. Lysine methylation can be mono, di and tri methylated while Arginine can be mono-methylated, symmetrically or asymmetrically di-methylated. Histone modifications by methylation are thought to be a more stable mark than the other PTMs, especially histone trimethylation as at the moment there are no known enzyme that can remove this type of methylated modification (148). Euchromatin is characteristically marked by di and trimethylation on H3K4 by specific HMTases (for example SET1/AS2 and SET7/9). This modification stimulates gene expression and a group of co activators including CHD1 binds to this methyl group and transcriptional machinery can also bind to this residue. In contrast methylation on H3K9 is associated with closed chromatin and marks heterochromatin. H3K27 methylation is also associated with closed chromatin and has been associated with pluripotency, developmental gene regulation and ESC function, and is catalysed by polycomb repressive complexes (PRCs). PRCs are thought to promote the tight packaging of chromatin, repress chromatin remodelling and block transcription machinery. Polycomb (PcG) proteins have a chromodomain which bind to methylated H3K27 and play a vital role in repression of transcription (108). Histone methylation was previously thought to be a stable and static PTM until the discovery of the first histone demethylase. Lysine-specific demethylase 1 (LSD1) which uses FAD as a cofactor and when in complex with Co-REST repressor complex it is able to demethylate nucleosomal histones such as mono and dimethylated H3K4, when complexed with androgen receptor demethylates H3K9. LSD1 alone cannot demethylate nucleosomes (142).

1.3.2.4 Ubiquitination

Ubiquitination is a very influential and essential mechanism in regulating the majority of the features of cell biology. The molecule ubiquitin is a small regulatory protein which is conjugated onto proteins either as a monomer or polymer. This PTM affects a range of cellular processes including degradation, cellular location, stability or activity of a protein and alter protein-protein and protein-DNA interactions.

1.3.2.4.1 Ubiquitination pathway

Ubiquitin can be attached to vast array of proteins and different types of ubiquitination can have very different effects on the protein as discussed, therefore the ubiquitination process requires a high specificity to the substrate. There are 2 E1s, at least 38 E2s and more than 1000 E3s that the human genome encodes. As the number of enzymes increases in this cascade so does the specificity of the next component. Specificity and sensitivity of the substrate protein recognition is largely carried out by the E3 ligase either on its own or in complex with a E2 (149).

Ubiquitin is a 76 amino acid which is transferred onto a K residue on target protein through a step wise process of enzymatic reactions with a E1 activating enzyme, an E2 conjugating enzyme and a E3 ubiquitin ligase, which is termed ubiquitination. The enzymatic cascade is initiated by a E1 activating enzyme which utilises ATP to form a thioester bond between its cysteine (C) in the active site the C-terminus of the G76 residue in ubiquitin. This process activates ubiquitin so it can be transferred to a E2 conjugating enzyme. This E1 activating enzyme interacts with a E2 conjugating enzyme and catalyses the transfer of ubiquitin from the E1 enzyme to the a C residue in the active site E2 enzyme forming a thiol ester bond with G 76 ubiquitin. The conjugated E2 then binds to a E3 ubiquitin ligase on which there are two different classes. The E3 ligase will either cause the direct transfer of the ubiquitin molecule onto a K target protein or onto a K acceptor in the E3 ligase or E3 bound target protein for E3 mediated ubiquitin transfer on a target protein. This mostly creates an amide isopeptide bond between the ϵ - amino group of a Lys in a target protein and the C-terminal G76 residue of ubiquitin (150). The majority of E3 ligases have a really interesting new gene (RING) domain or RING related E3s such as the U-box family which mediate the direct transfer of a activated ubiquitin from a E2 enzyme to the target protein. E3 ligase in the homologous to the E6AP carboxyl terminus (HECT) domain class conjugate ubiquitin on the C in the active site of the E3 creating a thioester intermediate which then transfers ubiquitin onto the target protein. Protein targets can be modified by a one ubiquitin on one (monoubiquitination) or more sites (multi- monoubiquitination) and repeated addition of ubiquitin molecules to existing ones to form chains of ubiquitin (polyubiquitination) (151). The traditional view of ubiquitination and what it is used for primarily is commonly polyubiquitination of proteins primarily as a mark for degradation by the 26S proteasome. Protein monoubiquitination has been shown as a vital player in regulating essential cellular functions which do not directly include protein degradation, such as the regulation of DNA repair, translation, and activation of kinases and transcription factors (149, 152).

Proteins can also be marked for ubiquitination and recognised and targeted by E3 ligases. An example of this are degrons which simulate the degradation of a proteins that are damaged, misfolded or abnormal via the proteasomal degradation pathway. This occurs primarily

through the N-end rule pathway and causes destabilisation of the N-terminal residue of a protein, termed N- degron. These are then recognised by a E3 ligases that contain a N-recognin sequences and with its cognate E2 enzyme polyubiquitinates the N-end rule substrates and so sending them to the 26S proteasome (153). Substrate markers for ubiquitination can also be generated through PTMs. An example of this in the context of nucleosome is CUL4 E3 ligase which binds to histones that are newly synthesised with an acetylated H3K56 and ubiquitinates H3K56 and so facilitating hand off H3-H4 from the histone chaperone Asf1 to others in nucleosome assembly (154).

DUBs are proteases which remove ubiquitin or ubiquitin like protein residues from target proteins and play essential roles in the ubiquitination pathway. DUBs recycle ubiquitin, reverse ubiquitin or ubiquitin like modifications of proteins, activate ubiquitin protein precursor and free unattached polyubiquitin chains. The human genome encodes for 100 DUBs which are separated into five families the ubiquitin C-terminal hydrolases (UCH), the ubiquitin specific protease (USP/UBP), the ovarian tumor (OTU), the Josephin domain are papain-like cysteine proteases and the fifth family JAB1/MPN/Mov34 metalloenzyme (JAMM) domain zinc-dependent metalloprotease family. Deubiquitination is a highly conserved and regulated process associated with many cellular process including the regulation of cell cycle progression, gene expression, DNA repair, kinase activation and proteasomal degradation. DUBs require interaction with either a substrate or scaffolding protein to allow for the catalytically competent conformation, this prevents DUBs acting on non-specific substrates. They are composed of catalytic, protein-protein interaction and ubiquitin binding domains which are involved in specificity, binding, localisation and function of DUBs. DUBs form multi protein complexes which are required for localisation and substrate specificity so it can function within a cell correctly. An example of this is the association of DUBs with E3 ligases and so consequently negatively regulating the conjugation of ubiquitin (155).

1.3.2.4.2 Ubiquitination of Histones

Ubiquitination of histones occurs mainly in the mono form which is not associated with degradation. The understanding of the effect of ubiquitin on histones is not as well understood as the other PTMs of histones but they have still be found to have critical functions in DNA repair and transcription. In cells H2AK119 and H2BK120 are some of the most ubiquitinated proteins in a cell which are high conserved and it has been estimated that 5-15% and 1-2% of all H2A and H2B respectively are modified in this way. H3 and H4 can also be ubiquitinated for example polyubiquitination of these is seen following UV irradiation, however the function of this PTM has not been elucidated. Monoubiquitination of H2A and H2B both play a clear role in transcription. H2A ubiquitination is associated gene silencing, ubiquitination on K119 by ubiquitin ligases that were discovered to by transcriptional repressor complexes e.g. PRC1 and has also been found to repress the methylation of H3K4 which is a transcription marker.

DUBs have been found to stimulate gene activation by deubiquitinating H2A. H2B on the other hand promote transcription activation through a number of ways by stimulating other PTMs and Pol II elongation. In yeast it was shown that ubiquitination of H2BK123 enhanced methylation of H3K4 which as stated before is a transcription marker. H2B ubiquitination facilitates Pol II elongation by stimulating the replacement of H2A/H2B dimers for the nucleosome (156, 157).

1.3.2.5 Poly(ADP-ribosyl)ation of Histones

PARPs are a family of enzymes that play vital roles in various cellular processes including DNA transcription, replication, repair and the modulation of chromatin structure. PARPs can achieve this by catalysing the transfer of ADP-ribose from donor nicotinamide adenine dinucleotide (NAD⁺) onto target proteins post translationally. The enzymatic reaction results in the covalent attachment of ADP-ribose to glutamine (Q), arginine (R) or K residues in acceptor proteins by a transesterification reaction. There are at least 18 PARPs that are encoded by different genes but share homology in a conserved catalytic domain. The functions of PARylation have been best identified for only a few PARPS; PARP1, PARP2 and tankyrases. There are four subfamilies which include: DNA-dependent PARPs (e.g. PARP1, PARP2, and PARP3), the tankyrases (e.g. PARP5B), the Cys-Cys-Cys-His (CCCH) PARPs (e.g. PARP7 and PARP12) and the macroPARPs (e.g. B-aggressive lymphoma protein 1) (158-160).

PARP1 is involved in the early recruitment of factors for DSB repair. PARP1 deficiency or inhibition leads to the delayed activation of DNA damage response proteins such as γ H2AX and p53 which are recruited to DSBs by ATM. ATM contains poly(ADP)ribose domains and its interactions with poly(ADP)ribose polymers stimulates its activity (158).

The poly(ADP-ribosyl)ation of nucleosome arrays has been shown to relax chromatin structure. PARP1 has been shown to modulate the composition of chromatin through facilitating the release of H1 and thus cause the recruitment of HGMGB1 and chromatin architectural protein to the oestrogen stimulated pS2 promotor (161). PARP1 has been found to regulate chromatin structure through preventing the demethylation of H3K4me3 by PARylating and inhibiting the recruitment of the K specific demethylase KDM5B and by the promoting the exclusion H1, causing the opening of promoter chromatin, thus regulating transcription (162). PARP1 activity can be simulated by lipopolysaccharide (LPS) to cause ADP-ribosylation of histones which destabilises the histone-DNA interactions in the nucleosome and so increasing the accessibility of the DNA promoters to nucleases. LPS stimulation induced ADP ribosylation at specific promoters facilitates NF- κ B recruitment and so the transcription of specific genes in macrophages (163). PAR chains have been suggested to stabilise histones that have been dissociated from DNA. A mesh of PAR chains are formed when large scale nucleosome eviction has occurred and so may function as a

scaffolding to maintain displaced histones locally. PARylation is also thought to maintain chromatin structure, and has been found to maintain heterochromatin and rDNA silencing (164).

1.3.3 Histone Chaperones

Histone chaperones are a group of proteins that regulate nucleosome assembly and can also disassemble nucleosomes. They are able to do this by binding to histones, there as two groups of histone chaperones, ones that bind to H3-H4 or H2A-H2B. However, some histone chaperones including facilities chromatin transcription (FACT) are able to bind both of these histone dimers. The negative charge of histones chaperones prevents non-specific aggregation of highly positively histones charged and negatively charged DNA. They are also involved in regulating critical steps when forming the histone octamer with DNA to make the nucleosome. Histones and DNA are unable to form nucleosomes on their own as histones tend to form aggregates with DNA by binding non-specifically, histone chaperones are therefore required for correct folding of the nucleosome (165). In nucleosome assembly firstly newly synthesised histones in the cytosol are localised to the nucleus by histones chaperones for example (Nucleosome assembly protein 1) Nap1, which are directly implicated in the transport of histones on DNA for nucleosome formation. They regulate enzymatic activity of histone modifiers with other histone binding proteins such as Anti-silencing factor 1 (Asf1) and RbAp46. They also maintain a pool of histones in case of cell stress, for example histone chaperones like Nuclear autoantigenic sperm protein (NASP) bind to histones and regulate supply of histones. They play key roles in many biological processes such as transcription, recombination, replication, DNA damage response and repair and cell cycle progression (166).

1.3.4 ATP – dependent chromatin remodelling complexes

ATP-dependent chromatin remodelling complexes alter chromatin organisation by causing the displacement of histones by utilising the energy from ATP hydrolysis to remove nucleosomes to expose DNA sequences, nucleosome sliding to expose (or bury) a DNA sequence and replacing pre-existing histones with specialised histone variants (167). They all share a range of similar features; common ATPase domain for remodelling and breaching histone DNA interfaces, strong affinity for the nucleosome, domains that recognise PTM of histones and utilise ATP hydrolysis to alter histone-DNA contacts. These remodelling complexes are divided into four different families which all have a common ATPase domain but are divided into different families by their unique flanking domains. The four families include the switching defective/sucrose nonfermenting (SW1/SNF), chromodomain, helicase, DNA binding (CHD), inositol requiring 80 (INO80) and imitation switch (ISWI) families that have been identified (106). All four are specialised for specific purposes and biological settings, by unique domains

residing in their catalytic ATPases and also by their unique associated subunits. Their structures are shown in figure 15. The SWI/SNF family acts by sliding and ejecting nucleosomes for many biological processes, but do little in chromatin assembly. However ISWI family remodellers optimise the spacing of nucleosomes, thus promoting chromatin assembly but repressing transcription. Some CHD remodellers slide or eject nucleosomes to stimulate transcription, conversely others have repressive roles. The INO80 family have diverse functions including histone variant exchange which comprise promoting DNA repair and transcription (167).

Figure from (167), Figure 2

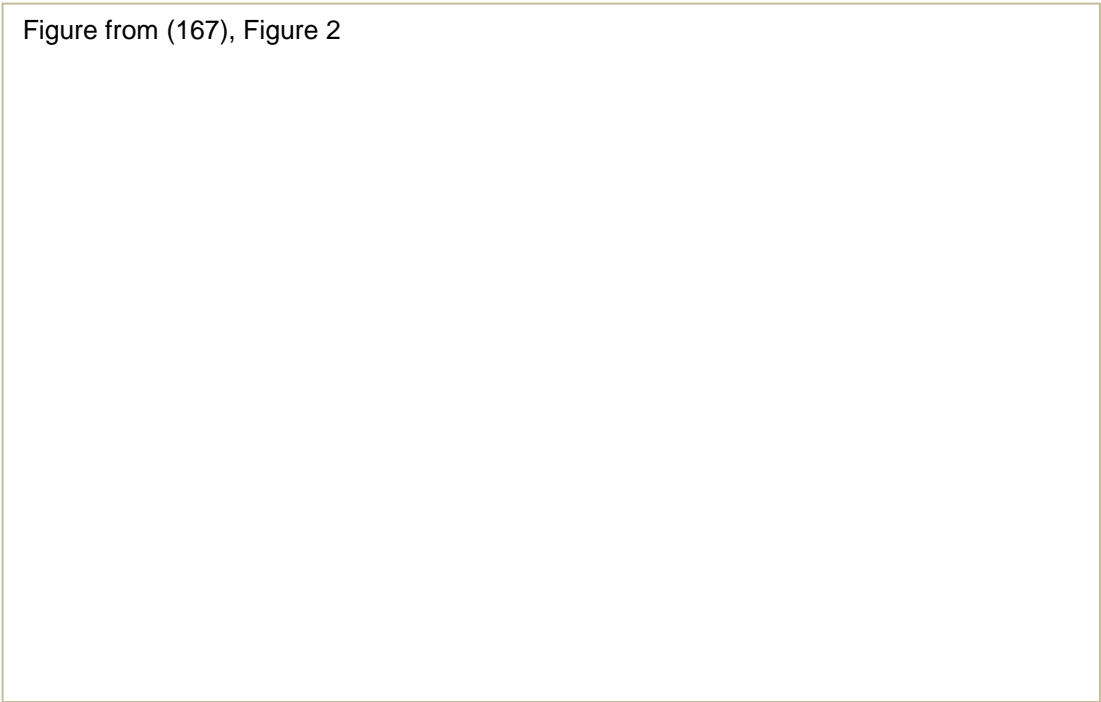


Figure 15: ATP-dependent chromatin remodelling families. All families share a SWI/SNF family ATPase subunit characterised by a ATPase domain which is in two sections, HELICc (orange) and DExx (red). These families are separated by domains that are within or adjacent to the ATPase domain, and are further defined by flanking domains (Bromodomain, helicase-SANT (HAS), SANT SLIDE module, tandem chromodomains). Figure is from (167).

1.3.5 Chromatin Dynamics in DNA repair

Changes in chromatin structure are essential in the response to DNA damage to regulate DNA repair and checkpoint signalling. To ensure genome integrity, DNA repair machinery must be able to access DNA lesions efficiently no matter what their position is in chromatin. The stability of the nucleosome can be altered through a number of ways; histone exchange, histone PTMs and the recruitment of ATP-chromatin remodelling complexes. Chromatin

remodelling in terms of DNA repair has been implicated mostly in the DSB and NER pathways which will be discussed in more detail below.

1.3.5.1 Histone Modifications

1.3.5.1.1 Histone Phosphorylation

Phosphorylation of H2AX on S 139 is the most established form of epigenetic change that occurs as a result of the DNA damage response (DDR). This is an early event which arises after DSB by either ataxia telangiectasia mutated (ATM) creating a chromatin mark. In DSB repair phosphorylated H2AX (γ -H2AX) is important for the accumulation of different repair proteins and signalling molecules, this concentrates repair proteins in small nuclear foci, ionising radiation-induced foci (IRIF) (168). The interaction between γ -H2AX and mediator of DNA damage checkpoint protein 1 (MDC1), a check point protein which is important for the function of γ -H2AX by increasing the levels of γ -H2AX along the chromatin fibre thus acting as spatial organiser (169). MDC1 also stabilises NBS1 (which is part of the homologous recombination essential MRN complex) and chromatin interaction at DSB (170, 171). MRN increases the levels of ATM and so increases the levels of γ -H2AX, this demonstrates a positive feedback loop with MDC1 to spread γ -H2AX across chromatin (170, 172). In addition when MDC1 and γ -H2AX are bound they act as a platform for other DDR proteins to interact, this includes checkpoint kinase 2 (CHK2), Rad51, ring finger protein (RNF)8 and 53BP1 (173). As described γ -H2AX functions as a spatial organiser for DSB repair directly and indirectly by promoting chromatin remodelling and concentrating repair proteins. DSB repair however is only slightly affected by the absence of γ -H2AX, suggesting its role is to cause a concentration of repair factors and its function to alter chromatin is not critical for repair. The activation of cell cycle checkpoints however is dependent on formation IRIF through γ -H2AX in response to low doses of ionising radiation (174) .

Histone H2B has been proposed to be phosphorylated on serine 14 at site where DSBs have occurred and form IRIF at late time points after irradiation, it has been suggested that this is maybe linked to chromatin condensation and apoptosis (175). Histone H2A in yeast showed that mutation of Serine 122 and 129 caused defects during DSB repair, with serine 122 having the strongest effect (176). Histone H4 has been suggested to be phosphorylated on serine 1 in response to DSBs by casein kinase II and phosphorylated H4 regulates chromatin acetylation by inhibiting NuA4-mediated acetylation of H4, this is thought to be important for normal gene expression and repair (177).

1.3.5.1.2 Histone Acetylation

Acetylation of histones has been found to be a key regulator of chromatin remodelling. In yeast studies investigating patterns of K residues in H4 tails that can be acetylated if mutated was

found to inhibit DSB and UV damage repair, this was associated with Esa1 NuA4 HAT acetylase complex (178). In DSB repair the TRRAP/TIP60 complex (mammalian homologue of NuA4) is thought to be required; studies have found the expression of mutated TIP60 which did not have acetyltransferase activity caused defective DSB repair and apoptosis (179). Reducing the TRRAP/TIP60 complex subunits caused deficient homologous recombination repair, however repair could be rescued by forcing chromatin unwinding, thus suggesting that the TRRAP/TIP60 complex was required to induce accessibility of chromatin to repair factors. The hyperacetylation of histone H4 is also important for the binding of repair proteins Rad51, 53BP1 and BRCA1 which require increased chromatin accessibility to bind (180, 181). In a study screening for histone modifications in response to DNA damage H3K9 and H3K56 acetylation was found to be significantly globally reduced (182).

NHEJ is initiated by the acetyltransferases p300 and CREB-binding protein (CBP) which accumulates around DSBs, acetylating H3 and H4 and so promoting the recruitment of Ku proteins (183). Males absent on the first (MOF), another acetyltransferase, also stimulates HR and NHEJ by increasing H4K16 acetylation in response to DSBs which is thought to facilitate BRCA1 and 53BP1 recruitment (184, 185). Acetylation of histones in DSB has been shown to be transient during different stages of the repair process. Acetylation of K on H3 and H4 during HR varies and the HDACs, Rpd3, Sir2 and Hst1 locate to site-specific DSB (186). HDACs 1 and 2 deacetylate H3 lysine 56 and H4 lysine 16 at DSBs and is required for efficient NHEJ repair, and is then followed by hyperacetylation. It has been suggested that deacetylation is important to repress transcription so repair is not hindered and that tightly bound chromatin is required to stop Ku proteins from slipping away thus keeping them concentrated (187).

In NER, total protein acetylation has been found to increase after UV irradiation and repair is boosted in nucleosomes which have been hyperacetylated, this was suggested to be because the DNA is made more accessible to repair proteins by histone acetyltransferases (188, 189). Changes in chromatin structure maybe induced by acetyltransferases controlling transcription of target genes or being attracted to certain DNA sequences following damage, this was proved in yeast that the repair and transcription of the MFA2 gene was dependent on GCN5 acetyltransferase (190). Following UV irradiation, GCN5 acetyltransferase is recruited to sites of damage and promotes H3K9 acetylation, H4K16 acetylation also increases however it is not known which enzyme catalyses this change but is speculated to be by MOF (184, 191).

Global histone acetylation as a result of DNA damage has been observed to increase chromatin accessibility and to increase repair efficiency. Following UV irradiation there is a increase in H3K9 and H3K14 in a p53 dependent manner causing chromatin relaxation. This is independent from repair proteins that are involved in damage recognition and is mediated by p300 acetyltransferase, which is also recruited by p53 to DNA damage (192, 193). The ING proteins regulate chromatin acetylation by associating with histone acetylases and

deacetylases, effecting NER. The interaction of p53 and p300 is stimulated by their binding to ING2. It has been shown that cells overexpressing inhibitor of growth 1 (ING1) protein, which are chromatin acetylation regulators, had an increased repair efficiency after UV damage, and its knockdown hindered repair, it was concluded that ING1 is required for global acetylation causing chromatin relaxation (194, 195).

1.3.5.1.3 Histone Ubiquitination

Ubiquitination of histones is a key process in DDR in DSB repair, and is used to recruit the repair proteins 53BP1 and BRCA1. The E3 ubiquitin ligase Ring finger protein 8 (RNF8) which accumulates at DSBs, monoubiquitinates H2A and H2AX which then catalyses the K63-linked ubiquitin chains with UBC1, that interact with MDC1 to recruit this protein to DNA damage sites (196-198). RNF168 another E3 ubiquitin ligase interacts with ubiquitinated H2A/H2AX to amplify its ubiquitination at sites adjacent to DSBs. The function of RNF168 is dependent on RNF8 to initiate ubiquitination of H2A/H2AXK 13 and 15. RNF168 and RNF8 serves to amplify the signal to the threshold level so that 53BP1 and BRCA1 can be recruited by altering the accessibility and so facilitating 53BP1 loading (199, 200). The ubiquitin E3 ligase HERC2 also localises to repair foci, it functions by binding and facilitating RNF8 and the E2 enzyme Ubc13 and so promoting Lys 63 polyubiquitin chains (198, 201). Histone H2B is also ubiquitinated as a result of DSBs on K120 by the RNF20-RNF40 dimer which is phosphorylated by ATM and then recruited to DSB. Without H2B ubiquitination, XRCC4 and Ku80 localisation is disturbed which leads to defects in DSB repair (202, 203).

H2A ubiquitination is also seen in NER following UV irradiation, this is dependent on CUL4A-DDB2 complex and the CAF1 histone chaperone, and as seen in DSB repair RNF8 is recruited to UV damage sites by MDC1 and UBC13 mediating ubiquitination. RNF2 knockdown has also been shown to perturb H2A ubiquitination after irradiation (204-207).

1.3.5.1.4 Histone methylation

Histone H3K4, 9, 27, 36 and 79 and H4K20 can be either mono, di or trimethylated. These types of PTMs are need for 53BP1 retention in chromatin containing DSBs and two have been implicated; H3K79 and H4K20 (208, 209). 53BP1 binds to methylated H3K79 and is important for RAD9 and RAD53 recruitment and activation, and have been shown to be defective in H3K79 and DOT1 methylase mutants. Levels of methylated H3K79 do not change as a result of DNA damage and it is suggested that DSBs induce changes in chromatin structure to expose methylated H3K79 (210, 211).

Dimethylation of H4K20 is required for 53BP1 accumulation by the Set9 methylase at DNA damage sites. Monomethylation in H4K20 mice after knockdown of Suv-20 methyltransferase

caused enhanced sensitivity to DNA damage. It has also been suggested that H4K20 dimethylation levels do not change following DNA damage but become exposed promoting 53BP1 binding. In a recent study however H4K20 levels increase locally following DSB by MMSET methyltransferase to accumulate 53BP1 at DSBs (212-214).

1.3.5.1.5 Histone Poly(ADP-ribosyl)ation

The roles of PARP1 in the DNA damage response have been studied extensively, various types of DNA damage cause the recruitment of PARP1 to sites of damage through its DNA binding activity. DNA binding induces the catalytic activity of PARP1 which results in the formation of PAR chains on itself, histone and non-histone proteins. Histone H2B and H3 are the main poly(ADP)ribosylation acceptors in response to DNA damage, minor amounts of H1 and H4 are also modified (215).

MOF-induced acetylation of H4K16 is required for the cellular DNA damage response and DSB repair. This site can also be poly(ADP)ribosylated by PARP1, crosstalk between these two types of modifications could conceivably occur in DSB repair. PARP1 *in vitro* is activated by oligonucleotides has been shown to be able to modify all 5 histones, the length of the poly(ADP)ribose chains was dependent on the NAD⁺ concentrations. PARP3 has been shown to interact with H2B, H3 and H1, poly(ADP-ribosyl)ation of H1 by PARP3 has been suggested following DNA DSBs (215).

In a recent *in vitro* study histones were found to be specifically modified following DNA DSBs by PARP1a and PARP2. PARP1a was found to mono ribosylate H2BE18 and 19. *In vitro* PARP1a was found to mono ribosylate H2BE18 and disruption of this site allowed for the ADP-ribosylation of H2E19. *In vivo* studies when generating mutations at these sites found that H2BE18 and 19 were the principal sites modified by PARP2 and PARP1a (215, 216).

In the NER pathway UV damage is recognised by XPC and RAD23B which associates with the complex DDB1-DDB2 that ubiquitinates the core histones to cause nucleosome displacement so repair can be initiated. XPC binds to the chained polymer poly(ADP-ribose) sites which is important for its recruitment to UV damage sites. PARP1 binding to DDB2 at these damage sites stimulates PARP1 activity, this increase in PARP1 activity causes ubiquitination-independent chromatin decondensation to facilitate UV damage repair. DDB2 stimulated PARylation of histones by PARP1 results in the recruitment of the ALC1 chromatin remodelling helicase through its PAR binding domains to further stimulate repair by the further recruitment of XPC (215, 217).

PARP1 has been suggested to facilitate nucleosome disassembly by PARylating histones to cause chromatin relaxation. this then causes the recruitment of multiple chromatin remodellers such as ALC1, SWI/SNF, SMARCA5 and CHD2 to make DNA accessible to repair. CHD2 which is recruited to DSBs in a PARP1-dependent manner, triggering the deposition of H3.3 at these regions to cause chromatin relaxation, promoting efficient repair by NHEJ (158).

PARP3 has been shown to nicked mononucleosomes which stimulate PARP3 trans-ribosylation activity on H2BE2. This suggests PARP3 is a nick sensor in nucleosomes, this study the presence of ribosylation of chromatin and DNA single strand breaks (218).

1.3.5.1.6 Histone Modifications in BER

There is very little evidence at this time for histone modifications in terms of BER, however there have been a couple of published studies which suggest the role of histone modifications. Histone acetylation has been suggested as TDG glycosylase interacts with transcriptional coactivators CREB binding protein (CBP) and p300 and the subsequent complexes were able to acetylate histones and process lesions (219). The DUB enzyme USP7 has been suggested to be involved in the regulation of oxidative damage repair through regulating mouse double minute 2 homolog (Mdm2) levels and so chromatin accessibility to proteins involved in DNA repair. It was suggested that USP7/Mdm2 dependent chromatin remodelling occurs through ubiquitination of H2B by Mdm2 to relax chromatin when a DNA lesion is recognised. Further investigation suggested that another E3 ligase regulated by USP7 may also be responsible for H2B ubiquitination (220). In another study a range of PTMs on histone H3 was analysed after DNA damaging agents in U2OS cells. Following methanesulfonate (MMS) a DNA alkylating agent, hydrogen peroxide causing DNA strand breaks and alkali labile sites and IR treatment there was a reduction in levels of H3S2, H3S28 and H3.3S31 phosphorylation and H3K9 and H3K56 acetylation. These findings of changes in H3 phosphorylations and acetylations suggest two responses to DNA damage, although this doesn't directly implicate BER, the DNA damaging agents mentioned do causing lesions which are processed by BER (182). In a study using mononucleosomes substrates nucleosomes were generated with site specific acetylated H3K14 or H3K56 and the rate of repair of uracil and single nucleotide gaps. These acetylated sites had no effect on uracil removal but decreased the gap filling ability of Pol β near the dyad axis suggesting acetylation of histones may promote alternative gap filling pathways (221).

1.3.5.2 Chromatin Remodelling

The INO80 family of ATP-dependent chromatin remodellers have the most known connection with DNA repair. In vitro INO80 is able to slide a mononucleosome from an end to a more central location along DNA and it is also involved in nucleosome eviction in vivo (167). In yeast studies INO80 is recruited by γ -H2AX to DSBs, and in strains lacking INO80 this hindered the 5' – 3' resection at DSB ends before strand invasion (222)]. Another study however did not find this to be the case but found RAD51 and RAD52 loading onto the 3' ends of the DSB was perturbed (223, 224). In mammalian cells however INO80 was not dependent on γ -H2AX but

the interaction of it with Arp8 was. Human cells with a knockdown of INO80 have shown reduced DSB repair due to its effect on Rad54B and XRCC3 transcription (223, 225). INO80 knockdown in mammalian cells causes defective HR repair as 53BP1 foci recruitment is impaired. It was found that the 5'-3' resection was impaired but not Rad51 was not affected. 53BP1 recruitment and resection are also defective in INO80 knockdown cells. Consequently, it has been suggested that INO80 participates in the initial stage of DSB end processing as the chromatin remodelling produced is necessary for the access the initial repair proteins (226). In yeast SWRI (INO80 sub family member) facilitates the localisation of KU proteins to damage sites in NHEJ (227). In mammalian cells the initial events of NHEJ is also dependent of SWI/SNF chromatin remodelling with the BRM1 subunit required for Ku70 recruitment and NHEJ (183). The BRG1 subunit is also required to bind to γ -H2AX nucleosome to cause hyperacetylation of H3 K9, K14, K18 and K23. BRG1 therefore increases the accessibility of ATM to cause additional H2AX phosphorylation. An interaction between BRCA1 and BRG1 has also been implicated in HR repair (228, 229).

Using dinucleosome substrates *in vitro* it was found that the 6-4PP excision was hindered by the dinucleosome which suggested that NER needs more room than the space provided by linker DNA to operate, and a number of studies have indicated chromatin remodelling activity (230). The essential protein CSB in TC- NER contain a SE12/SNF2 ATPase domain which has been shown *in vitro* to alter chromatin structure (231). Using a chromatin model *in vitro* the removal of acetylaminofluorene-guanine adduct near the nucleosome dyad was enhanced by SWI/SNF chromatin remodelling which was facilitated by XPA, XPC and RPA (232, 233). CPD repair is increased with mammalian SWI/SNF ATPase BRG1 subunit but not 6-4PP, and loss of BRG1 results in deregulation of checkpoints and increased apoptosis. The Brg1 subunit of SWI/SNF is recruited to UV-damage sites through an interaction with XPC (234, 235). In a yeast study Snf6 and Snf5, which are subunits of SNI/SNF, can be co-purified with Rad4 and RAD23, which are the homologues for APC and HR23B respectively and which is stimulated by UV induced damage and were required for complete NER (236). INO80 complexes are involved in NER, they are present at UV damage sites and their deletion eliminates the NER protein assembly (237).

1.4 BER in Chromatin

There is accumulating evidence for chromatin changes through histone modifications and chromatin remodellers being an integral part of the DNA DDR, particularly in DSB and NER as described above, with a number of histone modifications and chromatin remodelling events occurring at these specific lesions sites. Currently, evidence that chromatin changes occur to facilitate BER is limited. However, mononucleosome substrates containing site specific DNA base damage have been used *in vitro* to demonstrate that chromatin remodelling events are necessary to stimulate BER, particularly in occluded base damage site in the context of the nucleosome. Although the identity, mechanisms and enzymes involved in this process remain elusive.

1.4.1 Mononucleosome Substrates

Chromatin structure and proteins components are ever more linked to biological processes including transcription, recombination and DNA repair. Mononucleosome substrates have been used to analyse the activity of DNA repair enzymes, histone modifications and chromatin remodelling complexes (238-242). Nucleosome organisation regulates a range of cellular biological processes including DNA repair. Due to these findings of nucleosome dynamics much effort has put in to replicate these processes *in vitro* to build our understanding, which requires the reconstitution of chromatin components that have been utilised extensively. This allows the formation of model chromatin containing a distinct DNA sequences and the use of nucleosome positioning sequences for these which are a pivotal component of these studies to discover more about gene regulation and nucleosome structure and function particularly in DNA repair (243). Previous studies with mononucleosome substrates were limited to histones that had been extracted from chromatin (244). Histones were extracted from chromatin and were subsequently fractionated to purify each histone. However this approach was time consuming and relied on the availability of tissue or blood from an organism, histones degraded rapidly and the histone pool was very heterogeneous due to isotypes and PTMs of histones. Histones purified from recombinant sources (such as *Xenopus laevis*) however are homogenous (do not contain PTMs), are very pure and mutants or isotopes can be expressed. This advancement has allowed for resolution of the nucleosome to base pairs and structure of the mononucleosome to a high resolution (245, 246).

Variations in the B-DNA structure are sequence dependent and produce a definitive rotational and translational orientation, and histone octamer – DNA contacts interact at specific locations. Reconstituted nucleosomes have the same structural and physical properties of native nucleosomes in eukaryotes (243). Before the identification of the Widom 601 nucleosome positioning sequence (245), nucleosome positioning had a

somewhat limited positioning ability. A sequence with a preferential orientation may have several translational positions within 10bp resulting in a population which is heterogeneous with a set of favoured translational positions and no dominant orientation, which caused problems with *in vitro* investigations. The Widom 601 sequence was identified from a random DNA pool to bind to the histone octamer to form a nucleosome and has since become a standard sequence to use to reconstitute nucleosomes. When reconstituted in the nucleosome the 601 sequence has a near identical orientation to 147bp human α -satellite DNA nucleosome and the majority of DNA – histone octamer interactions are the same. The central 20bp of the 601 sequence and α -satellite nucleosome which conforms around the dyad have strikingly very similar conformations, which is related to the vast number of histone octamer – DNA interactions. There are some substantial differences however, the most important one being that the 601 sequence forms a 145bp nucleosome compared to α -satellite DNA which is 147bp. This is because of differences in the superhelical location at -5 and +5 where the 601 sequence DNA over coiled causing only 12bp of the 601 DNA in those locations instead of 13bp for the α –satellite, which causes some difference in histone octamer – DNA interaction at these positions (Figure 16) (247).

Figure from (247), Figure 4

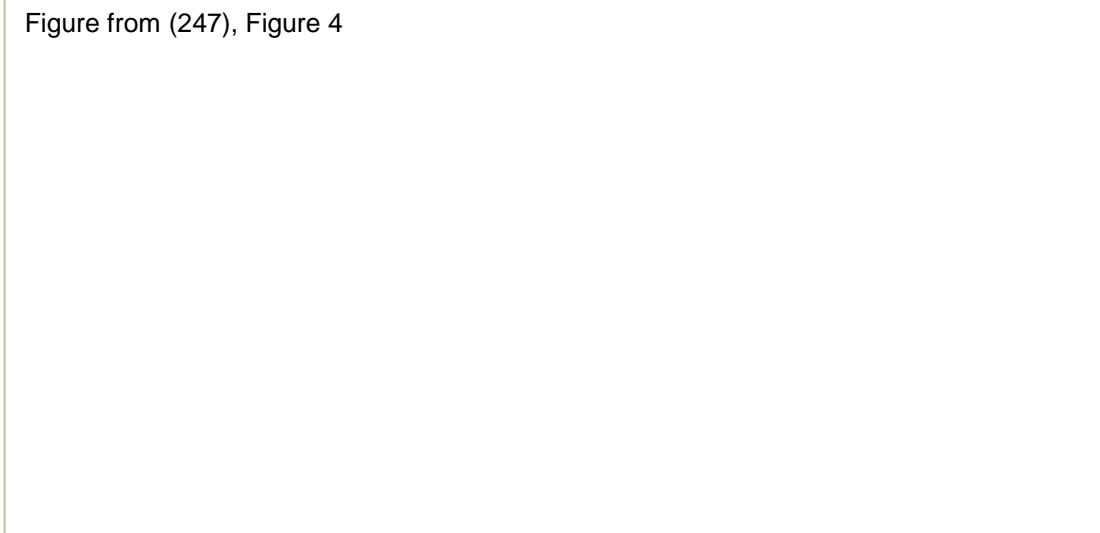


Figure 16; Comparing the Widom 601 Sequence with α -satellite DNA Nucleosome Core Particles. Image taken from Makde *et al* (247). (A) The Widom 601 sequence (blue) was aligned against α -satellite DNA (peach) in the context of a nucleosome core particle. The main differences between the two were found at the superhelical locations indicated to. The difference of the Widom 601 sequence is highlighted to in red and green in (B) and (C) at positions -5 and +5 respectively (numbers based on position from the nucleosome dyad).

1.4.2 Analysing BER *in vitro* utilising Mononucleosome Substrates

As most DNA nucleosome positioning sequences exhibit a preferred helical orientation, it is now possible to produce distinct model mononucleosomes to explore nucleosome influence and dynamics in many biological processes including BER. Several studies have reconstituted mononucleosomes with a specifically orientated DNA lesion to examine how BER enzymes recognise and process these lesions. It has been made clear through these studies that the processing of oxidatively damaged bases and AP sites, by DNA glycosylases and APE1 respectively, is dependent on the orientation of lesion and its position in relation to the nucleosome dyad. A lesion with the DNA backbone facing outwards away from the nucleosome are more efficiently processed by the enzymes than those facing inwards. DNA glycosylases and APE1, as previously mentioned, flip the damaged lesion or AP site out of DNA helix into a recognition site (64, 248, 249). In nucleosomes both of these proteins are able to process these types of DNA damages as long as the location of this damage is in an orientation so it can be flipped out of the helical formation without conflicting with the histone octamer. In contrast, DNA base lesions, AP sites and single nucleotide gap sites in occluded in regions of the nucleosome are inefficiently processed and are thought to require unwrapping of the DNA from the nucleosome to facilitate BER.. Presently it has been suggested that spontaneous and reversible unwrapping of nucleosomal DNA containing DNA base damage allows access to glycosylases and APE1 to the inwardly facing lesion. Lesions that are located in close proximity to the dyad axis are less efficiently processed than those located away from the dyad. Increased accessibility is thought to be achieved by currently unknown PTMs of histone and/or chromatin remodelling enzyme to facilitate repair (16). More specific details of the effects of chromatin on individual enzyme action are included below.

1.4.2.1 Activity of DNA glycosylases on nucleosomes

The efficiency of NTH1 in removing thymine glycol lesions (Tg) in different orientations on mononucleosomes has been measured. Outwardly facing Tg lesions were processed at a rate similar of that of naked DNA using low concentrations of NTH1. Inwardly facing Tg lesions were removed at a 10 fold decreased rate than free DNA, although increasing NTH1 to near physiological concentrations progressively increased Tg excision reaching 48 % relative to that of naked DNA, supporting the unwrapping hypothesis for inwardly facing lesions. Lesions near the dyad axis were only processed 22% as efficiently as naked DNA using the highest concentration of NTH1 (250). Increases in NTH1 concentration significantly increased the processing of the inwards facing lesions and notably the concentration of NTH1 used to efficiently process the inwardly facing Tg lesion was no higher than what was estimated to be present *in vivo*. This was thought to be due to NTH1 high specificity and low non-specific DNA binding. Using high NTH1 concentrations to process occluded sites can be linked to occurrence and extent of DNA unwrapping events from the nucleosomes to expose occluded

lesions (251). NEIL1 when used at a concentration similar to that expected *in vivo* was only able to excise 10% of Tg lesions facing inwards, compared to 50% when the lesion was facing outwards. This was thought to be due to NEIL1 poor specificity and is thought to require other proteins to increase its specificity (251).

The repair of 8-oxoG by OGG1 in nucleosomes is greatly impaired in *in vitro* mononucleosome studies. Using model dinucleosomes with a linker H1 proteins 8-oxoG lesions were positioned in either the linker DNA or within nucleosome. The absence of H1 in the linker produced similar removal rates of 8-oxoG as in free DNA however when H1 was associated with linker DNA there was a 10-fold decrease in the activity. In nucleosomal DNA, the processing of 8-oxoG was significantly impeded, with or without the linker H1 histone (252).

In a study from the Smerdon group, free DNA (not associated with a histone octamer) and mononucleosomes were constructed with G-uracil (U) mismatches. Mononucleosomes were constructed using the Widom 601 nucleosome positioning sequence containing a U rotationally positioned near the nucleosome dyad and were orientated so the DNA backbone was either positioned toward the histone octamer ('inwards') or away ('outwards'). The Mononucleosome substrates were compared with each other and with free DNA, analysing the activity of UDG and APE1 towards differently positioned and orientated U. Activity of UDG1 and APE1 was reduced 10-fold in mononucleosome substrates compared to free DNA and the U facing outwards was 2-3 fold more efficiently processed than U facing inwards. The next step of synthesis by Pol β was totally inhibited at both U orientations (253). In a more recent study by Smerdon's group they assessed the removal of varied translational positioned and orientated uracil's using UDG and APE1 using mononucleosome substrates using the Widom 601 nucleosome positioning sequence (Figure 17A). U were orientated either inwardly or outwardly facing positioned near the nucleosome dyad, and then at two different positions away from the nucleosome dyad as flexibility of DNA is thought to increase with distance from the nucleosome dyad. It was found that the rate of uracil removal using outwardly facing lesions was 2-10 fold greater than inwardly facing lesions. Inwardly facing lesions although not efficiently processed were more readily processed the further they were for the nucleosome dyad, outwardly facing lesions near the nucleosome dyad however were efficiently processed, see figure 17B.

Figure from (242), figure 1a and figure 2a

Figure 17; Uracil Rotational Orientation and Translational Position effect on the Activity of Glycosylase UDG1 and APE1. Image taken from Smerdon *et al* (242). (A) The crystal structure of the Widom 601 nucleosome core particle showing the translational position (numbered with respect of location from the dyad axis which is translational position 0) and orientation (DNA backbone outwards facing towards solvent labelled O and DNA backbone inwards facing towards the histone octamer labelled I) of U indicated to in black. (B) The percentage of incision of nucleosomal DNA following UDG1 and APE1 at different time point. Open symbols represent inwardly orientated U at translational positions; red square +4, blue circle +25, green circle -29 and purple triangle -49. Filled in shapes represent outwardly orientated U at translational positions; blue circle +29, purple triangle -35 and red square +10.

1.4.2.2 Activity of APE1 on nucleosomes

The activity of APE1 by has been measured, Hinz *et al* used mononucleosome substrates using the 601 Widom nucleosome positioning sequence with either a glycosylase generated AP site or a tetrahydrofuran (THF) AP site analog (synthetic AP-site which is more stable). These were placed, which when reconstituted in the nucleosome, were either inwards, outwards or in between inwards and outwards (mid). This study found there was virtually no difference in APE1 activity when using glycosylase generated AP sites or the THF AP site analog. Mononucleosome substrates with a synthetic AP site facing inwards were much less efficiently cleaved than those facing outwards or mid orientation. Association of APE1 with the mononucleosome was also found to was greatly reduced compared to free DNA. This was also lesion orientation dependent, the inwards facing THF had a much less association with APE1 supporting the idea of reduced APE1 activity in occluded lesion sites by the histone octamer (254).

1.4.2.3 Activity of Pol β on nucleosomes

The activity of Pol β has been found to be significantly reduced in the gap facing inwards compared to one outwardly facing (242), this has also been seen in other studies with Pol β (255). DNA glycosylases induce DNA to bend between 45°-70° (256), however for Pol β to function it needs to bend DNA by 90° opposite the single base gap. This severe bending of DNA may inhibit Pol β capacity function without altering the histone contacts. It has been suggested that Pol β on outwardly facing gaps can achieve its active configuration by disrupting enough of the histone contacts, but not when presented with one near the nucleosome dyad, where the DNA is tightly packed on both sides, explaining why Pol β has virtually no activity in the dyad regardless of orientation. This shows that the histone octamer causes varied levels of constraints in BER due to the different requirements of the BER enzyme (242).

Pol β activity was analysed following UDG and APE1 treatment using mononucleosome substrates where U was either facing outwards or inwards. Pol β activity in this study was found to be totally inhibited at both U orientations (253). In another study by the same group after UDG and APE1 treatment the gap filling function of Pol β was found to increase 3-fold when outwardly facing near the DNA ends than those of the same orientation near the dyad axis in the same orientation. This suggests that nucleosome unwrapping events are required for BER proteins to access these occluded regions to facilitate BER (242).

1.4.2.4 Activity of Lig III α -XRCC1

As described previously Pol β activity is significantly impeded by the nucleosome especially in the nucleosome dyad where its activity is virtually non-existent. However, it has been found that Lig III α -XRCC1 partially enhances the activity of Pol β to repair particularly inwardly facing gaps. Lig III α -XRCC1 was found to be noticeably active at high concentrations which lead to nucleosome disruption. As a result, the Lig III α -XRCC1 complex not only increased its own activity by nucleosome disruption at a single nucleotide gap site but also that of Pol β . This disruption in nucleosome – histone interaction is because DNA ligases function by encircling its DNA substrate, so to function in BER Lig III α -XRCC1 would require to disrupt the DNA- histone contacts (255).

1.4.2.5 APE1 activity using nuclear extracts in single and clustered DNA damage site

A characteristic of radiation generated DNA damage is clustered DNA damage which have been investigated to be more difficult to process than single lesions due to decreased efficacy in BER. In a recent study, mononucleosome substrates were produced using the Widom 601

nucleosome positioning sequence with either a single AP site, or two types of clustered sites; bistranded AP sites and a AP site with an opposing 8-oxoG lesion within a mononucleosome. Purified APE1 activity was significantly impeded in the single AP-site containing mononucleosome compared to incubation with the corresponding free DNA, however with nuclear extract CHO-K1 incubation the AP site was processed in free and mononucleosomal DNA at comparable rates. When analysing the bistranded AP sites mononucleosomes were efficiently cleaved using CHO-K1 extracts and the subsequent DSB caused nucleosomal DNA dissociation from the histone octamer. Using the 8-oxoG +1 from dyad axis to an AP site containing mononucleosome the AP site was efficiently cleaved however 8-oxoG processing was significantly impeded (in both the mononucleosome and free DNA), which was suggested to be due to OGG1 is unable to bind to when adjacent to a AP site (+1). The increase of APE1 activity in nuclear extract CHO-K1 was found not to be due to complete unwrapping of nucleosomal DNA from the histone octamer to produce free DNA, instead it was suggested the presence of a chromatin remodeller facilitates incision of the AP site (257).

1.4.3 Chromatin Remodelling factors

Very little is known about the potential histone chaperons and chromatin remodelling enzymes that may facilitate BER. SWI/SNF has been reported to stimulate the processing of 8-oxoG by each of the repair factors OGG1, APE1 and Pol β in nucleosomes reaching levels as those in free DNA. Likewise using oligonucleosome arrays containing a U were incubated with UDG, APE1 and Pol β *in vitro* Pol β activity was found to be significantly impeded, however ISW1 and ISW2 from yeast significantly increased Pol β activity (258). In nucleosomes with 8-oxoG lesions either positioned in linker DNA or within the nucleosome, the presence of remodels structure of chromatin (RSC) part of the SWI/SNF family enhanced the removal of 8-oxoG in the linker DNA and the nucleosome (252). In another study an 8-oxoG lesions was incorporated in two mononucleosome substrate near the dyad axis, one containing canonical histones and the other with variant H2A.Bbd. In both cases the removal, incision and gap filling activity of this lesion was significantly impeded in the mononucleosome compared to free DNA. The chromatin remodeller SWI/SNF was found to greatly increase the repair of 8-oxoG in canonical nucleosome but had a very weak effect on H2A.Bbd, through altering the DNA - histone octamer interactions and not mobilisation (nucleosome sliding) of nucleosome (259). In a recent study, evidence for histone chaperone activity in facilitating BER was suggested. The histone chaperone FACT was found to be released from transcription factors following oxidative stress and associate with repair proteins and chromatin remodelling complexes. FACT promotes UDG1 in removing uracil in mononucleosome substrates by boosting the chromatin remodelling activity of RSC, suggesting the role of these two proteins in facilitating the initial step in BER (241). There are very few studies of BER facilitated by chromatin remodelling activity *in vivo* and are mostly indirect. Utilising mutant yeast cells lacking in

certain subunits of SWI/SNF and INO80 chromatin remodelling complexes, these cells exhibit augmented sensitivity to methyl methanesulfonate (MMS) which suggest their role in chromatin remodelling in the presence of alkylated DNA lesions (260-262). In a more recent study, the STH1 ATPase subunit of RSC was depleted in yeast and caused an increased sensitivity to MMS and considerable inhibition of BER in the *GAL1* locus and genome wide. Throughout the genome chromatin DNA was found to be less assessable to micrococcal nuclease digestion without any change in BER gene expression (263). It is conceivable that PARP1 may regulate chromatin condensation to facilitate BER as it can ADP-ribosylate histones H2B and H1 which could cause nucleosome disruption, relaxing chromatin due to the added negative charge. PARP1 also inhibits histone demethylase KDM5B activity to create a more open chromatin state, although the roles of PARP in the context of chromatin is more associated with transcription regulation at this time (162, 264-266).

Chromatin remodellers involved in BER are significantly understudied, which is impeding our knowledge of the mechanism of BER in chromatin that is essential for genome stability and in maintaining human health.

1.5 Aims

The mechanism of BER and the major proteins involved are now well defined. However despite this knowledge, the epigenetic mechanisms and chromatin remodelling processes involved in the cellular response to DNA base damage that is processed by BER are poorly understood. Nucleosomes are constructed from 147 bp DNA which is wrapped around a histone octamer that comprises of two copies of H2A, H2B, H3 and H4. To access DNA, and therefore DNA damage, it is thought that chromatin remodelling is required to support DNA damage repair. This is thought to be achieved through histone PTMs on the N-terminal tails which contain lysine residues that can be modified through poly(ADP-ribosyl)ation, acetylation, methylation or ubiquitination. This then causes chromatin condensation or directly recruits chromatin remodelling factors which alter histone contacts through ATP hydrolysis. There is accumulating evidence for chromatin changes being an integral part of the DNA damage response, particularly in DSB repair and NER, with a number of histone modifications and chromatin remodelling events occurring at these specific lesion sites. Relating to BER, mononucleosome substrates containing DNA base damage have been used to predominately demonstrate that the orientation and translation position of base lesions greatly affects BER enzyme activity. However, the chromatin remodelling enzymes, the precise histone modifications and the histone modifying enzymes catalysing these that are necessary to stimulate BER and the mechanisms involved, remain unknown.

Therefore the study presented in this thesis aimed to identify specific histone modifications, the enzymes catalysing these, and the chromatin remodellers that are involved in the signalling and/or processing of DNA base damage during BER. In order to achieve this overarching aim, three key objectives were identified to drive the progress of this research as follows.

- I. The generation of mononucleosomes containing site-specific AP-site containing DNA damage.
- II. Establishment of *in vitro* BER assays using mononucleosomal DNA containing site-specific AP-site DNA damage in different orientations to examine differences in APE1 activity using purified protein and WCE.
- III. Use of fractionated HeLa cell WCE with mononucleosomal DNA containing site-specific AP-site DNA damage in order to identify novel enzymatic activities that stimulate APE1 activity.

CHAPTER II

MATERIALS AND METHODS

2.1 Materials

2.1.1 601 nucleosome positioning sequence

The Windom 601 strong nucleosome positioning was used for mononucleosome experiments Windom *et al* (245). The position of the synthetic AP-site (THF) was determined from the crystal structure and sequence published, Rodriguz *et al* (242). The cloning vector (P-GEM3Z with ampicillin resistance) containing the 256bp nucleosome positioning sequence was obtained from Prof Peter O'Neil (CRUK/MRC Oxford Institute for Radiation Oncology, University of Oxford, UK).

```

5' -GCTCGGAATTCTATCCGACTGGCACCGGCAAGGTCGCTGTTCAATACATG
3' -CGAGCCTTAAGATAGGCTGACCGTGGCCGTTCCAGCGACAAGTTATGTAC

CACAGGATGGTATATATCTGACACGTGCCTGGAGACTAGGGAGTAATCCC
GTGTCCTACCATATATAGACTGTGCACGGACCTCTGATCCCTCATTAGGG

CTTGCGGTTAAAACGCGGGGGACCACGCGTTGGTGCGTTTAAGCCGTG
GAACCGCCAATTTTGCGCCCCCTGGTGCGCAACCACGCAAATTCGGCAC

CTGGCGCTTGCTACGACCAATTGAGCGGCCTCGGCACCGGGATTCTCCAG
GACCGCGAACGATGCTGGTTAACTCGCCGAGCCGTGGCCCTAAGAGGTC

GGCGGCCGCGTATAGGGTCCATCACATAAGGGATGAACTCGGTCTTAAGA
CCGCCGGCGCATATCCCAGGTAGTGTATTCCCTACTTGAGCCAGAATTCT

ATCATGC-3'
TAGTACG-5'

```

Figure 18: Double strand 256bp DNA sequence for the 601 nucleosome positioning sequence. Figure show nucleotide sequence for the strong Windom 601 nucleosome positioning sequence. Nucleotides highlighted in yellow are a restriction digest site for Van91I and in green BglI. The nucleosome dyad is indicated to in black bold. The position of the tetrahydrofuran (AP site equivalent) is indicated to in red. An THF on the upper strand produced an outwards facing THF and when on the lower strand and inwards facing THF when reconstituted in the histone octamer.

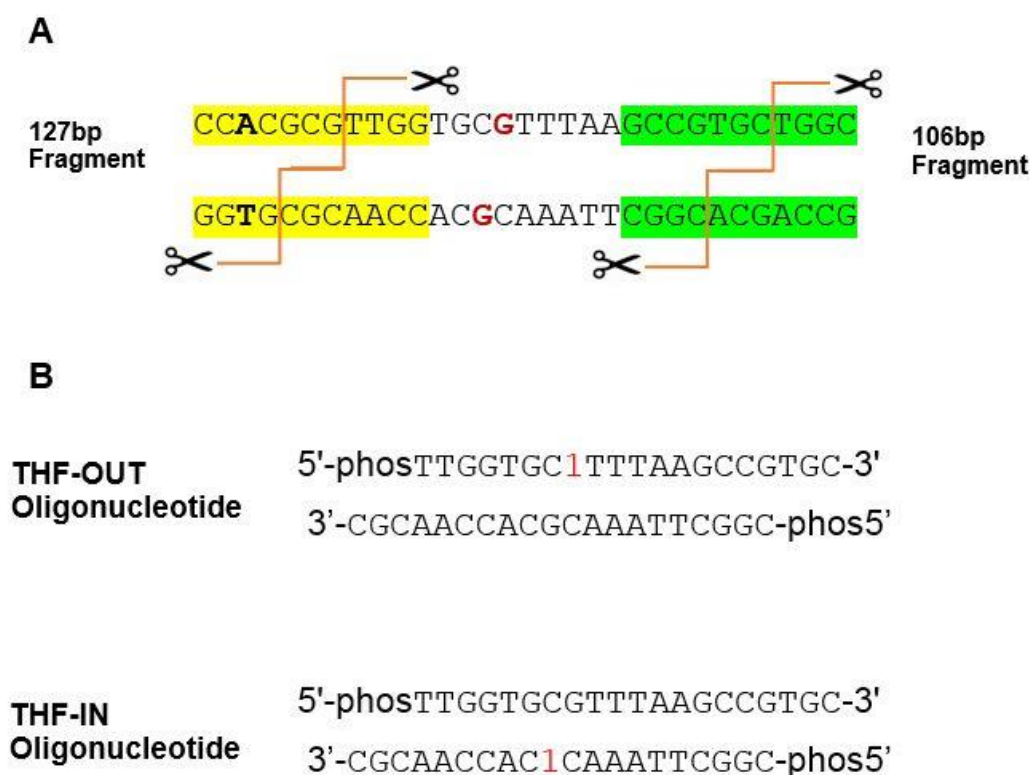


Figure 19: Restriction Digest cut sites and 17bp oligonucleotide insert. **A**, shows the cuts site from Van91 and BglI and the recognition sequences for each highlighted in yellow and green respectively from a sot segment of the 601 nucleosome positioning sequence (figure 18). The red lines through the DNA sequence show the specific cut site of each of the 5' and 3' DNA strands in which the enzymes cut to produce the 127bp and 106bp fragments. **B**, 17 bp oligonucleotide sequence which is ligated into the Widom 601 nucleosome positioning sequence with 3 base overhangs either the 5' or 3' ends depending on the orientation of the THF site (THF-OUT and THF-IN).

2.1.2 Oligonucleotides

2.1.2.1 Oligonucleotides for preparation of THF containing DNA

Fluorescently tagged primers were used to amplify the 601 nucleosome positioning sequence from the P-GEM3Z cloning vector (table 2). Due to the low intensity of IRDYE800 the fluorescent tags were set on the opposite forward and reverse primers for the THF facing inwards nucleosome (THF-IN). Unlabelled primers were also used to amplify the 601 nucleosome positioning sequence which was used in the nucleosome reconstitution as a carrier DNA to inhibit exonuclease activity in the BER *in vitro* assay (table 2). Short oligonucleotide sequences (table 3) were annealed together and used to introduce a THF

(labelled **1**) to the nucleosome DNA sequence, this is a stable equivalent of a AP site (as shown in Figure 19B)

	Primer Sequence
THF Facing Outwards Nucleosome (THF-OUT)	Forward. 5'-IRDYE700-GCTCGGAATTCTATCCGACTGGCACC GGCAAG-3' Reverse. 5'-IRDYE800-GCATGATTCTTAAGACCGAGTTCATCCCTTATGTG-3'
THF Facing Inwards Nucleosome (THF-IN)	Forward. 5'-IRDYE800-GCTCGGAATTCTATCCGACTGGCACC GGCAAG-3' Reverse. 5'-IRDYE700-GCATGATTCTTAAGACCGAGTTCATCCCTTATGTG-3'
Unlabelled 601 DNA sequence	Forward. 5'-GCTCGGAATTCTATCCGACTGGCACC GGCAAG-3' Reverse 5'. 5'-GCATGATTCTTAAGACCGAGTTCATCCCTTATGTG-3'

Table 2: Fluorescently 5' tagged primers for THF containing site DNA preparation. Table shows primer sequences for producing the fluorescently tagged 256bp nucleosome positioning sequence. Fluorescently tagged Primers were obtained from Integrated DNA technologies (Leuven, Belgium). The last row shows primer sequences for unlabelled 601 nucleosome positioning sequence, primers were obtained from Eurogentec (Seraing, Belgium).

	Oligonucleotide Sequence
THF-OUT	5'-phosTTGGTGC 1 TTTAAGCCGTGC-3' 5'-phosCGGCTTAAACGCACCAACGC-3'
THF-IN	5'-phosTTGGTGC GTTTTAAGCCGTGC-3' 5'-phosCGGCTTAAAC 1 CACCAACGC-3'

Table 3: Oligonucleotide sequences with a THF (1**) which is either outwards or inwards facing after nucleosome DNA reconstitution.** Sequences shown to create a 17bp oligonucleotide with either 5' or 3' 3 base overhang, with a THF indicated to as (**1**), this was positioned either on the upper strand THF facing outwards (THF-OUT) or lower strand THF facing inwards (THF-IN). Oligonucleotides were obtained from IDT technologies (Leuven, Belgium).

2.1.2.2 Real-time PCR primer sequences

Real time (RT) PCR primers (table 4) were used to measure the efficiency of siRNA knockdown of 11 E3 ubiquitin ligases in HeLa cells. Actin was used as an expression control and all results were normalised to this CT value.

Gene	RT-PCR primer Sequence	Amplicon (bp)
CUL4a	Forward. 5'-GGACCTCGCACAGATGTACC-3' Reverse. 5'-CGATCGCTGTTCCAAAAGTC-3'	104
RNF8	Forward. 5'-TGTGCTAGAGAATGAGCTCCAA-3' Reverse. 5'-TGTGGGCACAGTTCAAGG-3'	77
RNF168	Forward. 5'-GGCAAGAAAGCTAAGCATTGA-3' Reverse. 5'-GGGTGTAAGTGGATCAGATTTTCT-3'	94
DZIP3	Forward. 5'-TGCCCAAGATCTGATACAAGG-3' Reverse. 5'-CTCCAACACACCACCGTACA-3'	80
MSL2	Forward. 5'-CCCTTTCGTGCTGTGTTTG-3' Reverse. 5'-GCCTTTACAAGTTTTGCAGACAT-3'	95
RNF20	Forward. 5'-GGAGGAGCAGATAGAATACCTACAGA-3' Reverse. 5'-CCATTTTCAAGAGAGGAGTGCTTC-3'	77
RNF2	Forward. 5'-CGGCAGCTGATACCAGAGTC-3' Reverse. 5'-TGCACAGCCTGAGACATTG-3'	85
UBR2	Forward. 5'-CACTTTTCAAGGGCAGAACAG-3' Reverse. 5'-TTTGTCTTTTCAATTTCCGTTG-3'	61
BRCA1	Forward. 5'-TTGTTGATGTGGAGGAGCAA-3' Reverse. 5'-GATTCCAGGTAAGGGTTCC-3'	106
CUL1	Forward. 5'-CCTGGAATTATATAAACGACTTAAGGA-3' Reverse. 5'-TTCAGTACACTCTCATCCATCAAAT-3'	96
MULE	Forward. 5'-CAGCTCCAGCACTCAGTCAA-3' Reverse. 5'-TGAATGCTCTGGCTGCATAC-3'	63
ACTIN	Forward. 5'-AGGCACCAGGGCGTGAT-3' Reverse. 5'-CGCCCACATAGGAATCCTTCT-3'	52

Table 4: Real-time primer sequences for target gene. Primers were obtained from Eurogentec (Seraing, Belgium). Table shows target gene, primer sequence for both forward and reverse, and length of target sequence of gene.

2.1.2.3 SiRNA sequences

Small interfering mRNA (siRNA) sequences were used to interfere and knockdown the expression of specific genes as listed in table 5. A pool of 4 SiRNA sequences were used for every gene to increase the efficiency of the knockdown.

Target Sequence	GenBank Accession	SiRNA sequences
RNF20	NM_019592.6	5'-CCAAUGAAAUCAAGUCUAA-3' 5'-UAAGGAAACUCCAGAAUAU-3' 5'-GCAAAUGUCCCAAGUGUAA-3' 5'-AGAAGAAGCUACAUGAUUU-3'
MSL2	NM_018133.3	5'-GCAGUUCUGUUAUCAUUGG-3' 5'-UCUCUUAGCCAUAAUGUUU-3' 5'-CCAGUACACAUGAUGAUAA-3' 5'-GAGUAUAUAACACAGACUA-3'
RNF2	NM_007212.3	5'-GAGGUUAGCUUUAGAAGAA-3' 5'-GAGAAUACUGGAAAGUGA-3' 5'-GCACAGACGAGAUACAUA-3' 5'-GAGAAGCAGUAUACCAUUU-3'
DZIP3	NM_014648.3	5'-CAAAGUAAACUACAGACUAU-3' 5'-UGACAUAGAUCUACAGAA-3' 5'-GAUCAUGGCAUCUGCUUUA-3' 5'-GAAUACACCCUGAGAU-3'
UBR2	NM_015255.2	5'-GAAGUGUUCUGCUUUUUU-3' 5'-GCAGAACAAUACUCUAAUA-3' 5'-GAAGAAAGUACUCCUAAUA-3' 5'-CAAGAAACCUGGAUUAACA-3'
BRCA1	NM_007294.3	5'-CAGCUACCCUCCAUCAUA-3' 5'-GGGAUACCAUGCAACAUA-3' 5'-GAAGGAGCUUUCAUCAUUC-3' 5'-CAUGAAUUCUGUUGCUAUG-3'
RNF8	NM_003958.3	5'-AGAAUGAGCUCCAAUGUAU-3' 5'-CAGAGAAGCUUACAGAUGU-3' 5'-GAGGGCCAAUGGACAAUUA-3' 5'-CAUUUUGGAUCCUAAGUUG-3'
RNF168	NM_152617.3	5'-GGAAGUGGCUGAUGACUAU-3' 5'-GAAAUUCUCUCGUCAACGU-3' 5'-AGAAGGAGGUGGAUAAAGA-3' 5'-GAGUAUCACUUACGCGCUA-3'
MULE	NM_031407.6	5'-GCAAAGAAAUGGAUAUCA-3' 5'-GGAAGAGGCUAAUUGUCUA-3' 5'-UAACAUCAAUUGUCCACUU-3' 5'-GAAUUGGAUAUCAAACGUA-3'

Target Sequence	GenBank Accession	SiRNA sequences
CUL1	NM_003592.2	5'-CGACAGCACUCAAUUA-3' 5'-GGUUAUAUCAGUUGUCUAA-3' 5'-AGACUUGGAUUUCAGCAUU-3' 5'-CAACGAAGAGUUCAGGUUU-3'
CUL4A	NM_001008895.2	5'-GGAAGAGACUAAUUGC-3' 5'-GAACAGCGAUCGUAUCAA-3' 5'-GCAUGUGGAUUCAAAGUUA-3' 5'-GAACCAUAUUUUAGUGA-3'
HECTD1	NM_015382.3	5'-GAACUGGACUUCUUGUAU-3' 5'-GAAGAAUACCUUAUGG-3' 5'-GGACUUACCUAUUUCUAAA-3' 5'-GUUAAUAGCUGUACUAGAA-3'
YBX1	NM_004559.4	5'-GAGAGACUGUGGAGUUUGA-3' 5'-GCGGAGGCAGCAAUGUUA-3' 5'-GCAGACCGUAACCAUUAUA-3' 5'-GUAAGGAACGGAUAUGGUU-3'
YBX3	NM_003651.4	5'-GGAAUAUCUGCGCAGUGU-3' 5'-GGACAGACCUUGACCGUC-3' 5'-AGACGUGGCUACUAUGGAA-3' 5'-CAACGUCAGAAUGGAUUAU-3'

Table 5: siRNA pool sequences for knockdowns. SiRNA pools were obtained from Dharmacon (Lafayette, Colorado USA). Each SiRNA pool contains 4 individual oligonucleotides (5nmol) lyophilised. SiRNA were diluted to 10µM with RNase-free water in a Tissue culture hood with laminar flow. SiRNA was mixed on an orbital shaker for 30 minutes at room temperature and aliquoted.

2.1.3 Antibodies

Antibodies were used to probe for specific proteins in western blotting to confirm their presence and levels of expression in protein lysates.

Antibody	Reactivity	Concentration (mg/ml)	Dilution	Molecular weight (kDa)	Source
Ubiquitinated Lys119 Histone H2B	Mouse monoclonal	1	1:1000	25	2B Scientific
Ubiquitinated Lys 120 Histone H2A	Mouse monoclonal	1	1:1000	25	Millipore
Actin	Mouse monoclonal	26.1	1:20,000	42	Sigma Aldrich
APE1	Mouse Monoclonal	1	1:10,000	34	Novus Biologicals
His-tag	Mouse monoclonal	0.2	1:1000	N/A	Millipore
CUL4A	Rabbit polyclonal	1	1:5,000	88	Abcam
DDB1	Rabbit polyclonal	0.81	1:2,500	127	Abcam
Mule	Rabbit polyclonal	1	1:2000	482	Bethyl Labs
CHIP	Rabbit polyclonal	1	1:1000	35	Abcam
HECTD1	Rabbit polyclonal	1	1:1000	280	Bethyl Labs
YBX1	Rabbit polyclonal	1	1:1000	50	Bethyl Labs
YBX3	Rabbit Polyclonal	1	1:1000	53	Bethyl Labs

Table 6: Primary Antibodies. Reactivity, concentration, dilution and molecular weight for each primary antibody are shown in table. Antibodies were diluted in Odyssey blocking buffer (Li-cor biosciences, Lincoln, Nebraska, USA). and 1x Phosphate buffered saline (PBS, Fisher scientific UK, Loughborough, UK) 1:1 with 1% tween-20 (Sigma Aldrich, St. Louis, Missouri, USA) and applied to Immobilon-FL polyvinylidene difluoride (PVDF) membranes (Sigma Aldrich, St. Louis, Missouri, USA). Antibodies were obtained from 2B Scientific (Oxford, UK), Abcam, (Cambridge UK), Sigma Aldrich (St. Louis, Missouri, USA), Novus Biologicals, (Ontario, Canada), Merck-Millipore (Watford, UK) and Bethyl Labs, (Montgomery, Texas, USA).

Secondary Antibody	Dilution
IR Dye 800 goat anti-mouse IgG	1:10,000
IR Dye 680 goat anti-rabbit IgG	1:10,000
IR Dye 800 goat anti-mouse IgG	1:10,000
IR Dye 800 goat anti-rabbit IgG	1:10,000

Table 7: Secondary antibodies. Fluorescently tagged secondary antibodies were applied to PVDF membranes (Sigma Aldrich, St. Louis, Missouri, USA) after primary antibody incubation. The corresponding reactivity was selected so secondary antibody could bind to primary antibody. All secondary antibodies were obtained from Li-cor biosciences (Lincoln, Nebraska, USA).

2.1.4 Tissue culture reagents

HeLa cells and AG06173 lung fibroblasts were obtained from Dr Grigory L. Dianov, CRUK/MRC Oxford Institute for Radiation Oncology, University of Oxford, UK). All tissue culture reagents were obtained from Sigma Aldrich (St. Louis, Missouri, USA) as listed below.

- Dulbecco's Phosphate-buffered saline (PBS)
- Trypsin -EDTA solution 0.25% (2.5g porcine trypsin and 0.2g EDTA. 4Na /L of Hank balanced salt solution with phenol red)
- Dulbecco's Modified Eagle's Medium (DMEM) with hydroxyethyl piperazineethanesulfonic acid (HEPES) modification, 4500mg/L 25mM HEPES and sodium bicarbonate, sterile filtered was supplemented with 10% fetal bovine serum (FBS, non-USA origin, sterile filtered) 2mM L-glutamine, 100U penicillin, 0.1mg streptomycin and 1% MEM Non-essential amino acid solution

2.2 Transformation of competent cells

DH5 α cells (Invitrogen, Waltham, Massachusetts, USA) or Rosetta2(DE3)pLysS (Merck-Millipore, Watford, UK) were thawed on ice and mixed gently using a pipette tip. DH5 α cells were transfected with 1 ng purified plasmid and incubated on ice for 30 minutes. The cells were then heat shocked for 20 seconds at 42°C and then left for a further 2 minutes on ice. 10 times warmed lysogeny broth (LB) (2.5 % (w/v) LB granule (Fisher Scientific UK, Loughborough, UK), 0.5 % (w/v) NaOH, pH 7.2) was then added and the cells incubated at 37°C on a shaking incubator for 1 hour. 100 μ l of cells was removed and spread on LB agar plates (2.5 % (w/v) LB granules, 1.5 % (w/v) agar, 0.5 % NaOH and the correct antibiotic (50 μ g/ml ampicillin or 34 μ g/ml kanamycin (Fisher Scientific UK, Loughborough, UK)). These were then incubated at 37°C overnight. Successfully transformed colonies were selected and grown overnight in 5 ml LB containing 50 μ g/ml ampicillin or 34 μ g/ml at 37°C on a shaking platform overnight.

2.2.1 Purifying DNA from bacterial cultures

The overnight cultures were then centrifuged at 5000 x g for 5 minutes to form a pellet and supernatant aspirated. DNA was purified following the QIAprep® Spin Miniprep Kit, manufacturer's protocol (Qiagen, Hilden, Germany) and eluted in TE buffer. The concentration of the DNA was measured using a Nanodrop ND-1000 spectrometer (software version V3.7.1), (Thermo Scientific, Massachusetts, USA) at a wavelength of OD 260nm.

2.3 Polyacrylamide gel electrophoresis (PAGE)

Samples were diluted in 5x EMSA loading buffer (30 % glycerol, 0.25 % xylene cyanol and 0.25 % bromophenol blue (Fisher Scientific UK, Loughborough, UK) and electrophoresed on an 8 % polyacrylamide gel using acrylamide/bis-acrylamide solution 19:1 40 % (w/v) (National Diagnostics, Nottingham, UK) with a 1.5 mm 10-well comb inserted in 0.5x TBE (44.5 mM Tris, 44.5 mM boric acid and 1 mM EDTA (Sigma Aldrich, St. Louis, Missouri, USA) using the Hoefer™ SE400 vertical electrophoresis unit (Fisher Scientific UK, Loughborough, UK), 0.4 % APS and 0.04 % *N,N,N',N'*-Tetramethylethylenediamine (TEMED, Biorad Laboratories Ltd, Hercules, California, USA) were used to initiate polymerisation. Samples were electrophoresed for 3 hours at 175 V and the unit covered for light protection of the fluorescent tags. The gel was then imaged using the Odyssey image analysis system (DNA gel, 0.75mm offset, 680/800 channels).

2.4 Denaturing PAGE

A 8 % polyacrylamide denaturing (7 M urea) polyacrylamide gel in 1x TBE (90 mM Tris, 90 mM Boric acid, 2 mM EDTA) using acrylamide/bis-acrylamide solution 29:1 40% (w/v) (National Diagnostics, Nottingham, UK) was prepared fresh on the day of use and the solution sterile filtered (0.45 µm syringe filter). The Hoefer SE400 vertical electrophoresis unit was used and the solution was poured between glass plates after 0.4 % APS and 0.04 % TEMED were used to initiate polymerisation, and a 1.5 mm 15 well comb inserted. Once polymerised, the gel was pre run to warm the gel to around 40°C by electrophoresis for 10 minutes at 350 V, and wells were washed out using 1x TBE prior to sample loading. Samples were mixed 1:1 with formamide loading dye (formamide 0.025 % (w/v) (9 5% (w/v) Sigma Aldrich St. Louis, Missouri, USA) , heated at 95°C for 5 minutes and loaded onto the 8 % polyacrylamide denaturing gel and electrophoresed for 1 hour at 350 V.

2.5 Sodium dodecyl sulphate polyacrylamide gel electrophoresis (SDS-PAGE) and Western blotting

2.5.1 SDS-PAGE

Proteins were separated by sodium dodecyl sulphate polyacrylamide gel electrophoresis (SDS-PAGE). Gels were prepared by mixing the components of the separating gel together (377 mM Tris HCl pH 8.8, 0.2 % SDS, 2 mM EDTA, and the appropriate concentration of acrylamide/bis solution 30:0.8 (Bio-Rad Laboratories Ltd, Hercules, California, USA). 1 % APS and 0.1 % TEMED were added to initiate polymerisation and the gel poured into a 1.5 mm empty gel cassette until three quarters full and the gel allowed to set following overlay with 100 % ethanol. The percentage gel used was dependent on the size of protein being analysed. The 5 % stacking gel (62.5 mM Tris HCl pH6.8, 0.2 % SDS, 2 mM EDTA, 5 % acrylamide/bis solution 30:0.8 and 10 % APS and 1 % TEMED) was then added to the remaining quarter of the gel cassette, following removal of the ethanol, and either a 10-well or 15-well 1.5 mm comb added and the gel allowed to set. Samples were diluted in SDS-PAGE loading buffer (25 mM Tris pH 6.8, 2.5 % β-mercaptoethanol, 1 % SDS, 5 % glycerol 0.5 mg/ml bromophenol blue, 1 mM EDTA) and proteins denatured by heating at 95°C for 5 minutes. Electrophoresis was performed in 1x Tris-glycine (TGS) SDS buffer, 0.025M Tris, 0.192M glycine and 0.1% SDS, pH 8.5 (Fisher Scientific UK, Loughborough, UK) for 2 hours at 125 V (unless otherwise stated) in the XCell SureLock Mini Cell (Life Tehnologies). The Precision Plus Protein All Blue Pre-stained Protein Standards, Bio-Rad Laboratories Ltd (Hercules, California, USA) were used as standard markers ranging from 10 kDa to 250 kDa.

2.5.2 SDS-PAGE gel protein staining.

The SDS-PAGE gel following electrophoresis (2.5.1) was then rinsed in water and Instant Blue (Expedeon, San Diego, California, USA) added so it covered the gel and incubated on a rotating platform for >15 minutes. The gel was then imaged using the Odyssey image analysis system.

2.5.3 Western Blots

Proteins were separated by SDS-PAGE (see 2.5.1) and transferred onto an Immobilon-FL PVDF membrane (Millipore) by electrophoresis at 25 V for 90 minutes in transfer buffer (25mM Tris pH 8.3, 192mM glycine (Fisher scientific UK, Loughborough, UK), 20% methanol) using the XCell II blot module (Life Technologies, Woolstone, UK). The PVDF membrane was blocked in Odyssey blocking buffer which was diluted 1:1 in 1x PBS for 1 hour at room temperature. The blocking buffer was removed and the membrane probed with the appropriate primary antibody diluted to the relevant concentration (see table 5) in Odyssey blocking buffer and 1XPBS (1:1), 0.1 % tween-20 and incubated overnight at 4°C on a rocking platform. The membrane was then washed three times for 5 minutes with 1x PBS containing 0.1% tween-20 and the relevant secondary added diluted to the suggested ratio (see table 6) in Odyssey blocking buffer and 1X PBS (1:1) with 0.1% tween-20 for 1 hour at room temperature. The membrane was washed as before and an additional final wash was performed with 1x PBS prior to imaging using the Odyssey Image Analysis System.

2.6 HeLa whole cell extract preparation

HeLa whole cell extract (WCE) was prepared as previously described (267). HeLa cell pellets (Cilbiotech, Mons, Belgium) were resuspended in one packed cell volume of buffer I (10 mM Tris-HCl pH 7.8), 200 mM KCl (Sigma Aldrich St. Louis, Missouri, USA), 1 µg/ml of each protease inhibitor; aprotinin, pepstatin, chymostatin and leupeptin (Sigma Aldrich St. Louis, Missouri, USA), 100 µM Phenylmethylsulfonyl fluoride (PMSF) and 1 mM N-ethylmaleimide (NEM, Sigma Aldrich St. Louis, Missouri, USA). Following resuspension two pack cell volumes of buffer II (10 mM Tris-HCl pH 7.8, 600 mM KCl, 40 % glycerol, 2 mM EDTA, 0.2 % NP-40 and 1 µg/ml of each of protease inhibitor, 100 µM PMSF and 1 mM NEM) was added and thoroughly mixed. Cell suspension was mixed by rotation for 30 minutes at 4°C, centrifuged at 72000 x g for 20 minutes at 4°C and supernatant collected and stored at -80°C.

2.6.1 Protein Concentration

Prepared HeLa WCE protein concentration was measured using the Bradford assay using the protein assay dye reagent (Biorad Laboratories Ltd, Hercules, California, USA) to measure the absorbance reading at an optical density of 595 nm using a UV spectrometer. 0.2 mg/ml BSA was used as a protein standard for reference for protein concentration calculation below.

$$BSA = 0.2 / Ab_{BSA} = V$$

$$\text{Samples concentration} = V \times Ab_{\text{sample}} \times \text{dilution factor}$$

2.7 Preparation of purified APE1

2.7.1 Overexpression of his-tagged APE1

His-tagged pET14b APE1 plasmid (provided by Prof Dianov, Oxford Institute for Radiation Oncology) was transformed into Rosetta2(DE3)pLysS bacterial cells, and a colony picked and cultured overnight with 5 ml LB with 30 µg/ml kanamycin (Fisher Scientific UK, Loughborough, UK) and 34 µg/ml chloramphenicol (following 2.2 transformation). If the culture was turbid 300 µl culture was added to 30 ml LB with 30 µg/ml kanamycin and 0.1 % glucose and grown at 37°C at 225 rpm shaking until turbid ($OD_{600} \sim 0.6$ to 0.8). The entire culture was expanded to 300 ml with LB and antibiotic and glucose and incubated with shaking until turbid (OD_{600} 0.6 to 0.8). Protein expression was induced with 1 mM IPTG and incubated at 30°C with shaking for 3 hours. The culture was centrifuged at 5000 x g for 2 minutes, the supernatant aspirated, and pellets were then stored at -80°C.

2.7.2 Purification of his-tagged APE1

The bacterial cell pellet containing overexpressed his-tagged APE1 was resuspended in lysis buffer (25 mM Tris-HCl (pH8), 0.5 M NaCl, 5 % glycerol, 5 mM imidazole, pH 8 (Sigma Aldrich St. Louis, Missouri, USA), 100 mM PMSF and 1 µg/ml of each protease inhibitor; leupeptin, chemostatin, pepstatin and aprotinin). 2 mg lysozyme was added and the cells were incubated on ice for 15 minutes. Cells were lysed by sonication for 3x15 second pulses with 30 seconds intervals on ice. Lysates were transferred to 50 ml Oakridge tubes and centrifuged at 23,000 x g or 20 minutes at 4°C. The supernatant was collected and filtered through a 1 µm syringe prefilters, and then a 0.45 µm syringe filter. A 1 ml HisTrap column (GE Healthcare, Little Chalfont, UK) was attached to the AKTA purifier FPLC and the column washed in the same lysis buffer as above (except 0.1mM PMSF was used). The lysate was added to the column and washed thoroughly until no more protein eluted. Bound proteins were collected by gradient elution with 20 ml lysis buffer and elution buffer (25 mM Tris-HCl pH8, 0.5 M NaCl, 5 % glycerol, 500 mM imidazole and 0.1 mM PMSF) collecting 0.5 ml fractions. Fractions were

analysed by SDS-PAGE and western blotting (see 2.5) using anti-His antibodies to select fractions with purified his-tagged APE1.

2.8 Immunodepletion of proteins

Protein A magnetic agarose beads (Qiagen, Hilden, Germany) were inverted to resuspend beads and 30 µl removed into a fresh 1.5 ml tube for each depletion and control. Beads were washed with 500 µl 1X PBS and a magnetic rack used to attract the beads and the PBS removed and repeated three more times. Beads were resuspended in 300 µl 1x PBS and 0.5 µg antibody when immunodepleting APE1 and 10 µg when immunodepleting HECT Domain E3 Ubiquitin Protein Ligase 1 (HECTD1) added (see table 6 for concentrations). A control of beads without antibody was also prepared for each immunodepletion. Beads were incubated at 4°C on an oscillating platform for 3 hours. The magnetic rack was used again to attract beads and PBS/unbound antibody removed. Beads were washed in 500 µl buffer (50mM Tris-HCl pH 8, 50 mM KCl, 1 mM EDTA, 5 % glycerol) and buffer removed using the magnetic rack and this was repeated three more times. Cell extract (100 µg) was diluted to 200 µl with buffer and added to beads-antibody, and beads alone as a control, and incubated overnight at 4°C on a rotator. The magnetic rack was used to attract beads and the immunodepleted extract removed into a fresh tube. The protein concentration of the cell extract was measured using a Nanodrop ND-1000 spectrometer (software version V3.7.1) at a wavelength of OD 280nm. The immunodepleted extract was analysed using SDS-PAGE and Western blotting (see 2.5) to check for immunodepletion efficiency.

2.9 Tissue Culture

Tissue culture work was carried out in a class II hood with laminar flow (Esco Global, Barnsley, UK) and cleaned with 70 % ethanol thoroughly before and after use. Trypsin, PBS and complete DMEM media (containing 10 % FBS, 2 mM glutamine and 1 % pen-strep) were warmed in a water bath at 37°C prior to use. All tissue culture work was performed using an aseptic technique. All plastics were tissue culture grade and cells were grown in a humidified cell culture incubator in 5 % CO₂ at 37°C.

2.9.1 Defrosting cells

Vials of cells were removed from liquid nitrogen storage, rapidly defrosted for 1 minute in a 37°C water bath, centrifuged at 2000 x g for 5 minutes and DMSO removed. The cell pellet was then diluted in complete DMEM media to 10 ml and transferred to a T75 flask. Cells in the flask were transferred to a humidified cell culture incubator at 5 % CO₂ at 37°C. Once cells were approximately 80 - 90 % confluent the cells were sub-cultured.

2.9.2 Sub Culturing

Once cells had reached approximately 80 % confluence, cells were sub-cultured by aspirating DMEM media from the T75 flask, and washing cells with 10 ml PBS. Cells were then treated with 1 ml trypsin and incubated for 2 minutes (or until cells had lifted from the tissue culture flask base) at 37°C in a tissue culture incubator. Trypsin was neutralised using 9 ml media and cells were sub cultured 1:10 for both HeLa and AG06173 lung fibroblasts. Therefore, 1 ml of cells was transferred to a fresh T75 flask with 25 ml DMEM media and cells cultured in a tissue culture incubator.

2.9.3 Harvesting Cells

Cells (in 100 mm dishes) were removed from the tissue culture incubator, and plates washed with 5 ml cold PBS and aspirated. A further 5 ml of cold PBS was added and cells were carefully scraped off using a cell scraper and added to a 15 ml tube, this was repeated again with another 5 ml cold PBS. Cells were centrifuged at 2000 x g for 5 minutes at 4°C and the supernatant removed. 1 ml cold PBS was used to resuspend the cell pellet which was transferred to a 1.5 ml tube and centrifuged for 5 minutes at 3000 xg at 4°C. The supernatant was removed and cells pellets frozen at -80°C.

2.10 Preparation site-specific THF containing DNA

The plasmid P-GEM3Z containing the Widom 601 nucleosome positioning sequence was transformed and purified from DH5α cells (following 2.2 transformation and DNA purification).. The 601 sequence was then amplified using polymerase chain reaction (PCR) and the central 17bp with 3 base pair overhangs either side (5' or 3' depending on the THF orientation) was removed using a restriction digest and replaced by a duplex oligonucleotide containing a THF by sequential ligation. The THF containing DNA was then purified for use in DNA repair assays either without (free DNA) or with mononucleosome reconstitution.

2.10.1 Amplification of 601 nucleosome positioning sequence

Polymerase chain reaction (PCR) was used to amplify the 601 nucleosome positioning sequence from the P-GEM3Z plasmid. The standard conditions for PCR were 200 μM dNTPS (Sigma Aldrich, St. Louis, Missouri, USA), 1x Phusion HF buffer, 2 mM MgCl₂, Phusion Hot Start II DNA polymerase (Fisher Scientific UK, Loughborough, UK), 0.3 μM of each forward and reverse primers (see table 3) and 25 pg/μl P-GEM3Z plasmid made up to 50 μl with distilled water. Primers were fluorescently tagged with either IR700 (visualised as red) and IR800 (visualised as green) so DNA could be imaged using the Odyssey image analysis

system (Li-cor Biosciences, Lincoln, Nebraska, USA). To create enough 256 bp DNA product, 15 PCR reactions were completed and pooled together. To perform the PCR, 1 cycle of initial denaturation was used for 5 minutes at 95°C, this was then followed by 35 cycles of denaturation at 98°C for 30 seconds, annealing at 57°C for 30 seconds and extension at 72°C for 30 seconds. After this cycling there was a final extension step at 72°C for 5 minutes. The 256bp nucleosome positioning sequence was checked using a 1.5 % agarose gel (broad range agarose) in 1x TAE using a 100 bp DNA ladder and 1X loading buffer (all obtained from Fisher Scientific UK, Loughborough, UK) and electrophoresed at 100 V for 1 hour. The 256 bp substrate was visualised using the Odyssey image analysis system (Li-cor Biosciences, Lincoln, Nebraska, USA).

The PCR reactions were pooled and purified using the QIAquick PCR purification kit according to manufacturer's instructions (Qiagen, Hilden, Germany), split across three columns and eluted in TE buffer. Eluted DNA was combined into a 1.5 ml amber tube for light protection and the concentration measured using Nanodrop ND-1000 spectrometer at a wavelength of OD 260nm.

2.10.2 Restriction digests of the 601 nucleosome positioning sequence

The central 17 bp and 3 base overhangs either side (either on the 3' or 5' ends depending on THF orientation, will just be called 17 bp from here onwards) from the 601 nucleosome positioning sequence 256 bp PCR product was removed by restriction digest using 20 U BglI and 50 U XbaI restriction enzymes with 1 x Buffer R (Fisher Scientific UK, Loughborough, UK) and incubated overnight at 37°C on a shaking platform. To check the efficiency of the restriction digests the digest products, 127bp and 106bp were separated and analysed by 8% PAGE (2.3). After efficient restriction digest of the central 17bp from the 601 nucleosome positioning sequence, the entire sample was loaded onto an 8 % PAGE to separate the digest products and electrophoresed and analysed as before. The digest products were then excised from the gel by aligning the Odyssey image analysis system printed image with the gel and the 127bp and 106bp removed using a scalpel blade, and sliced into small pieces and placed into separate 1.5 ml amber tube. To purify the DNA from gel the freeze/squeeze method (268) was used by freezing the gel pieces at -80°C for a minimum of 20 minutes and the DNA extracted.

2.10.3 DNA Purification from gel pieces

DNA (127 bp and 106 bp separated fragments) in gel pieces following freezing were incubated in TE buffer (10 mM Tris, pH 8 and 1 mM EDTA) at 37°C for 3 hours with shaking and the TE buffer was removed and filtered through 0.45µM Spin-X columns by centrifugation at 20,000 x g for 1 minute. The flow through was collected and transferred to 1.5 ml tubes, the 127 bp and 106 bp digest products were kept separate. Fresh TE buffer was added to the gel pieces and incubated for at least 1 hour and the TE buffer was removed and filtered as before. The gel pieces were then added to the Costar Spin-X centrifuge tube filter (0.45µm, Sigma Aldrich, St.Louis, Missouri, USA) and centrifuged for 5 minutes to remove any residual TE buffer. The filtrates were combined and then concentrated using Amicon Ultra 0.5 ml devices (10 kDa molecular weight cut off (MWCO), EMD Millipore Darmstadt, Germany) for each of the digest products to approximately 50 µl and the concentration checked using Nanodrop ND-1000 spectrometer at a wavelength of OD 260nm. The purification of the two digest products was checked and analysed using PAGE (2.3) on an 8 % polyacrylamide gel.

2.10.4 Preparation of duplex oligonucleotide

The duplex oligonucleotide was prepared for ligation by mixing either the two single strands (20 bases) DNA sequences for THF-OUT or THF-IN (table 3) at 10 pmol for each with 200 mM NaCl in TE buffer. The oligonucleotides were then heated at 95°C for 5 minutes in a metal heat block and then the heat block was removed from the heater (with the sample still in) and allowed to cool to room temperature for approximately 2 hours, this allowed the strands to anneal together. After annealing they formed a 17 bp oligonucleotide with 3 base overhangs either 5' for THF-OUT or 3' for THF-IN, this oligonucleotide will now just be called 17bp duplex oligonucleotide from now on.

2.10.5 Sequential ligation of restriction digest products

The 127 bp DNA from the restriction digest was ligated to the 17bp duplex oligonucleotide which was added in 3 times excess of the 127 bp DNA with 5 U T4 DNA ligase and 1x T4 DNA ligase buffer (Thermo Scientific, Massachusetts, USA) and incubated overnight at 4°C . The efficiency of the ligation was checked and analysed against the 127 bp DNA using 8% polyacrylamide electrophoresed and the 147 bp IR700 tagged ligated DNA visualised. If ligation was unsuccessful, then more duplex oligonucleotide DNA and T4 ligase was added and ligation repeated. The samples were heated at 65°C for 10 minutes to inactivate T4 DNA ligase and denature any duplex oligonucleotide DNA. The DNA was then purified by using the MinElute reaction clean-up kit following manufacturer's instructions (Qiagen, Hilden, Germany). DNA was eluted by two sequential elutions with buffer EB into a 1.5 ml amber tube

following incubation of the column with this buffer for 1 minute and then centrifugation for 1 minute at 17,900xg.

For the second ligation, the 147 bp ligated DNA and the remaining 106 bp DNA fragment were mixed together with 5 U T4 DNA ligase and 1x T4 DNA ligase buffer and incubated overnight at 4°C. The efficiency of the ligation was checked and analysed as with the first ligation and the fully ligated 256bp DNA gel purified, extracted from gel pieces, concentrated and purity checked as stated previously (2.2.5). The concentration of the final 256 bp DNA containing a synthetic THF was determined using Nanodrop ND-1000 spectrometer (software version V3.7.1) at a wavelength of OD 260nm and stored at -20°C until required.

2.11 Expression and purification of Recombinant histones

E.coli were transformed with expression vector *Xenopus Laevis* histones (H2A, H2B, H3 and H4) obtained from Professor Karolin Luger (University of Colorado Boulder, Boulder, USA) and histones were overexpressed following Isopropyl β -D-1-thiogalactopyranoside (IPTG) induction. The bacteria were harvested, the cells lysed and the recombinant histones purified from inclusion bodies by size and ion-exchange chromatography under denaturing condition using AKTA-FPLC. Histones were refolded and combined during dialysis to form the histone octamer and purified using a high salt buffer using a size exclusion column and a FPLC. The purity and stoichiometry of the histone octamer was analysed using SDS-PAGE. Protocol was followed from Luger *et al* (246).

2.11.1 Recombinant Histone Expression

Rosetta2(DE3)pLysS *E.coli* cells were transformed with 0.25 ng pET-expression vector for H2A, H2B and H3, whereas the pET-expression vector for H4 was transformed into Rosetta2(DE3) cells (Both Rosetta Competent Cells, obtained from Merck-Millipore (Watford, UK)). Cells were incubated on ice for 10 minutes, heat shocked for 30 seconds at 42°C and returned to ice for at least 2 minutes. 10 times the volume of cells/plasmid of pre-warmed 2x TY media (1 % (w/v) bacto tryptone, 1 % (w/v) yeast extract, 0.5 % (w/v) NaCl, pH 7 (all Sigma Aldrich, St.Louis, Missouri, USA) and incubated on a shaking platform for 1 hour at 37°C. A third of the cells were plated onto TYE agar plates (1 % bacto tryptone, 0.5 % yeast extract, 0.8 % NaCl, 1.5 % (w/v) agar, 50 μ g/ml ampicillin and 34 μ g/ml chloramphenicol (Fisher Scientific UK, Loughborough, UK)) and incubated overnight at 37°C. In four separate universal tubes 1 ml 2xTY media (with added 50 μ g/ml ampicillin, 34 μ g/ml chloramphenicol and 0.1% glucose (Sigma Aldrich, St. Louis, Missouri, USA) was inoculated with a single colony from each agar plate and incubated at 37°C with shaking until turbid (optical density (OD)₆₀₀ ~ 0.4). 0.5 ml was removed from each culture and added to 10 ml 2xTY (supplements added as

previously) and incubated with shaking as before until turbid ($OD_{600} \sim 0.4$). 8 ml of each culture added to 500 ml 2xTY (supplements added as before) in 2 litre conical flasks and incubated with shaking for a third time until turbid ($OD_{600} \sim 0.4$). Histone expression was induced by adding 0.2 mM IPTG (Fisher Scientific UK, Loughborough, UK) to each culture and incubated at 30°C with shaking for 2 hours. Cells were harvested in 500 ml centrifuge bottles and centrifuged at 3000 x g for 10 minutes at room temperature and the supernatant removed. Each cell pellet was re-suspended in 10 ml wash buffer (50 mM Tris pH 7.5, 100 mM NaCl, 1 mM EDTA, 5 mM β -mercaptoethanol, 0.3 mM PMSF (Sigma Aldrich, St. Louis, Missouri, USA) and transferred to 50ml centrifuge tubes and stored at -80°C.

2.11.2 Inclusion body preparation

The histone proteins are expressed in insoluble form and have to be isolated from inclusion bodies following cell lysis. To do this, the bacterial cells in wash buffer were thawed at 37°C, 10 mg lysozyme (Sigma Aldrich, St. Louis, Missouri, USA) was added and incubated on ice for 30 minutes. The lysates were then sonicated for 2x30 second pulses with 30 second intervals on ice and lysates were transferred to 50 ml Oakridge tubes, (Eppendorf, Hamburg, Germany), and centrifuged at 23,000 x g or 20 minutes at 4°C. The supernatant was removed and 10 ml wash buffer added (made up as previously with added 1% Triton X-100, (Fisher Scientific UK, Loughborough, UK)). Lysates were further sonicated and centrifuged a further three times as before, on the final resuspension 10 ml wash buffer was added without Triton. H4 was an exception, this protein was only sonicated, centrifuged and re-suspended in wash buffer the once as it is prone to lysis. After this final wash step, all histones were centrifuged for a final time, the supernatant poured off and stored at -20°C. Histone purification involved a two-step purification procedure involving gel filtration followed by ion-exchange chromatography using an AKTA fast protein liquid chromatography (FPLC, GE Healthcare, Little Chalfont, UK) under denaturing conditions. Each histone protein was purified separately.

2.11.3 Recombinant Histone Purification by gel filtration chromatography

A fresh 9 M urea (Fisher Scientific UK, Loughborough, UK) stock solution was made in water with heating and deionised using 1 % amberlite IRN150 mixed bed resin (Sigma Aldrich, St. Louis, Missouri, USA) and incubated for 30 minutes at room temperature, prior to filter sterilising using a 0.45 μ m filter. This was used to make up the gel filtration buffer (20 mM sodium acetate pH 5.2, 1 M NaCl, 7 M urea 1 mM EDTA and 5 mM β -mercaptoethanol (Sigma Aldrich St. Louis, Missouri, USA)) and cooled to 4°C. A 320ml Sephacryl S-200 gel filtration column, (GE Healthcare, Little Chalfont, UK) was attached to an AKTA FPLC purifier and equilibrated with gel filtration buffer for 1.5 column volumes at 1.5 ml/min. 400 μ l Dimethyl sulfoxide (DMSO, Sigma Aldrich, St. Louis, Missouri, USA) was added to one of the histone pellets and then minced with a spatula and 10 ml 1x unfolding buffer (7 M guanidinium HCl

(Fisher scientific UK, Loughborough, UK), 20 mM Tris pH 7.5, 10 mM Dithiothreitol (DTT, Sigma Aldrich, St.Louis, Missouri, USA) was added dropwise and the mixture stirred for 1 hour using a magnetic stirrer and stir bar. This was then centrifuged at 23,000 x g for 20 minutes at room temperature, the supernatant removed and filtered using syringe prefilters (1 µm). The sample was then loaded onto the gel filtration column using a 10 ml superloop (GE healthcare, Little Chalfont, UK), at 1.5ml/min. After approximately 85 ml the protein started to elute and 4 ml fractions were collected until the UV signal reduced and stabilised so no more protein was being eluted. The peak fractions were analysed by 16 % SDS-PAGE and gel staining (2.5.1 and 2.5.2 respectively) to identify those containing the relevant histones.

2.11.4 Recombinant Histone Purification by FPLC ion-exchange chromatography

Peak fractions from gel filtration chromatography (2.3.3) that contained histones as analysed by SDS-PAGE were dialysed in snakeskin dialysis tubing (35 mm Dry ID, 7 kDa MWCO, Thermo Fisher Scientific, Massachusetts, USA) in 2 litres of distilled water containing 2 mM β-mercaptoethanol at 4°C for 2 hours. The water was then replaced with fresh water and 2 mM β-mercaptoethanol and dialysed overnight at 4°C. The dialysed fractions were collected and concentrated by Amicon Ultra centrifugal concentrators (3 kDa MWCO, Merck-Millipore, Watford, UK) to approximately 1-2 ml. A 1 ml HiLoad 16/10 sepharose high performance MonoS column (GE Healthcare, Little Chalfont, UK), was attached to AKTA FPLC and the column was equilibrated with cold low salt buffer (20 mM NaAc pH 5.2, 0.1 M NaCl, 7 M urea (prepared from 9 M deionised stock), 1 mM EDTA, 5 mM β-mercaptoethanol) for 3 column volumes at 1 ml/min. The dialysed histone sample was then loaded onto the column and washed until no more protein eluted. Histone proteins were gradient eluted from the column using 20 ml low salt buffer and high salt buffer (20 mM NaAc pH 5.2, 1 M NaCl, 7 M urea (prepared from 9 M deionised stock), 1 mM EDTA, 5 mM β-mercaptoethanol) at 1 ml/min collecting 0.5 ml fractions. The peak fractions were analysed by 16 % SDS-PAGE as previous. Fractions identified to contain histones were pooled and dialysed in snakeskin dialysis tubing (35 mm Dry ID, 7 kDa MWCO) in 2 litres water with 5 mM β-mercaptoethanol at 4°C overnight. This was then replaced with fresh water and 5 mM β-mercaptoethanol for 4 hours, the dialysed fractions collected and concentrated to 0.5 ml using Amicon Ultra centrifugal filter (3 kDa MWCO). The concentration of the histones was measured Nanodrop ND-1000 spectrometer at a wavelength of OD 280nm using molecular weights and extinction coefficients (ε) in table 8. Histones were aliquoted in the following equimolar amounts ready for octamer preparation; 2mg H2A, 2mg H2B, 2.25mg H3, 1.17mg H4 and stored at -80°C.

Histone	Molecular weight (kDa)	ϵ (cm/M) x 10 ³
H2A	13.96	4.05
H2B	13.77	6.07
H3	15.27	4.04
H4	11.24	5.4

Table 8: Histone molecular weights and molar extinction coefficients – Molecular weight and ϵ was used to determine the concentration of each histone using a nanodrop.

2.11.5 Refolding of the Histone Octamer

Each histone aliquot was dissolved to a concentration of 2 mg/ml using 1.25x unfolding buffer (25 mM Tris-HCL pH 7.5, 8.75 M guanidinium HCL, 12.5 mM DTT) resulting in a final concentration of 1x unfolding buffer. Histones were incubated on ice for 2 hours to allow the proteins to unfold. All the histones were then mixed together and an equal volume of 1x unfolding buffer added to create a 1 mg/ml solution. Histones were dialysed in snakeskin dialysis tubing (35 mm Dry ID, 7 kDa MWCO) in 600 ml refolding buffer (10 mM Tris-HCl pH7.5, 2 M NaCl, 1 mM EDTA, 5 mM β -mercaptoethanol) for 6 hours at 4°C and then dialysed overnight in fresh refolding buffer. The histones were further dialysed for 4 hours in fresh refolding buffer. The dialysed histone octamer was centrifuged at 23,000 x g for 20 minutes at 4°C and the supernatant collected and concentrated using Amicon Ultra centrifugal concentrators (10 kDa MWCO) to 400 μ l. This was then loaded on a 24 ml Superdex 200 10/300GL gel filtration column (GE Healthcare, Little Chalfont, UK), attached to a FPLC and previously equilibrated with refolding buffer and 0.5ml fractions collected until the UV signal reduced and stabilised. Peak fractions were analysed using 16 % SDS-PAGE and gel staining using Instant blue (2.3.4 and 2.3.5) and fractions containing the histone octamer in the correct equimolar ratios were pooled and concentrated to 0.5 ml using Amicon Ultra centrifugal concentrators (10 kDa MWCO). A Nanodrop spectrometer at a wavelength of OD 280nm was then used to check the concentration of the histone octamer was approximately 10 mg/ml (absorbance at 0.45 for a 1 mg/ml solution), and then 40 % glycerol and 2 M NaCl was added and the histone octamer stored at -20°C.

2.12 Analysing APE1 activity in mononucleosomal and free DNA

Mononucleosome substrates were created with the free THF containing DNA and the histone octamer, both prepared as described above. The level of activity of purified, recombinant APE1 using mononucleosome substrates with a THF facing either outward or inwards from

the nucleosome core was measured and the activity compared between the two substrates. These substrates were also incubated with HeLa whole cell extract (WCE). The activity of APE1 and HeLa WCE using THF containing free DNA was also used as a control.

2.12.1 Nucleosome Reconstitution

The nucleosome reconstitution mix was prepared by mixing 5 pmol fluorescently-labelled 256 bp THF DNA, 75 pmol unlabelled 601 nucleosomal DNA sequence (using non fluorescent primers (see table 2) but amplified using same PCR reaction and cycles as the preparation of THF containing DNA), 50 µg bovine serum albumin (BSA) molecular biology grade (New England Biolabs Ltd, Luton, UK), 0.01 % NP-40, 2 M NaCl, 94 pmol Histone Octamer in a final volume of 280 µl distilled water. The total volume increased to approximately 300 µl after dialysis. All volumes were adjusted if less DNA was used. The mix was then incubated for 10 minutes at room temperature and transferred to 6.4 mm diameter dialysis tubing 8 kDa MWCO (Fisher Scientific UK, Loughborough, UK) which had been rinsed with distilled water and 0.1 mg/ml BSA prior to use. The nucleosome reconstitution mix was then dialysed in 500 ml of decreasing concentrations of NaCl; 1.6 M, 1.2 M, 0.8 M, 0.6 M, 0.2 M, 0.075 M NaCl, with 10 mM Tris HCl pH 7.4, 1 mM EDTA and 5 mM β-mercaptoethanol for 1.5 hours each and the final dialysis left overnight (0.075 M NaCl). The nucleosome reconstitution was removed from the dialysis tubing into a 1.5 amber tube and the efficiency of the nucleosome reconstitution analysed using a 0.7 % agarose gel in 0.02x TAE buffer and 5 nM SYTO60 red fluorescent nucleic acid stain. 50 fmol of the nucleosome reconstitution and free DNA (from preparation of free DNA) with 5xloading buffer were loaded onto the agarose gel with a 100 bp DNA ladder and electrophoresed at 75 V for 1.5 hours and imaged using the Odyssey Image Analysis system. Successful nucleosome reconstitution was visualised as a shift to a heavier molecular weight of approximately 700 bp (but not high molecular weight species indicative of protein aggregates) to form a mononucleosome substrate with a THF facing either outwards or inwards from the nucleosome (depending on which tagged 256 bp THF DNA substrate used). The mononucleosome substrate was stored at 4°C.

2.12.2 Preparation of Free DNA

Free DNA was prepared as a control, to mimic the conditions of the nucleosome. In this instance, 5 pmol labelled 256 bp THF containing DNA was mixed with 75 pmol unlabelled 601 nucleosomal DNA sequence, 50 µg BSA, 0.075 M NaCl, 10 mM Tris-HCl pH 7.4, 5 mM β-mercaptoethanol and the volume made up to 300µl with distilled water and stored at 4°C.

2.12.3 *In Vitro* BER Repair Assay and DNA extraction

A reagent mix (Mix A) was prepared on ice containing 1 x BER buffer (40 mM Tris-HCl pH 8, 5 mM MgCl₂, 0.1 mM EDTA, 0.5 mM DTT), 2 mM ATP, 1 µg BSA (deacetylated) and 50 fmol DNA (either free DNA or mononucleosomal DNA) and made up to 6 µl with distilled water per reaction. An enzyme/extract mix (Mix B) was prepared with increasing concentrations of purified his-tagged APE1 or HeLa whole cell (WCE) diluted buffer in RWDB buffer (25 mM Tris HCl pH 8, 100 mM KCl, 12 mM MgCl₂ 1 mM EDTA, 17 % glycerol, 2 mM DTT). Where indicated, reactions were also supplemented with 5 mM Nicotinamide adenine dinucleotide (NAD, Sigma Aldrich St. Louis, Missouri, USA), 0.7 pmol UBE1 activating enzyme, 2.5 pmol E2 conjugating enzymes (a combination of 10 different E2s pooled in equimolar ratios; UbE2H, Cdc34, UbE2D1, UbE2D2, UbE2D3, UbE2E1, UbE2L3, UbE2L6 and UbE2C) and 0.6 nmol ubiquitin (Boston Biochemicals, Cambridge, Massachusetts, USA). The His-tagged E1 and E2s (UBE1) were prepared by Dr Jason Parsons following overexpression of the proteins in bacterial cells, and purified by His-trap chromatography similar to APE1 described above (2.4.4.2). Mix A was added to Mix B and incubated at 30°C for set time periods (either 10 minutes or 1 hour). The reaction was stopped by adding to a final concentration 20 µM EDTA and 0.4 % SDS in a final volume of 25 µl with distilled water. 50 µl phenol:chloroform:isoamyl alcohol 25:24:1 (Sigma Aldrich St. Louis, Missouri, USA) was further added and the sample was vortexed and centrifuged at 15,000 x g for 1 minute. The upper aqueous (DNA containing) layer was removed and transferred to a fresh 1.5ml tube. 50 µl chloroform:isoamyl alcohol 24:1 (Sigma Aldrich St. Louis, Missouri, USA) was then added and the sample was centrifuged again and the upper aqueous layer removed, this step was then repeated. The aqueous layer was then mixed with 10 µg glycogen, 1/10 volume of 3 M NaAc pH 5.2 and 2.5 volumes of cold 100% ethanol. Samples were mixed by inverting the tubes 3 to 5 times and incubated at -80°C for >1 hour. Samples were centrifuged at 16,000 x g for 30 minutes and the supernatant aspirated, 3 volumes of cold 70% ethanol added and centrifuged for a further 10 minutes and the supernatant aspirated. Pellets were left to air dry for 5 minutes and 10 µl TE buffer added and pellets thoroughly resuspended. Samples were analysed by 8% denaturing PAGE (2.4).

2.13 HeLa Cell Fractionation

Candidate histone modifiers (eg. E3 ubiquitin ligases, chromatin remodellers) were fractionated and purified by sequential chromatography of HeLa cell pellets. Individual fractions were analysed using the mononucleosome THF facing inwards substrate, which is not efficiently repaired by recombinant APE1 only, utilising the BER assay after each chromatography step. Fractions that stimulated recombinant APE1 activity for incision of the THF (active fractions) above the threshold value (60 fmol APE1 added which causes ~20 %

incision) were pooled and further fractionated by chromatography to further purify histone modifiers.

2.13.1 Preparation of HeLa Whole cell extract for Phosphocellulose Chromatography

HeLa WCE was prepared (as shown in (2.6) using 20 g HeLa cell pellets) and dialysed to reduce NP-40 and KCl concentrations using snakeskin dialysis tubing (35 mm Dry ID, 10 kDa MWCO, Thermo Fisher Scientific, Massachusetts, USA) in 3 litres of 150 mM KCL buffer (1 mM DTT, 100µM PMSF) for 12 hours at 4°C. The WCE was centrifuged at 72000 x g to remove precipitated proteins for 20 minutes at 4°C, and the supernatant filtered through a 1 µm syringe prefilter and then through a 0.45 µm syringe filter.

2.13.2 Phosphocellulose Chromatography

A 250 ml phosphocellulose column, prepared using P-11 cellulose and an XK50/20 column (GE Healthcare, Little Chalfont, UK), was equilibrated in PC150 buffer (50 mM Tris-HCl pH 8, 150 mM KCl, 1 mM EDTA, 5 % glycerol, 1 mM DTT, 1 mM PMSF) using an AKTA purifier FPLC. HeLa WCE was loaded onto the column and unbound protein were eluted and collected until the UV signal stabilised, this was designated the PC150 fraction. Proteins that were bound to the column were eluted by PC1000 buffer (50 mM Tris-HCl pH 8, 1000 mM KCl, 1 mM EDTA, 5 % glycerol, 1 mM DTT, 1 mM PMSF), this was designated the PC1000 fraction.

2.13.4 Ion exchange chromatography (MonoQ)

A 20 ml HiLoad 16/10 Q Sepharose high performance column (GE Healthcare, Little Chalfont, UK) was equilibrated in Mono Q buffer 1 (50 mM Tris-HCl pH 8, 50 mM KCl, 1 mM EDTA, 5 % glycerol, 1 mM DTT, 1 mM PMSF) by washing in three column volumes using a AKTA purifier FPLC. The PC150 fraction (collected following phosphocellulose chromatography) was diluted 1:1 with a no salt buffer (50 mM Tris-HCl pH 8, 1 mM EDTA, 5 % glycerol) and passed over the column. Following washing of the column for 3-5 volumes, proteins were eluted using a 400 ml salt gradient using Mono Q buffer II (50 mM Tris-HCl pH 8, 1000 mM KCl, 1 mM EDTA, 5 % glycerol, 1 mM DTT, 1 mM PMSF) and 4 ml fractions collected. 500 µl aliquots from each fraction were concentrated using a Amicon Ultra 0.5 ml devices (10MWCO) by centrifugation at 15000 x g to 50 µl and then buffer exchanged (50 mM Tris-HCl pH 8, 50 mM KCl, 1 mM EDTA, 10 % Glycerol, 1 mM DTT, 1 mM PMSF) prior to analysis of activity using concentrated (10 x) fractions.

2.13.5 Gel filtration

Using an AKTA purifier FPLC, a 24 ml Superdex 200 10/300GL column (GE Healthcare, Little Chalfont, UK) was equilibrated in PC150 buffer (see 2.5.2). For each identified activity eluting from the MonoQ chromatography, 4 ml fractions were pooled and concentrated using Amicon Ultra 15 ml centrifugal concentrators (10 kDa MWCO) to 500 µl at 15000 x g. The concentrated samples were then individually loaded onto the gel filtration column and 0.5 ml fractions collected until the UV signal stabilised. Fractions were analysed for activity and active fractions were pooled for the next chromatography stage.

2.13.6 Final Ion exchange (MonoQ) chromatography

A 1 ml MonoQ 5/50 GL column (GE Healthcare, Little Chalfont, UK) was equilibrated in MonoQ buffer I (see 2.13.4). Active fractions from the gel filtration chromatography stage were loaded onto the column and the column washed with buffer for 3-5 column volumes. Proteins were eluted using a 20 ml salt gradient using Mono Q buffer II (see 2.5.5) in 0.5 ml fractions. Fractions were analysed for activity and the most active fraction from each activity was analysed by mass spectrometry by Dr Deborah M Simpson (Centre for Proteasome Research, University of Liverpool) to identify candidate E3 ubiquitin ligases and/or chromatin remodellers.

2.14 Seeding cells for RNA interference

2.14.1 Seeding cells for preparation of WCE

Cells were removed from T75 flasks using trypsin (see 2.9.2 above), and following neutralisation with complete DMEM media, cells were counted using a haemocytometer. Cells were subsequently seeded at 0.5×10^6 cells per 100 mm dish 10 ml complete DMEM media, or 1.5×10^5 cells per 35 mm dish in 2 ml complete DMEM media. Cells were grown until 70-80 % confluence before RNA interference.

2.14.2 RNA interference

Cellular protein levels were down-regulated by siRNA-mediated mRNA depletion. siRNA primers for target proteins are shown in table 4. Lipofectamine RNAiMAX (Invitrogen, Waltham, Massachusetts, USA) was used to transfect cells with siRNA sequences. Cells were seeded in either 100 mm or 35 mm dishes until 30-50 % confluent. Per 100 mm dish, 10 µl lipofectamine RNAiMAX was added to 0.5 ml DMEM media (no supplements added) and separately 40 nM siRNA was added to 0.5 ml DMEM media (no supplements added), these were mixed by inversion 5 times and incubated for 5 minutes. The lipofectamine

RNAiMAX mix was added to the siRNA mix, mixed by inversion as before and incubated for a further 10 minutes. This 1 ml solution was added drop wise to cells and dishes transferred to a tissue culture incubator where they were incubated for 48 hours. For 35 mm dishes, 2.5 µl Lipofectamine RNAiMAX and 40 nM siRNA was added to cells in 250 µl using the same method.

2.15 Reverse Transcription and Real-time PCR

The RNeasy Mini kit (Qiagen, Hilden, Germany) was used to extract RNA from cell pellets following manufacturer's instructions. Briefly pelleted HeLa cells following siRNA knockdown were resuspended in 350 µl buffer RLT and mixed with 350 µl 70% ethanol, the total mixture was transferred to a RNeasy Mini spin column and centrifuged at 8000xg for 15 seconds (all centrifugations were at this speed and time for the rest of the protocol unless stated). 700 µl Buffer RW1 was added to column and centrifuged, 500 µl buffer RPE was then added twice and centrifuged after each addition. The column was then dried by centrifugation for 1 minute and 30 µl RNase free water added and then centrifuged for 1 minute to elute RNA. The concentration of RNA was measured using a Nanodrop ND-1000 spectrometer (software version V3.7.1) at a wavelength of OD 260nm. The GoScript™ Reverse Transcription System (Fitchburg, Wisconsin, USA) was used to generate cDNA from purified mRNA according to manufacturer's instructions. Briefly up to 5µg RNA (concentrations were kept the same siRNA knockdowns and the control) was incubated with 0.5µg Oligo(dT)₁₅ at 70°C for 5 minutes and ice for 5 minutes. The reverse transcription mix was made with the following components, 4 µl GoScript™ 5x reaction buffer, 1.4mM MgCl₂, 0.5mM PCR nucleotide mix, 0.5µl Recombinant RNasin ribonuclease inhibitor, 1µl GoScript™ reverse transcriptase and made up to 15 µl with nuclease free water, the 5µl RNA and primer mix was then added. This mix was incubated at 25°C for 5 minutes for annealing, extended by heating at 42°C for 1 hours and the reverse transcriptase inactivated by incubation at 70°C for 15 minutes. SYBR® Select Master Mix (Thermo Scientific, Massachusetts, USA) was utilised to amplify cDNA using primers in table 4 for quantitative Real Time PCR analysis using the 7500 Real Time PCR system (Applied Biosystems, Warrington, UK) software version v2.3. A cycle threshold value (CT) was provided of the run for the gene/s of interest and the reference gene actin following their knockdown by SiRNA. Further calculations (see below) determined relative quantities of mRNA (RQ value) and so statistical analysis of knockdown efficiency could be calculated. The RQ value allowed us to analyse if successful knockdown of target genes was successful.

$$\begin{aligned}\Delta CT &= CT_{\text{gene}} - CT_{\text{reference gene}} \\ \Delta\Delta CT &= \Delta CT_{\text{control}} - \Delta CT_{\text{treatment}} \\ RQ &= 2^{\Delta\Delta CT}\end{aligned}$$

2.16 Clonogenic survival assay

HeLa cells were seeded on 35 mm dishes at 1.5×10^6 cells and transfected with siRNA targeting each of the genes YBX1, YBX3, and HECTD1 and a control (lipofectamine RNAiMAX only) as in section 2.6.4. After 48 hours, cells were irradiated at 0-4 Gy using the CellRad X-ray irradiator (Faxitron, Tucson, Arizona, USA) at 3 Gy/min. Following irradiation the media was aspirated, cells were washed in 1 ml PBS, 200 μ l trypsin added to the cells which were incubated at 37°C until cells lifted of the tissue culture dishes. Trypsin was neutralised in 800 μ l media and cells counted using a haemocytometer. A defined number of cells were seeded in 2 ml complete DMEM media at two different cell densities in triplet for each irradiation treatment in 6-well plates. Number of HeLa cells seeded per well in a 6 well plate, for lipofectamine RNAiMAX only and YBX1 SiRNA; 0 Gy 250 and 500, 1 Gy 500 and 1000, 2 Gy 1000 and 2000, 4 Gy 2000 and 4000, and for HECTD1 and YBX3 SiRNA; 0 Gy 500 and 1000, 1 Gy 1000 and 2000, 2 Gy 2000 and 4000, 4 Gy 4000 and 8000. The cell numbers were increased for increasing ionising radiation doses and double the number of cells were used for HECTD1 and Y-Box proteins 3 (YBX3) compared to the control and YBX1 which allowed for cell plating efficiencies. The plates were incubated in a tissue culture incubator at 37°C, 5 % CO₂ for 7-10 days when colonies were clearly visible (>50 cells/colony). Cells were fixed and stained by removing media, washing the cells in PBS, and adding 0.5 % crystal violet in 6 % glutaraldehyde (bot Fisher Scientific UK, Loughborough, UK) for 1 hour. The dye was removed and plates washed in water and allowed to dry overnight. The GelCount colony counter (Oxford Optronix, Oxford, UK) was used to accurately count the numbers of colonies. The average plating efficiency for the untreated control plate was calculated by the number of colonies, divided by how many cells were plated and the average calculated for the two seeding density triplicates. To determine the surviving fraction, the surviving counts for each condition was divided by the number of cells plated times by the average plating efficiency.

2.17 Alkaline COMET assay

The alkaline comet assay was used to study repair kinetics following irradiation as described (269). Therefore HeLa cells and AG06173 lung fibroblasts that had been transfected with siRNA for either HECTD1 or YBX3 were trypsinised, diluted to 1×10^5 cells/ml and 250 μ l cell suspension placed into a 24 well plate. Cells were irradiated with 1.5 Gy using the CellRad X-ray irradiator at 3 Gy/min. Following irradiation, 1 ml 1 % low melting point agarose (Fisher Scientific UK, Loughborough, UK) in PBS was added to the cell suspension and which was then added to a pre-coated microscope slides (800 μ l 1 % normal melting point agarose in distilled water) which had been allowed to dry overnight. A 22 x 50 mm cover slip was added and the slides were kept on ice to allow the agarose with cells to set, and then placed in a 37°C humidified incubator for a selected length of time to allow for DNA repair. At the end of the repair time, coverslips were removed and slides were placed into coplin jars containing

cold lysis buffer (2.5 M NaCl, 100 mM EDTA, 10 mM Tris base, pH 10.5 and containing 10 % DMSO and 1 % tween-20 added just before use). Cells were left to lyse for >1 hour at 4°C. Slides were transferred to an electrophoresis tank and slides immersed in cold electrophoresis buffer (300 mM NaOH, 1 mM EDTA, 1 % DMSO, pH>13). Electrophoresis was performed at 25 V for 25 minutes ensuring the current was 300 mA by adding or removing buffer. The slides were removed and covered with 1 ml neutralisation buffer (500 mM Tris-HCl pH 8) for 5 minutes and repeated a further two times and slides air dried overnight. Slides were rehydrated with distilled water for 30 minutes and 1 ml SYBR Gold (Fisher Scientific UK, Loughborough, UK) diluted 1:20,000 diluted in distilled water (pH 8) added for 30 minutes. Slides were then air dried overnight. Slides were imaged using the BX61 Olympus microscope and 10x magnification (Olympus, Shinjuku, Japan) by taking 10 images per slide, containing at least 5 cells per image, using two slides per time point and therefore counting 100 cells in total. The experiment was performed in triplicate. Images were analysed using Komet 6.0 software (Andor Technology, Belfast) in order to calculate % tail DNA values.

CHAPTER III

RESULTS I

Generation of the Mononucleosome Containing Site Specific Damage

3.1 Introduction

Chromatin is a tightly packed unit of DNA, histones and non-histone proteins as described previously. Access to occluded sites is facilitated through chromatin remodelling events which make DNA more accessible to proteins involved in many biological processes such as DNA transcription and replication. This process is also required for DNA repair, however evidence for this has mainly been focussed on DSB repair and NER, and that occurring during BER is limited. However it is thought that chromatin remodelling occurs due to published studies indicating that certain BER enzymes are significantly less efficient at sterically occluded sites; particularly when lesions where the DNA backbone is facing inwards and when they are located near the dyad axis (94) (242, 254). Nevertheless, the precise mechanisms and enzymes involved to facilitate BER by remodelling such as PTM events and chromatin remodellers are unknown at this time. I hypothesised that a PTM event by a histone modifying enzyme takes place that is either sufficient enough alone to cause chromatin relaxation, or actively recruits an ATP-dependent chromatin remodelling complex to cause chromatin relaxation allowing access to occluded sites and so facilitating BER.

To look at nucleosome dynamics *in vitro* during BER, I aimed to firstly mononucleosome substrates were generated that contained a synthetic AP site (THF) either with the DNA backbone facing inwards (THF-IN) or facing outwards (THF-OUT), which allowed us to examine APE1 activity in the nucleosome context. To achieve this the Widom 601 nucleosome sequence was used due to its strong nucleosome positioning ability, and the DNA was then subsequently engineered to contain a THF lesion within the central 17bp region removed, either on the upper DNA strand (5' → 3') or lower strand (3' → 5'). The THF was chosen as it displays virtually no difference with regards to APE1 activity compared to glycosylase generated AP sites, but importantly is much more stable. The histone octamer was made using recombinant histone proteins from *Xenopus Laevis*, which are commonly used to generate *in vitro* mononucleosomes as the histones are homologous and are of a high purity (246). The substrates were designed so that when the THF was located on the upper strand, an THF-OUT mononucleosome was formed when the THF site containing DNA was

reconstituted with the histone octamer, Alternatively, an THF-IN containing mononucleosome substrate was generated when the lower strand contained a THF (see figure 20 for their positions within the crystal structure of the Widom 601 sequence mononucleosome). These positions were equivalent to +12 for THF-OUT and +11 for THF-IN when counting from the nucleosome dyad axis based on sequences from Smerdon *et al* (242). These mononucleosome substrates were then used to analyse the effect of orientation on APE1 activity.

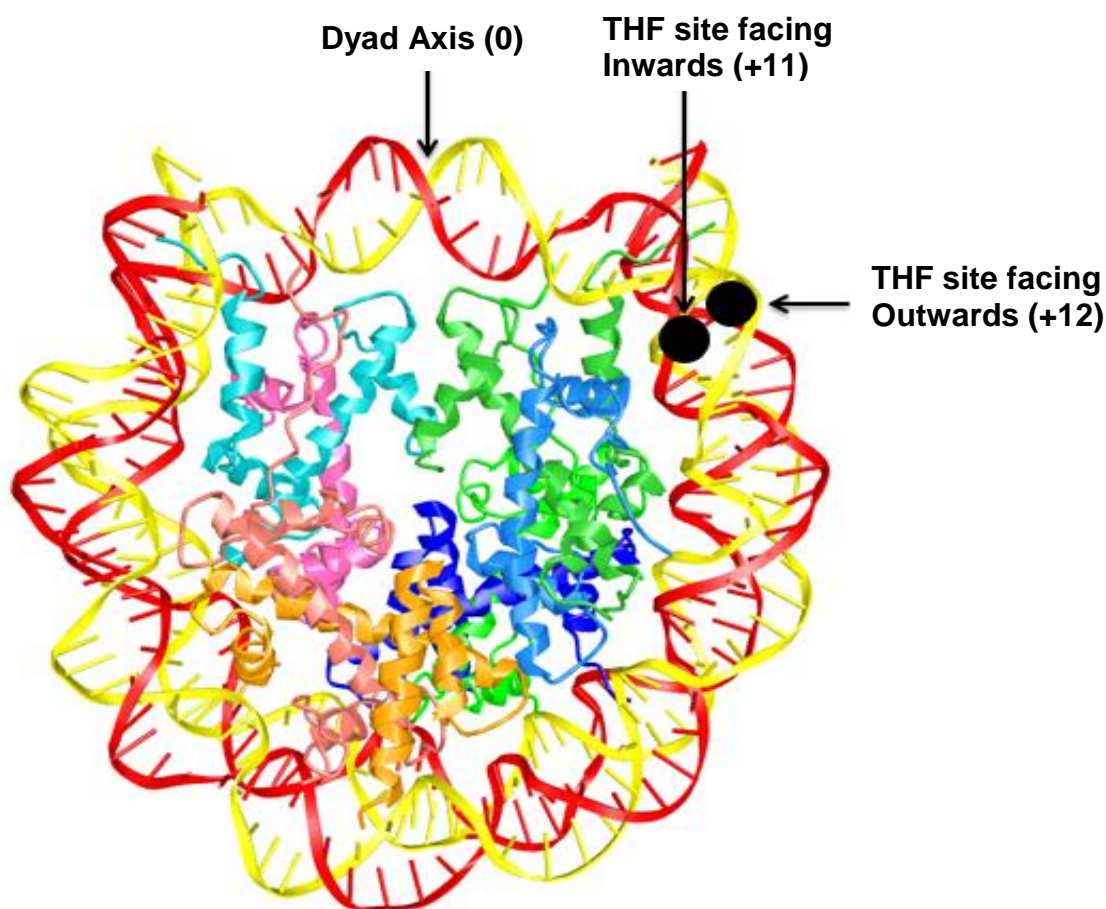


Figure 20; Positions of THF sites in the crystal structure of the nucleosome core particle containing the Widom 601 nucleosome. Crystal structure PDB ID [3LZ0](#) obtained and modified from (270) orientation 1. The crystal structure of the Widom 601 nucleosome core particle showing the translational position (numbered with respect of location from the dyad axis which is translational position 0) and orientation (DNA backbone outwards facing towards solvent and DNA backbone inwards facing towards the histone octamer labelled) of THF sites in reconstituted mononucleosomes indicated to in black circles.

3.2 Preparation site specific THF site containing DNA

To produce mononucleosome substrates containing site specific THF sites to analyse APE1 activity, it was initially important to formulate a method producing a segment of DNA with nucleosome interacting properties containing these damaged sites. Two DNA substrates were generated containing a site specific THF site either on the upper or lower strand in the central area of the DNA sequence. Restriction sites and the location of the THF site can be found in Chapter 2 Materials (2.1.1, figure 18 and 19). The Widom 601 sequence was amplified from a plasmid using PCR and the central 17 bp removed using restriction enzymes to produce two DNA sequence fragments which were purified from one another. A 17 bp duplex oligonucleotide containing a THF either on the upper or lower strand was prepared and sequentially ligated to each of the purified DNA sequence fragments from the restriction digest from the Widom 601 nucleosome positioning sequence. This method resulted in the production of two site specific THF site DNA substrates, which when reconstituted with the histone octamer, formed mononucleosomes with the DNA backbone containing the THF facing either inwards or outwards, figure 21.

3.2.1 Amplification of 601 nucleosome positioning sequence

The Widom 601 wild- type nucleosome positioning sequence which has strong nucleosome affinity was amplified from the P-GEM3Z plasmid by PCR using primers containing 5'-fluorescent labelled dye; IRDye800 (green tagged) or IRDye700 (red tagged) on either the forward or reverse primers, which was dependent on which type of THF site was generated. The IRDye700 was always located on the strand of DNA that contained the THF due to the increased signal intensity of this tag so THF incision could be better visualised using the Odyssey Image Analysis system. The schematic diagram in Figure 21 shows the process in which substrate DNA was created and then wrapped around a histone octamer to reconstitute the nucleosome. Following PCR to amplify the 601 nucleosome positioning sequence, a restriction digest removed the central 17bp region leaving 127 bp and 106 bp DNA products. A 17 bp oligonucleotide with a THF was sequentially ligated to the 127 bp and 106 bp PCR products. This produced a DNA fragment of 256 bp containing a THF which could then be reconstituted with a histone octamer to form a nucleosome.

Figure 22A shows the 256 bp 601 nucleosome positioning sequence PCR product that was produced following PCR in yellow as it contained both IRDye700 and IRDye800 5' tagged ends. PCR reactions were equally efficient whether a 5'-IRDye700 labelled primer was used to amplify the upper strand (Figure 22Ai) or whether a 5'-IRDye800 labelled primer was used (Figure 22Aii). The fluorescent primers used are also clearly visible underneath each of the

PCR products. The 256 bp DNA was subsequently purified using a PCR purification kit and the yield was found to be approximately 100 µg for 15 PCR reactions that were pooled.

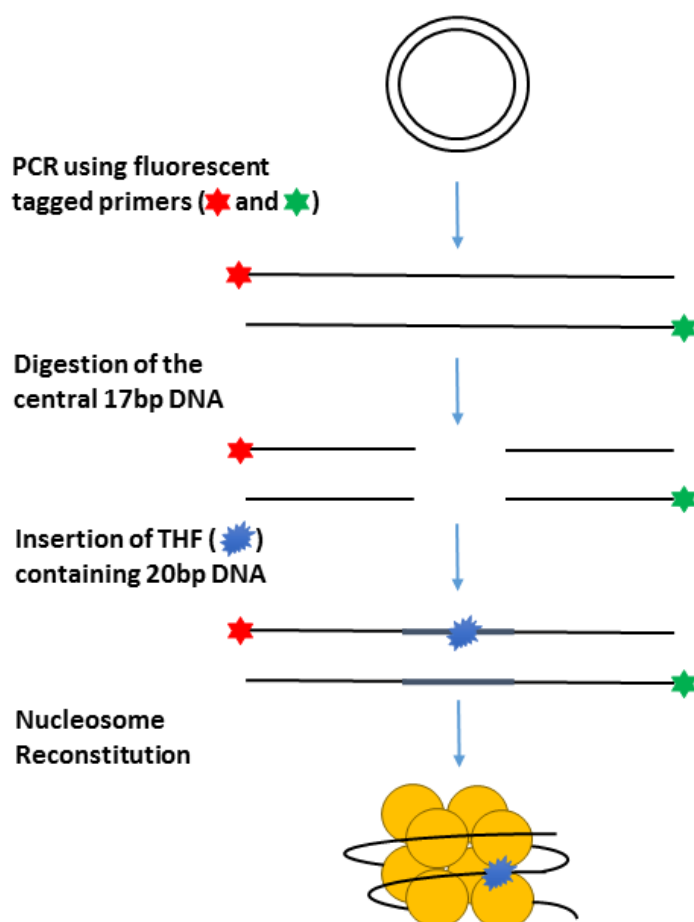


Figure 21; Schematic diagram showing the formation of the THF containing DNA and nucleosome. The 256 bp Widom 601 nucleosome positioning sequence was amplified from a plasmid using PCR using fluorescently tagged primers shown as red and green stars in the diagram. The central 17 bp was then removed by utilised a digest to produce a red tagged (red star) 127 bp digest product and green tagged (green star) 106 bp digest product (when producing a THF-OUT mononucleosome). A 17 bp oligonucleotide (shown in grey) containing a THF (blue shape) was then sequentially ligated to the 127 bp and 106 bp DNA producing the final 256 bp DNA which was then reconstituted with the histone octamer to form the nucleosome.

3.2.2 Restriction digest of the 601 nucleosome positioning sequence

Following purification of the 601 nucleosome positioning sequence, the restriction digest enzymes *Van91I* and *BglI* were utilised to remove the central 17 bp region, the position and area these enzymes cut is also shown in Figures 18 and 19 in Chapter 2 Materials (2.1.1). These enzymes produce sticky ends which are DNA overhangs that facilitate the subsequent ligations (Figure 19). After the Widom 601 nucleosome positioning sequence was treated with these enzymes the 100 % efficiency of the digestion was assured producing 106 bp and 127 bp DNA segments (Figure 22B, lane 2) in comparison to the original PCR product (Figure 22B, lane 1). Digestion efficiency was the same whether 5'-IRDye700 labelled primer was used to amplify the upper strand (Figure 22Bi) or whether a 5'-IRDye800 labelled primer was used (Figure 22Bii). As a result, following digestion the 127 bp DNA segment is either visualised as a red band (Figure 22Bi) or a green band (figure 22Bii), and vice versa for the 106 bp segment. The 127bp and 106 bp DNA segments were then purified from each other using PAGE separation and gel extraction, and their effective purification and quality analysed (Figure 22Ci and Cii).

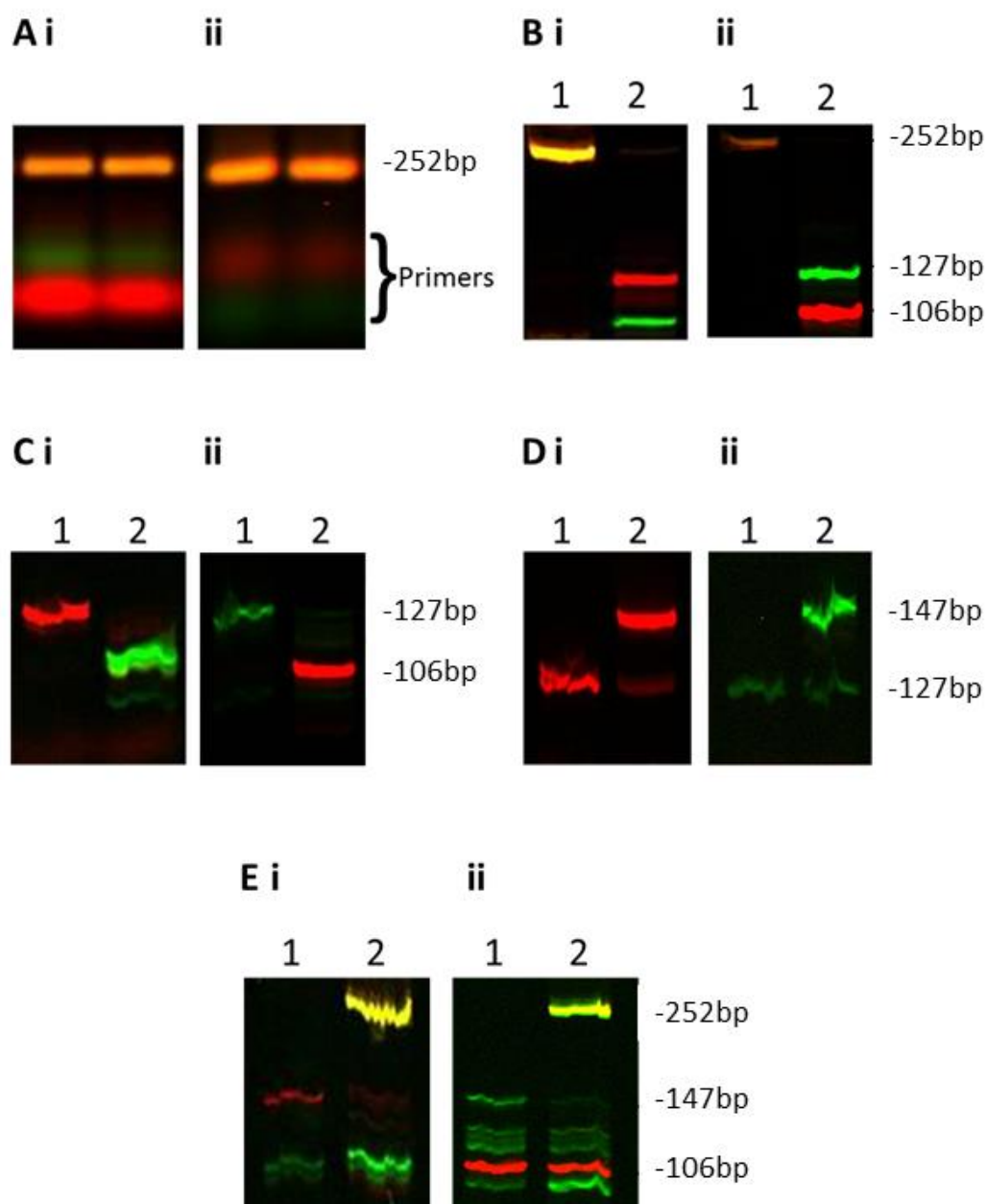


Figure 22: DNA Substrate Preparation containing a site specific THF site. **A**, PCR of nucleosome positioning 601 wild-type sequence containing both the IRDye800 and IRDye700 florescent tags separated by electrophoresis on a 1.5 % agarose gel at 100 V for 1 hour. **B**, Products before (lane1) and after digestion (lane 2) with BglI and Van91 yielding the 127 bp and 106 bp products. **C**, After gel purification of the 127 bp (lane 1) and 106 bp (lane 2) products. **D**, Before (lane 1) and after ligation (lane 2) of the 127 bp band with the 17 bp duplex oligonucleotide. **E**, Before (lane 1) and after the second (lane 2) ligation using the 147 bp and 106 bp products, producing a 256 bp product containing a THF. DNA substrate preparation using either 5'-IRDye700 labelled primer to amplify the upper strand (i) or the lower strand (ii) are shown. All PAGE gels (B, C, D and E) contained 8 % polyacrylamide and 0.5x TBE, and were run for 2.5 h at 175 V.

3.2.3 Sequential ligation of restriction digest products

The 127 bp and 106 bp DNA segments from the 601 nucleosome positioning sequence were ligated sequentially to maximise ligation efficiency to a pre-prepared 17 bp duplex oligonucleotide with complementary sticky ends, the sequence of these is shown in figure 19B and table 3 in Chapter 2 Materials (2.1.2). Two oligonucleotide duplexes corresponding to different orientations of the THF site (THF-OUT and THF-IN) were used. The 127 bp was initially ligated to the 17 bp oligonucleotide duplex, which was successful as a ligated 147 bp DNA segment was observed for both DNA substrates utilising either a 5'-IRDye700 labelled (Figure 22Di, lane 2) or a 5'-IRDye800 labelled (Figure 22Dii, lane 2) 127 bp fragment. This was purified using the MinElute reaction clean up kit and then ligated to the 106 bp DNA segment. Successful ligation was evidenced by the formation of the full 256 bp substrate DNA, utilising a 5'-IRDye700 labelled 147 bp segment in combination with a 5'-IRDye800 labelled 106 bp segment (Figure 22Ei, lane 2). Or of ligation of a 5'-IRDye800 labelled 147 bp segment with a 5'-IRDye700 labelled 106 bp segment (Figure 22Eii, lane 2). The full 256 bp substrate DNA produced a yellow coloured band, being the combination of both the IRDye700 and IRDye800 DNA ends. This was then purified using gel extraction and used in the nucleosome reconstitution with the prepared histone octamer. At this point, I had now successfully developed a method to generate substrate DNA containing a site specific THF site which I could use to examine APE1 incision activity rates. Substrates were labelled so the IRDye700, the most intense signal when imaging was on the DNA strand which would be incised by APE1 (so the upper strand for THF-OUT and the lower strand for THF-IN) so the incision rate by APE1 could be better visualised.

3.3 Expression and purification of recombinant histones for histone octamer preparation

E.coli were individually transformed with expression vectors for *Xenopus Laevis* histones (H2A, H2B, H3 and H4) and the proteins overexpressed following IPTG induction. The bacteria were harvested, the cells lysed and the recombinant histones purified from inclusion bodies by size exclusion and ion-exchange chromatography under denaturing conditions (7 M urea), using an AKTA purifier FPLC. The histones were then unfolded, combined together in equimolar ratios, and refolded to form the histone octamer. The octamer was subsequently purified in high salt containing buffer using a size exclusion column and an FPLC. The strategy of the histone purification process is shown in figure 23.

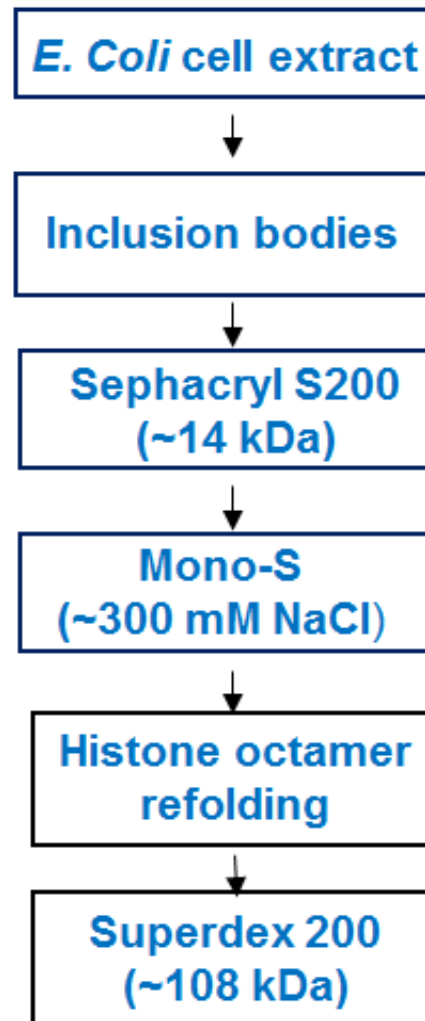


Figure 23: Steps of the purification process of histones and refolding of the histone octamer. Flow chart shows the stages in the purification process of histones and finally refolding of the histone octamer. Firstly each histone was overexpressed in *E.coli* following IPTG induction and bacterial cells were harvested and lysed. Histones were then separately purified from inclusion bodies by size exclusion chromatography using a Saphacryl S200 column eluting at around 14 kDa and ion exchange chromatography using a Mono-S column eluting at around 300 mM NaCl, both purification steps were under denaturing conditions (7M urea). The presence of histones in fractions was analysed by SDS-PAGE and instant blue protein staining. Once purified histones were mixed in equimolar ratios and allowed to refold to form the histone octamer. The histone octamer was purified by size exclusion chromatography using a Superdex 200 column with a high salt buffer (2 M NaCl) and proteins eluted around 108 kDa. The purity and stoichiometry of the histone octamer was analysed by SDS PAGE and protein staining and histone octamer containing fractions pooled.

3.3.1 Recombinant Histone Purification by gel filtration chromatography

Once individual histones H2A, H2B, H3 and H4 had been expressed in *E.coli* following IPTG induction, bacterial cells were harvested and lysed, and histones purified from inclusion bodies under denaturing conditions. This initial step of purification was by gel filtration chromatography using a Sephacryl S200 column in combination with an AKTA purifier FPLC. The UV trace and fractions number collected when protein started to elute from AKTA FPLC which correlates to the amount of protein that is being eluted are shown for each of the four histones; H2A (Figure 24Ai), H2B (Figure 24Bi) H3 (Figure 25Ai) and H4 (Figure 25Bi). In general these traces show two major peaks, the first relating to bacterial protein contaminants, and the second later peak relating to the histone of interest. The proteins within these fractions were separated by SDS PAGE and proteins stained (Figure 24Aii, 24Bii, figure 25Aii and 25Bii, for H2A, H2B, H3 and H4, respectively). H2A and H2B have molecular weights of 13.96 and 13.77 kDa respectively and these proteins were shown to elute in fractions 11-15 for H2A and 10-14 for H2B (Figure 24Aii and Bii). Note that the upper band are the full length histones and the lower band corresponds to histones that are slightly degraded. H3 and H4 have molecular weights of 15.27 kDa and 11.24 kDa, respectively. Fractions 8-13 for H3 and fractions 13-19 for H4 were found to contain these histones (Figure 25Aii and Bii). Of note is the very low concentration of H4 in the UV trace and SDS PAGE protein stained gel (Figure 25Bii), which has been previously documented (246). Fractions containing the individual histones were pooled together for further protein purification by ion-exchange chromatography.

3.3.2 Recombinant histone purification by ion-exchange chromatography

Pooled fractions for each histone were dialysed in distilled water containing 2 mM β -mercaptoethanol and then purified by ion-exchange chromatography using a MonoS column using an AKTA purifier FPLC, again under denaturing conditions. Fractions were collected following salt gradient elution and proteins levels and fraction numbers are shown on the UV traces (Figure 26Ai for H2A; Figure 26Bi for H2B; Figure 27Ai for H3; Figure 27Bi for H4). Fractions containing protein were separated by SDS PAGE and analysed by protein staining (Figure 26Aii for H2A; Figure 26Bii for H2B; Figure 27Aii for H3; Figure 27Bii for H4). Fractions 13-19 contained protein for H2A and degraded H2A was observed in fractions 8-12 (Figure 26Aii). Fractions 16-21 contained H2B and degraded H2B was found in fractions 8-15 (Figure 26Bii). Fractions 14-21 contained full length H3 protein and its degraded form in fractions 10-13 (Figure 27Aii). Fractions 12-14 had H4 protein present and H4 degradation (lower band) based on the SDS-PAGE protein stained gel, although protein levels for H4 were extremely low (Figure 27Bii). Fractioning containing individual histones were pooled, dialysed in distilled water containing 2 mM β -mercaptoethanol and then concentrated. The protein concentration measured for each histone using molecular weights and extinction coefficients were as follows; H2A 6 mg, H2B 7 mg, H3 12 mg and H4 1.16 mg per 2 litre bacterial culture.

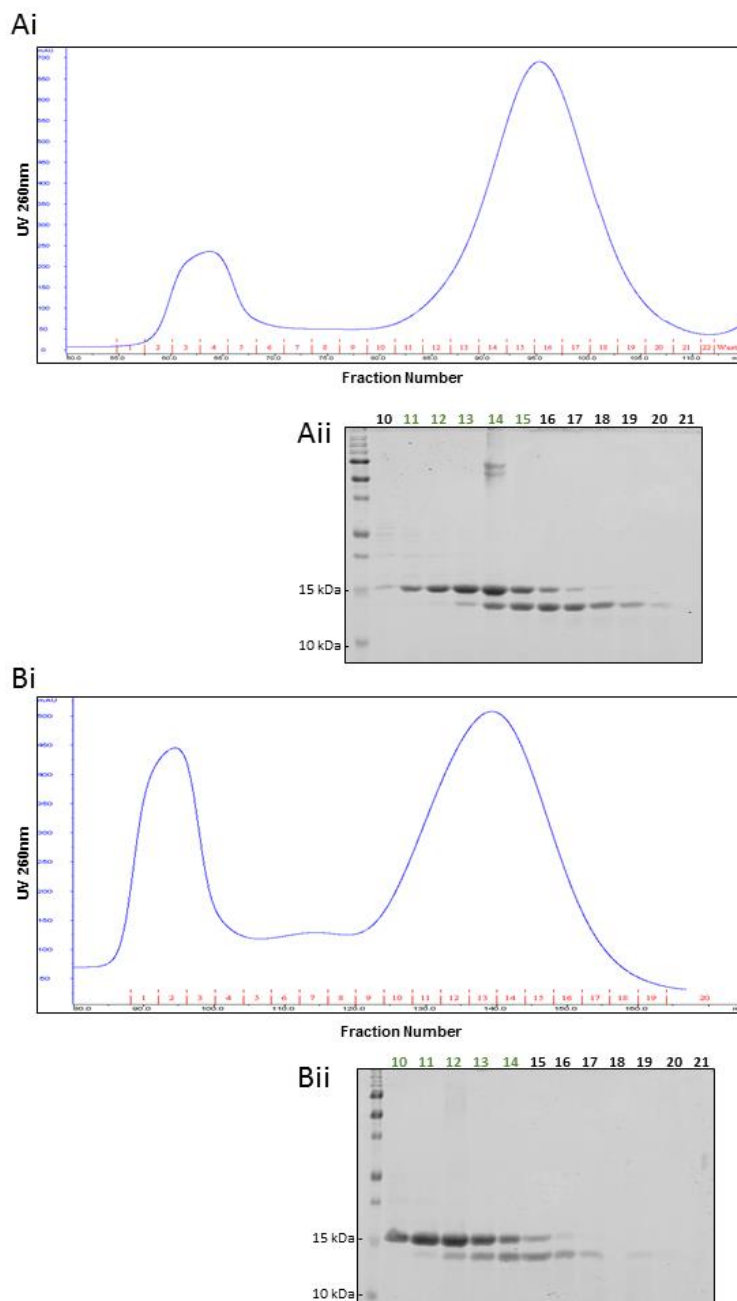


Figure 24: Purification of recombinant histones H2A and H2B by gel filtration chromatography. Following protein overexpression, the recombinant histones were initially purified by a gel filtration column Sephacryl S-200 for size exclusion chromatography under denaturing conditions (7 M urea) and an FPLC. **Ai** (H2A) and **Bi** (H2B), UV traces from FPLC are shown for histones with the fraction number shown below in red. **Aii** (H2A) and **Bii** (H2B) fractions were probed for histones using a SDS gel stained with Instant blue for each histone (fraction number indicated to in each image) with protein marker for 10 kDa to 250 kDa, the fraction designated to in green were pooled. All SDS-PAGE gels contained 16 % polyacrylamide and run for 2.5 h at 175 V.

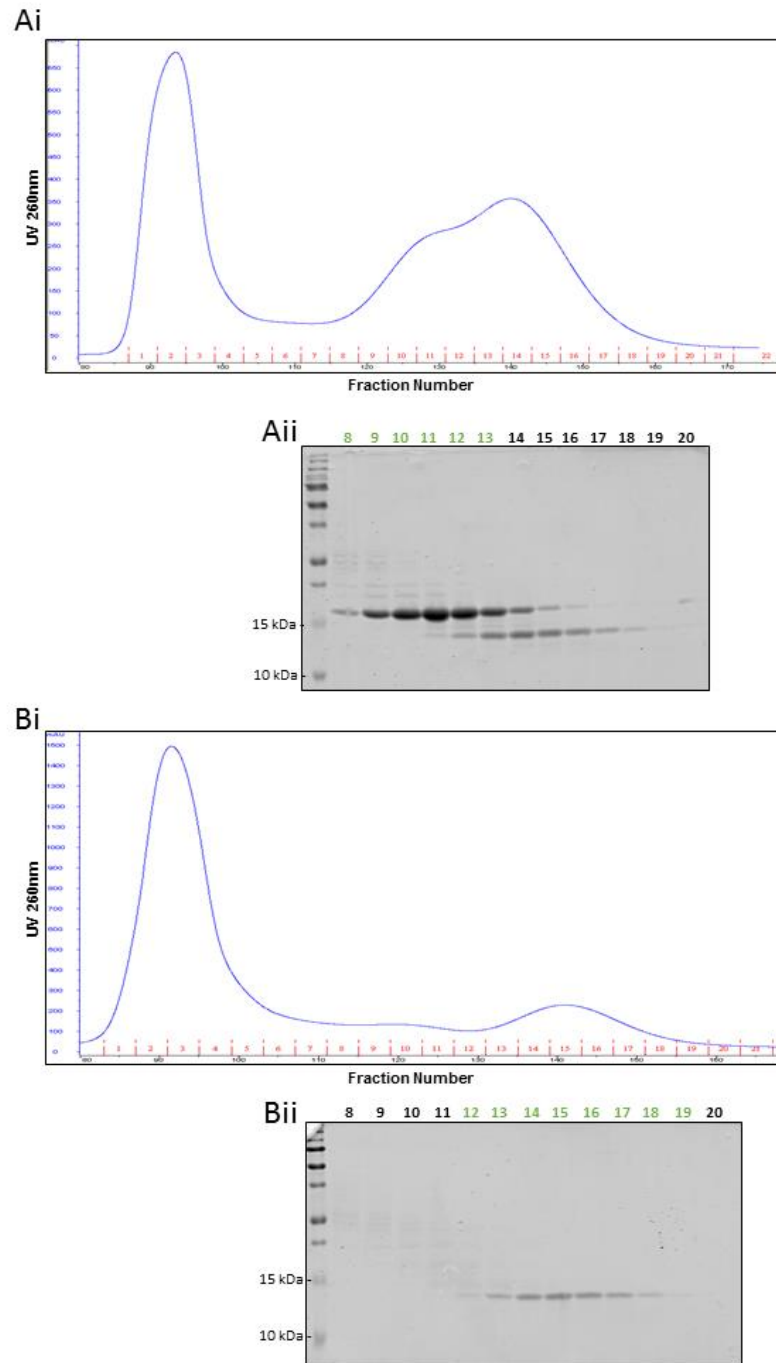


Figure 25: Purification of recombinant histones H3 and H4 by gel filtration chromatography. Following protein overexpression, the recombinant histones were initially purified by a gel filtration column Sephacryl S-200 for size exclusion chromatography under denaturing conditions (7 M urea) and an FPLC. **Ai** (H3) and **Bi** (H4), UV traces from FPLC are shown for histones with the fraction number shown below in red. **Aii** (H3) and **Bii** (H4) fractions were probed for histones using a SDS gel stained with Instant blue for each histone (fraction number indicated to in each image) with protein marker for 10 kDa to 250 kDa, the fraction designated to in green were pooled. All SDS-PAGE gels contained 16 % polyacrylamide and run for 2.5 h at 175 V.

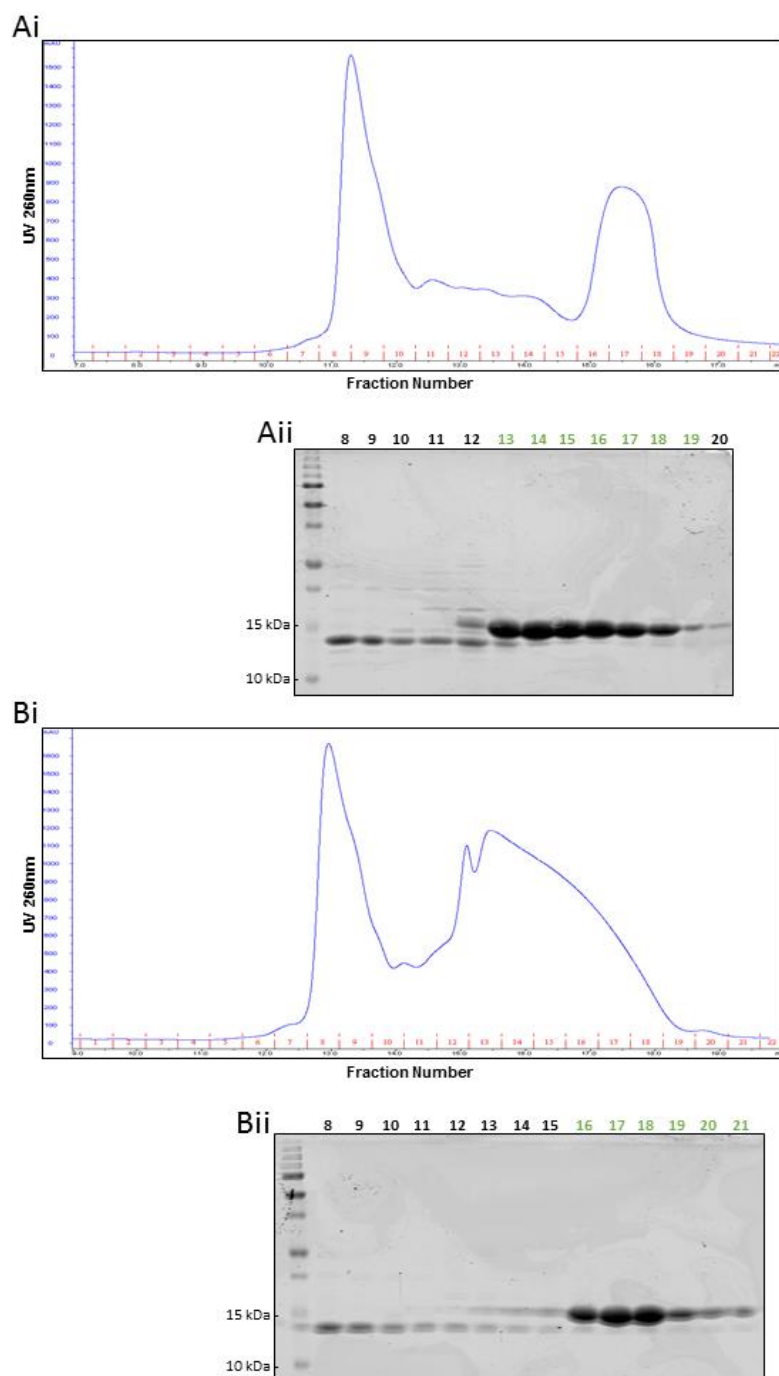


Figure 26: Purification of recombinant histones H2A and H2B by ion-exchange chromatography. Following initial histone purification by gel filtration the pooled fractions were then separated by an ion exchange column Mono S under denaturing conditions (7 M urea) to further purify the histones. **Ai** (H2A) and **Bi** (H2B), the UV traces from FPLC are shown for each histone with the fraction number shown below in red. **Aii** (H2A) and **Bii** (H2B), fractions where major UV peaks were seen were probed for histones using a SDS gel stained with Instant blue for each histone (fraction number indicated to in each image) with protein marker for 10 kDa to 250 kDa, the fractions designated to in green were pooled. All SDS-PAGE gels contained 16 % polyacrylamide and run for 2.5 h at 175 V.

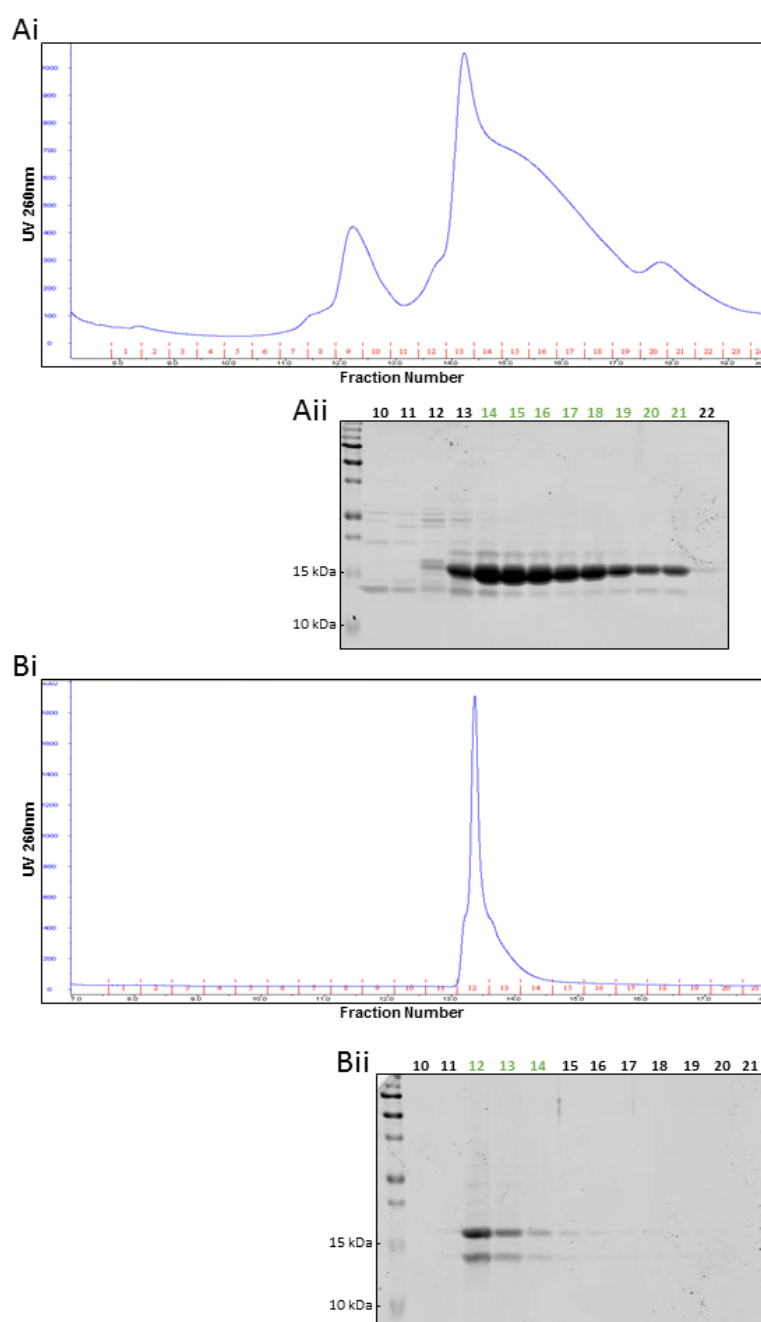


Figure 27: Purification of recombinant histones H3 and H4 by ion-exchange chromatography. Following initial histone purification by gel filtration the pooled fractions were then separated by an ion exchange column Mono S under denaturing conditions (7 M urea) to further purify the histones. **Ai** (H3) and **Bi** (H4), the UV traces from FPLC are shown for each histone with the fraction number shown below in red. **Aii** (H3) and **Bii** (H4), fractions where major UV peaks were seen were probed for histones using a SDS gel stained with Instant blue for each histone (fraction number indicated to in each image) with protein marker for 10 kDa to 250 kDa, the fractions designated to in green were pooled. All SDS-PAGE gels contained 16 % polyacrylamide and run for 2.5 h at 175 V.

Following purification of each histone, it was found that the concentration of H4 was too low for generating the histone octamer and therefore the purification of H4 was repeated, but with the modifications as follows. After sonication and centrifugation the subsequent wash steps were removed prior to purification by Sephacryl S200 gel filtration. Fractions were collected and the UV trace obtained from the FPLC are shown (Figure 28Ai) in addition to separation of proteins by SDS PAGE and analysis by protein staining using a protein marker 10 kDa to 250 kDa (Figure 28Aii). Fractions 12-19 were shown to contain H4, which were then pooled, dialysed and then purified by ion-exchange chromatography using a MonoS column. Fractions were collected and the UV trace obtained from the FPLC is shown (Figure 28Bi) and the fractions separated by SDS PAGE and analysed by protein staining (Figure 28Bii). A small amount of degraded H4 was seen in fractions 8-13, whereas fractions 14-20 contained full length H4 protein. Therefore these latter fractions were pooled, and the total yield of H4 obtained was 18 mg per 2 L bacterial culture. This amount of H4 was sufficient enough with the other histones (H2A, H2B and H3) to form the histone octamer.

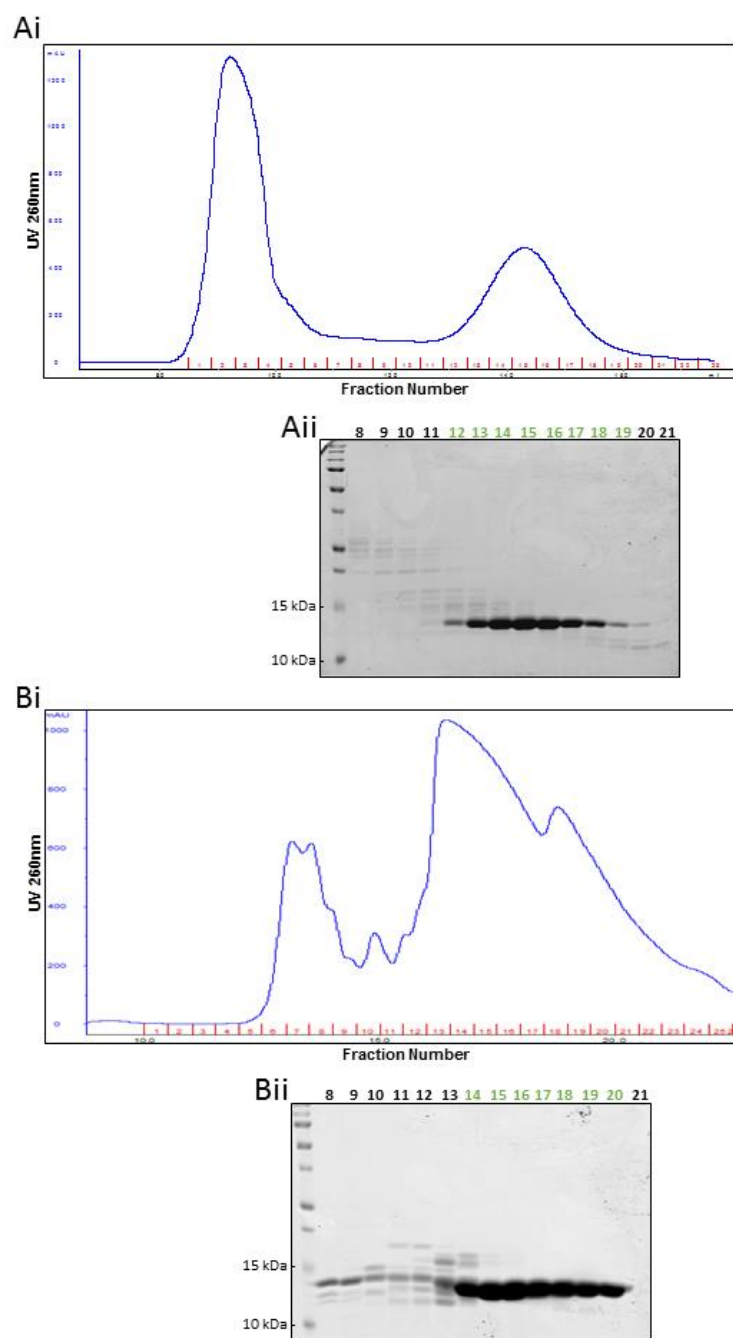


Figure 28: Purification of Histone H4. Following protein overexpression in *E. coli*, recombinant histone H4 was purified by a two-step purification process under denaturing conditions (7 M urea) utilising an FPLC as previous, but including a minor modification whereby the wash steps following sonication were removed to improve H4 purification yield. **Ai (H4)** UV trace and **Aii (H4)** SDS PAGE gel stained with Instant blue from FPLC from the gel filtration column Sephacryl S-200 for size exclusion chromatography, where the fraction numbers indicated in green were pooled. **Bi (H4)** UV trace and **Bii (H4)** SDS PAGE gel stained with Instant blue from the fractions separated by an ion exchange column Mono S, and where the fractions indicated in green were pooled. All SDS-PAGE gels contained 16 % polyacrylamide and run for 2.5 h at 175 V.

3.3.4 Refolding of the Histone Octamer

Purified histones were mixed in equimolar ratios in an unfolding buffer, dialysed in refolding buffer and the subsequent octamer formed was purified by gel filtration chromatography using a Superdex 200 column. Fractions were collected and the UV trace obtained from the AKTA FPLC are shown (Figure 29A) in addition to separation of proteins by SDS-PAGE and analysis by gel protein staining (Figure 29B). Fractions 28-32 contain H2A and H2B dimers which have failed to form the octamer fully with H3 and H4, however fractions 23- 27 show histone octamer formation at the expected molecular weight (~108 kDa). These fractions containing the histone octamer were pooled, concentrated and glycerol added to stabilise the octamer prior to storage. This octamer preparation acted as a source for use in the nucleosome reconstitution with the site specific THF site containing DNA to generate the mononucleosome substrates.

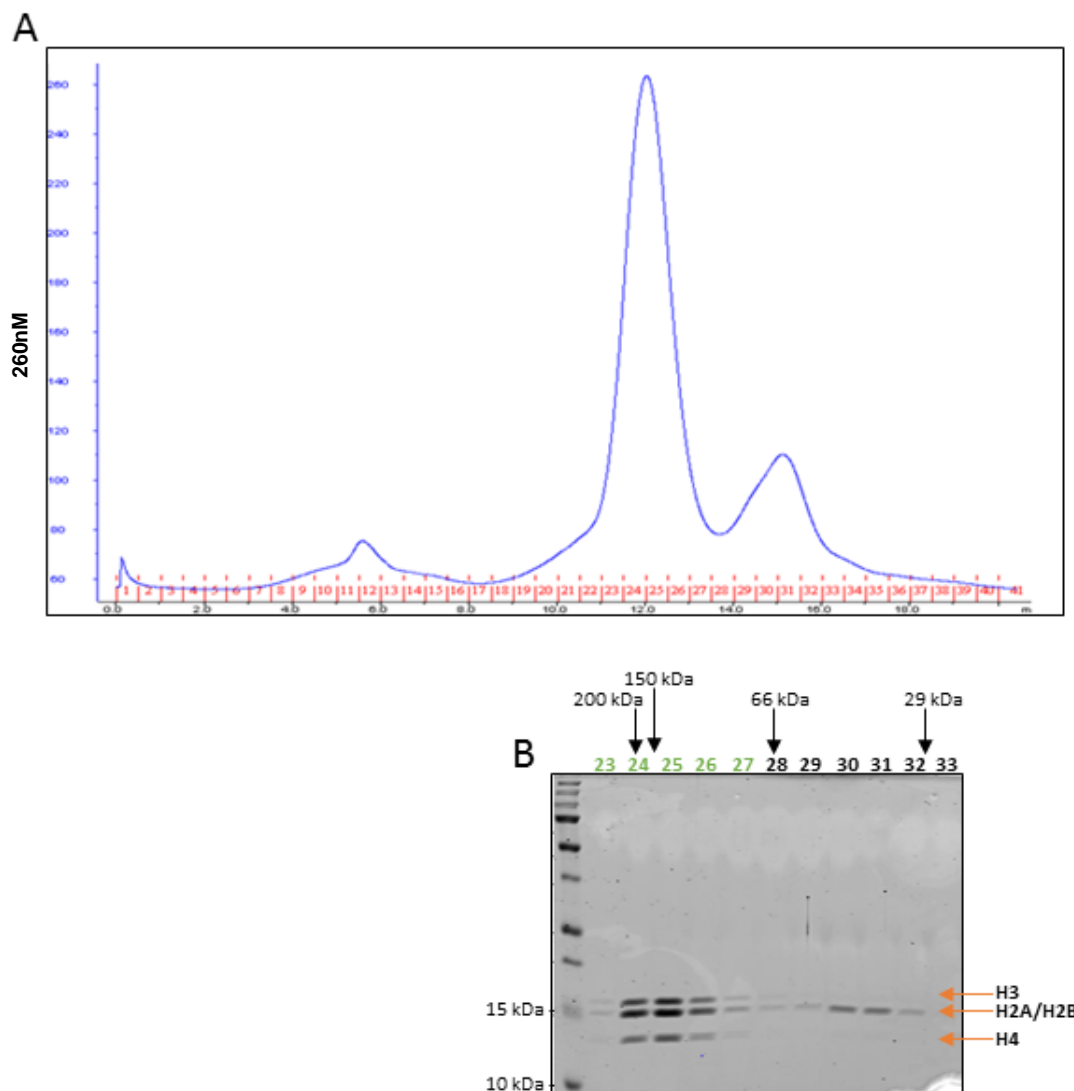


Figure 29: Refolding of the histone octamer. Histones were mixed together in equimolar ratios in unfolding buffer, refolded to form the octamer using a high salt buffer (2 M NaCl) and purified using gel filtration chromatography using a Superdex 200 column. **A**, UV trace from FPLC for the histone octamer purification. **B**, SDS-PAGE gel stained with Instant blue used to check for fractions containing the histone octamer. Fractions indicated in green contained the histone octamer and fractions indicated in orange contained H2A-H2B dimer. All SDS-PAGE gels contained 16 % polyacrylamide and run for 2.5 h at 175 V.

3.4 Generation of mononucleosomes containing site-specific DNA damage

Mononucleosomes were reconstituted by incubation of the purified histone octamer with the THF site containing substrate DNA (either THF-IN or THF-OUT), using salt gradient dialysis. This was achieved by mixing the octamer and DNA in an optimum ratio promoting mononucleosome formation, in a high salt (2 M NaCl) containing buffer. The reconstitution

was then dialysed in buffers containing reducing concentrations of salt, to stimulate mononucleosome substrate formation, which was confirmed by agarose gel electrophoresis by a shift in the DNA to a higher molecular weight species.

3.4.1 Optimising Nucleosome reconstitution

The optimal substrate DNA: histone octamer ratio was investigated to determine which ratio provided the best nucleosome reconstitution, whilst minimising any substantial aggregate formation. Nucleosome reconstitutions were analysed by agarose gel electrophoresis using a number of different electrophoresis conditions to fully determine the degree of reconstitution. This was firstly achieved using nucleosomal DNA that had been directly prepared by PCR using the Widom 601 sequence in the presence of unlabelled PCR primers, and which hadn't been modified to contain any THF sites. Gels were stained with SYTO60 Red Fluorescent Nucleic Acid stain and visualised using the Odyssey Image Analysis System. The results show that the DNA alone (256 bp) runs at the expected molecular weight following analysis by either a 0.5 % agarose gel in 0.5 x TAE (Figure 30A, lane 1) or a 0.7 % gel in 0.2 x TAE (Figure 30B, lane 1). Following addition of the histone octamer to the DNA for nucleosomal reconstitution, a shift to a higher molecular weight (700 bp) species can be observed. When the TAE concentration was too high at 0.5X TAE the DNA appeared to be partially stripped from the histone octamer (Figure 30A), whereas using a 0.2X TAE concentration appeared to keep the nucleosome intact (Figure 30B). Near full nucleosome reconstitution was observed using a DNA:octamer ratio of 1:1 (lane 4, Figure 30B), although at 1:1.2 (lane 5), 1:1.4 (lane 6), and particularly 1:1.6 (lane 7) DNA: histone octamer ratios, there appeared to be smearing above the mononucleosome band which was indicative of aggregate formation. It was therefore concluded that the optimal DNA:octamer ratio for promoting mononucleosome formation, whilst limiting aggregate formation, was 1:1.

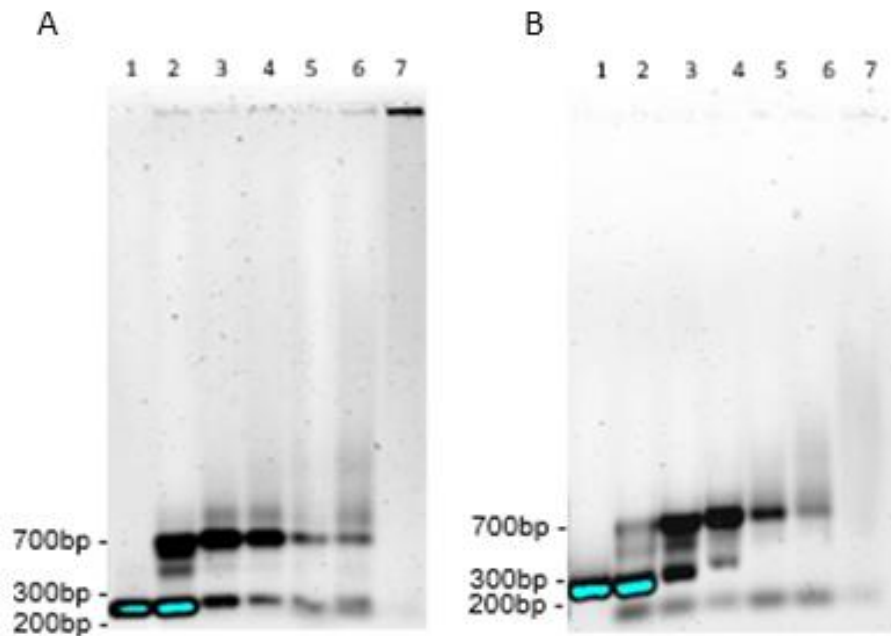


Figure 30: Generation of a Mononucleosome containing unlabelled DNA comparing agarose gel conditions and DNA :histone octamer ratio. Nucleosome reconstitution was compared to free DNA on agarose gels, whereby a shift from the 256 bp free DNA prep (lane 1 in all) to high molecular weight species, indicating nucleosome formation (~700 bp). **A** and **B**, increasing DNA:histone octamer ratios of 1:0.6 (lane 2), 1:0.8 (lane 3), 1:1 (lane 4), 1:1.2 (lane 5), 1:1.4 (lane 6) and 1:1.6 (lane 7). **A**, 0.5 % in 0.5xTAE and **B**, 0.7 % in 0.2x TAE. All agarose gels and DNA was separated using electrophoresis at 75 V for 1.5 h. A 100 bp ladder was used to identify the size of the DNA

3.4.2 Generation of the THF site facing outwards and inwards mononucleosomes

Following optimisation, the 1:1 DNA: histone octamer was used for all subsequent nucleosome reconstitutions. Figure 31 show mononucleosome formation for both the THF-OUT (A) and THF-IN (B) from the nucleosome using the 100 bp DNA ladder. A shift from the lower molecular weight of 256 bp for free DNA (from free DNA prep) to a higher molecular weight of approximately 750 kDa indicating nucleosome formation is visualised for both the THF-OUT and THF-IN generated mononucleosomes. These successfully generated mononucleosomes could then be used in repair assays to measure the activity of APE1 on both these substrates.

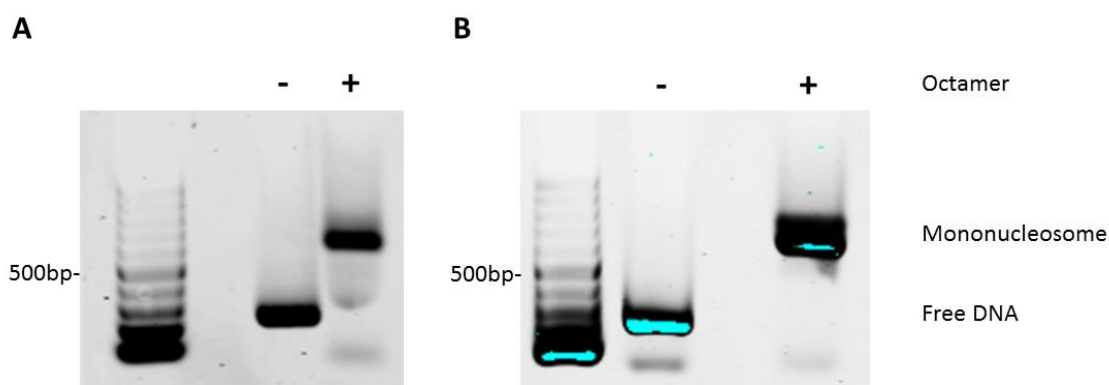


Figure 31: Generation of a Mononucleosome containing an THF. Nucleosome reconstitution was compared to free DNA (lane 1), whereby a shift from the 256 bp free DNA prep to high molecular weight species (lane 2), was observed when the nucleosome was formed. The 1:1 DNA: histone octamer ratio was used. **A**, THF-OUT. **B**, THF-IN. DNA was separated using a 0.7 % agarose gel and electrophoresed at 75 V for 1.5 h. A 100 bp ladder (right hand lane) was used to identify the size of the DNA

3.5 Summary

To investigate the effect of possible histone modifiers or ATP chromatin remodellers on BER in chromatin, it was necessary to generate mononucleosome substrates. Two mononucleosome substrates were designed to contain THF site lesions in different orientations in order to examine the effect of processing by APE1, both in the absence and presence of chromatin remodelling activities. According to previously published data, one of these synthetic AP site (THF) containing substrates is easily accessible to APE1 as the DNA backbone is facing outwards away from the histone octamer, whereas the other with the DNA backbone containing the THF site facing inwards towards the histone octamer is thought to be more inaccessible. These substrates would allow us to determine if the orientation does indeed affect recombinant APE1 activity *in vitro* as seen in similar previous studies, but more importantly to investigate what enzyme/protein factors potentially stimulate APE1 towards the more sterically occluded THF site. In this Chapter, I have now shown that a methodology is in place to generate mononucleosome substrates containing site-specific THF sites.

The Widom 601 sequence was selected due to its strong nucleosome positioning affinity. This was amplified from a plasmid using fluorescently labelled primers so that the DNA could be easily visualised using the Odyssey system. The central 17 bp DNA segment was excised by restriction enzyme digests and replaced by two sequential DNA ligations with a 17 bp oligonucleotide duplex containing a THF either on the upper or lower strand of the DNA. The position of the THF in the DNA sequence had been determined using the Widom 601 nucleosome crystal structure so one sequence would contain a THF in an orientation so the backbone was facing outwards, THF-OUT (+12) and the other sequence containing a THF facing inwards, THF-IN (+11). This process resulted in producing two substrates containing a site specific THF site DNA sequence which could then be used in combination with a histone octamer to create a mononucleosome substrate. It should be noted that previously published methodology generating substrate DNA has involved using radiolabelled DNA for detection, and now our newly designed method completely avoids the use of this harmful radioactivity. Instead, our novel method incorporates 5'-fluorescently labelled DNA which is easier and safer to work with, but also can be quantitatively analysed using the Odyssey Image Analysis System. This is crucial for the analysis of accurate incision rates of the substrate DNA by purified enzymes and cell extracts, which will be discussed in subsequent chapters.

The histone octamer was successfully prepared following individual overexpression of each *Xenopus Laevis* recombinant histone in *E.coli*. Histones were able to be purified using gel filtration and ion exchange chromatography under denaturing conditions, and subsequently unfolded and refolded to form the histone octamer, as previously reported (246). It had previously been noted that histone H4 appeared to be prone to proteolysis, so I made modifications to the inclusion body preparation step before gel filtration chromatography to prevent this. Indeed, I demonstrated that this was able to successfully increase the yield of full

length histone H4. Histone octamer formation was then proven successful, as shown following gel filtration chromatography purification, to contain two of each of the histones H2A, H2B, H3 and H4. Mononucleosome substrates (THF-OUT and THF-IN) were finally prepared by mixing AP site containing DNA with the histone octamer, and a 1:1 ratio of DNA:octamer was found to be the most efficient. This is consistent with previously reported data (246).

In summary, I have devised and optimised a methodology to generate site specific THF site mononucleosome substrates. These can then be used to compare APE1 activity on the two different orientations; THF-OUT and THF-IN, in an *in vitro* repair assay using recombinant APE1 and cell extracts which will be presented in the next chapter. This optimised methodology could also now be used to generate a wide range of different substrates such as a gap, nick or damaged DNA bases so multiple BER activities could be tested in future work.

CHAPTER IV

RESULTS II

BER *in vitro* assays using mononucleosomal DNA containing site-specific DNA damage in different orientations to examine difference in APE1 activity

4.1 Introduction

The short patch BER pathway, the predominant repair pathway for DNA base damage as described previously. The mechanisms and DNA repair proteins involved in BER are now well established, however the precise mechanism of BER in terms of chromatin is very poorly understood. There is accumulating evidence for chromatin remodelling in DNA repair, however this has been more directed towards DSB repair and NER.

Chromatin remodelling is governed by two groups of proteins; histone modifying enzymes and ATP-dependent chromatin remodelling complexes, as described. PTMs influence the DNA and histone octamer interface causing relaxation (or tightening) of the DNA, causing structural changes and manipulating electrostatic interactions. These PTMs of histones can also result in the recruitment of a ATP-dependent chromatin remodelling complex. The family of ATP-dependent chromatin remodelling complexes regulate exposure of DNA by moving (sliding, twist or loop), ejecting or exchanging histones through the hydrolysis of ATP. Chromatin remodelling factors have been implicated in DNA repair; however at this time specific chromatin remodelling factors in BER remain unknown.

Our current understanding of BER within nucleosomes is that the activity of glycosylases, APE1 and Pol β *in vitro* is dependent on the helical orientation and translational position of the particular substrate lesion as described (242, 254, 255, 257, 271). It is thought that partial reversible unwrapping of nucleosomal DNA from the histone octamer facilitates access to these sterically occluded DNA base damage sites *in vivo*, achieved by currently unknown PTMs of histones and/or chromatin remodelling enzymes that facilitate repair. However evidence for the existence of these enzymes, and ultimately of chromatin remodelling required for BER *in vivo*, is lacking.

Therefore my aim for this chapter was to establish if the occluded THF-IN mononucleosome could be more efficiently processed in the presence of factors that could stimulate chromatin remodelling events. This was achieved by comparing APE1 incision using either the

recombinant form and APE1 in HeLa WCE which contains chromatin remodelling factors using the THF-OUT and THF-IN mononucleosomes. Firstly, it was important to conclude if there was any sequence bias between the two oligonucleotide DNA substrates containing a site specific THF site using the BER *in vitro* repair assay in the presence of recombinant APE1 and APE1 in HeLa WCE. There was minimal difference in incision between the two DNA substrates so the THF-IN and THF-OUT mononucleosome were used in the BER *in vitro* assays. Assays were supplemented with ubiquitination supporting factors and NAD to promote ubiquitination and poly(ADP)ribosylation events which have both been implicated heavily in DNA repair and chromatin remodelling activity in the DDR in DSB and NER, strengthening the interest to investigate these two PTMs. This laboratory also has a strong area of interest in ubiquitination and strategies to identify E3 ligases using similar techniques as shown in thesis, which have been successful (267, 272). Once the correct assay conditions had been established and if the THF-IN mononucleosome was more efficiently processed by APE1 following the addition of these chromatin remodelling factors in HeLa WCE, then HeLa WCE would be fractionated to discover the precise proteins that regulate this change in activity of APE1 by a chromatin remodelling event.

4.2 BER *in vitro* assays using free and mononucleosomal DNA containing site-specific DNA damage; THF-OUT and THF-IN

The first step was to develop an optimised protocol to analyse the *in vitro* repair of THF-OUT and THF-IN in naked DNA (mononucleosome free), as well as that for THF-OUT and THF-IN within a mononucleosome. The DNA substrates would largely be incubated with increasing concentrations of purified APE1 or with HeLa WCE (in the presence of buffer containing ATP and BSA to stabilise proteins), and therefore the DNA would have to be extracted from excess protein by phenol chloroform and ethanol precipitation. It was thought that because of the presence of chromatin remodellers and/or histone modifiers in HeLa WCE, that the occluded THF-IN site would be much more readily processed by APE1 in HeLa WCE compared to just purified APE1 alone. Once the DNA was purified, this would have to be separated by denaturing (7 M urea) PAGE in order to separate the cleaved 137 bp product for THF-OUT or 119 bp for THF-IN, from the 256 bp substrate. The location of incision of the substrate THF-containing DNA by APE1 and the products that are visualised following incision are shown in figure 32. Substrates and products were then analysed by using the Odyssey Image Analysis System to quantify the degree of THF incision (percentage cleavage).

Substrate

5' –GCTCGGAATTCTATCCGACTGGCACCGGCAAGGTCGCTGTTCAATACATG
 3' –CGAGCCTTAAGATAGGCTGACCGTGGCCGTTCAGCGACAAGTTATGTAC

CACAGGATGGTATATATCTGACACGTGCCTGGAGACTAGGGAGTAATCCC
 GTGTCCTACCATATATAGACTGTGCACGGACCTCTGATCCCTCATTAGGG

APE1 incision (THF-OUT)

↓

CTTGGCGGTTAAAACGCGGGGGACCAACGCGTTGGTGC1TTTAAGCCGTG

GAACCGCCAATTTTGCGCCCCCTGGTGCACCAACCAC1CAAATTCGGCAC

APE1 incision (THF-IN)

↑

CTGGCGCTTGCTACGACCAATTGAGCGGCCTCGGCACCGGGATTCTCCAG
 GACCGCGAACGATGCTGGTTAACTCGCCGGAGCCGTGGCCCTAAGAGGTC

GGCGGCCGCGTATAGGGTCCATCACATAAGGGATGAACTCGGTCTTAAGA
 CCGCCGGCGCATATCCCAGGTAGTGTATTCCTACTTGAGCCAGAATTCT

ATCATGC–3'
 TAGTACG–5'

Product

THF-OUT

5' **IRDYE700**–GCTCGGAATTCTATCCGACTGGCACCGGCAAGG
 TCGCTGTTCAATACATGCACAGGATGGTATATATCTGACACGTG
 CCTGGAGACTAGGGAGTAATCCCCTTGGCGGTTAAAACGCGGGG
 GACCAACGCGTTGGTGC

THF-IN

CAAATTCGGCACGACCGCGAACGATGCTGGTTAACTCGCCGGAG
 CCGTGGCCCTAAGAGGTCCCGCCGGCGCATATCCCAGGTAGTGT
 ATTCCCTACTTGAGCCAGAATTCTTAGTACG–**IRDYE700** 5'

Figure 32: DNA sequence for THF-OUT and THF-IN before and after incision of APE1.

Figure shows the substrate sequence for THF-OUT with the THF (1) on the upper strand of the 256 bp Widom nucleosome positioning sequence and THF-IN with the THF (1) on the lower strand. The nucleosome dyad is shown in black bold and the 17 bp oligonucleotide insertion is shown in blue bases. The product DNA sequence with the more intense IRDYE700 fluorescent tag for 137 bp THF-OUT and 116 bp THF-IN are shown.

4.2.1 Optimising gel conditions for denaturing (7 M urea) PAGE

It was firstly important to optimise gel and running conditions so the substrate and product bands on the denaturing (7 M urea) PAGE gels could be separated, visualised and ultimately quantified with confidence. Optimisations for gel quality were achieved using the free THF-OUT DNA using recombinant APE1 only. Initially, following phenol chloroform extraction the DNA from the BER reactions was ethanol precipitated. This led to smearing on gels and aggregates in the well following incubation of the substrate with an increasing concentration of APE1 (0-14.3 fmol; Figure 33A). It was thought that residual phenol in the reactions was causing this smearing effect, so a wash step using isoamyl alcohol after phenol chloroform extraction was added in an attempt to remove phenol. However again, incubation of free THF-OUT with increasing concentrations of APE1 (0-3.57 fmol) led to smearing on the gel (Figure 33B). Therefore a second, additional wash step of isoamyl alcohol was added. This increased the quality of the substrate and product bands visually, reduced the amount of smearing and no aggregates were seen in the wells of the gel as a consequence of thoroughly removing all the phenol from the reaction (Figure 33C). However there was still some minor smearing on the gel below the substrate band. As the 8 % denaturing (7 M) acrylamide (19:1 acrylamide/bis-acrylamide) gel was made from a stock solution, I further examined whether making this fresh would improve the using the same increasing concentrations of APE1, and indeed when this was performed very little smearing on the gel was observed (Figure 33D). Further changing the acrylamide/bisacrylamide gel ratio from 19:1 to 29:1, additionally improved the substrate and product band quality (Figure 33E). Now that the gel image quality, and in particular the product and substrate bands were optimised, substrate DNA from BER reactions could be extracted, separated and quantified with confidence and allow us to accurately determine the relative activity of both recombinant APE1 and HeLa WCE on THF-OUT and THF-IN containing DNA.

4.2.2 BER *in vitro* assays using free THF-OUT and THF-IN DNA

Before looking at THF incision using the THF-OUT and THF-IN mononucleosome substrates, it was important to see if there was any sequence specific differences in the incision of the free DNA for THF-IN and THF-OUT using recombinant APE1 and HeLa WCE. This is to ensure that any potential differences observed in the incision of the THF-IN and THF-OUT containing mononucleosomes, was not caused by a different sequence context. The percentage cleavage from three independent BER assays using titrations of APE1 and HeLa WCE were performed for both the THF-OUT and THF-IN, free DNA substrates. A concentration range was selected so a maximum of ~40 % incision was observed. Using increasing concentrations of both recombinant APE1 and HeLa WCE had a positive linear correlation in the percent incision of the AP sites in both THF-OUT and THF-IN (Figure 34A-D). THF-OUT free DNA using recombinant APE1 had slightly more percentage incision at all concentrations compared to THF-IN substrate, with the biggest difference occurring at highest

concentration, suggesting that there is a mild sequence specific effect on incision by APE1 (Figure 34A and 34C). In contrast, using HeLa WCE at the three lowest concentration points showed very minimal difference in percentage incision between THF-OUT and THF-IN, although at the two highest concentrations of HeLa WCE there was a slight increase in THF-OUT incision compared to THF-IN. There does therefore appear to be a very marginal bias towards increased AP-site incision of the THF-OUT free DNA, possibly due to the sequence surrounding the THF site. As shown in figure 32 the sequence surrounding the THF site for the THF-IN is in a GC rich region either side, whereas the THF-OUT neighbours AT. However it was predicted that the difference in THF incision between these two THF-OUT and THF-IN substrates when reconstituted into mononucleosomes would be more substantial, and that this would negate the very slight bias in free DNA substrates.

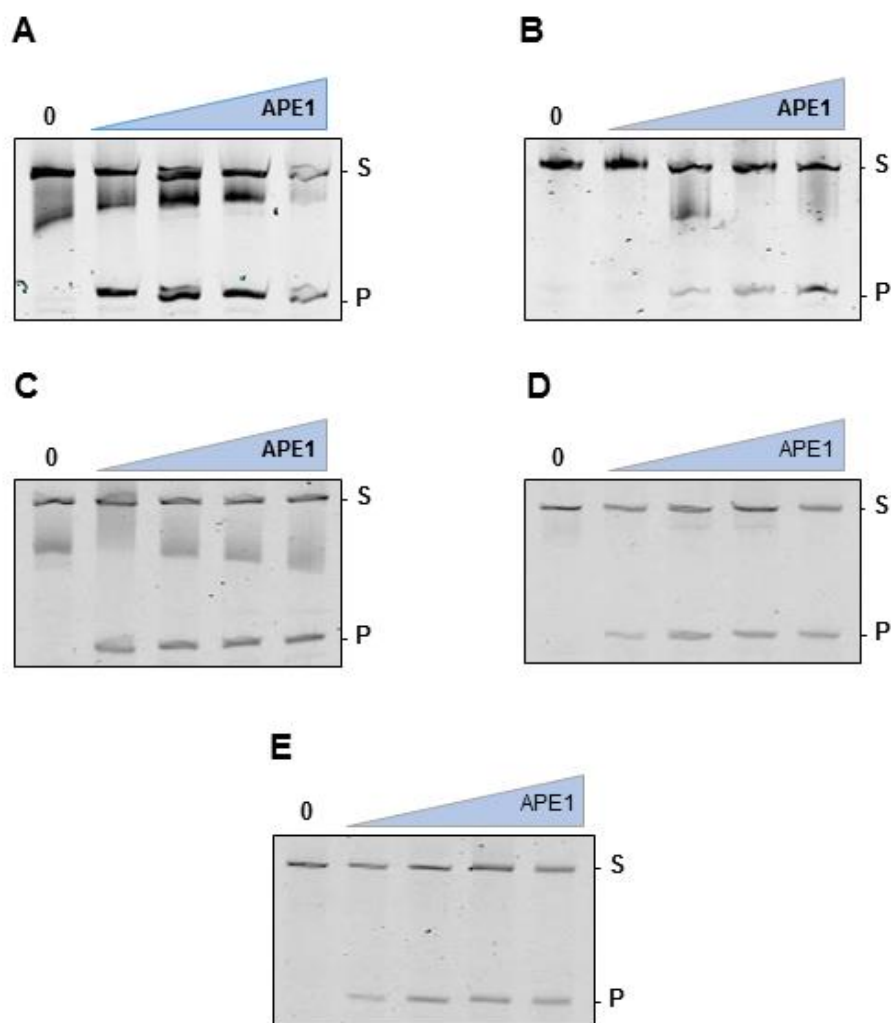


Figure 33: Optimising gel condition for BER *in vitro* assays using AP-O free DNA and purified APE1. For all, 8 % denaturing (7 M) PAGE gels (19:1 acrylamide/bisacrylamide, unless stated) in 1X TBE were electrophoresed to separate DNA at 350 V for 1.25 hours and visualised using the Odyssey Image Analysis system (IRDYE700). S refers to the substrate DNA and P the product DNA after APE1 incision. **A**, APE1 concentrations 0, 1.8, 3.6, 7.1, 14.3 pmol, DNA was extracted by phenol chloroform and then ethanol precipitated. **(B-E)** APE1 concentrations used were 0, 0.35, 0.9, 1.79, 3.57 pmol. **B**, after phenol chloroform extraction, DNA was washed with isoamyl alcohol and then ethanol precipitated. **C**, Underwent two washes with isoamyl alcohol and then ethanol precipitated. **D**, 19:1 acrylamide/bis-acrylamide freshly prepared, **E**, 29:1 acrylamide/bis-acrylamide freshly prepared.

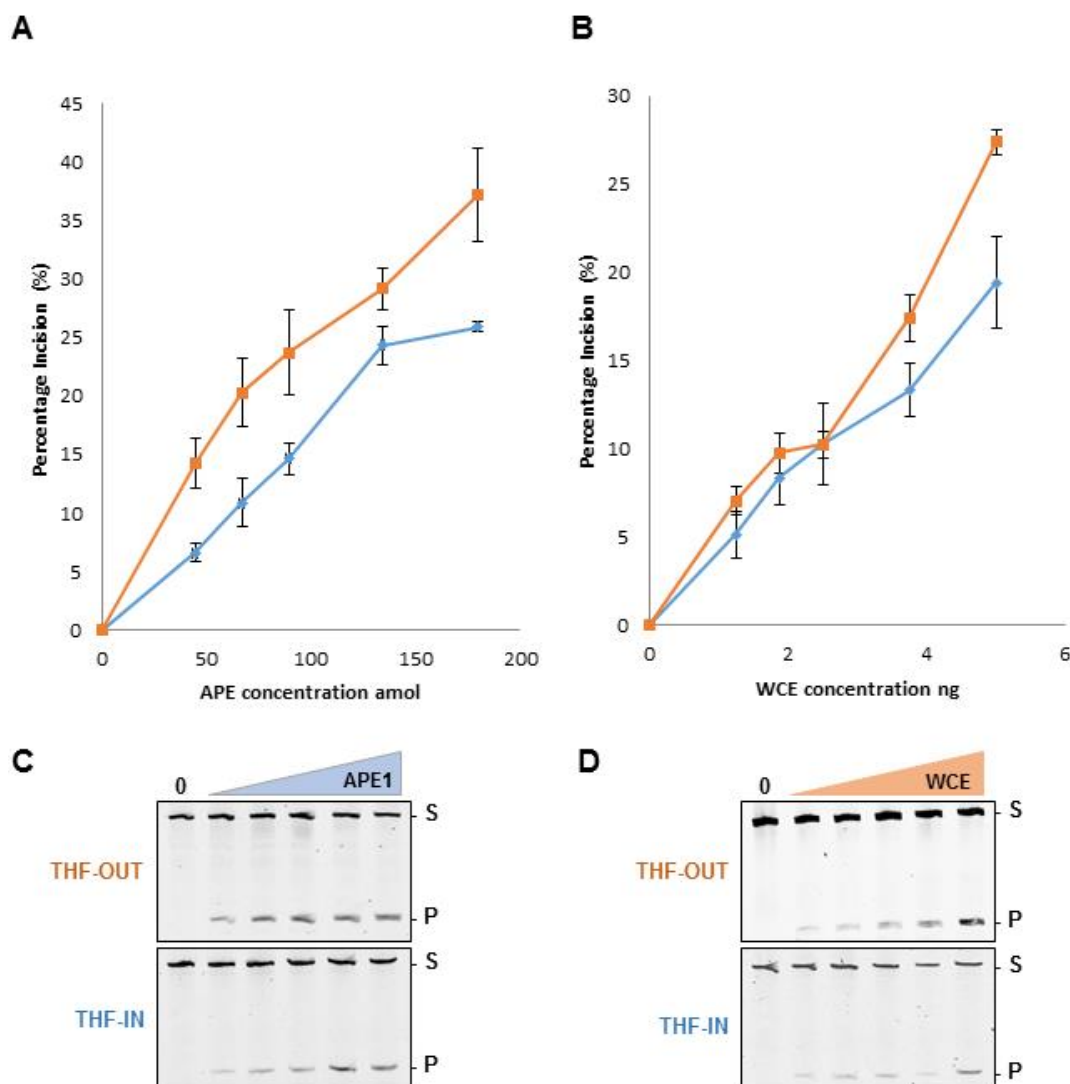


Figure 34. *In vitro* BER assays using Free DNA Substrates containing an AP site for either THF-OUT (orange) or THF-IN (blue). For both free DNA substrates, representative denaturing (7 M) PAGE gels are shown for various APE1 titrations (0-180 amol) (**C**, THF-OUT and THF-IN free DNA substrates) and HeLa WCE using concentrations (0- 5 ng) **D**, THF-OUT and THF-IN free DNA substrates). These were incubated with the substrate DNA for 10 minutes at 30°C. PAGE gels were quantified using the Odyssey Image Analysis system and the mean and standard deviation calculated for both substrates. S refers to the substrate DNA and P the product DNA after APE1 incision. **A**, APE1 titration for THF-OUT (orange) and THF-IN (blue) and **B**, WCE titration for both THF-OUT (orange) and THF-OUT (blue) DNA substrates. All denaturing PAGE gels contained 8 % polyacrylamide, 7M Urea and 1x TBE, and run for 1.25 h at 350V.

4.2.3 Quantifying APE1 concentration in HeLa WCE

The concentration of APE1 in HeLa WCE was measured using quantitative Western blotting, in order to correlate the amount of WCE used in the *in vitro* BER assays, to that of recombinant APE1 only. Therefore known and increasing amounts of HeLa WCE, plus recombinant APE1, were separated on a 10 % SDS polyacrylamide gel and probed for APE1 (34 kDa) using anti-APE1 antibodies. It was found that 300 fmol recombinant APE1 was approximately equivalent to 5 µg HeLa WCE, and that the highest concentration used of APE1 (1200 fmol) was equal to 20 µg HeLa WCE (Figure 35). So extrapolating backwards, 1 µg HeLa WCE was be approximately equivalent to 60 fmol recombinant APE1. From this we could roughly estimate how much APE1 in HeLa WCE was causing a certain level of incision and how this compared to recombinant APE1.

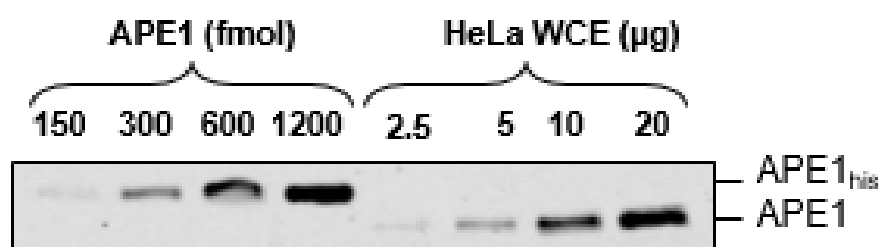


Figure 35: Quantifying APE1 concentration in HeLa WCE. APE1 concentration in HeLa WCE was estimated by using known amounts of HeLa WCE and quantifying them against known concentrations of purified his-tagged APE1. A 10 % SDS polyacrylamide gel was used to separate proteins by electrophoresis at 125 V for 2 h with a 10 kDa to 25 kDa protein marker and proteins transferred onto a membrane. APE1 was then detected by Western blotting and the Odyssey Image Analysis system was used to visualise and quantify APE1 protein concentration.

4.2.4 BER *in vitro* assays using THF-OUT and THF-IN mononucleosome substrates

THF site incision was compared between the THF-OUT and THF-IN mononucleosome substrates, using recombinant APE1 and HeLa WCE. The percentage incision from at least three independent BER assays using titrations of APE1 and HeLa WCE were performed for both THF-OUT and THF-IN mononucleosome substrates. As expected, the concentrations of APE1 and HeLa WCE required to cause incision of THF-OUT and THF-IN mononucleosomes were much higher (~1000-fold) than what was used to cause incision of free DNA, confirming that the nucleosome in general hinders access of APE1 to DNA. I also discovered that the THF-IN mononucleosome substrate is much less efficiently cleaved than the THF-OUT substrate using recombinant APE1 (Figure 36A and C). Indeed cleavage of THF-IN only

reached 20 % with 200 fmol APE1 whereas this was as high as 60 % with THF-OUT. This was expected due to the inability of APE1 to access the THF site within the THF-IN mononucleosome substrate. However, HeLa WCE displayed a very similar pattern to recombinant APE1, in that the THF-IN mononucleosome substrate was much less efficiently cleaved than the THF-OUT substrate (Figure 36B and D). Indeed, an approximate 3-fold higher concentration of HeLa WCE was required to incise the THF site to a similar efficiency in THF-IN versus that in THF-OUT, which was similar to the results with recombinant APE1 only. This was surprising given that I had hypothesised that WCE (due to the presence of histone modifiers and chromatin remodellers) would be able to catalyse the cleavage of the THF site both in the THF-IN and THF-OUT substrates to a similar efficiency. Of note are the concentrations used of HeLa WCE, which is roughly equivalent to the same amount of recombinant APE1 as determined by quantitative Western blotting. Indeed based on figure 35, 1 µg HeLa WCE is approximately equivalent to 60 fmol of recombinant APE1, which means that the graphs are virtually directly comparable to one another. Therefore under these conditions, no significant difference was observed in cleaving both substrates when comparing APE1 to HeLa WCE (Figure 36A and B). As the reaction conditions contained minimal factors required for histone PTMs and chromatin remodelling (only ATP added which promotes histone phosphorylation and ATP-dependent chromatin remodellers), I proposed that the addition of other factors promoting other histone PTMs would be required to promote APE1 incision of THF-IN. For example, DNA repair has been shown to be increasingly dependent on ubiquitin-dependent processes, so supplementing reactions with factors supporting ubiquitination could be one approach. Secondly, reactions had only a short incubation time (10 min) so it was thought that this was not sufficient time to allow for remodelling of the mononucleosomes following incubation with HeLa WCE specifically.

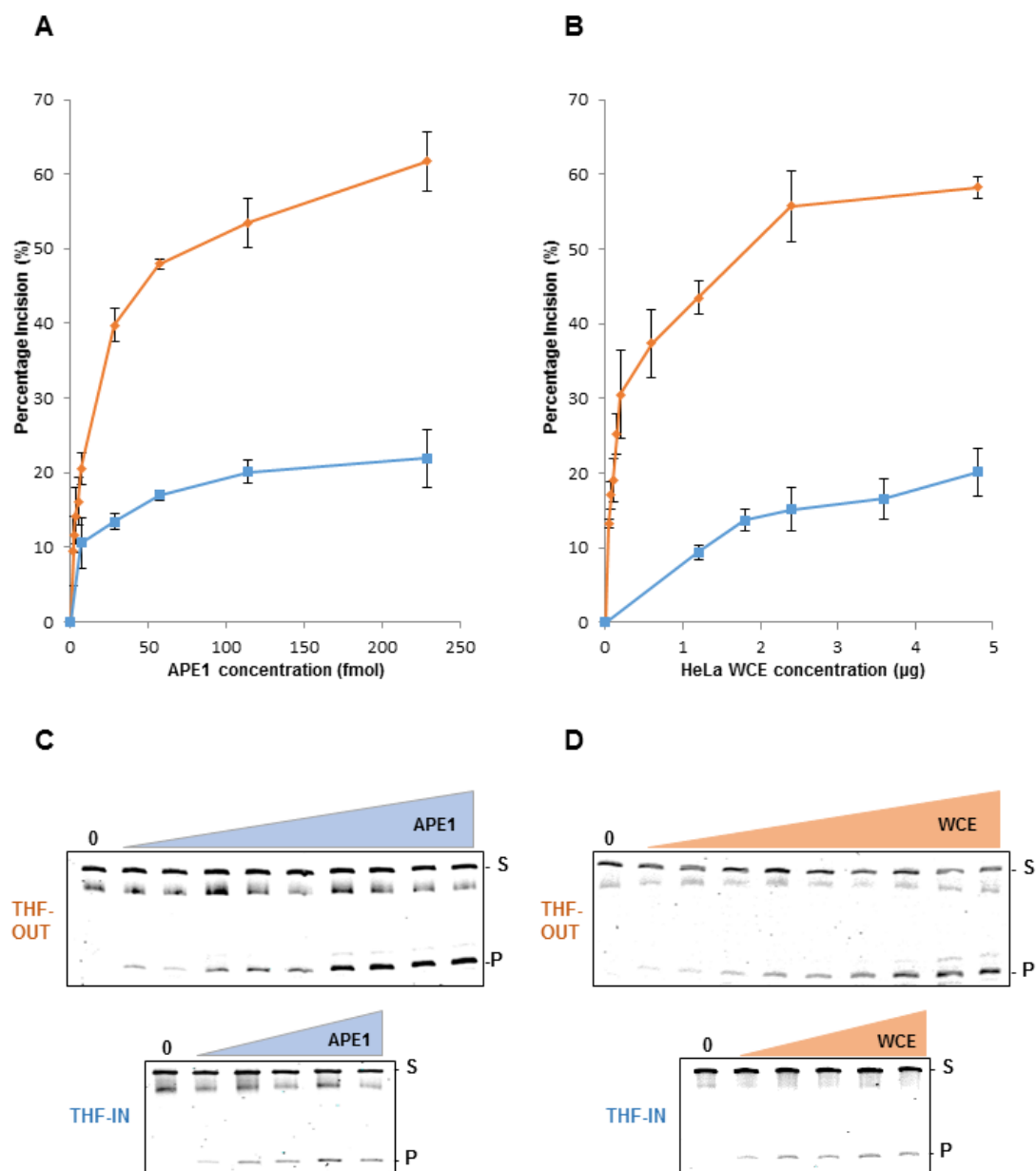


Figure 36: *In vitro* BER assays using mononucleosome substrates containing an THF-OUT (orange) or THF-IN (blue). For both mononucleosome substrates percentage incision was quantified from denaturing (7 M) PAGE gels using the Odyssey Image Analysis system and the mean and standard deviation calculated for both substrates from at least three independent experiments. **A**, Purified APE1 concentration titration (0-229 fmol) using THF-OUT (orange) and THF-IN (blue) mononucleosomes and **C**, representative gels shown for each. **B**, HeLa WCE concentration titration (0-4.8 μg) using THF-OUT (orange) and THF-IN (blue) mononucleosomes and **D**, representative gels shown for each. All denaturing PAGE gels contained 8 % polyacrylamide, 7 M Urea and 1x TBE, and run for 1.25 h at 350 V.

4.3 BER *in vitro* assays using HeLa WCE in the presence of ubiquitin and other factors

Due to the observed lack of difference in incision of the THF-IN mononucleosome substrate by HeLa WCE, it was predicted that the extracts are potentially deficient in factors stimulating histone modifications and/or chromatin remodelling. In the first instance, it was therefore assessed whether addition of ubiquitin (therefore promoting histone ubiquitylation) would enhance cleavage of the THF-IN mononucleosome substrate, which is more difficult to repair. To achieve this, a time course experiment was performed using a defined amount of HeLa WCE in the absence and presence of ubiquitin in the BER *in vitro* assay. Using a time course experiment also allowed us to examine whether chromatin remodelling factors needed a longer time period (than the 10 minutes used in the first experiments) to catalyse nucleosome relaxation events. Secondly the addition of other factors including phosphocreatine (PC) and phosphocreatine kinase (PCK; to regenerate ATP concentrations), NAD (to promote ADP-ribosylation) and E1, E2 enzymes (further supporting ubiquitylation) in promoting AP site incision within a mononucleosome was assessed. Cumulatively, this would indicate the precise conditions, and ultimately indicate the factors and enzymes, that are necessary for chromatin remodelling of THF sites during BER.

4.3.1 BER *in vitro* time course assays using HeLa WCE and ubiquitin with THF-IN and THF-OUT

To examine the effect of adding ubiquitin and incubation time on incision of the THF-IN mononucleosome substrate by HeLa WCE, a specific concentration of WCE (1.3 μ g) which caused approximately 10 % incision after 10 min incubation (see Figure 36A) was used, with and without supplementary ubiquitin added (0.6 nmol) and the reaction continued up to 1 h. Ubiquitination of histones has been shown to be a vital event in the DDR in DSB and NER. The percentage incision from at least three individual BER assays for each time course experiment was quantified from denaturing (7 M) PAGE gels. Firstly it was noted that increasing the incubation time of the THF-IN mononucleosome with WCE from 10-60 min in the absence of ubiquitin had a very minimal effect on AP site incision without ubiquitin, only increasing incision by <5% from 10 minutes to 1 hour (Figure 37A, light purple line and Figure 37C). However the percent cleavage of the THF site within THF-IN by HeLa WCE was significantly higher in the presence of ubiquitin at all time points compared to when ubiquitin was not added (Figure 37A, dark purple line and Figure 37C). Indeed, there was an approximate 2.4-fold increase in percentage incision of the THF with ubiquitin added. In the presence of ubiquitin, the increase in time seemed to allow possible chromatin remodelling factors to have a significant effect on the accessibility of the THF site in the THF-IN mononucleosome, increasing incision from ~17 % at 10 min to ~37 % at 1 h.

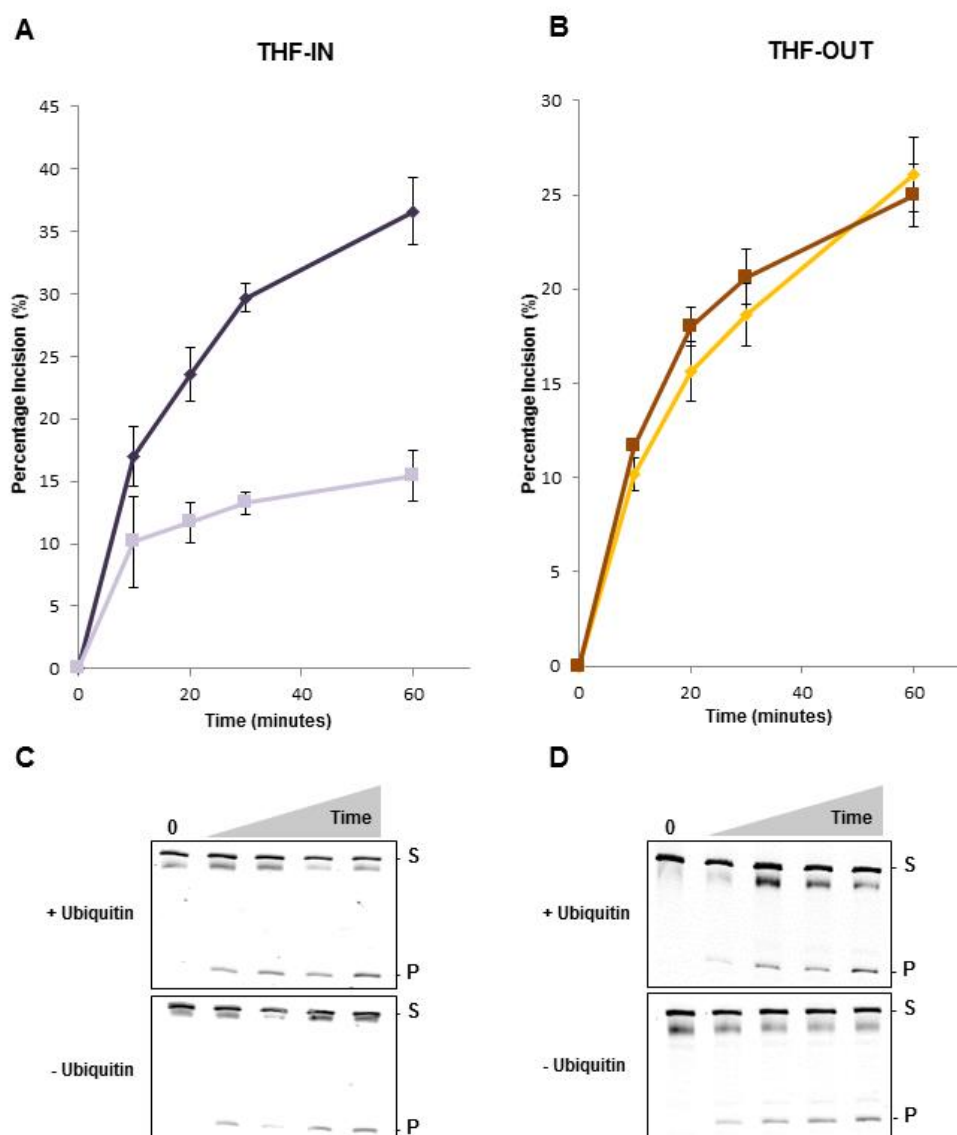


Figure 37: *In vitro* BER assays time course using THF-IN and THF-OUT mononucleosomes with HeLa WCE plus and minus ubiquitin. THF-IN and THF-OUT mononucleosomes were treated with 1.3 μ g and 0.04 μ g HeLa WCE respectively, plus and minus 0.6nmol ubiquitin. Reactions were stopped after 10, 20, 30 and 60 minute and the percentage cleavage of the mononucleosome substrates was quantified from denaturing (7 M) PAGE gels using the Odyssey Image Analysis system and the mean and standard deviation calculated. The dark purple (A) and brown (B) represent result with ubiquitin and light purple (A) and yellow (B) without ubiquitin. **A**, THF-IN mononucleosome substrate. **B**, THF-OUT mononucleosome substrate. Representative denaturing PAGE gels are shown plus and minus ubiquitin for each Mononucleosome **C**, THF-IN and **D**, THF-OUT. All denaturing PAGE gels contained 8 % polyacrylamide, 7 M Urea. The percentage incision from at least three independent BER assays for each time course experiment were quantified from denaturing (7 M) PAGE gels.

To analyse whether this increase in THF site incision activity was specific to the THF-IN mononucleosome, the same time course was utilised with the THF-OUT mononucleosome, albeit using a lower amount of HeLa WCE as necessary (0.04 μ g). The percentage incision from at least three and we expected that because the THF site in the THF-OUT mononucleosome is already very accessible to APE1 that there wouldn't be much difference in APE1 percentage incision. This was indeed the case as there was virtually no difference in incision of the THF-OUT substrate in the presence or absence of ubiquitin (Figure 37B and D), and both substrates reached ~25 % incision following 1 h incubation. These data strongly suggested that the effect of ubiquitin could be specific to histone modifications and/or chromatin remodelling of the THF-IN substrate which is difficult to repair. Therefore, the increased activity of APE1 present in HeLa WCE to the THF-IN mononucleosome appears to be ubiquitin dependent, and could either be due to an increase in accessibility from dissociation of the DNA from the histone octamer, or because ubiquitination on the N-terminal of histones causes relaxation of the mononucleosome structure.

4.3.2 BER *in vitro* time course assays using HeLa whole cell extract and Ubiquitin with THF-IN free DNA

As the addition of ubiquitin was found to stimulate the cleavage of the THF site in THF-IN mononucleosome substrate by APE1 present in HeLa WCE, I further examined whether this effect was specific to histone modifications and/or chromatin remodelling, and not related to modification (ie. ubiquitination) of APE1 protein itself present in the WCE. Therefore the same time course was completed using the THF-IN substrate in free DNA. The percentage incision from at least three independent BER assays for each time course experiment was quantified from denaturing (7 M) PAGE gels. It was found that addition of ubiquitin had no effect on the cleavage of the AP site in THF-IN free DNA by HeLa WCE. In fact, incision of the THF site in the THF-IN free DNA marginally decreased in the presence (Figure 38A, dark green line and Figure 38B) compared to the absence (Figure 38A, light green line and Figure 38B) of ubiquitin. Nevertheless, both substrates appeared to reach ~45-50 % incision following 1 h incubation. This suggested that ubiquitin appears to be having a specific effect on mononucleosomal containing DNA damage and not on APE1 itself.

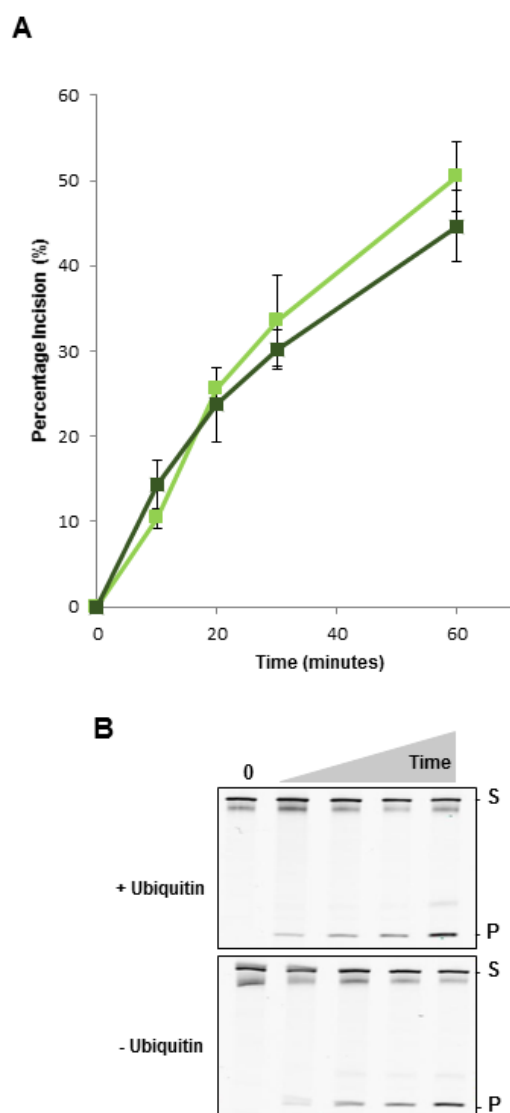


Figure 38: *In vitro* BER assays time course using free THF-IN DNA substrate HeLa WCE plus and minus ubiquitin. THF-IN free DNA was treated with 1 ng HeLa WCE, plus and minus 0.6 nmol ubiquitin. Reactions were stopped after 10, 20, 30 and 60 minute and the THF-IN DNA substrates percentage cleavage was quantified from denaturing (7 M) PAGE gels using the Odyssey Image Analysis system and the mean and standard deviation calculated from three experiments. **A**, Graph showing with and without ubiquitin, the dark green represent result with ubiquitin and light green without. **B**, Representative denaturing PAGE gels are shown plus and minus ubiquitin for each THF-IN free DNA substrate. All denaturing PAGE gels contained 8 % polyacrylamide, 7 M Urea and 1x TBE, and run for 1.25 h at 350 V.

4.3.3 BER *in vitro* time course assays analysing different conditions using HeLa WCE with THF-IN mononucleosome

As I established that adding just ubiquitin was able to specifically stimulate incision of THF within the THF-IN mononucleosome substrate, I further examined the effect of different supplementary components added to the *in vitro* reaction to optimise the conditions for maximal THF cleavage. These included PC and PCK (to regenerate ATP concentrations), NAD (to promote ADP-ribosylation) and E1, E2 enzymes in the presence and absence of ubiquitin (promoting further ubiquitylation). These conditions were compared against the standard reaction (no supplements) using HeLa WCE (1.3 µg) and the THF-IN mononucleosome substrate at two incubation time points (30 and 60 min).

The standard reaction containing just HeLa WCE (plus ATP) yielded just 17 % and 21 % THF incision at 30 and 60 min incubation time, respectively (Table 9). As seen previously, in the presence of ubiquitin the percentage incision increased at both time points (32 % and 30 %, respectively), further supporting a dependence on ubiquitination on THF-IN processing. On addition of BSA, the percentage incision of the THF-IN mononucleosome substrate only marginally increased at 30 and 60 min incubation time (20 % and 26 %) compared to the standard reaction (17 % and 21 %), indicating potential stabilisation of protein factors by additional protein. The combination of both BSA and ubiquitin together only produced a marginal increase in incision of THF-IN (31 % and 37 %), particularly after 60 min incubation, compared to ubiquitin alone (32 % and 30 %). The addition of NAD appeared to increase the incision of THF-IN mononucleosome substrate reaction (23 % and 31 %) compared to the standard reaction alone (17 % and 21 %), suggesting that poly (ADP-ribosylation) stimulates THF cleavage. Addition of PC and CPK to facilitate phosphorylation had only a marginal effect on incision (18 % and 25 %), although the presence of PC/PCK and NAD significantly increased incision by at 30 and 60 min incubation time (39 % and 44 %) in comparison to the standard reaction alone (17 % and 21 %). Interestingly, addition of an E1 activating enzyme and a pool of ten E2 conjugating enzymes (further supporting ubiquitination) did not cause a significant increase in THF-IN incision (22 % and 26 %) compared to reactions containing ubiquitin alone (32 % and 30 %). However, when E1/E2 enzymes, ubiquitin and NAD was added together to the BER assay, the percentage incision of the THF site in THF-IN mononucleosome substrate was significantly increased (56 % and 67 %), suggesting that a ubiquitination event in addition to an NAD-dependent process (eg. poly(ADP-ribosylation)) was taking place to making the AP site more accessible. Lastly, further adding PC and PCK to this reaction did not cause any additional increase in THF incision, and in fact this slightly decreased APE1 activity (31 % and 42 %). Consequently, these findings suggest that components supporting both ubiquitination (E1, E2 and ubiquitin) and poly(ADP-ribosylation) (NAD) are required for maximal APE1 activity on THF-IN, and could be acting on histone proteins making the THF site in the THF-IN mononucleosome substrate more accessible to

APE1 within HeLa WCE and this effect was investigated further. In contrast, an ATP regenerating system (PC and PCK) does not appear to be essential for the efficiency of the THF-IN incision reaction, suggesting that there is sufficient ATP within the reaction to support any potential phosphorylation events.

Reaction Conditions	Minutes	Percent Incision (%)
Standard Reaction	30	17.0
	60	20.5
0.6nmol ubiquitin	30	32.0
	60	30.1
6µg BSA	30	20.4
	60	25.5
6µg BSA and 0.6nmol Ubiquitin	30	30.7
	60	36.5
5mM NAD	30	23.4
	60	30.7
25mM PC and 10ng CPK	30	18.3
	60	25.1
25mM PC, 0.5µg CPK, 5mM NAD	30	39.1
	60	43.8
0.7 pmol E1, 2.5 pmol E2s and 0.6nmol Ubiquitin	30	22.4
	60	25.7
0.7 pmol E1, 2.5 pmol E2s, 0.6nmol Ubiquitin and 5mM NAD	30	55.7
	60	66.9
0.7pmol E1, 2.5 pmol E2s, 0.6nmol Ubiquitin, 5mM NAD, 25mM PC and 10ng CPK	30	30.7
	60	41.5

Table 9; BER *in vitro* time course assays analysing different conditions using HeLa WCE with THF-IN Mononucleosome. Reactions were stopped after 30 and 60 min in the presence of HeLa WCE (1.3 µg) and the various components, and the THF-IN DNA substrate percentage cleavage was quantified from denaturing (7M) PAGE gels using the Odyssey Image Analysis system. The standard reaction (HeLa WCE) was supplemented with various components to stimulate with ubiquitination (0.7pmol E1, 2.5pmol E2 and/or 0.6nmol ubiquitin), phosphorylation via ATP regeneration (25mM PC and 10ng PCK), and poly(ADP-ribosyl)ation (NAD). The percentage incision for each of these varying condition is shown after 30 and 60 minutes from one independent experiment.

4.3.4 BER *in vitro* time course assays using both HeLa WCE and purified APE1 in the presence of ubiquitin, E1/E2s and NAD using THF-IN mononucleosome substrate

Now that the reaction conditions had been optimised for maximal THF site incision of the THF-IN mononucleosome substrate, particularly by supplementation with ubiquitin, E1/E2 enzymes and NAD, I examined the full time course (0-60 min) of repair of this substrate again using both HeLa WCE and purified APE1. I anticipated that stimulation of THF incision activity would only be observed with HeLa WCE (containing histone modifiers and chromatin remodellers) and not with purified APE1 only. The percentage incision from at least three independent BER assays for each time course experiment was quantified from denaturing (7 M) PAGE gels. In previous experiments using recombinant APE1 only, the THF-IN mononucleosome substrate was only incised to ~20 % with 57-230 fmol APE1 following a 10 minute incubation (Figure 36A). The addition of ubiquitin, E1/E2 enzymes and NAD to recombinant APE1 (57 fmol) over the time course of incision of the THF-IN mononucleosome substrate similarly did not appear to dramatically affect THF site incision (Figure 39A, green line and Figure 39B) as this only reached ~20 % and ~30 % after 20 min and 60 min incubations, respectively. This suggests that ubiquitin, E1/E2 enzymes and NAD are only having a minimal effect on recombinant APE1 activity. In contrast, THF-IN mononucleosome substrate incision by HeLa WCE in the presence of these components was significantly enhanced, especially after 20 min incubation. Whilst THF site cleavage was found previous to be only ~12 % and 15 % with HeLa WCE and 23 % and 37 % with HeLa WCE with ubiquitin after 20 and 60 min incubation, respectively (Figure 37A), the addition of ubiquitin, E1/E2 enzymes and NAD increased this to ~45 % and 67 % (Figure 39A, grey line and Figure 39B). This suggests that this significant difference when using HeLa WCE is because of ubiquitination event by a E3 ubiquitin ligase, in combination with poly(ADP-ribosyl)ation in the presence of NAD, which was either causing a structural change in the mononucleosome through histone PTMs, or is actively recruiting an ATP-dependent chromatin remodeller. The effect of these additional factors was further analysed using both the THF-OUT and THF-IN mononucleosomes to compare the difference in THF incision with either recombinant APE1 or HeLa WCE.

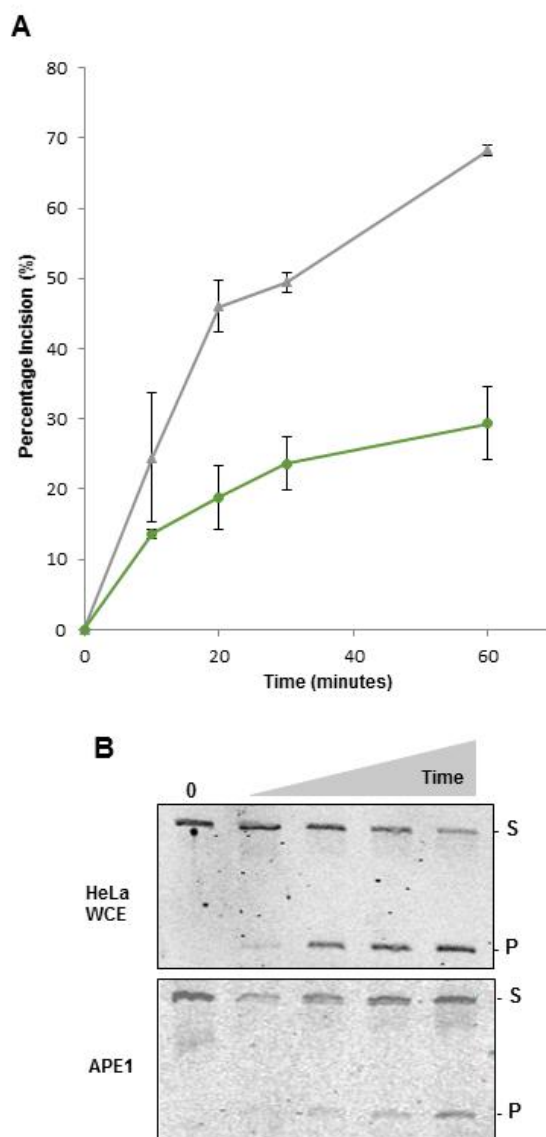


Figure 39: *In vitro* BER assays time course using THF-IN mononucleosome substrate with HeLa WCE or purified APE1 in the presence of ubiquitin, NAD and E1/E2 enzymes. Reactions were stopped after 10, 20, 30 and 60 minute and the THF-IN mononucleosome substrate with either APE1 or HeLa WCE in the presence of 0.7 pmol E1 and 2.5 pmol E2s and 5mM NAD, percentage cleavage was quantified from denaturing (7 M) PAGE gels using the Odyssey Image Analysis system and the mean and standard deviation calculated. **A**, Graph showing with 1. 3 μ g HeLa WCE (grey) and purified 57 fmol APE1 (green). **B**, Representative denaturing PAGE gels for both HeLa WCE and purified APE1 using THF-IN mononucleosome substrate. All denaturing PAGE gels contained 8 % polyacrylamide, 7 M Urea and 1x TBE, and run for 1.25 h at 350 V.

4.3.5 BER *in vitro* assays with HeLa WCE and purified APE1 in the presence of supplementary ubiquitin, E1/E2 enzymes and NAD using THF-OUT and THF-IN mononucleosome substrates

APE1 incision was compared between the THF-OUT and THF-IN mononucleosome substrates, using titrations of recombinant APE1 and HeLa WCE with all factors required to support ubiquitination (ubiquitin, E1/E2 enzymes) and poly(ADP-ribosyl)ation (NAD), which in the previous section, I demonstrated caused maximal THF site cleavage of the THF-IN mononucleosome substrate. The percentage incision from at least three independent BER assays using titrations of recombinant APE1 and HeLa WCE were performed for both THF-OUT and THF-IN mononucleosome substrates containing the THF site. The dramatic difference in incision of the THF-OUT versus the THF-IN mononucleosome substrate by recombinant APE1 alone previous shown (Figure 34A), albeit following 10 min incubation, was replicated under conditions using increasing concentrations of recombinant APE1 in the presence of E1/E2 enzymes, ubiquitin and NAD following 60 min incubation (Figure 40A and 40C). Indeed APE1 was able to efficiently cleave the THF site in THF-OUT, but was significantly impeded by the THF site in THF-IN. At the highest concentration of APE1 (230 fmol), the percentage difference in incision between THF-OUT and THF-IN was 3.9-fold. However, using increasing concentrations of HeLa WCE, THF-IN mononucleosome was much more efficiently incised in the presence of E1/E2 enzymes, ubiquitin and NAD, and appeared to be approaching the levels of THF site incision of the THF-OUT mononucleosome substrate (Figure 40B and D). Indeed, at the final concentration point there was only a 1.2-fold difference in cleavage between THF-OUT and THF-IN mononucleosome substrates. Therefore the addition of E1/E2 enzymes, ubiquitin and NAD has greatly improved accessibility and incision of the THF site in THF-IN compared to HeLa WCE alone (Figure 36B). On direct comparison of recombinant APE1 versus the comparative levels of APE1 present in HeLa WCE using the THF-IN mononucleosome substrate, recombinant APE1 (57 fmol) produced ~13 % incision, however in HeLa WCE (1 µg, equivalent) incision significantly increased to ~52 %. In contrast with the THF-OUT mononucleosome substrate at the same concentrations of APE1 and HeLa, virtually the same level of incision of the THF site was observed (73% and 75%, respectively). These findings provide further strong evidence that the increase in activity of APE1 in HeLa WCE on the THF-IN mononucleosome substrate could be due to an increase in accessibility from dissociation of the DNA from the histone octamer by PTM (eg. ubiquitination or poly(ADP-ribosyl)ation) on the N-terminal tails of histones which were either causing a structural change or recruiting an ATP-dependent chromatin remodeller.

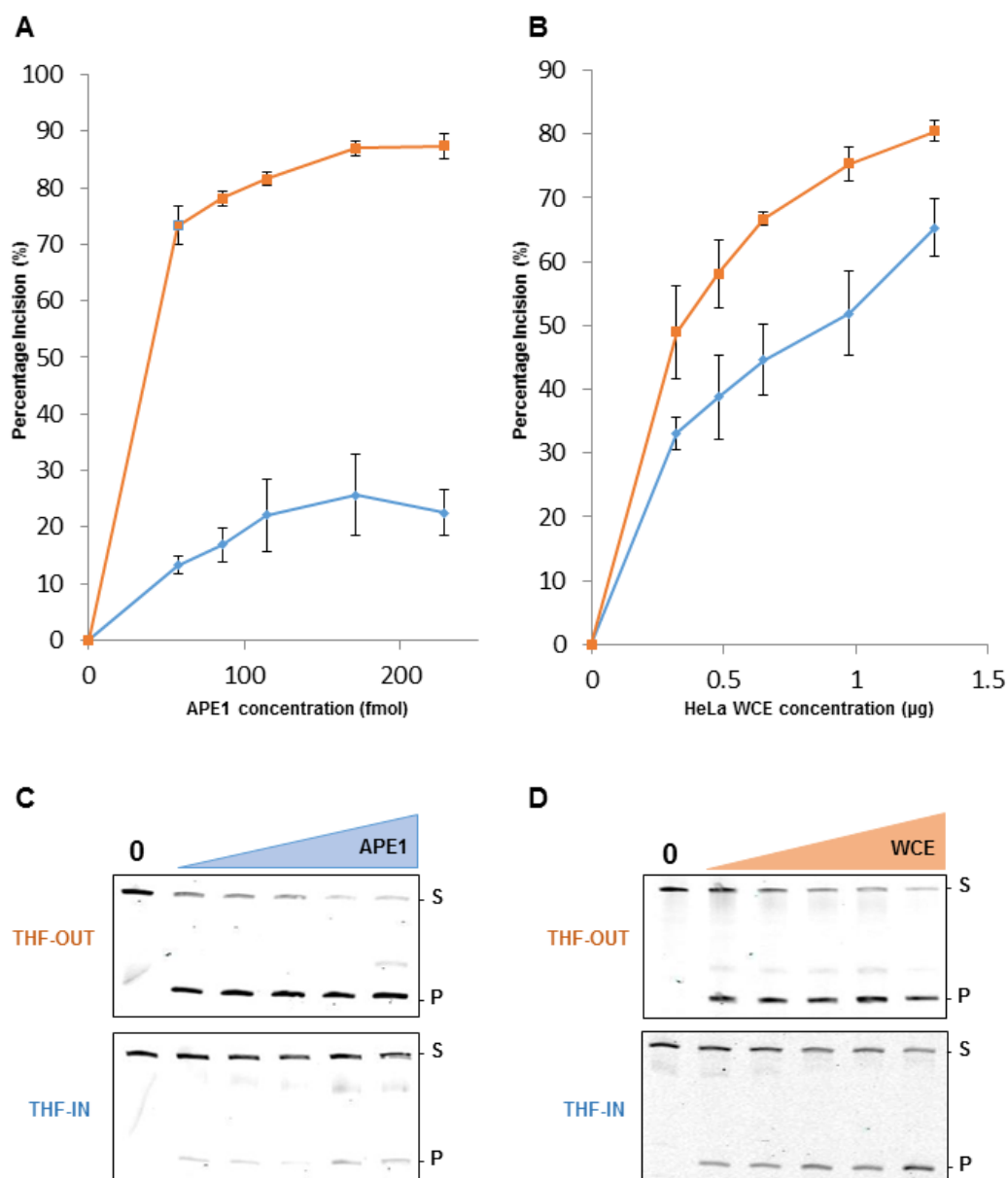


Figure 40: *In vitro* BER assays using mononucleosome substrates containing an THF-OUT (orange) or THF-IN (blue) with factors added to support ubiquitination and poly(ADP-ribosylation). For both mononucleosome substrates, percentage cleavage was quantified from denaturing (7 M) PAGE gels using the Odyssey Image Analysis system and the mean and standard deviation calculated for both substrates. Each reaction was supplemented with 0.7 pmol E1 and 2.5 pmol E2s, 5 mM NAD and 0.6 nmol ubiquitin. **A**, Purified APE1 concentration titration (0-229 fmol) using THF-OUT (orange) and THF-IN (blue) mononucleosomes and **C**, representative gels shown for each. **B**, HeLa whole cell extract concentration titration (0-1.3 μg) using THF-OUT (orange) and THF-IN (blue) mononucleosomes and **D**, representative gels shown for each. All denaturing PAGE gels contained 8 % polyacrylamide, 7 M Urea and 1x TBE, and run for 1.25 h at 350 V.

4.4 Analysing structural changes in the THF-IN mononucleosome following BER *in vitro* assay in the presence of additional factors.

The THF-IN mononucleosome was analysed for any structural changes following the BER *in vitro* assay using HeLa WCE in the presence of ubiquitin (plus E1 and E2 enzymes) and NAD. It was thought that perhaps the increase of APE1 activity towards THF with these added factors was promoting accessibility through a PTM (e.g. ubiquitination or poly(ADP-ribosyl)ation) on the N-terminal tails of histones causing a structural change or recruiting an ATP-dependent chromatin remodeller. The THF-IN mononucleosome was therefore analysed to see if the DNA was completely unwrapped from the histone octamer and so making the THF site more accessible to APE1, but also whether the histones were being directly ubiquitinated.

4.4.1 Modifications and structural changes the THF-IN mononucleosome following BER *in vitro* assay in the presence of ubiquitin

To analyse whether the THF-IN mononucleosome substrate DNA following incubation with HeLa WCE and ubiquitin was destabilised, thus promoting dissociation of the DNA from the histone octamer, the reaction was analysed by agarose gel electrophoresis to see if the nucleosome was still fully reconstituted and the structure maintained. The mononucleosome was found to still remain intact following incubation with HeLa WCE and ubiquitin when compared to free DNA (Figure 41A), suggesting that the nucleosome structure is not completely disrupted, and that possibly a partial, localised unwrapping event could be taking place. Since the incision of THF-IN by HeLa WCE was ubiquitin-dependent, possible histone modifications on the mononucleosome were analysed using Western blotting probing for H2A ubiquitination on K119 and H2B on K120, common PTM modifications of histones involved in DNA repair. The THF-IN mononucleosome substrate was incubated in the presence and absence of HeLa WCE and ubiquitin for 1 h and six reactions of each were pooled and separated by SDS-PAGE and analysed by Western blotting. Using the H2A K119 antibodies appeared show non-specific binding to a protein (largely at 10 kDa) in HeLa WCE but there was no evidence of H2A monoubiquitination appearing at ~25 kDa (Figure 41B). Similarly, the appearance of H2B K120 ubiquitination of histones in THF-IN by HeLa WCE was not evident (Figure 41C). Whilst this is not conclusive evidence for the lack of histone H2A lysine 119 and H2B lysine 120 ubiquitination induced by HeLa WCE, this does suggest that these particular PTM associated with DNA repair are not induced in THF-IN. However it should be noted that very low amounts of histones (<75 ng) are associated with THF-IN mononucleosome DNA which makes them difficult to analyse using this approach and further experimentation is necessary.

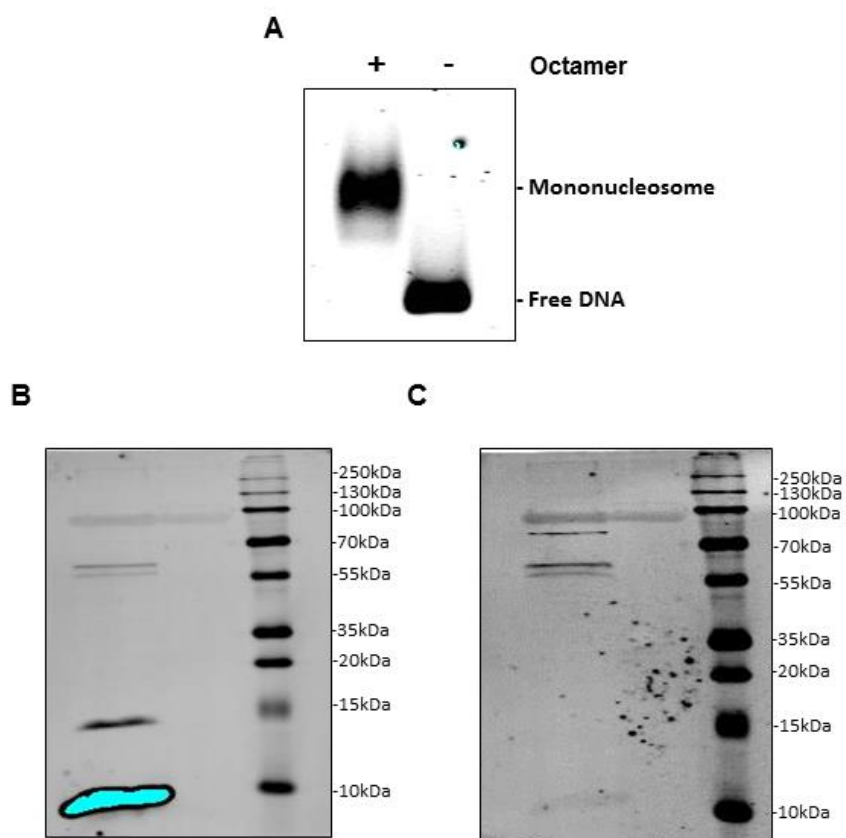


Figure 41: Analysing structural changes and modifications of THF-IN mononucleosome substrate. THF-IN mononucleosome substrate was treated with 1.3 μg HeLa WCE and 0.6 nmol ubiquitin using the BER *in vitro* assay and incubated for 1 h. **A**, after incubation the nucleosome was analysed using a 0.7 % agarose gel in 0.2x TAE containing SYTO60 using 50 fmol free DNA as a control and electrophoresed for 1.5 hat 75 V. **B and C**, Following incubation, 6 reactions in the presence (lane 1) or absence (lane 2) of HeLa WCE were pooled and electrophoresed on a 16 % SDS polyacrylamide gel with a 10 kDa to 250 kDa protein marker at 125 V for 2 h. Following electrophoresis proteins were transferred onto a membrane and analysed using western blotting probing for **(A)** H2A ubiquitination on Lys 119 and **(B)** H2B on Lys 120. Gel and Western blots were visualised using the Odyssey Image Analysis system.

4.4.2 Structural changes the THF-IN mononucleosome following BER *in vitro* assay in the presence of ubiquitin, E1/E2s and NAD

Following incubation of THF-IN with E1/E2 enzymes, NAD and ubiquitin in the BER *in vitro* assay with the THF-IN mononucleosome substrate, reactions were also analysed by agarose gel electrophoresis to examine if the DNA was dissociating from the histone octamer. The THF-IN mononucleosome appeared to remain intact following incubation when compared to the free DNA (Figure 42). Interestingly, there was an increase in smearing up the gel, suggesting a shift in the mononucleosomal DNA above the very defined mononucleosome band at 800bp. Whilst the nature of this smear requires further investigation, it does suggest that proteins such as ubiquitin or poly(ADP)ribose are binding to the THF-IN mononucleosome causing the gel shift, and we speculate that this could potentially be a histone modifier and/or chromatin remodeller.

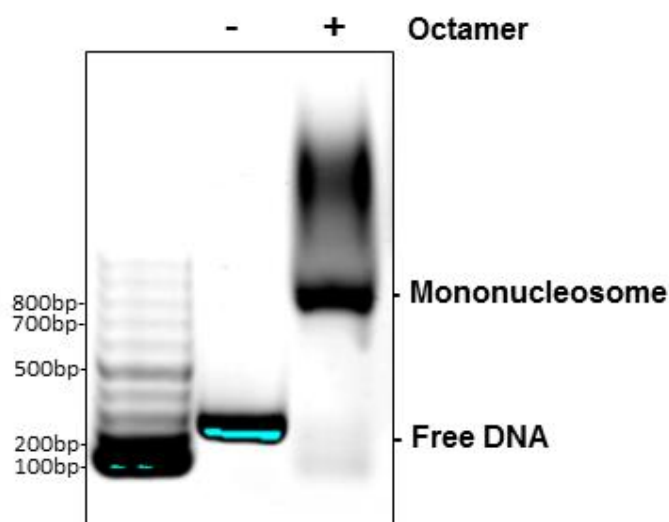


Figure 42: Analysing major structural changes in the THF-IN mononucleosome substrate with HeLa WCE in the presence of ubiquitin, NAD and E1/E2s. After 60 min incubation of the THF-IN mononucleosome substrate with HeLa WCE and ubiquitination factors (0.6 nmol ubiquitin, 0.7 pmol E1, 2.5pmol E2s and 5mM NAD), reactions were analysed against free THF-IN DNA as a control by 0.7 % agarose gel in 0.2x TAE using SYTO60. Agarose gels were electrophoresed at 75 V for 1.5 h and visualised using the Odyssey Image Analysis system

4.5 Summary

To examine whether PTMs by histone modifying enzymes and/or ATP-dependent chromatin remodelling complexes could facilitate APE1 in DNA repair, a BER *in vitro* assay was established to measure the repair of a THF site in THF-OUT which is easily accessible and THF-IN which contains an occluded lesion, using recombinant APE1 and HeLa WCE. We hypothesised that recombinant APE1 would efficiently incise the THF site in THF-OUT due to its increased accessibility but its activity towards the THF site in THF-IN would be significantly impeded as this site is sterically occluded. However, because HeLa WCE contains possible histone modifying enzymes able to induce PTMs on the N-terminal tails of histones and ATP-chromatin remodelling complexes that could remodel the nucleosome to make the THF site in THF-IN more accessible, it was hypothesised that this would increase incision by APE1. A direct comparison between recombinant APE1 and HeLa WCE in this context has not previously been reported.

A protocol to analyse the *in vitro* repair of THF sites in free DNA, as well as a THF site present within a mononucleosome at two different orientations, THF-OUT and THF-IN, was developed. Initially recombinant APE1 and HeLa WCE was incubated with THF-OUT and THF-IN free DNA for 10 min and the percentage incision quantified. This showed a slight bias in incision towards the THF-OUT free DNA compared to the THF-IN free DNA using both recombinant APE1 and HeLa WCE, although this difference was very minimal and probably due to the THF site being positioned in different sequence contexts. Using the same BER *in vitro* assay, but incorporating the THF-IN and THF-OUT mononucleosome substrates, it was found that recombinant APE1 and HeLa WCE (quantified by Western blotting to contain roughly the same amount of APE1 as used in comparison to recombinant APE1) were able to incise the THF site in the THF-OUT mononucleosome effectively but were both impeded to the THF in THF-IN. This was initially surprising as it was thought that the histone modifiers and/or chromatin remodellers present in HeLa WCE would cause the THF site in THF-IN to become more accessible by remodelling the DNA around the histone octamer. Therefore two points were further investigated; the short amount of time that the mononucleosomes were incubated (10 min) which is not sufficient time for remodelling to take place, and secondly the requirement of additional factors necessary for effective incision of the THF site. To tackle these points, the BER *in vitro* assay using a defined amount of HeLa WCE with the THF-IN mononucleosome substrate was analysed in a time course experiment, but also in the same experiment, the presence and absence of ubiquitin to promote ubiquitination events was investigated and subsequently the percentage incision of the THF site was monitored. In the absence of ubiquitin, the THF-IN mononucleosome substrate was still inefficiently processed by HeLa WCE up to 1 hour incubation times indicating that the time of the reaction was, at least partially, not a contributory factor in the lack of THF site incision. However in the presence of ubiquitin, the percentage incision increased dramatically demonstrating that a ubiquitination-dependent process was stimulating accessibility and incision of the THF site. It

was found that this increase in incision was not due to the DNA completely dissociating from the histone octamer as analysed by gel electrophoresis, so it was thought a partial unwrapping event could be taking place as a result of ubiquitination, possibly through ubiquitination of one of the histones. To rule out the possibility that ubiquitination of APE1 itself was increasing its activity, both THF-IN free DNA and the THF-OUT mononucleosome substrate incision was analysed using the same time course with HeLa WCE in the presence of ubiquitin. These two substrates were incised by HeLa WCE to the same level with and without ubiquitin. This suggested that ubiquitination was increasing THF site incision activity not by ubiquitination of APE1 itself, but potentially of histone proteins facilitating increased access of APE1 to the occluded THF site in THF-IN.

Since ubiquitin was found to stimulate incision of the THF site within the THF-IN mononucleosome substrate by HeLa WCE, several other components were added to the BER *in vitro* assay in a small scale experiment designed to optimise the conditions for maximal THF site cleavage by HeLa WCE. The concentration of ATP supporting phosphorylation events was thought not to be a factor in improving THF site incision as the addition of PC and PCK which regenerates ATP had no effect. However, addition of NAD, which is required for poly(ADP-ribosyl)ation, plus all factors required to stimulate ubiquitination (ubiquitin, E1/E2 enzymes) did produce a significant increase in THF site incision in the THF-IN mononucleosome substrate. Time course experiments were repeated using HeLa WCE with these additional components added using THF-IN mononucleosome substrate, and it was observed that the incision of THF-IN was extensively increased compared to reactions in the absence of these factors. Further titrations experiments of HeLa WCE (at 1 hour incubation) with these factors added using both the THF-IN and THF-OUT mononucleosome substrates revealed that in fact the incision of the THF-IN mononucleosome substrate by HeLa WCE was approaching the levels of incision of the THF-OUT mononucleosome substrate, which is easily accessible. Indeed when comparing relative levels of APE1 in HeLa WCE to recombinant APE1 there was found to be a 4-fold increase in incision of the THF-IN mononucleosome when using the same amount of APE1 in HeLa WCE compared to recombinant APE1. In contrast THF site in the THF-OUT mononucleosome was found to have similar levels of incision when using the same amount of APE1 in HeLa WCE and recombinant APE1. This strongly indicated that these additional factors supporting ubiquitination and poly(ADP-ribosyl)ation events were greatly stimulating THF site accessibility using THF-IN by HeLa WCE. In contrast, there was still a significant difference in incision of the THF-IN versus THF-OUT mononucleosomes substrates with recombinant APE1, demonstrating a dependence on proteins present within the HeLa WCE. Indeed as incision was largely stimulated by E1/E2 enzymes and ubiquitin, this suggested the presence of an E3 ubiquitin ligase in the WCE which was causing ubiquitination of one of the histone proteins in the histone octamer, which was either causing a structural change in the mononucleosome, or recruiting an ATP-dependent chromatin remodelling complex making the occluded THF site in THF-IN more

accessible to APE1. Again, this event was found not to occur through complete unwrapping of the nucleosomal DNA from the histone octamer so a partial unwrapping event could be taking place. The identity of potential E3 ubiquitin ligase(s) or PARPs that are driving this effect in HeLa WCE was then the subject of further experiments.

CHAPTER V

RESULTS III

Identification of histone modification/chromatin remodelling factors that stimulate APE1 activity towards the THF-IN mononucleosome substrate

5.1 Introduction

As discussed in the previous chapter a ubiquitination or poly(ADPribose)ation event was hypothesised to be taking place on histones causing increased accessibility of the THF-IN mononucleosome to APE1 in HeLa WCE with factors to support these two PTMs. At this stage I focused on the ubiquitination event that was thought to be taking place. This was partly due to the expertise of this laborator, but more importantly because of its known roles in the DDR in DSB repair and NER for chromatin remodelling to facilitate repair. Ubiquitin is a small regulatory protein which is covalently added onto substrate proteins, termed ubiquitination, which can affect protein stability, activity and protein-protein or protein-DNA interactions, as discussed previously. RNF8 and RNF168 have been found to ubiquitinate H2A and H2AX on K13 and 15 and form K63-linked chains increasing the accessibility of DSBs and so facilitating the loading of 53BP1 (197, 199). PTM of histones can also recruit ATP-dependent chromatin remodelling complexes. For example, INO80 is recruited to DSB by γ H2AX to allow access of the initial repair proteins by chromatin remodelling to facilitate resection of DSB (226). These complexes regulate chromatin by repositioning nucleosomes, removing and expelling histone proteins and so altering the accessibility of certain regions of DNA to proteins for biological process including DNA damage repair.

The evidence for the role of histone modifications and ATP-dependent chromatin remodelling complexes in BER is limited. Data from other Groups and the data provided in this thesis (Chapter IV) show that the orientation and translational position of DNA base damage impacts the activity of BER proteins. Indeed, I have shown that a synthetic THF site with the backbone facing outwards away from the octamer (THF-OUT) is efficiently incised by APE1 using both recombinant APE1 and HeLa WCE. In contrast, a THF site with the DNA backbone which is facing inwards toward the histone (THF-IN) is inefficiently cleaved by recombinant APE1, although when using HeLa WCE in the presence of factors that stimulate ubiquitination, the THF site is more efficiently cleaved. This suggested that there was a ubiquitination-dependent event, catalysed by an E3 ubiquitin ligase, occurring on a histone protein within the histone

octamer which caused a structural change in the nucleosome, or stimulated the recruitment of a ATP-dependent chromatin remodelling complex causing the THF site in THF-IN to become more accessible.

Therefore the aim of this chapter was to identify the E3 ligase and/or the chromatin remodelling factors present in HeLa WCE that were stimulating BER. Two approaches were used to achieve this goal. Firstly, a candidate approach was used whereby E3 ligases known to be involved in other types of DNA repair and histone modifications were depleted by siRNA knockdowns in HeLa cells, and the effect of these examined on the incision activity of recombinant APE1 on the THF-IN mononucleosome substrate *in vitro*. Secondly, a biochemical fractionation approach was utilised, which is a strong and successful approach in Dr Parsons' laboratory, which involves separation of proteins from HeLa WCE by sequential chromatography and testing the activity of individual fractions in stimulating recombinant APE1 activity towards the THF-IN mononucleosome substrate. Fractions, and ultimately purified proteins, were then identified by mass spectrometry. Using both approaches, and once candidates have been identified, DNA damage repair kinetics and survival following IR in cells could be analysed to further confirm their role in BER during the cellular DNA damage response.

5.2 A candidate approach to discover the possible E3 ubiquitin ligase responsible for ubiquitinating histones

In the previous chapter, it was discovered that when factors were added to HeLa WCE to stimulate ubiquitination (E1, E2s, ubiquitin) but also poly(ADP-ribosyl)ation (NAD) the THF-IN mononucleosome substrate was significantly more efficiently incised by APE1 present in WCE, compared to recombinant APE1 which had very little activity on the substrate. Therefore, it was hypothesised that an E3 ubiquitin ligase was ubiquitinating one or more of the histone proteins present in the histone octamer and either destabilising the DNA:histone octamer interaction, or causing the recruitment of an ATP-dependent chromatin remodeller, either of which could promote the THF site in the THF-IN mononucleosome substrate to become more accessible to APE1 in HeLa WCE. To specifically identify the E3 ubiquitin ligases involved in this process, eleven enzymes previously associated with other DNA repair pathways and histone ubiquitination were selected and their possible effect in stimulating THF site cleavage by APE1 was analysed. These enzymes were male-specific lethal-2 (MSL2), ubiquitin protein ligase E3 component N-recognin 2 (UBR2), RNF168, ring finger protein 20 (RNF20), DAZ Interacting Zinc Finger Protein 3 (DZIP3), CUL4A, cullin-1 (CUL1), ring finger protein 2 (RNF2), RNF8, Mcl-1 ubiquitin ligase E3 (MULE) and BRCA1, see table 10 for their suggested functions. This was achieved by siRNA knockdowns of each of the eleven E3 ligases for 48 h in HeLa cells. Following siRNA treatment, cells were harvested and cell extracts prepared for use in BER *in vitro* repair assays to quantitatively analyse any difference

in the incision by recombinant APE1 of the THF-IN mononucleosome substrate in the absence of each E3 ubiquitin ligase or PARP. Assays were performed in the presence of factors to support ubiquitination (E1, E2, ubiquitin) and poly(ADP-ribosyl)ation (NAD) and reactions were analysed by denaturing (7 M urea) PAGE prior to quantification using the Odyssey Image Analysis System to determine the degree of THF site incision for each of the E3 ligase knockdowns compared against a Lipofectamine (transfection reagent only) control.

Ubiquitin E3 Ligase	Association with Histones and/or DNA Repair
BRCA1	Key HR factor and ubiquitinates several key proteins at DSBs including H2A K127-129 (with BARD1). (273)
CUL1	In complex with SKP1-Cul1-F-box to increase JMJD2/KDM4 histone demethylases turnover to regulate chromatin modifications (274)
CUL4A	Catalyses the ubiquitination of H3 and H4 in response to UV irradiation (275)
DZIP3	Targets H2A K119 ubiquitination (276)
MSL2	Ubiquitinates H2B K34 <i>in vitro</i> and Drosophila. Located on in an inaccessible area of nucleosome structure, ubiquitination of this residue would likely cause significant alteration of the nucleosome (277)
MULE	Regulator of BER. Ubiquitinates histones and likely plays a role in chromatin condensation (278, 279)
RNF2	Monoubiquitinates H2A K119 and 120 to help in the recruitment of phosphorylated ATM to DSBs, and so reduces γ H2AX (280)
RNF8	Ubiquitinates H1 and monoubiquitinates H2A/H2AX which catalyses K63 linked ubiquitin chains with UBC1 to recruit RNF168 (196)
RNF20	Monoubiquitinates H2B on K120 to promote chromatin remodelling a HR (203)
RNF168	Ubiquitinates H2A K13 and K15 leading to the recruitment of 53BP1 and other DSB repair proteins (204)
UBR2	Ubiquitinates histones H2A and H2B in spermatocytes and somatic cells for chromosome stability. UBR2 deficient chromosomes showed defects in DSB repair (281)

Table 10: Candidate E3 Ligases for stimulation of THF-IN incision. Eleven E3 ligases were selected for the mini screen to test for THF-IN incision activity by APE1 in HeLa WCE following SiRNA knockdown. E3 Ligases were selected based on their known activity in DNA repair and/or histone modifications.

5.2.1 Analysing the efficiency of the knockdown for each E3 ubiquitin ligase in HeLa cells

Firstly, the efficiency of the siRNA knockdowns were determined using quantitative PCR (qPCR). RNA was extracted from HeLa cell pellets and utilised to prepare cDNA. Primers for each E3 ubiquitin ligase gene, and actin as the reference gene, were assessed by qPCR and a threshold cycle (Ct) value was determined for each gene knockdown. Each knockdown was performed in triplicate and averaged before the knockdown efficiency was calculated. The majority of siRNA knockdowns for each E3 ubiquitin ligase gene were greater than 85 % (apart from DZIP3 which still had a 76 % knockdown) as shown in figure 43. It was concluded from this that the E3 ligase knockdowns were successful and so the HeLa cell pellets for each siRNA treatment could be utilised for preparing WCE. These extracts could then be used in the BER *in vitro* assay to see if there were any differences in THF site incision of the THF-IN mononucleosome substrate in the absence of each of the E3 ubiquitin ligases.

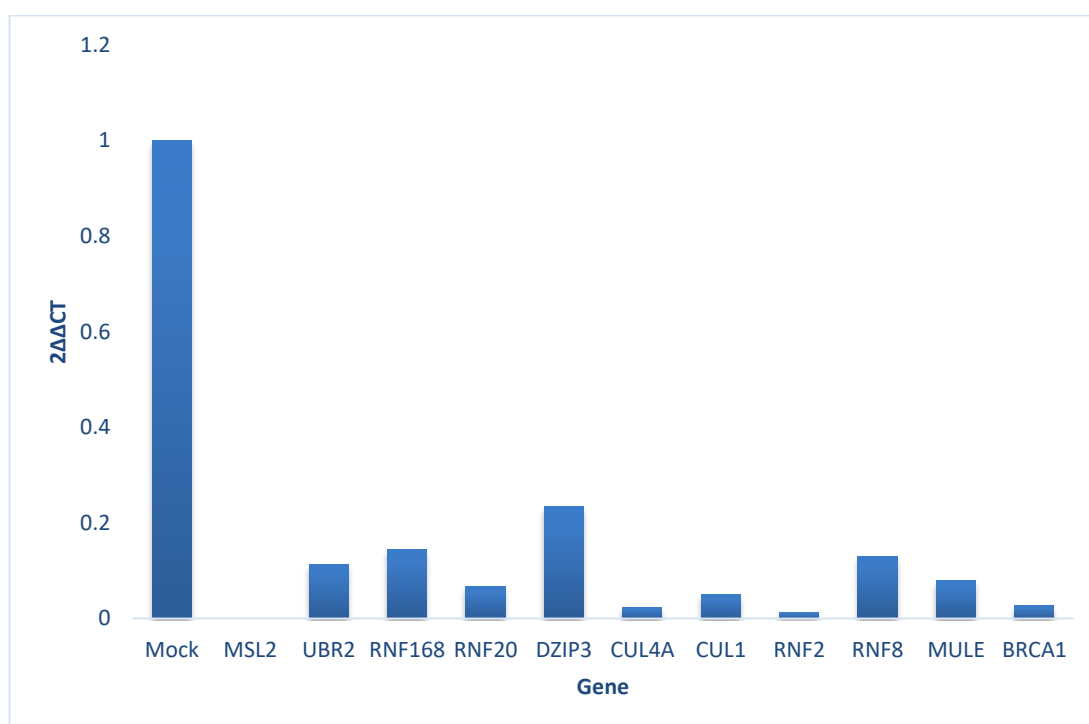


Figure 43: Percentage knockdown for each siRNA candidate E3 Ligases. The percentage knockdown for each E3 ligase was quantitated by RT-PCR and the gene levels of mRNA (RQ value) calculated from the CT value for the RT-PCR run. Bar chart shows the mock (lipofectamine only) normalised to 1 and the relative gene levels after siRNA knockdown. Each was done in triplicate and the average CT value calculated. A non template control (just primers, no cDNA) was also run for each primer to check for any contamination which could alter results.

5.2.2 BER *in vitro* assay with titrations of E3 ubiquitin ligase knockdown HeLa WCE with THF-IN mononucleosome

To analyse if there were any differences in incision rates of recombinant APE1 in HeLa WCE on the THF-IN mononucleosome substrates, siRNA knockdown of the eleven E3 Ligases in HeLa cells were performed, WCE was prepared and two concentration points were analysed (0.65 and 1.3 μ g) for each E3 ubiquitin ligase knockdown, using Lipofectamine (transfection reagent only) as a control. WCE were incubated with the THF-IN mononucleosome substrate (1 h at 30°C), and the percentage incision of this substrate from two independent BER assays using these concentrations for each E3 ubiquitin ligase knockdown was analysed by denaturing (7 M urea) PAGE, quantified using the Odyssey Image Analysis System and averaged. I found that there was no dramatic difference in percentage incision of the THF-IN mononucleosome substrate between any of the E3 ligase knockdowns compared to the control (Figure 44A, 44B and 44C). Using 0.65 μ g HeLa WCE, all E3 ubiquitin ligase knockdowns lay within a maximum of 8 % range of the control, and at 1.3 μ g WCE, this difference decreased slightly to 5 %. Only a knockdown of CUL4A or RNF2 appeared to show any decrease in incision of THF-IN at the two concentrations of WCE tested. Nevertheless, this indicated that there was no significant differences in THF site incision in the absence of these selected E3 ligases. To examine whether there may be a delay in the kinetics of APE1 activity in HeLa WCE following an E3 ubiquitin ligase knockdown, a small time course was utilised to see if there were any differences in percent incision of the THF-IN mononucleosome substrate.

5.2.3 BER *in vitro* assay time course with E3 ubiquitin ligase knockdown HeLa WCE with THF-IN mononucleosome

A time course was used to analyse if there was any significant difference in the kinetics of THF site incision using HeLa WCE (1.3 μ g) for each E3 ubiquitin ligase siRNA knockdown, in comparison to Lipofectamine (transfection reagent only) as a control. WCE were incubated with the THF-IN mononucleosome (10 and 30 min), and the percentage incision of the substrate from two independent BER assays using these time points for each E3 ubiquitin ligase knockdown was analysed by denaturing (7 M urea) PAGE, quantified using the Odyssey Image Analysis System and averaged (Figure 45A, 45B and 45C). After 10 min, the percentage incision of the THF-IN mononucleosome substrate for all E3 ubiquitin ligase knockdowns (apart from MSL2) were slightly below the control, with the lowest two corresponding to RNF8 (figure 45A) and MULE (figure 45C) at 27 % and 28.5 % respectively compared to the control at 39 %. However the efficiency of incision of both RNF8 and MULE depleted WCE appeared to increase at 30 min, where they were similar to that observed with the control WCE. After 30 min, the biggest difference in incision activity compared to the

control was with CUL1 knockdown, although this only differed by 8 % (figure 45B). Furthermore a depletion of UBR2, RNF168 and DZIP3 (in addition to CUL1) led to consistent decreases in the incision of THF-IN at both 30 and 60 min incubation. However, due to these minor differences, again it was concluded that there was no significant and dramatic decreases in THF site incision of the THF-IN mononucleosome substrate by APE1 present in HeLa WCE when these selected eleven E3 ligases, associated with other DNA repair pathways, were absent. This could be for several reasons. Firstly, that there were multiple E3 ubiquitin ligase activities that were compensating for each other when one was depleted and so the THF site was still being made accessible to APE1. Secondly, that there were other E3 ligase(s), or other ubiquitin-dependent activities, that had not been selected for analysis. Due to the complexity of these results combined with the small changes observed, it was determined that a WCE fractionation approach using sequential chromatography was utilised to identify and purify potential activities that stimulate APE1 activity towards the THF site in the THF-IN mononucleosome substrate.

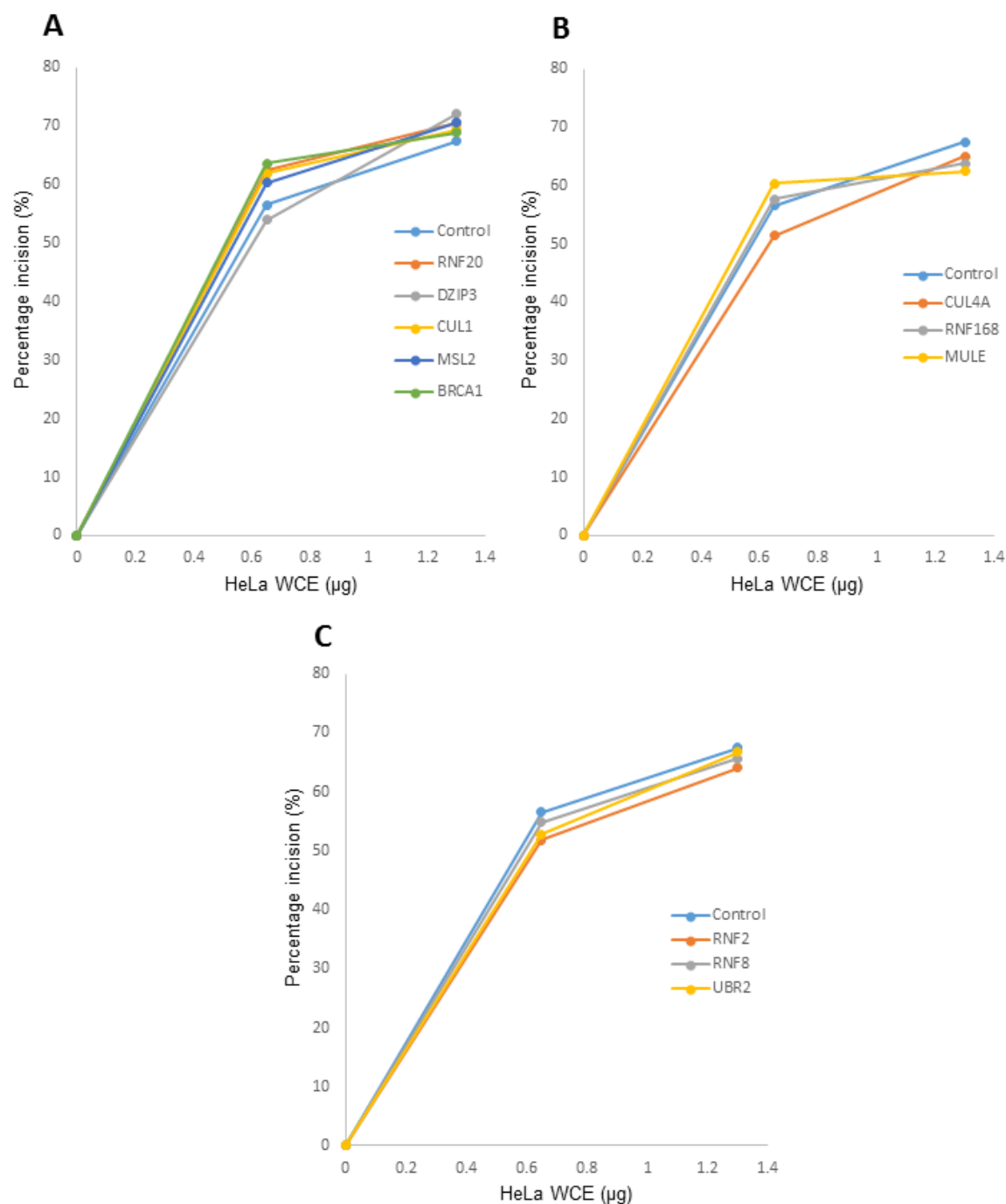


Figure 44: The effect of candidate siRNA E3 ubiquitin ligase knockdowns titrations on the BER *in vitro* assay with THF-IN mononucleosome. The BER *in vitro* assay was used with factors to stimulate ubiquitination (0.7 pmol E1, 2.5 pmol E2 and 0.6 nmol ubiquitin) to analyse to the effect of HeLa WCE prepared from each siRNA E3 ligase knockdown on the AP site incision of THF-IN mononucleosome using A, B, C, titrations of each HeLa cell extract (0.65 μg and 1.3 μg) for 1 h at 30°C. Graphs show the average from two separate experiments quantified from denaturing (7 M) PAGE gels contained 8 % polyacrylamide, 7 M Urea and 1x TBE, and run for 1.25 h at 350 V.

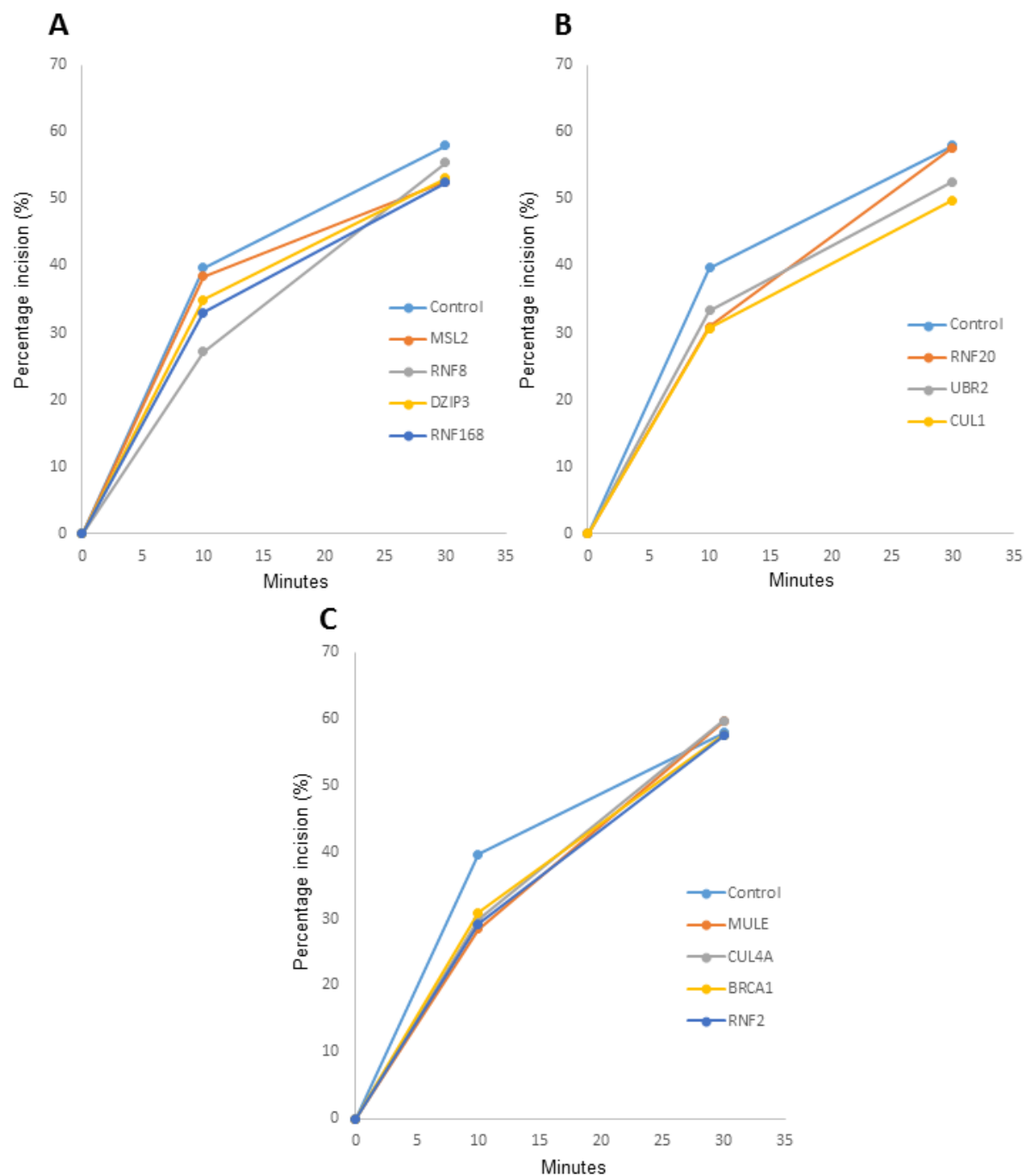


Figure 45: The effect of candidate siRNA E3 ubiquitin ligase knockdowns on the BER *in vitro* assay using a time course with THF-IN mononucleosome. The BER *in vitro* assay was used with factors to stimulate ubiquitination (0.7 pmol E1, 2.5 pmol E2, 0.6 nmol ubiquitin and 5mM NAD) to analyse the effect of HeLa WCE prepared from each siRNA E3 ligase knockdown on the AP site incision of THF-IN mononucleosome using, A, B, C, a time course (10 and 30 min) following incubation with each of the HeLa WCE (1.3 µg). The key for both A and B is shown on the right. Graphs show the average from two separate experiments quantified from denaturing (7 M) PAGE gels contained 8 % polyacrylamide, 7 M Urea and 1x TBE, and run for 1.25 h at 350 V.

5.3 Fractionation of HeLa WCE to identify novel activities that stimulate APE1 activity towards the THF site in THF-IN mononucleosome substrate

Candidate histone modifying activities, E3 ubiquitin ligases and potentially ATP-dependent chromatin remodelling complexes were aimed to be discovered using sequential chromatography of HeLa WCE in combination with the BER *in vitro* assay containing the THF-IN mononucleosome substrate. This approach has been very successful in Dr Parsons' laboratory to identify other enzymatic activities, largely E3 ubiquitin ligases, that regulate various BER proteins (267, 272, 282, 283). HeLa WCE was therefore fractionated by sequential chromatography using, 1. phosphocellulose, 2. ion exchange, 3. gel filtration and 4. a final polishing ion exchange chromatography step. The 250ml phosphocellulose column was used initially to separate DNA and non-DNA binding proteins, this column has a very high binding capacity (10mg/ml) so could take up to 2.5g protein. Once the active fraction from the phosphocellulose fractionation had been established then this fraction was put over a 20ml MonoQ, which also had a very high binding capacity (60mg/ml) so could take up to 1.2g of proteins. Active fractions then underwent gel filtration chromatography to help determine the molecular weight of the partially purified activity, and the active fractions put over a final MonoQ column as a polishing step. We couldn't use the gel filtration before the first MonoQ, as the sample volume for gel filtration needs to be extremely low (<5% of the column volume) to improve separation. Following each chromatography step, protein fractions were analysed using the BER *in vitro* assay incorporating the THF site in THF-IN mononucleosome substrate in the presence of recombinant APE1, to identify those that stimulate APE1 activity above the basal level observed with the protein alone, as a control. Active fractions were pooled and were subsequently fractionated by the next chromatography stage until the fractionation was performed to completion, at which point fractions were analysed by mass spectrometry. Candidates were selected based on how high their Mascot score was, this is the probability that the protein is present in the sample based on matching of the sequences identified by mass spectrometry with the peptide sequence databases. Therefore the higher the Mascot score (which is also related to the number of peptides recognised and the sequence coverage), then the more likely the protein is there. Generally proteins with a mascot score of ~50 or less have low probability.

5.3.1 Phosphocellulose chromatography of HeLa WCE

HeLa WCE was prepared from 20 g cell pellets and was firstly fractionated by Phosphocellulose chromatography. Phosphocellulose mimics DNA, particularly being negatively charged, and proteins were then eluted into two fractions by salt elution. PC150 (elution at 150 mM KCl) largely contains non-DNA binding proteins and the subsequent generation of PC1000 (elution at 1000 mM KCl) largely contains DNA binding proteins. Due to the presence of endogenous APE1 within these fractions that may interfere with analysis of

stimulation of THF site incision activity by recombinant APE1, this endogenous protein was firstly aimed to be removed by immunodepletion.

5.3.1.1 Immunodepletion of APE1 in HeLa WCE, PC150 and PC1000

APE1 was immunodepleted in HeLa WCE, in addition to the PC150 and PC1000 fractions, to attempt to remove/reduce any residual, endogenous APE1 incision activity. Magnetic beads bound with APE1 primary antibodies were used for immunodepletion of the extracts which was performed overnight at 4°C, prior to analysis by Western blotting following 10 % SDS-PAGE. It can be seen that endogenous APE1 present in the WCE, is also present in the PC1000 fraction as expected, since APE1 displays DNA binding activity (Figure 46A). PC150 only contains very little/trace amounts of APE1. After immunodepletion, APE1 was successfully depleted by ~82 % from HeLa WCE but this had limited success (~20 %) in PC1000, which could not be improved. Nevertheless, with this in mind, APE1 immunodepleted fractions were examined for stimulation of recombinant APE1 activity using the THF-IN mononucleosome substrate.

5.3.1.2 BER *in vitro* assays to analyse APE1 stimulation in PC150 and PC1000

The BER *in vitro* assay containing factors added to stimulate ubiquitination (E1, E2, ubiquitin) and poly(ADP-ribosyl)ation (NAD) was utilised to analyse THF site incision of the THF-IN mononucleosome substrate with HeLa WCE, PC150 and PC1000 after APE1 immunodepletion, in the absence and presence of recombinant APE1. Reactions were incubated for 1 h and analysed by denaturing (7 M urea) PAGE and gels quantified by comparing the cleaved 119 bp THF-IN incision product to the 256 bp substrate using the Odyssey Image Analysis System for determining the percentage incision of this substrate. Purified APE1 only (57 fmol) produced ~20 % incision of the THF site in the THF-IN mononucleosome, which was used as a baseline value (Figure 46B and 46C). If after addition of recombinant APE1 to the extracts that the incision activity increased above this baseline value, then it was predicted that there were histone modifiers (eg. E3 ubiquitin ligases) or chromatin remodelling factors (eg. ATP-dependent chromatin remodelling complexes) that were causing the THF site in the THF-IN mononucleosome to become more accessible to APE1 and so increasing the percentage incision. A fixed amount of HeLa WCE, PC150 and PC1000 (1.3 µg) with THF-IN mononucleosome substrate were then incubated with and without recombinant APE1. Incision of THF-IN by HeLa WCE increased from 13 % to 36 % when recombinant APE1 was added, an increase of 23 %, which is similar to that for recombinant APE1 only. Likewise, addition of recombinant APE1 to PC1000 only increased THF site incision by ~13 % (from 33% to 46%). In contrast, THF site incision by PC150 increased from 0.8 % to 37 % in the absence and presence of recombinant APE1, an increase

of ~36 %, This was significantly more than the baseline value observed with recombinant APE1 only, suggesting that there are E3 ubiquitin ligase(s) and/or chromatin remodelling factors largely in PC150 that are increasing the accessibility of the THF site in THF-IN mononucleosome substrate to recombinant APE1. Therefore, the PC150 fraction was further fractionated to identify novel activities that stimulate recombinant APE1 activity.

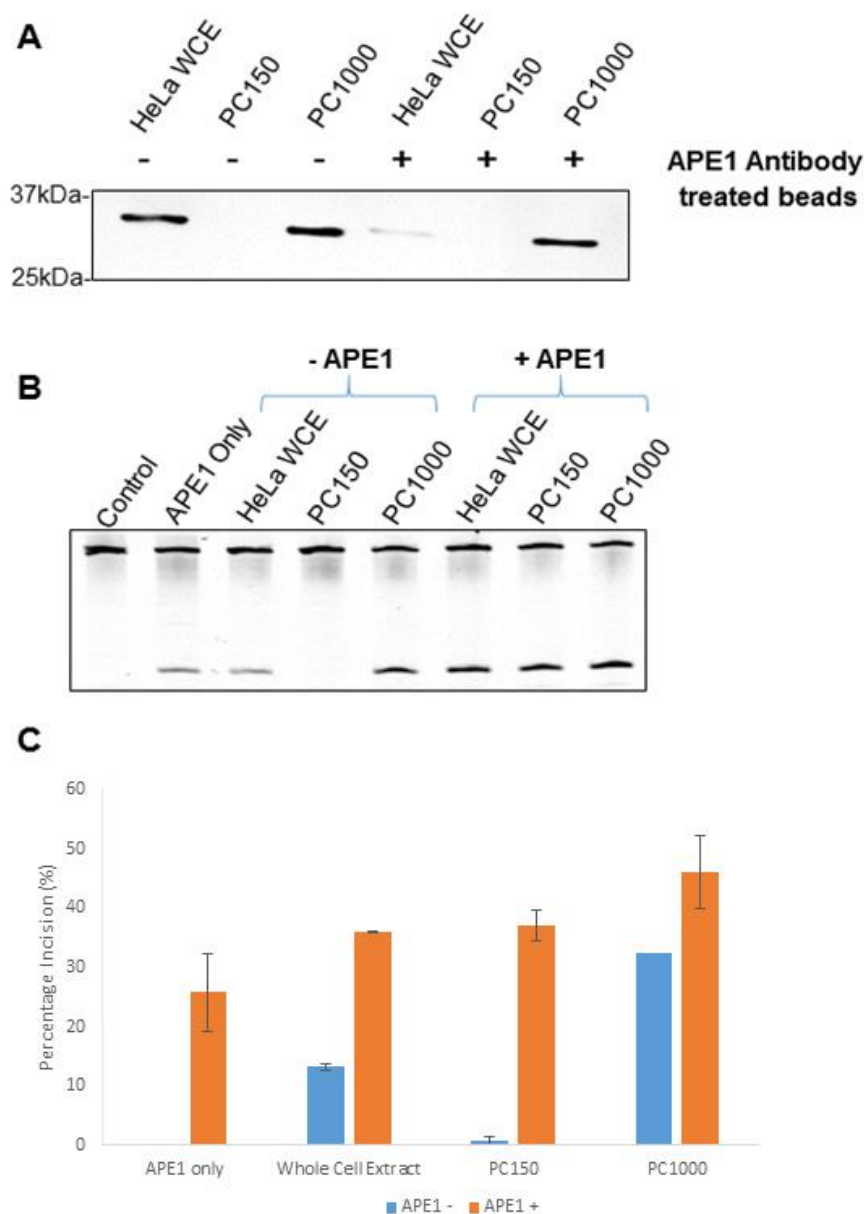


Figure 46: Analyses of APE1 stimulation by WCE, PC150 and PC1000 fractions; APE1 was immunodepleted from HeLa WCE, PC150 and PC1000 and the efficiency of the immunodepletion determined by analysis of extracts (10 μ g) on a 10 % SDS polyacrylamide gel which was probed for APE1 by Western blotting (A). Immunodepleted HeLa WCE, PC150 and PC1000 in the absence and presence of purified APE1 (57 fmol) were used in the BER *in vitro* assay with THF-IN mononucleosome and incubated for 1 h at 30°C with additional factors (0.7 pmol E1, 2.5 pmol E2, 0.6 nmol ubiquitin and 5 mM NAD) (B). Purified APE1 was used as a control which produces around ~20-25 % incision of this substrate, which was as the threshold value which is shown. All other values for HeLa WCE, PC150 and PC1000 have had the threshold value deducted to show the stimulation of APE1 above the threshold. Percentage incision was quantified from denaturing (7 M) PAGE and the average quantifications for two independent experiments are shown and the standard error (C).

5.3.2 Ion exchange chromatography of the PC150 fraction of HeLa WCE

The PC150 fraction (~1 g total protein) was fractionated by ion exchange chromatography using a 20 ml Mono Q column utilising an increasing salt gradient to elute protein fractions. This resulted in the generation of >80 protein fraction, therefore alternate fractions were analysed for their ability to stimulate the THF site incision activity of recombinant APE1. Any endogenous/residual APE1 activity present in the fractions was also determined by analysis of fractions in the absence of recombinant APE1 using the THF-IN mononucleosome substrate. Reactions were incubated for 1 h at 30°C with factors to support ubiquitination (E1, E2, ubiquitin) and poly(ADP-ribosyl)ation (NAD), separated by denaturing (7 M urea) PAGE and gels quantified by comparing the cleaved 119 bp THF-IN incision product to the 256 bp substrate using the Odyssey Image Analysis System to quantify the degree of THF site incision.

5.3.2.1 Identifying novel activities for stimulation of APE1 activity from ion exchange chromatography of PC150

Fractions from Mono Q fractionation of the PC150 fraction of HeLa WCE were buffer exchanged to ensure that the level of salt in each fraction was approximately the same (50 mM KCl). The BER *in vitro* assay was employed to analyse THF site incision of the THF-IN mononucleosome with factors added to support ubiquitination and poly(ADP-ribosyl)ation. Recombinant APE1 only (57 fmol) was added to the reactions to examine if protein within the fractions could stimulate APE1 activity above the baseline value of ~20 %. Recombinant APE1 only reactions (but still with ubiquitination/poly(ADP-ribosyl)ation stimulating factors) was always completed with every set of reactions as a control, and deducted from the percentage incision found in the fractions it was used in. This then showed the increase in incision that was not related to recombinant APE1 only, but related to factors stimulating APE1 activity, such as E3 ubiquitin ligase(s) and ATP-dependent chromatin remodelling complexes. Alternate protein fractions generated from the Mono Q chromatography (Figure 47A) from fraction 6 to 76 were analysed for this APE1 stimulating activity (Figure 47B and 47C, blue line). Three main stimulatory activities were identified; from fractions 34 – 42 (activity 1; Figure 47Bi) peaking at fraction 36 at ~37 % incision above the baseline value, fractions 46 – 52 (activity 2; Figure 47Bii) peaking at fraction 50 at ~36 % incision, and fractions 63 to 76 (activity 3; Figure 47Biii) the strongest activity with the last six fractions producing up to 40 % incision above the baseline value. Their elution position in the FPLC UV trace is shown (Figure 47A). A smaller incision activity was noticed between fractions 20 to 28 with the peak fraction being at fraction 25 producing ~14 % incision above the baseline value. The BER *in vitro* assay was repeated on the three strongest activities, and although percentage incision did vary for activities 1 and 2, there were still three defined activities where the percentage incision above the baseline value for activity were observed (Figure 47C, grey line). To determine if these

were genuine APE1 stimulating activities, fractions had to be analysed further for any residual/endogenous APE1 which could be producing one or more of identified activities and so are not directly related to APE1 stimulation.

5.3.2.2 Analysing fractions for residual APE1 incision activity

Fractions were examined for any endogenous/residual APE1 incision activity, by performing BER *in vitro* assays in the absence of recombinant APE1, therefore eliminating any false positives in APE1 stimulating activities. Therefore alternate fractions from 18 to 54 and 60 to 76 (where the major APE1 stimulatory activities were discovered) were tested for THF site incision activity with the THF-IN mononucleosome in the BER *in vitro* assay with factors added to stimulate ubiquitination/poly(ADP-ribosyl)ation. Fractions 20 to 22 were found to produce a spike in THF site incision activity (~15 % incision above baseline levels; Figure 47C, orange line). This appeared to partially overlay with the small activity that was seen with fractions 18 to 28 in the presence of recombinant APE1 (Figure 47C, blue line) suggesting that this small activity was probably accountable to residual, endogenous APE1 in the fractions. At the position of the three other identified APE1 stimulatory activities, however, negligible THF site activity was observed. Therefore these activities were pooled separately and further fractionated separately in order to purify and identify the proteins responsible for stimulating APE1 activity.

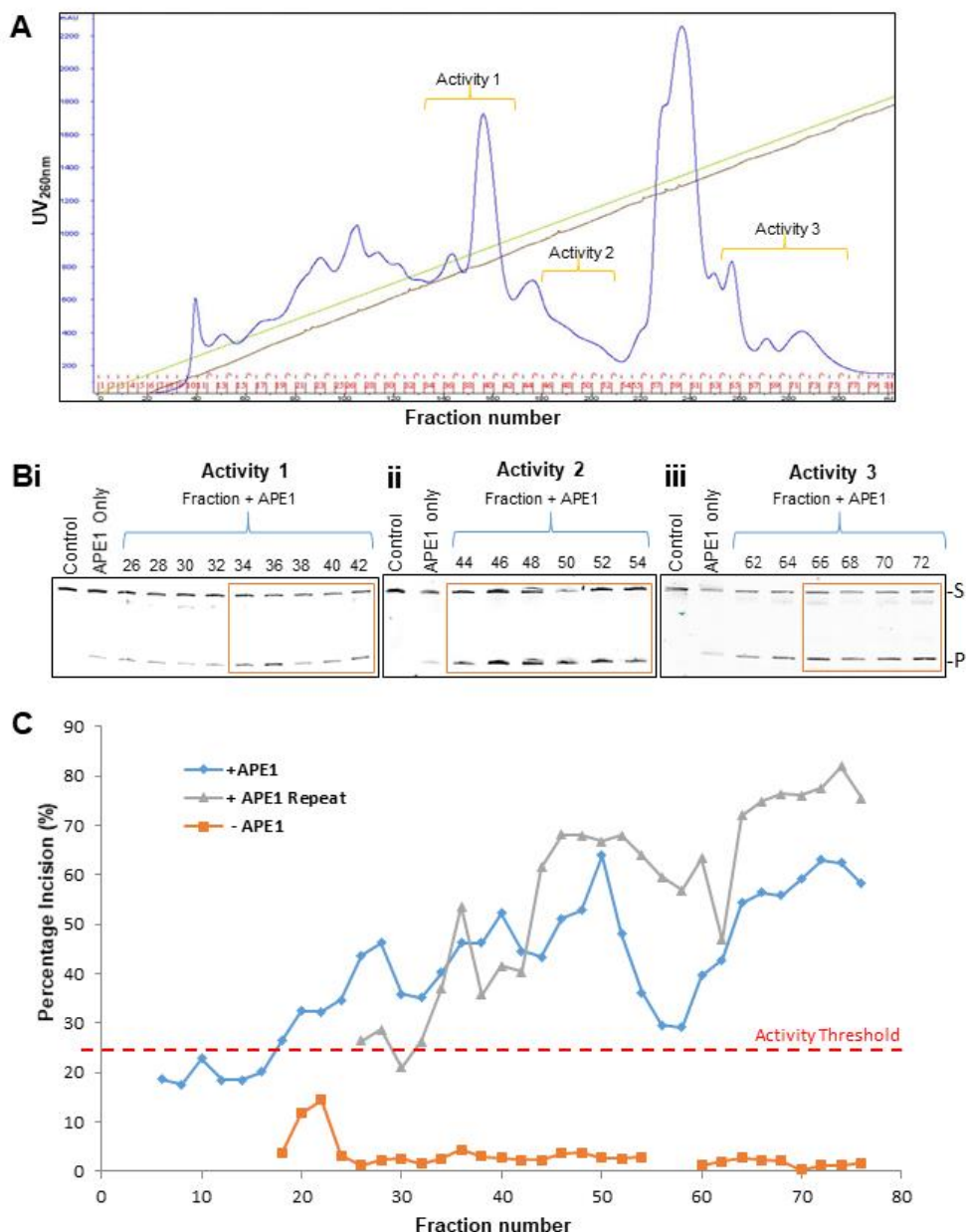


Figure 47; Mono Q chromatography of HeLa PC150. Proteins within HeLa PC150 were fractionated by Mono Q chromatography shown is the FPLC UV trace (A). The relative THF site incision activity on the THF-IN mononucleosome substrate by protein fractions was tested using the BER *in vitro* assay with additional ubiquitin stimulating factors (0.7 pmol E1, 2.5 pmol E2, 0.6 nmol ubiquitin and 5 mM NAD) added in the presence of APE1 (57 fmol) and incubated for 1 h at 30°C. Representative gels from three activities identified by denaturing (7 M) PAGE gels are shown for activity 1 (Bi), activity 2 (Bii) and activity 3 (Biii). Quantification of these gels (blue line) and a repeat analysis on the active fractions (grey line) are also shown (C), where threshold incision activity of the purified APE1 only, producing 24 % incision is shown as a red dashed line. Fractions that stimulated APE1 activity above this baseline are suspected to have chromatin remodelling factors and/or E3 ligases.

5.3.3 Further fractionation of the three activities and identifying candidate proteins that stimulate APE1 activity

Now that three activities stimulating APE1 activity on the THF-IN mononucleosome substrate has been identified, each activity was further fractionated in order to purify protein activity to near homogeneity. This was achieved using sequential gel filtration chromatography and a final polishing step involving ion exchange chromatography. As above, fractions were analysed for stimulation of recombinant APE1 incision activity on the THF-IN mononucleosome substrate using the BER *in vitro* assay, with a focus on identifying incision activities above the baseline value obtained using recombinant APE1 only. Reactions were incubated for 1 h at 30°C with factors to support ubiquitination (E1, E2, ubiquitin) and poly(ADP-ribosyl)ation (NAD), separated by denaturing (7 M urea) PAGE and gels quantified by comparing the cleaved 119 bp THF-IN incision product to the 256bp substrate using the Odyssey Image Analysis System to quantify the degree of THF site incision. Active fractions were pooled after the gel filtration chromatography step and underwent further fractionation using the final ion exchange chromatography step. Active fractions at this final step from each of the three activities were analysed by mass spectrometry. Candidate proteins in the fractions were subsequently analysed for their alignment, as determined by Western blotting, against the activity of the fractions at each chromatography step in order to clarify the identification of the proteins which are stimulating APE1 through making the THF site more accessible in the THF-IN mononucleosome substrate. The most active fraction was also tested with and without factors supporting ubiquitination to examine whether the identified activities were dependent on ubiquitination or not. The process to identify proteins stimulating APE1 will be discussed for each activity separately.

5.3.3.1.1 Gel filtration chromatography of activity 1

Fractions 34 to 42 from the Mono Q chromatography stage equating to activity 1 (Figure 47A) were pooled and fractionated using a gel filtration (24 ml Superdex 200) column. Fractions were collected (Figure 48A) and subsequently analysed for APE1 stimulatory activity using the BER *in vitro* assay incorporating the THF-IN mononucleosome substrate, with a particular focus on identifying fractions containing THF site incision activity above the baseline value of recombinant APE1 only. The activities of alternate fractions from 14 to 40 where protein eluted were tested. I found that the percentage incision of the THF site was found to exceed the baseline value using fractions 16 to 30 by up to 15 % (Figure 48B and 48C). Fractions 16 to 30 were therefore pooled and further fractionated by ion exchange chromatography.

5.3.3.1.2 Ion exchange chromatography of activity 1

Fractions 16 to 30 from the gel filtration stage were fractionated by ion exchange chromatography using a 1 ml Mono Q column (Figure 49A). Initially very little APE1 stimulatory activity on the THF-IN mononucleosome substrate was observed with these fractions using the BER *in vitro* assay. Fractions were therefore buffer exchanged into a low salt buffer (50 mM KCl) and concentrated further prior to analysis. On retesting these fractions, an increase in THF site incision activity, above the baseline value for recombinant APE1 only, in fractions 16-17 was observed when alternate fractions were analysed using the BER *in vitro* assay from fractions 8 to 20 (Figure 49B and 49C). Activity was reproducibly higher in these fractions (by up to 25 %), despite the activity appearing to reduce between fractionation columns. Fraction 16 was subsequently analysed by mass spectrometry in order to examine the proteins contained within, and particularly to discover whether any candidate E3 ubiquitin ligase(s) and ATP-dependent chromatin remodelling complexes were present.

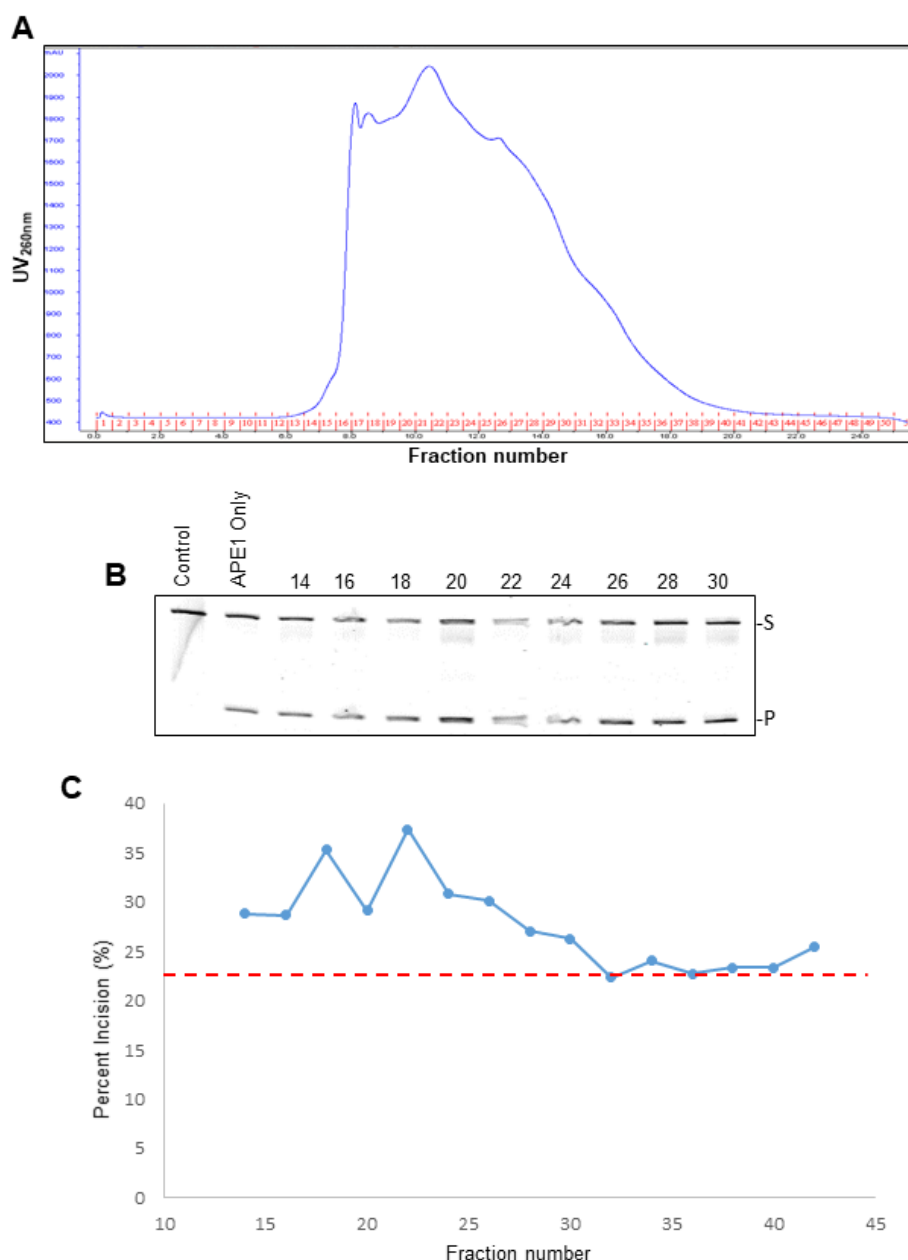


Figure 48; Gel filtration chromatography of activity 1. Fractions 34 to 42 from Mono Q chromatography were pooled and fractionated using gel filtration (Superdex 200) chromatography and the resulting FPLC UV trace is shown (A). The relative THF site incision activity of fractions on the THF-IN mononucleosome substrate, in the presence of purified APE1 (57 fmol), was tested using the BER *in vitro* assay with additional ubiquitin stimulating factors (0.7 pmol E1, 2.5 pmol E2, 0.6 nmol ubiquitin and 5 mM NAD) added and incubated for 1 h at 30°C. Reactions were separated by denaturing (7 M) PAGE and a representative gel is shown (B). Quantification of THF site incision from these gels are also shown as an average of two independent experiments, where the threshold incision activity of purified APE1 only, producing 22 % is shown as a red dashed line (C).

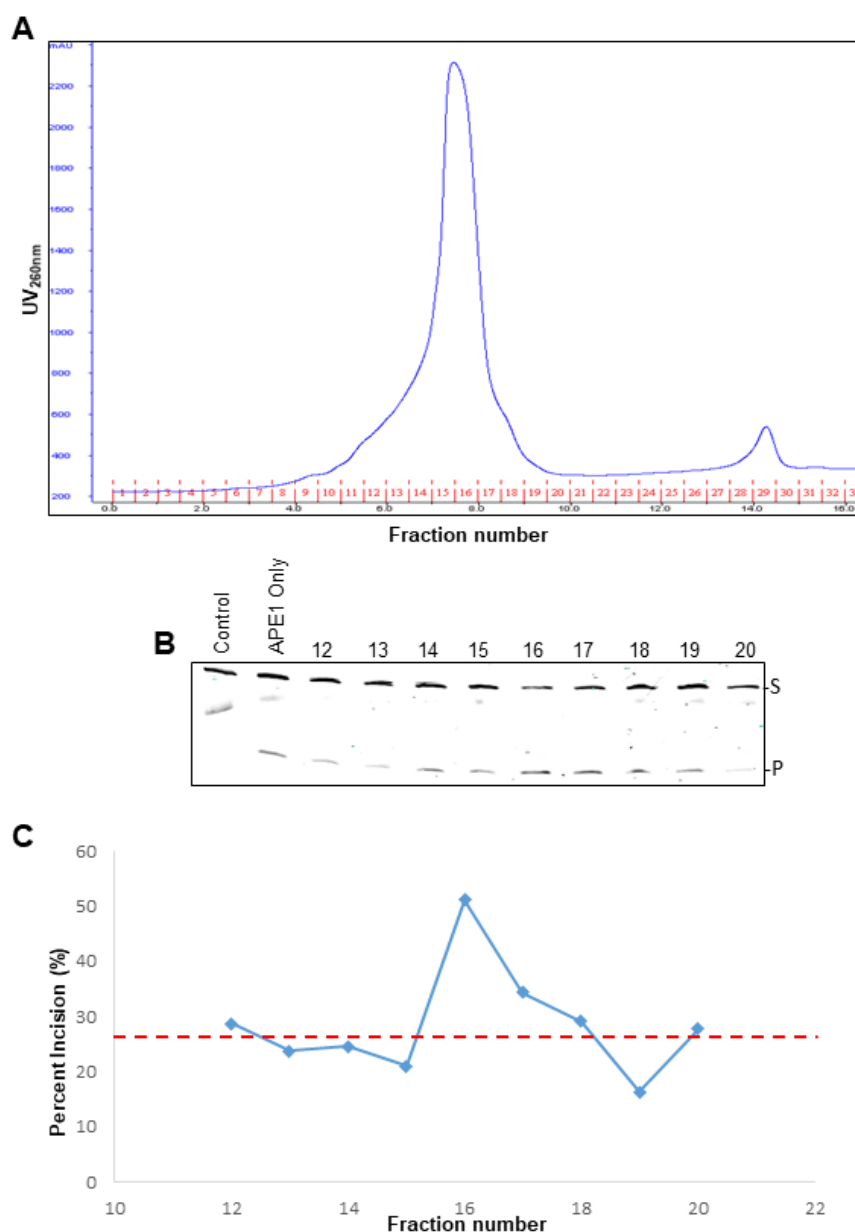


Figure 49: Ion exchange chromatography of activity 1. Fractions 18 to 30 from gel filtration chromatography were pooled and fractionated using 1 ml Mono Q column and the resulting FPLC UV trace is shown (A). The THF site incision activity of fractions on the THF-IN mononucleosome substrate, in the presence of purified APE1 (57 fmol), was tested using the BER *in vitro* assay with additional ubiquitin stimulating factors (0.7 pmol E1, 2.5 pmol E2, 0.6 nmol ubiquitin and 5 mM NAD) added and incubated for 1 h at 30°C. Reactions were separated by denaturing (7 M) PAGE gels and a representative gel is shown (B). Quantification of THF site incision from these gels are also shown as an average of two independent experiments, where the threshold incision activity of purified APE1 only, producing 25 % incision has been shown as the red dashed line (C).

5.3.3.1.3 Mass spectrometry of fraction 16 from ion exchange chromatography of activity 1

The most active fraction from the final ion exchange (Mono Q) chromatography step, fraction 16, was analysed by mass spectrometry to identify candidate proteins. A selection of the top mascot score proteins are shown in table 11 and a full list is provided in Appendix 1. As I originally identified that factors supporting ubiquitination (but also poly(ADP-ribosyl)ation) were required for improving THF site accessibility to APE1 present in WCE, the major focus was predominately on identifying candidate E3 ubiquitin ligases, but also ATP-dependent chromatin remodelling complexes that could be recruited after ubiquitination, that were present. However, other proteins were not immediately excluded. Interestingly, in this particular fraction we discovered that the E3 ubiquitin ligases HECTD1 and Hsc-70-interacting protein (CHIP) were among the top scoring proteins, achieving Mascot scores of 591 and 536, respectively. Therefore these candidate enzymes were analysed further, particularly for their presence in active fractions, and their alignment with APE1 stimulatory activity.

Accession	Description	Mascot Score
P07900	Heat shock protein HSP90-alpha	3426
P08238	Heat shock protein HSP90-alpha	3379
P49736	DNA replication licensing factor MCM2	652
P33993	DNA replication licensing factor MCM7	645
Q9ULT8	E3 ubiquitin protein ligase HECTD1	591
Q9UNE7	E3 ubiquitin protein ligase CHIP	536

Table 11; Mass Spectrometry results for activity 1. Fraction 16, the most active fraction for activity 1 purified by the final ion exchange (Mono Q) chromatography column, was analysed by mass spectrometry to identify candidate proteins. The top mascot scoring proteins are shown in the table and the candidate E3 ligases (HECTD1 and CHIP) are shown in bold.

5.3.3.1.4 Alignment of CHIP and HECTD1 with the APE1 stimulatory activity from each of the chromatography steps for activity 1

The alignment of the candidate E3 ubiquitin ligases CHIP and HECTD1 against the APE1 stimulatory activity profile from each chromatography stage was analysed using Western blotting to confirm their presence and levels in fractions compared to the THF-IN incision activity profile. Protein fractions were separated by either 6 % (HECTD1) or 10 % (CHIP) SDS-PAGE, transferred onto a PVDF membrane and the presence of these proteins in fractions were probed for using Western blotting in combination with the Odyssey Image Analysis System.

5.3.3.1.4.1 Ion exchange chromatography alignment of the activity 1 profile to CHIP and HECTD1

Alternate fractions 32 to 44 from the initial ion exchange (Mono Q) chromatography stage, containing activity 1, were analysed for the presence of HECTD1 and CHIP proteins. Both of these candidate proteins were present in the fractions, although the protein levels of CHIP in the fractions did not appear to perfectly align with the APE1 stimulatory incision activity profile (Figure 50Ai and 50Aii). The highest levels of CHIP were found in fractions 32 and 34 whereas the activity was seen predominantly in fractions 36 to 42. Consequently, CHIP was thought not to be a major candidate for stimulating APE1 activity on a mononucleosome substrate containing a THF site. In contrast, HECTD1 protein levels do appear to correlate well with the position of stimulatory incision activity. Levels of HECTD1 are maximal in fraction 38, although there is a significant amount of protein present within fractions 34-44 which contains APE1 stimulatory activity. HECTD1 was therefore further characterised in the subsequent chromatography stages.

5.3.3.1.4.2 Gel filtration chromatography alignment of the activity 1 profile to HECTD1

Alternate fractions 18 to 26 from the gel filtration (Superdex 200) chromatography stage were analysed for the presence of HECTD1, and its alignment to the APE1 stimulatory incision activity profile. Similar to the previous Mono Q column, HECTD1 was found to be present in significant amounts in these active fractions (Figure 50Bii), and the levels of HECTD1 did align, to some degree, with the APE1 stimulatory activity profile (Figure 50Bi). The alignment of HECTD1 protein was next analysed with the final ion exchange chromatography stage.

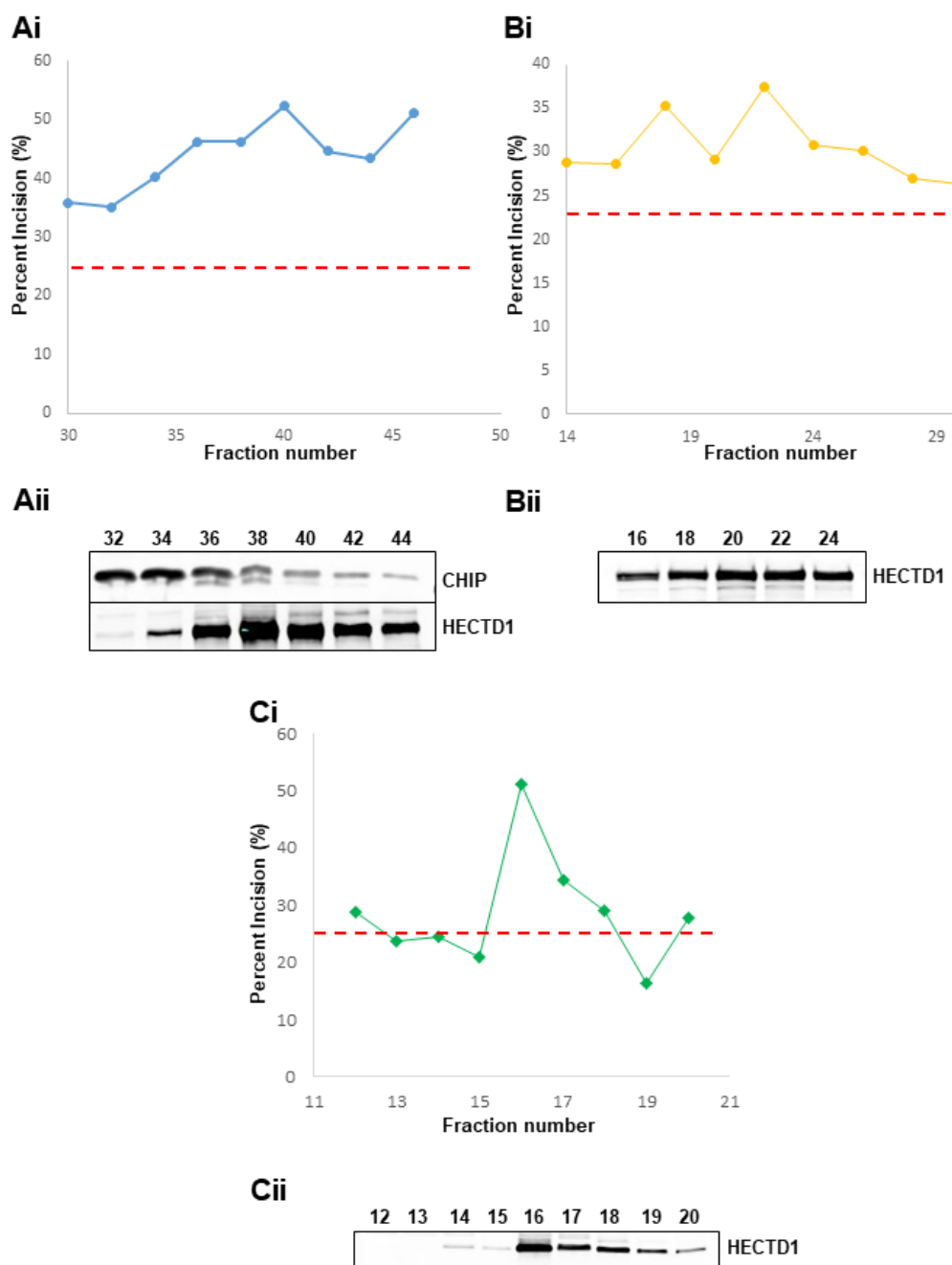


Figure 50: Alignment of candidate proteins to the activity profiles of activity 1 for each of the sequential chromatography stages. CHIP and HECTD1, identified from mass spectrometry, were analysed for their alignment to the activity profiles of each chromatography step (Ai, Bi, Ci). Protein fractions from active regions were separated by 6 % (for HECTD1) or 10 % (for CHIP) SDS polyacrylamide gels and transferred onto a PVDF membrane. Fractions were analysed for the respective proteins by Western blotting (Aii, Bii, Cii). Figures shows protein alignments for the initial ion exchange Mono Q column (Ai and ii), the gel filtration Superdex 200 column (Bi and ii) and the final ion exchange Mono Q column (Ci and Cii). The activity threshold of APE1 is shown as the red dashed line in each of the graphs.

5.3.3.1.4.3 Final ion exchange chromatography alignment of the activity 1 profile to HECTD1

The alignment of HECTD1 protein with the APE1 stimulatory incision activity profile from the final ion exchange (Mono Q) chromatography stage was analysed. At this point we would expect the alignment to be strong as the activity, and indeed protein, is highly purified. Fractions 12 to 20 were analysed for HECTD1 and indeed the protein was found to be present in fractions 16 to 20, with a trace amounts in fraction 14 and 15 (Figure 50Cii). The highest levels of HECTD1 were found in fraction 16 and this aligned perfectly with the APE1 stimulatory activity profile where the activity was the strongest in this fraction (Figure 50Ci and 50Cii). The activity then decreased from fractions 17 to 19, which also matches with a decrease in HECTD1 protein. This provided clear evidence that HECTD1 is most likely the enzyme that catalyses activity 1. The most active fraction (16) was then analysed for its dependence on ubiquitination by removing the ubiquitination supporting factors in the *in vitro* BER assay.

5.3.3.1.4.4 Analysing ubiquitination dependence of activity 1

As HECTD1 was identified as the most likely protein stimulating the activity of APE1 on a THF-IN mononucleosome substrate (activity 1), and as HECTD1 is an E3 ubiquitin ligase, the activity within the purified protein fractions should show dependence on ubiquitination supporting factors in the BER *in vitro* assay. Therefore it was important to assess whether this stimulation in APE1 activity was dependent on ubiquitination, which would further support evidence that HECTD1 is the enzyme responsible for this effect. Fraction 16 from the final Mono Q chromatography stage was titrated into the BER *in vitro* assay using the THF-IN mononucleosome substrate containing APE1 (57 fmol) and ubiquitin (6 nmol), and the assay was performed either in the presence or absence of E1/E2 enzyme pool which would support ubiquitination. Similar to previous experiments, recombinant APE1 only was used as a control under these conditions which was deducted from the percentage THF site incision caused by the fraction so that the amount of APE1 stimulation could be directly determined. Whilst the THF incision activity was relatively low and quite variable, ubiquitination was found to be required for the full activity of purified fraction 16 in stimulating APE1 mononucleosome activity on THF-IN (Figure 51A and 51B). Indeed, using volumes of 0.5 μ l and 2 μ l of fraction 16 the activity was significantly increased in the presence of E1/E2 enzymes compared to when these were not, as there was a 4-fold and 4.8-fold percentage incision increase, respectively. The effect of removing HECTD1 from fraction 16 by immunodepletion was attempted as we would expect that when HECTD1 is depleted, then the APE1 stimulatory activity would decrease.

5.3.3.1.4.5 The effect of HECTD1 immunodepletion from fraction 16 of activity 1

HECTD1 was attempted to be immunodepleted from the active final Mono Q chromatography fraction 16, containing activity 1, to see if its removal from the fraction decreased the observed stimulation in APE1 activity on the THF-IN mononucleosome substrate. This is due to my hypothesis that HECTD1 ubiquitinates histones to make the THF site in THF-IN more accessible to APE1 and so stimulates its activity. To achieve this, HECTD1 antibody was bound to magnetic beads, and fraction was added and incubated overnight with the antibody magnetic beads, with beads alone used as a control. Immunodepletion of HECTD1 from the fraction was analysed by 6 % SDS-PAGE and Western blotting for HECTD1. Unfortunately, despite several attempts, the best immunodepletion result attained was only ~25 % immunodepletion of HECTD1 (Figure 52A). Nevertheless, the control and HECTD1 immunodepleted extracts were analysed in the BER *in vitro* assay using the THF-IN mononucleosome substrate with factors added to stimulate ubiquitination/poly(ADP-ribosyl)ation in the presence of recombinant APE1 using a reaction time course (0-80 min). A slight decrease in percentage incision of the THF site by APE1 was observed, especially at the last two time points (60 and 80 min) which saw a decrease of ~17 % and ~9 % respectively (Figure 52B and 52C). This correlated with a lack of efficient immunodepletion of HECTD1, although no further conclusions could be established from this result. Therefore in order to examine HECTD1 further, an siRNA knockdown of HECTD1 in cultured cells was used to analyse if the enzyme was having effect on DNA damage repair kinetics and survival following IR.

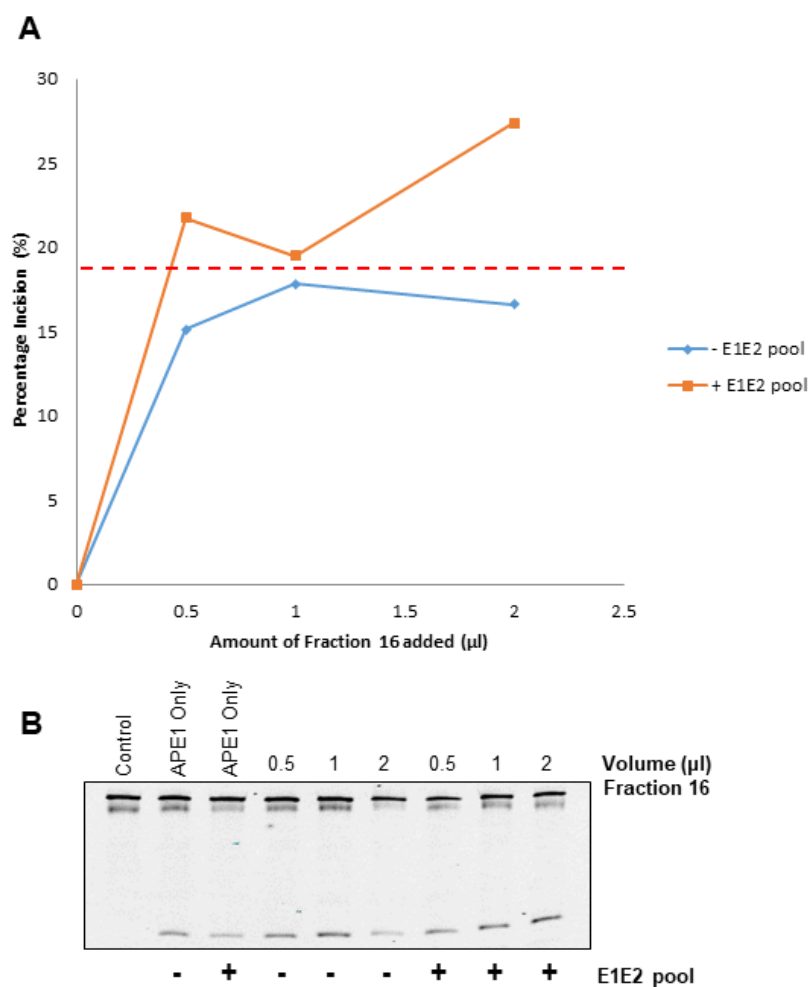


Figure 51: Analysing the ubiquitination dependence of activity 1. Fraction 16 from the final Mono Q chromatography stage from activity 1 was analysed for its dependence on ubiquitination using the BER *in vitro* assay to analyse the repair activity on the THF-IN mononucleosome substrate. Fraction 16 (0.5-2 μl) was incubated with APE1 (57 fmol) and ubiquitin (0.6nmol) with and without the E1/E2 enzyme pool, and the THF-IN substrate incubated for 1 h at 30°C. Percentage substrate incision was averaged from two separate experiments (A), and a representative denaturing (7 M) PAGE gels (B) is shown. Incision with the APE1 only control threshold is shown as the red dashed line.

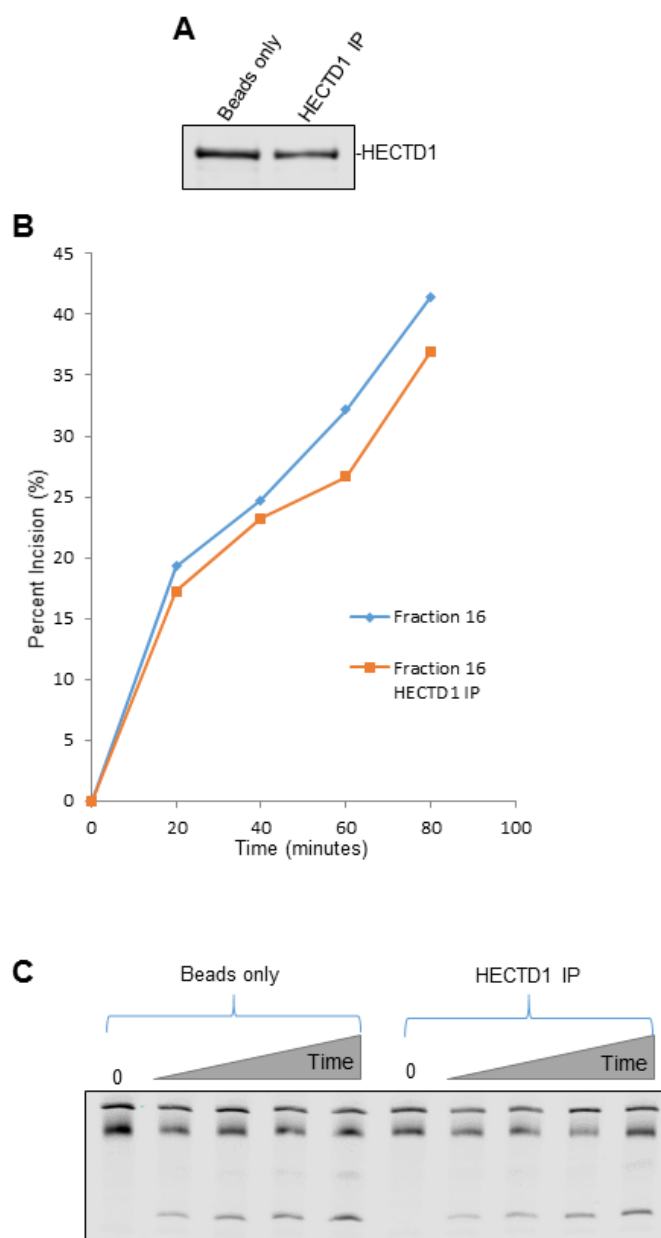


Figure 52: HECTD1 immunodepletion from fraction 16 from the final ion exchange chromatography. Following immunodepletion (IP) of HECTD1 from fraction 16 using HECTD1 antibody with magnetic beads, and using beads alone as a control, the fractions were separated on 6 % SDS-PAGE, proteins transferred onto a PVDF membrane which was then analysed for HECTD1 by Western blotting to check the efficiency of HECTD1 IP (A). Fractions were then used in the BER *in vitro* repair assay to analyse the repair of the THF-IN mononucleosome substrate at different time points (with 0.6 nmol ubiquitin, 0.7 pmol E1, 2.5 pmol E2s and 5 mM NAD) (0-120 min). The percentage THF site incision quantification (B) and the denaturing (7 M) PAGE gel that was quantified (C) are shown.

5.3.3.2.1 Gel filtration chromatography of activity 2

Active fractions 46–52 containing activity 2 from the first ion exchange Mono Q chromatography stage (Figure 47A) were pooled and fractionated using the gel filtration (24 ml Superdex 200) column (Figure 53A). Fractions were collected and analysed for APE1 stimulatory activity on the THF-IN mononucleosome substrate using the BER *in vitro* assay by examining activity above the baseline value of recombinant APE1 only in the presence of ubiquitination/poly(ADP-ribosyl)ation factors. Alternate fractions from 14 to 40 were tested for APE1 stimulatory activity. I found that percentage incision of the THF in THF-IN exceeded the baseline value in fractions 14 to 28 (Figure 53B and 53C). APE1 stimulatory activity appeared to be maximal using fractions 18-26, where it reached ~20 % incision above that using recombinant APE1 alone. Therefore fractions 16 to 26 were pooled and fractionated by ion exchange chromatography.

5.3.3.2.2 Ion exchange chromatography of activity 2

Fractions 16-26 from the gel filtration (Superdex 200) chromatography stage were fractionated by ion exchange chromatography using a 1 ml Mono Q column (Figure 54A). Alternate fractions 10 to 32 were analysed using the BER *in vitro* assay containing the THF-IN mononucleosome substrate in the presence of recombinant APE1 and ubiquitination/poly(ADP-ribosyl)ation factors. Maximal APE1 stimulatory activity appeared to be around fraction 21, which was ~20 % above baseline levels (Figure 54B and 54C). Therefore this fraction was chosen for analysis by mass spectrometry to identify candidate E3 ubiquitin ligase(s) and ATP-dependent chromatin remodelling complexes.

5.3.3.2.3 Mass spectrometry of fraction 21 from ion exchange chromatography of activity 2

The most active fraction from the final ion exchange (Mono Q) chromatography step, fraction 21, was analysed by mass spectrometry to identify candidate proteins. A selection of the top mascot score proteins are shown in table 12 and a full list is provided in Appendix 2. As factors to promote ubiquitination (but also poly(ADP-ribosyl)ation) were initially found to stimulate APE1 activity by WCE on the THF-IN mononucleosome substrate, the identification of candidate E3 ubiquitin ligase(s) was of interest, in addition to any ATP-dependent chromatin remodelling complexes that could be recruited after ubiquitination. However, other proteins that were identified were not completely excluded. In this particular fraction, the E3 ubiquitin ligases MULE and the DNA damage-binding protein 1 (DDB1) which is a core component of the cullin (CUL4A and CUL4B) E3 ubiquitin ligase complex had high mascot scores of 1041 and 167, respectively. In fact CUL4A was also identified in the mass spectrometry results, however it had a lower mascot score of 42. MULE and DDB1 were therefore analysed for their presence and alignment in purified fractions containing APE1 stimulatory activity.

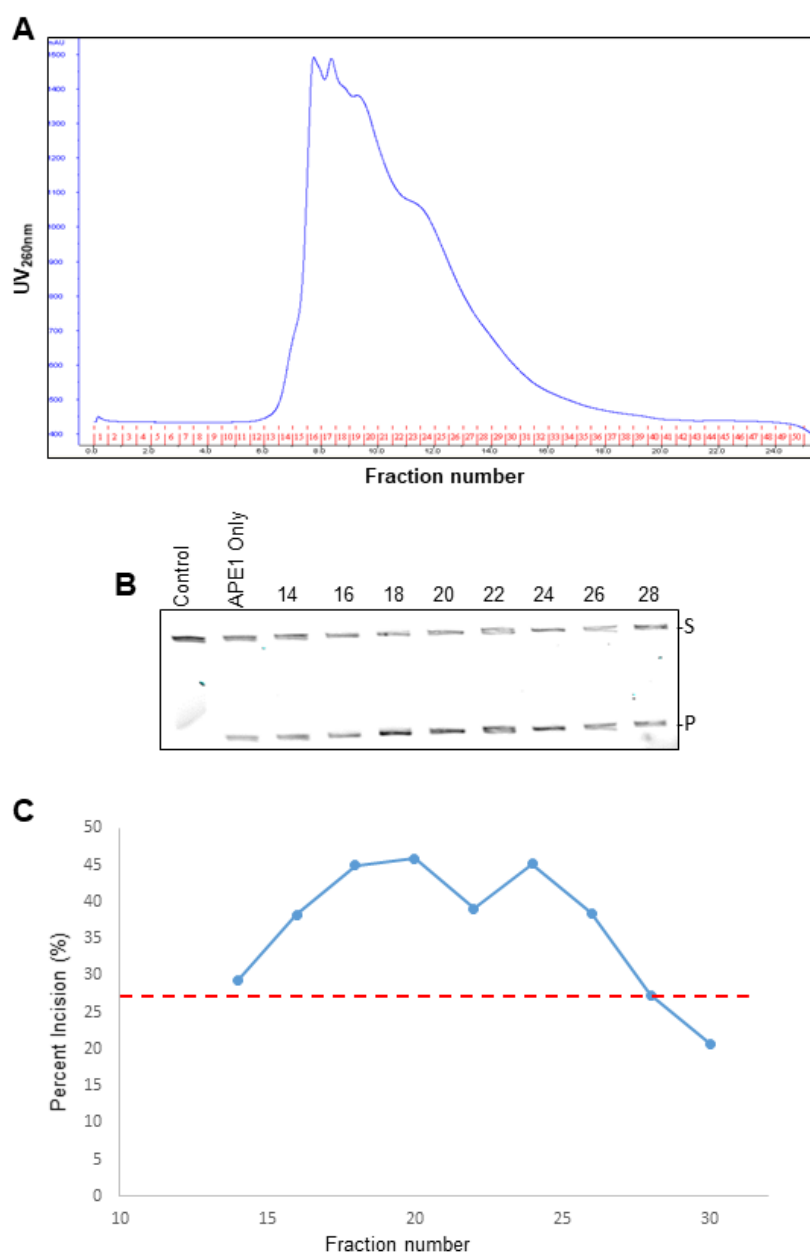


Figure 53: Gel filtration chromatography of activity 2. Fractions 46 to 52 from the first ion exchange (Mono Q) chromatography stage were pooled and fractionated using gel filtration (Superdex 200) chromatography and the resulting FPLC UV trace is shown (A). The repair activity of fractions on the THF-IN mononucleosome substrate using the BER *in vitro* assay with ubiquitin factors (0.7 pmol E1, 2.5 pmol E2, 0.6 nmol ubiquitin and 5 mM NAD) added in the presence of APE1 (57 fmol) was performed by incubation for 1 h at 30°C. Reactions were separated by denaturing (7 M) PAGE gels and a representative gel is shown (B). Quantification of THF site incision from the average of two independent experiments of these gels are also shown, where incision activity of the activity threshold purified APE1 only, producing 27% incision is shown as the red dashed line (C).

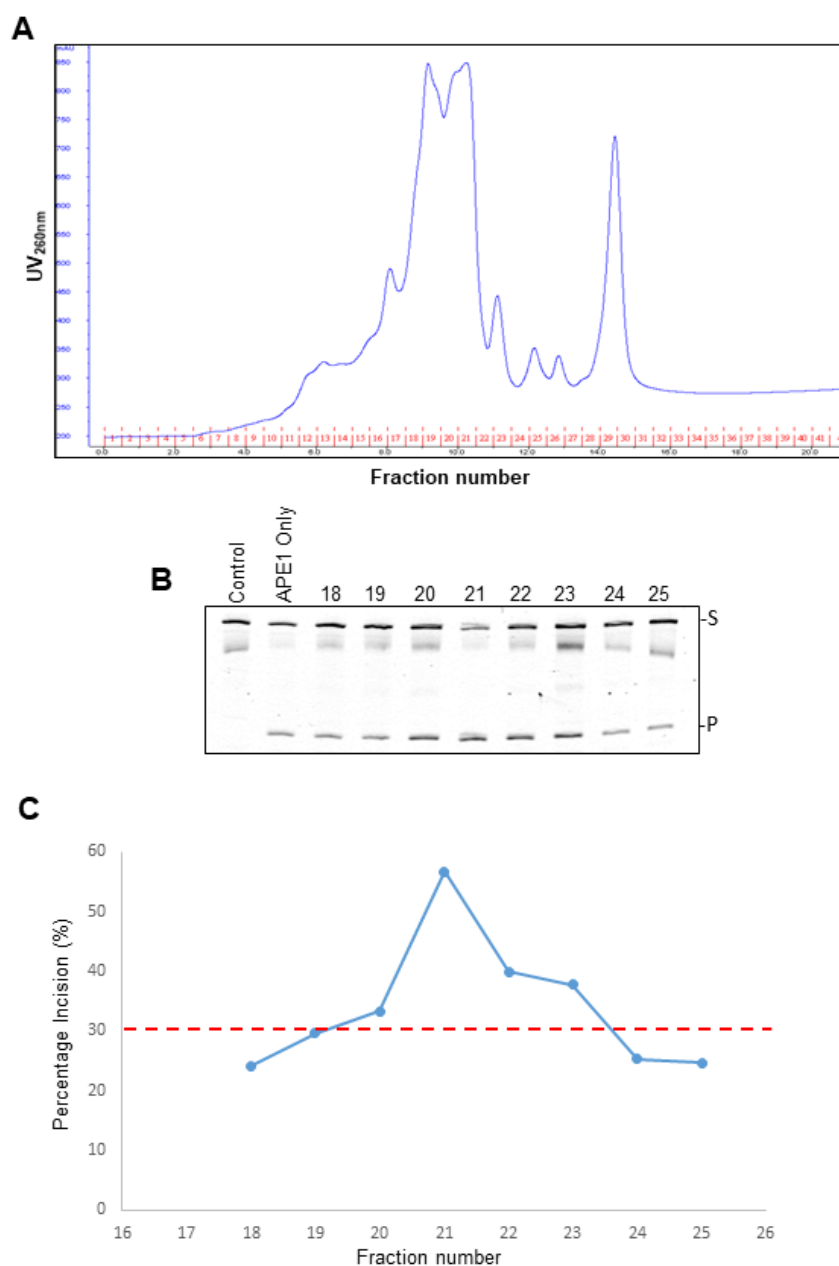


Figure 54; Ion exchange chromatography of activity 2. Fractions 16 to 26 from gel filtration (Superdex 200) chromatography were pooled and fractionated by ion exchange chromatography using 1 ml Mono Q column and the resulting FPLC UV trace is shown (A). The repair activity of fractions on the THF-IN mononucleosome substrate using the BER *in vitro* assay with ubiquitin factors (0.7pmol E1, 2.5pmol E2, 0.6nmol ubiquitin and 5mM NAD) added in the presence of APE1 (57 fmol) were performed by incubation for 1 h at 30°C. Reactions were separated by denaturing (7 M) PAGE gels and a representative gel is shown (B). Quantification of AP site incision from these gels are also shown as an average of two independent experiments, where incision activity of the activity threshold purified APE1 only, producing 30 % incision is shown by the red dashed line (C).

Accession	Description	Mascot Score
O15355	Protein phosphatase 1G	1581
Q7KZ85	Transcription elongation factor SPT6	1446
P49792	E3 SUMO-protein ligase RanBP2	1138
Q7Z6Z7	E3 ubiquitin-protein ligase MULE	1041
Q86VP6	Cullin-associated NEDD8-dissociated protein 1	241
Q16531	DNA damage-binding protein 1	167

Table 12: Mass Spectrometry results for activity 2. Fraction 21, the most active fraction for activity 2 purified by the final ion exchange (Mono Q) chromatography column, was analysed by mass spectrometry to identify candidate proteins. The top mascot scoring proteins are shown in the table and the candidate E3 ligases are shown in bold.

5.3.3.2.4 Alignment of MULE and DDB1 with the activity from each of the chromatography steps for activity 2

The alignment of the candidate E3 ubiquitin ligase proteins MULE and DDB1 to the APE1 stimulatory activity profile for activity 2 from each of the chromatography stages was analysed using Western blotting to confirm their presence and levels in fractions compared to the activity profile. Protein fractions were separated on a 6 % (MULE) and 10 % (DDB1) SDS-PAGE gel, transferred onto a PVDF membrane and the presence of each of these proteins in fractions were probed for using Western blotting in combination with the Odyssey Image Analysis System.

5.3.3.2.4.1 Ion exchange chromatography alignment of the activity 2 profile to MULE and DDB1

Alternate fractions 46 to 56 from the initial ion exchange (Mono Q) chromatography stage containing activity 2 were analysed for the presence of MULE and DDB1. Indeed significant amounts of both of these candidate proteins were found to be present in the fractions (Figure 55Ai and 55Aii). However their elution profile did not appear to align well with the APE1 stimulatory activity profile of activity 2. Both proteins appear to peak at fraction 46 (and possibly earlier) and then decreased across the fractions, especially MULE, whereas THF-IN stimulatory incision activity peaked at fraction 50 and decreased either side of this. Although the alignment of proteins to the activity profile didn't match completely, MULE and DDB1 alignment was still further characterised in the subsequent chromatography steps.

5.3.3.2.4.2 Gel filtration chromatography alignment of the activity 2 profile to MULE and DDB1

Alternate fractions 16 to 30 from the gel filtration (Superdex 200) chromatography of activity 2 were analysed for the presence of MULE and DDB1, and for their alignment to the APE1 stimulatory incision activity profile. From the activity profile, the highest APE1 stimulatory activity on THF-IN seemed to be within fractions 18 to 26 where they appeared relatively the same intensity (Figure 55Bi). MULE was found to be present in fraction 18, albeit at a low concentration, peaks at fraction 20 and then reduces in quantity up to fraction 28 (Figure 55Bii). DDB1 also follows a similar trend to MULE being present in low amounts in fraction 18, although the levels appear to stay the same in fractions 20 to 26 and then reducing at fraction 28. Both proteins again do not appear to align greatly with the activity profile, particularly as activity is largely maximal in fraction 18 where the amounts of both proteins are low. However despite this, the alignment of these proteins in the final ion exchange chromatography step was analysed.

5.3.3.2.4.3 Final ion exchange chromatography alignment of the activity 2 profile to MULE and DDB1

Every fraction from fraction 17 to 25 from the final ion exchange (Mono Q) chromatography of activity 2 was probed for MULE and DDB1, but also CUL4A, for completion. CUL4A was found to be present in the mass spectrometry results at a low mascot score, but it is well known to form E3 ubiquitin ligase complexes with DDB1. The peak fraction for APE1 stimulatory activity was fraction 21, with the two fractions either side of it showing some degree of THF-IN stimulatory incision activity (Figure 55Ci). The protein levels of MULE did not appear to correlate with the alignment of activity, as its highest presence appeared to be in fractions 19 and 20. DDB1, however, was present in all fractions from 17 to 24 but peaked at fraction 21, and fractions either side of it (20 and 22) also had higher levels of DDB1 protein compared to the other fractions (Figure 55Cii). This showed some degree of alignment with APE1 stimulatory activity, although not greatly particularly as DDB1 was found in fractions 17-19 where there is no activity, although this activity may be dependent on protein abundance. As expected, CUL4A showed a similar elution profile to DDB1 given that they form protein complexes. These data largely suggest that neither MULE or DDB1 align extremely well with APE1 stimulatory activity on a THF-IN mononucleosome substrate, although CUL4A and DDB1 should not be excluded entirely. Therefore, it was important to analyse whether the stimulatory activity in these fractions had any dependence on ubiquitination.

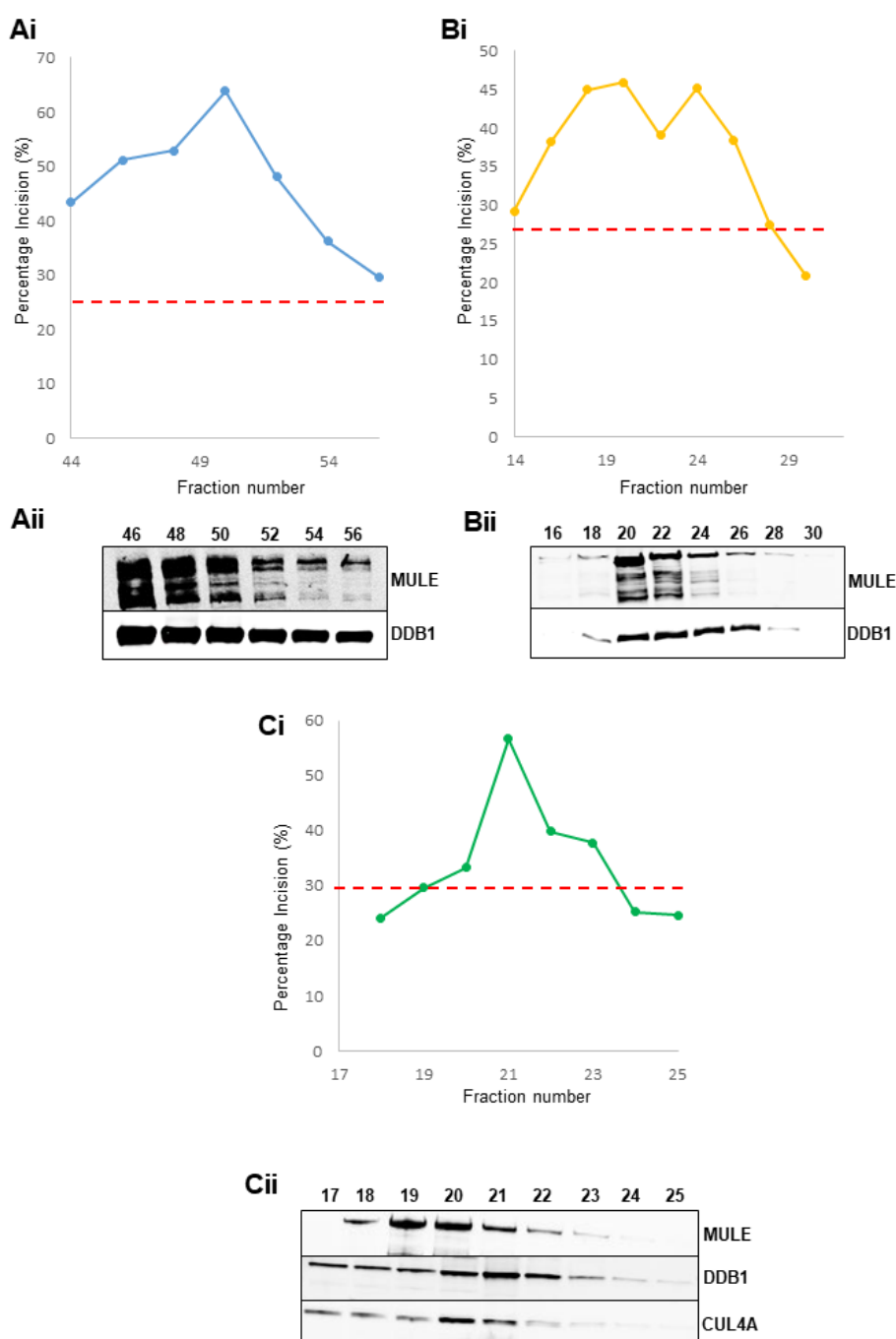


Figure 55: Alignment of candidate proteins to the activity profiles of activity 2 for each of the sequential chromatography stages. MULE and DDB1, identified from mass spectrometry, were analysed for their alignment to the activity profiles of each chromatography step (Ai, Bi, Ci). Protein fractions were separated on a 6 % (for MULE) or 10 % (for DDB1 and CUL4A) SDS polyacrylamide gels, transferred onto a PVDF membrane and analysed by Western blotting for the respective proteins (Aii, Bii, Cii). Figure shows protein alignments for the initial ion exchange (Mono Q) column (Ai and ii), gel filtration (Superdex 200) column (Bi and ii) and the final ion exchange (MonoQ) chromatography column (Ci and Cii). The activity threshold of APE1 is shown as the red dashed line in each of the graphs.

5.3.3.3.4.4 Analysing ubiquitination dependence of activity 2

The two candidate proteins MULE and DDB1 identified from mass spectrometry of activity 2 showed poor alignment to the activity profile for APE1 stimulation on a THF-IN mononucleosome substrate. This raised the possibility that this activity may not be ubiquitination/E3 ubiquitin ligase dependent and that a different method to stimulate APE1 incision (eg. phosphorylation of histones, chromatin remodelling) may be responsible. Since we used ubiquitination supporting factors in the BER *in vitro* assay, it was important to assess whether this stimulation in APE1 activity was dependent on these factors. Active fraction 21 from the final ion exchange (Mono Q) chromatography stage was titrated into the BER *in vitro* assay using the THF-IN mononucleosome substrate containing recombinant APE1 (57 fmol) and ubiquitin (0.6 nmol) in the absence and presence of the E1/E2 enzyme pool, to see if ubiquitination was key for this activity. The average THF site incision from two experiments was determined, and as previous, recombinant APE1 only was used as a control which was deducted from the percentage incision using the fraction so that the amount of stimulation could be determined. Interestingly, and in contrast to activity 1, the activity of fraction 21 from activity 2 was found not to be dependent on ubiquitination. Indeed the level of APE1 stimulation of incision of THF-IN was virtually the same in the absence and presence of E1/E2 enzymes (Figure 56A and 56B). It was therefore decided that this activity, at this point, would not be followed further as this would potentially require extensive further analysis of mass spectrometry data and subsequent testing of alternative candidate enzymes involved in other PTM events.

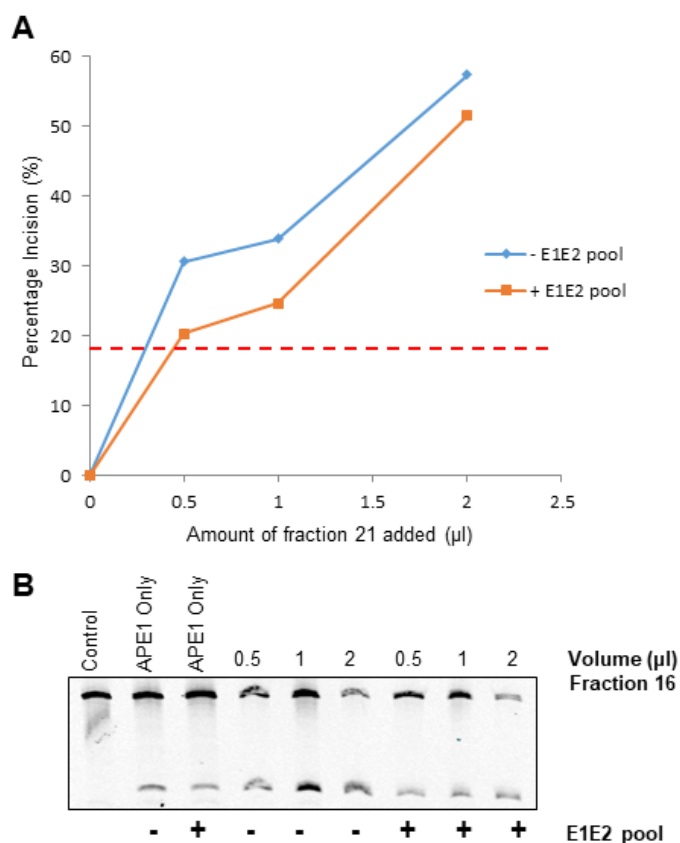


Figure 56: Analysing the ubiquitination dependence of activity 2. Fraction 21 from the final ion exchange (Mono Q) chromatography stage of activity 2 was analysed for the dependence on ubiquitination. The fraction (0.5-2 µl) was tested in the BER *in vitro* assay using the THF-IN mononucleosome substrate with APE1 (57 fmol) and ubiquitin (0.6 nmol), with and without the E1/E2 enzyme pool, which was incubated for 1 h at 30°C. Percentage substrate incision was averaged from two separate experiments (A), and a representative denaturing (7 M) PAGE gels (B) is shown. Incision with the APE1 only control activity threshold is shown as the red dashed line.

5.3.3.3.1 Gel filtration chromatography of activity 3

Active fractions 63 to 76 from the initial ion exchange (Mono Q) chromatography stage (Figure 47) were pooled and fractionated using the gel filtration (24 ml Superdex 200) column (Figure 57A). Fractions were collected and analysed for APE1 stimulatory activity on the THF-IN mononucleosome substrate using the BER *in vitro* assay by examining activity above the baseline value of recombinant APE1 only. Alternate fractions 14 to 38 where protein eluted were tested for APE1 stimulatory activity. The percentage incision of THF in the THF-IN mononucleosome substrate was found to exceed the baseline value using fractions 16 to 32 (Figure 57B and 57C). The peak of activity was at fraction 18 which caused an ~25 % increase in incision above the baseline value using recombinant APE1 only. Fractions 16 to 24, where the highest activity was seen, were pooled and fractionated by ion exchange chromatography.

5.3.3.3.2 Ion exchange chromatography of activity 3

Fractions 16 to 24 from the gel filtration (Superdex 200) chromatography stage were pooled and fractionated by ion exchange chromatography using a 1 ml MonoQ column (Figure 58A). Every fraction from 25 to 31 was then analysed for APE1 stimulatory activity by the BER *in vitro* assay using the THF-IN mononucleosome substrate. This showed that activity was predominantly present in fractions 28 and 29 (Figure 58B and 58C). Indeed the highest increase in THF site incision percentage was ~10-15 % and therefore fraction 29 was analysed by mass spectrometry to identify potential candidate E3 ubiquitin ligase(s) and ATP-dependent chromatin remodelling complexes.

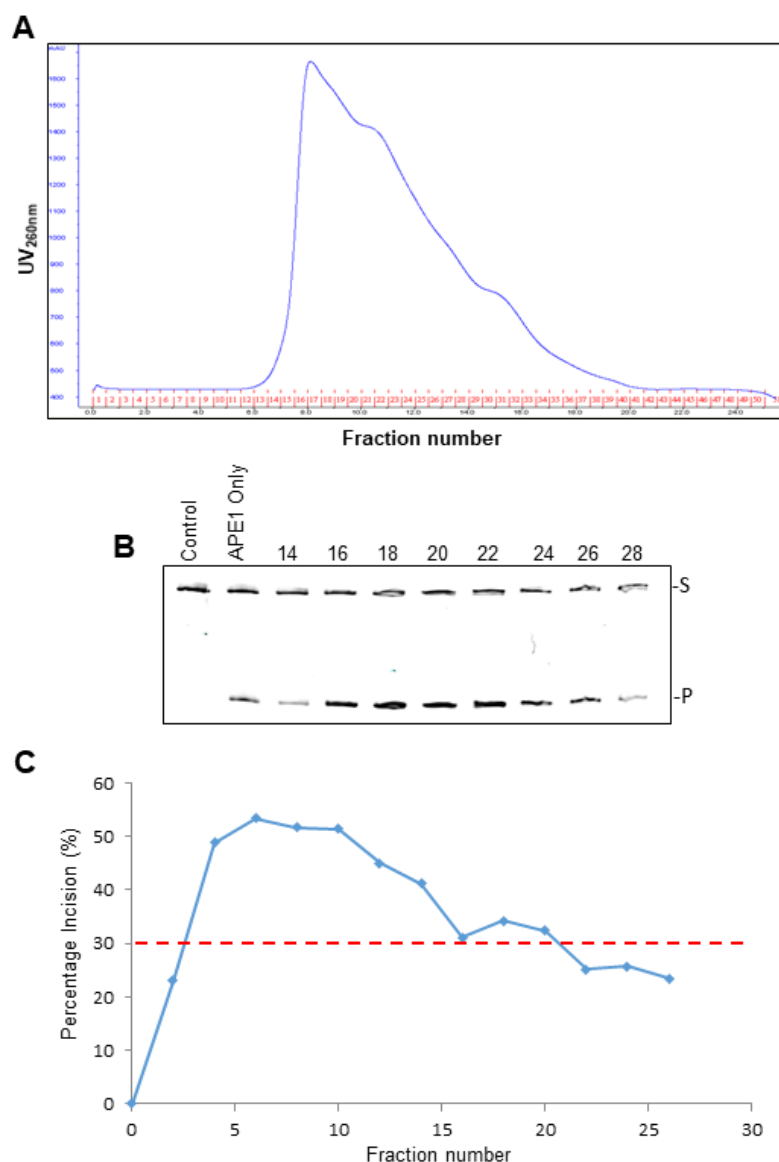


Figure 57: Gel filtration chromatography of activity 3. Active fractions 63 to 76 from the first (Mono Q) chromatography stage were fractionated using gel filtration (Superdex 200) chromatography and the resulting FPLC UV trace is shown (A). The repair activity of fractions on the THF-IN mononucleosome substrate using the BER repair assay with APE1 (57 fmol) and ubiquitin (0.6 nmol) added was performed for 1 h at 30°C. Reactions were separated by denaturing (7 M) PAGE gels and a representative gel is shown (B). Quantification of AP site incision from these gels are also shown as an average of two independent experiments, where incision activity of purified APE1 only, the threshold activity, producing 30 % incision is shown by the red dashed line (C).

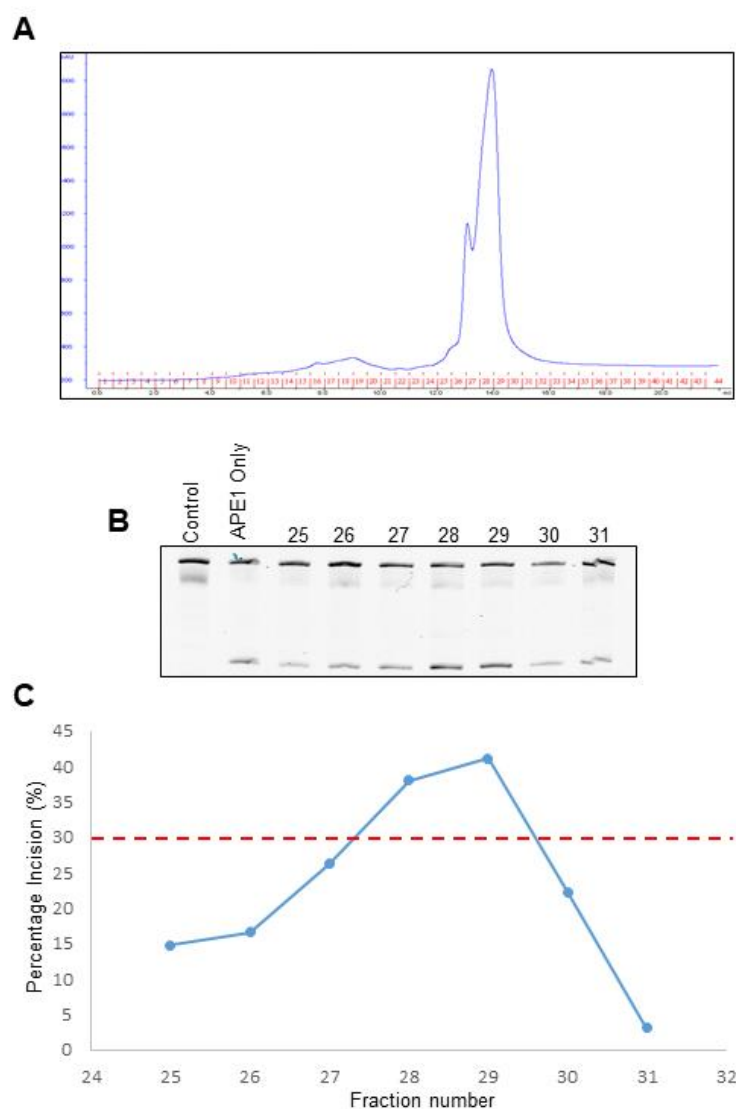


Figure 58: Ion exchange chromatography of activity 3. Active fractions 16 to 24 from gel filtration (Superdex 200) chromatography stage were pooled, fractionated using ion exchange (Mono Q) column and the resulting FPLC UV trace is shown (A). The repair activity of fractions on the THF-IN mononucleosome substrate using the BER repair assay with APE1 (57 fmol) and ubiquitin (0.6 nmol) added was performed for 1 h at 30°C. Reactions were separated by denaturing (7 M) PAGE gels and a representative gel is shown (B). Quantification of THF site incision from these gels are also shown as an average of two independent experiments, where incision activity of purified APE1 only, the threshold value, producing 30 % incision is shown by the red dashed line(C).

5.3.3.3.3 Mass spectrometry of fraction 29 from ion exchange chromatography of activity 3

The most active fraction from the final ion exchange (Mono Q) chromatography step from activity 3, fraction 29, was analysed by mass spectrometry to identify candidate proteins. A selection of the top mascot score proteins are shown in table 13 and a full list is provided in appendix 3. As factors used to promote ubiquitination (but also poly(ADP-ribosyl)ation) were initially found to increase APE1 incision of the THF-IN mononucleosome substrate, the identification of any E3 ubiquitin ligases were of interest, as were the presence of any ATP-dependent chromatin remodelling complexes that could be recruited after ubiquitination. Surprisingly, none of these types of proteins were identified from mass spectrometry. In fact two Y-Box binding proteins (YBX), were the top two proteins identified from mass spectrometry, which were nuclease-sensitive element-binding protein 1 (YBX1) and Y-box binding protein 3 (YBX3) with Mascot scores of 917 and 459, respectively. Therefore, YBX1 and YBX3 were analysed for their presence and alignment in fractions containing APE1 THF-IN stimulatory activity.

Accession	Description	Mascot Score
P67809	Nuclease-sensitive element-binding protein 1 (YBX1)	917
P16989	Y-box binding protein 3 (YBX3)	459
P68363	Tubulin alpha-1B chain	345
P07437	Tubulin beta chain	293

Table 13: Mass Spectrometry results for activity 3. Fraction 29 the most active fraction for activity 3 purified from the final ion exchange (Mono Q) chromatography stage was analysed by mass spectrometry to identify candidate proteins. The top mascot scoring proteins are shown in the table and the interesting candidate proteins are shown in bold.

5.3.3.3.4.1 Ion exchange chromatography alignment of the activity 3 profile to YBX1 and YBX3

Alternate fractions 64 to 76 from the initial ion exchange (Mono Q) chromatography stage where APE stimulatory activity was discovered were analysed for the presence of YBX1 and YBX3 by Western blotting. Both of these candidate proteins were present in the fractions, although the antibodies for YBX3 were not of particularly good quality (Figure 59Ai and 59Aii). However it appeared as though the signal for YBX3 does not align particularly well with the activity profile as the protein appeared the most abundant in fractions 64-66 and decreased thereon, whereas APE1 stimulatory activity on the THF-IN mononucleosome substrate appeared to increase from fractions 64 to 74. The protein levels of YBX1 also appeared higher in fractions 64 and 66, which then decreases in the other fractions (68 to 76), although this seemed to occur to a lesser extent than with YBX3. Nevertheless, the alignment of YBX1 and YBX3 were further characterised in the subsequent chromatography steps

5.3.3.3.4.2 Gel filtration chromatography alignment of the activity 3 profile to YBX1 and YBX3

Every fraction from fractions 17 to 25 from the gel filtration (Superdex 200) chromatography stage were examined for the presence of YBX1 and YBX3 by Western blotting, and for their alignment to the APE1 stimulatory incision activity profile on the THF-IN mononucleosome substrate. From the activity profile the highest activity appeared to be in fractions 18 to 24 with the peak activity at fraction 18 (Figure 59Bi). YBX1 and YBX3 were again found to present in all active fractions from 17 to 25. The levels of both proteins peaked at fraction 17 and 18, and then decrease to fraction 25 which aligns, to some degree, with the APE1 stimulatory activity profile (Figure 59Bi and 59Bii). As both proteins appeared to display some alignment with the activity profile, this was further assessed in the final ion exchange chromatography step.

5.3.3.3.4.3 Final ion exchange chromatography alignment of the activity 3 profile to YBX1 and YBX3

Every fraction from fraction 25 to 33 from the final ion exchange (Mono Q) chromatography stage where APE1 stimulatory activity was present were examined for YBX1 and YBX3 by Western blotting. The two fractions that produced APE1 stimulatory activity on the THF-IN mononucleosome substrate were fractions 28 and 29 (Figure 59Ci). YBX1 was found to be present in fractions 27 to 29 and YBX3 largely present in fractions 27 and 28. Interestingly the antibodies for YBX3 detected the protein well in these fractions, indicating that YBX3 is indeed increasing in abundance following purification. However, both of these were proteins appear to be present in fraction 27, where little APE1 stimulatory activity was seen, and activity was

also observed in fraction 29 there was very little YBX3 (Figure 59Ci and 59Cii). Therefore, it was difficult to conclude whether YBX1 or YBX3 are or are not causing the APE1 stimulatory activity observed. The dependence of fraction 29 for ubiquitination was therefore examined further.

5.3.3.3.4.4 Analysing ubiquitination dependence of activity 3

The two candidate proteins, YBX1 and YBX3, identified from mass spectrometry of the final ion exchange (Mono Q) chromatography stage showed some degree of alignment to the activity profile for APE1 stimulatory activity on the THF-IN mononucleosome substrate. It was thought that either these proteins were stimulating APE1 activity on their own, or acting in concert with another as yet unidentified enzyme present in the purified fraction thereby making the THF site in the THF-IN mononucleosome substrate more accessible to APE1. As we used factors (E1, E2, ubiquitin) but also poly(ADP-ribosyl)ation (NAD) in the BER *in vitro* assay, it was important to assess whether this stimulation in APE1 activity was particularly ubiquitination dependent. Fraction 29 from the final ion exchange (Mono Q) chromatography column was titrated into the BER *in vitro* assay using the THF-IN mononucleosome substrate with APE1 (57 fmol) and ubiquitin (0.6 nmol), in the absence or presence of the E1/E2 enzyme pool to examine if ubiquitination was key for this activity. The average THF site incision within THF-IN from two experiments was calculated and recombinant APE1 only was used as a control which was deducted from the percentage incision by the fractions so that the amount of stimulation could be determined. Interestingly, ubiquitination was found to greatly stimulate this activity as there was a dramatic reduction in THF incision in the absence of the E1/E2 enzyme pool (Figure 60A and 60B). As this activity was found to be largely ubiquitination-dependent, and that YBX1 and YBX3 are not known as E3 ubiquitin ligases, it was predicted that these proteins maybe facilitating ubiquitination of histones by an associated E3 ligase present in the fractions that makes the AP site more accessible. It was therefore interesting to examine the effect of an siRNA knockdown of YBX1 and YBX3 in cells to analyse if these proteins are controlling DNA damage repair kinetics and survival following IR.

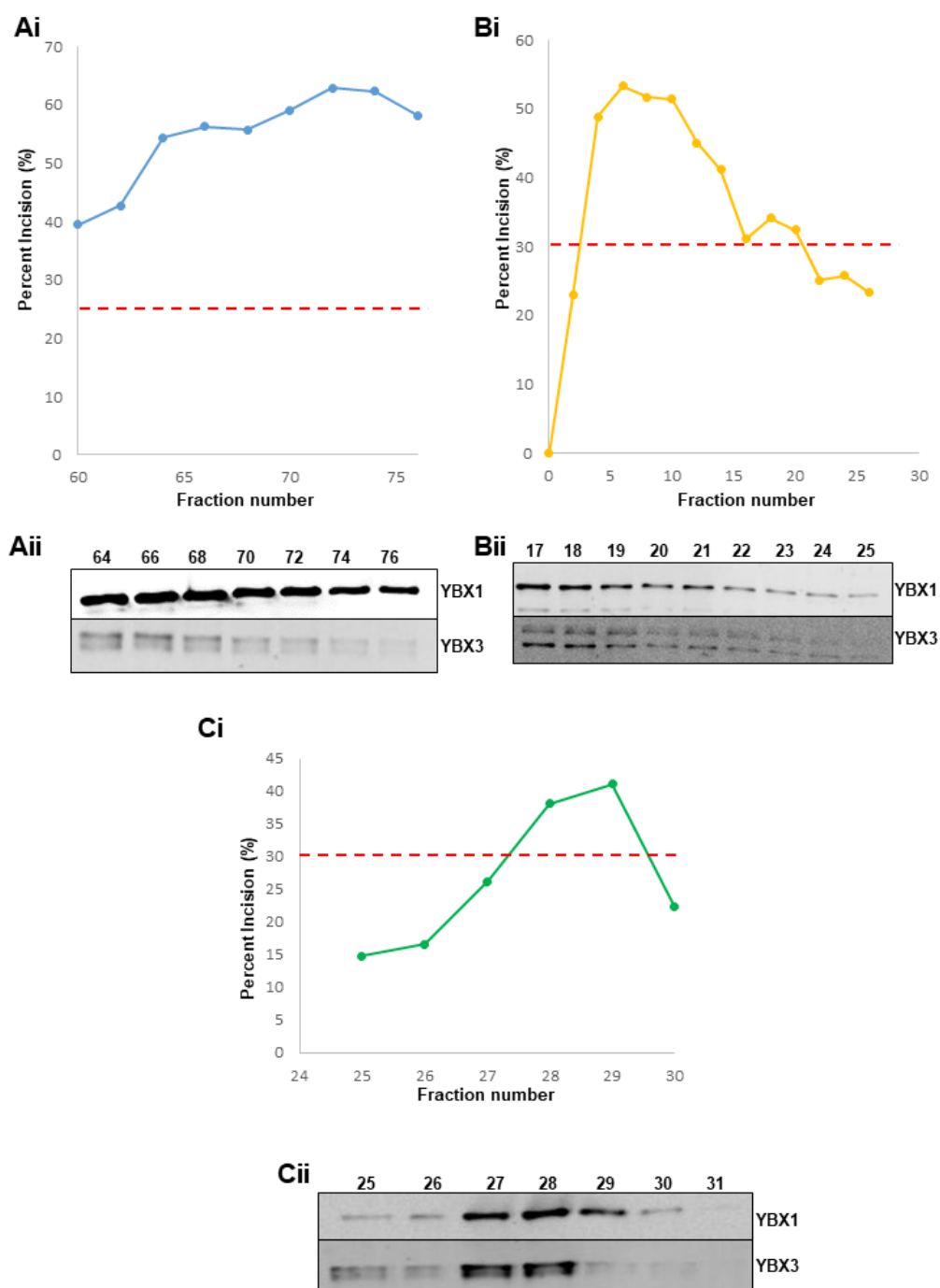


Figure 59: Alignment of YBX1 and YBX3 to the activity profiles of activity 3 for each of the sequential chromatography stages. YBX1 and YBX3, identified from mass spectrometry, were analysed for their alignment to the activity profiles of each chromatography step (Ai, Bi, Ci). Protein fractions were loaded onto 10 % SDS polyacrylamide gels, transferred onto a PVDF membrane and analysed by Western blotting for the respective proteins (Aii, Bii, Cii). Figures show protein alignments for the initial ion exchange (Mono Q) column (Ai and ii), the gel filtration (Superdex 200) column (Bi and ii) and the final ion exchange (Mono Q) chromatography column (Ci and Cii). The activity threshold of APE1 is shown as the red dashed line in each of the graphs.

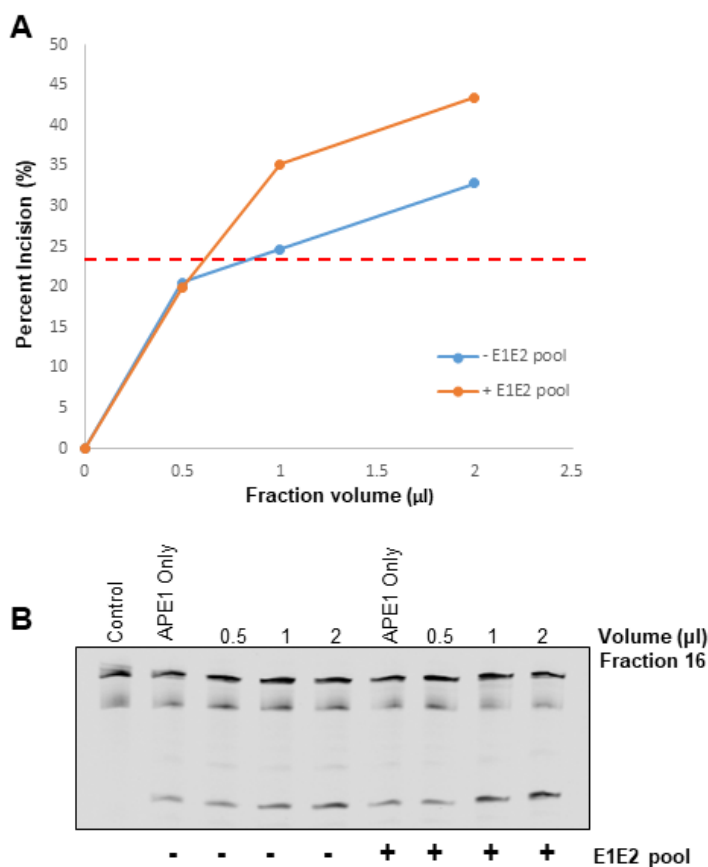


Figure 60: Analysing the ubiquitination dependence of activity 3. Fraction 28 from the final ion exchange (Mono Q) chromatography stage of activity 3 was analysed for the dependence on ubiquitination. The fraction (0.5-2 μl) was tested in the BER *in vitro* assay using the THF-IN mononucleosome substrate with APE1 (57 fmol) and ubiquitin (0.6nmpmol), with and without the E1/E2 enzyme pool, which was incubated for 1 h at 30°C. Percentage substrate incision was averaged from two separate experiments (A), and a representative denaturing (7 M) PAGE gels (B) is shown. Incision with the APE1 only control, the threshold value, is shown by the red dashed line.

5.4 Analysing IR-induced DNA damage repair kinetics and cell survival following siRNA knockdown of candidate proteins

The results shown previously suggest that the candidate proteins identified (HECTD1, YBX1 and YBX3) maybe stimulating APE1 activity by increasing the accessibility of sterically occluded AP sites through histone modifications and/or chromatin remodelling. If these proteins were required in cells to promote DNA repair and were thus depleted, this should reduce the ability of the cells to repair DNA damage and also sensitise the cells to DNA damaging agents (eg. ionising radiation (IR)). IR was selected as a DNA damaging agent due to its use in cancer therapy and so making this work more translational. IR does have its disadvantages however, it causes a range on DNA damages; base damages, SSBs and DSBs and so is not specific to BER. MMS is a specific base damaging agent, due to its ability as a DNA alkylating agent but using this would have little translational impact to cancer therapy. The candidate proteins were therefore knocked down in cells using siRNA prior to irradiation. Cell survival was then measured using clonogenic assays, whereas the comet assay was used to analyse DNA damage repair kinetics following individual candidate protein knockdowns.

5.4.1 Knockdown of HECTD1, YBX1 and YBX3 in HeLa cells

HeLa cells were treated with siRNA (40 nM) for each of the candidate proteins HECTD1, YBX1 and YBX3 with Lipofectamine RNAiMAX for 48 h, in addition to a control using the transfection reagent only, so the knockdown efficiency could be compared. Cells were harvested, lysed and protein concentration measured. The efficiency of knockdown for each protein compared to the control was assessed by SDS-PAGE and Western blotting for each of the candidate proteins using the Odyssey Image Analysis System (Figure 61A-C). This revealed that all three candidate proteins were efficiently knocked down by siRNA in HeLa cells, by ~88 %, ~84 %, ~92 %, and for HECTD1, YBX3 and YBX1 respectively. The same conditions were therefore used prior to the clonogenic assay and comet assay.

5.4.2 Analysing IR-induced cell survival after YBX1, YBX3 and HECTD1 knockdown

To assess whether the siRNA knockdown of YBX1, YBX3 and HECTD1 separately in HeLa cells affected cell survival in response to IR-induced DNA damage, the clonogenic assay was utilised. Following a 48 h knockdown of each of these proteins, using transfection reagent only as a control, the cells were irradiated with increasing doses of x-rays (0-4 Gy). Cells were then trypsinised and a defined number of cells seeded in triplicate in 6-well plates for each siRNA knockdown and irradiation condition. The cell numbers were increased for increasing radiation doses and double the number of cells were used for HECTD1 and YBX3 siRNA treated cells,

compared to the control and YBX1 treated cells, to allow for cell plating efficiencies. Cells were incubated for ~7 days, and cells fixed and stained as long as there were more than >50 cells/colony. Colonies were then counted using the GelCount colony analyser and the relative colony formation (surviving fraction) of each siRNA knockdown condition compared to the untreated control was determined.

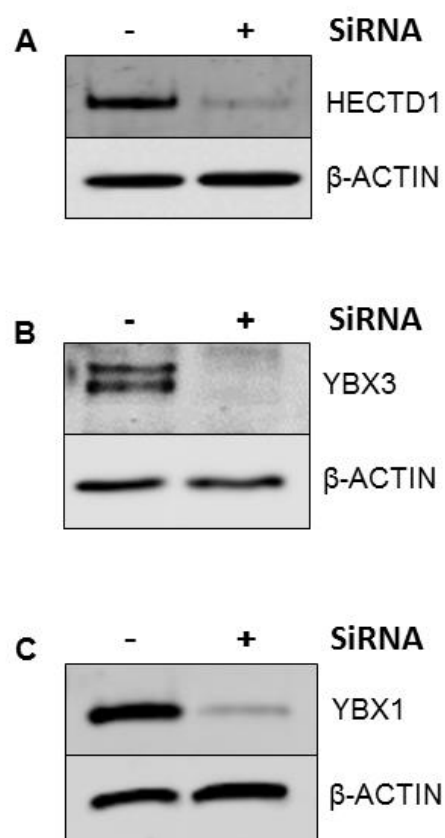


Figure 61: Knockdown of HECTD1, YBX1 and YBX3 in HeLa cells. HeLa cells were treated with siRNA (40 nM) for either HECTD1, YBX1 or YBX3 for 48 h, or using Lipofectamine RNAiMAX only as a control. Cells were harvested, lysed and protein concentration was measured using the Bradford assay. Cell lysates (10 µg) were separated on SDS polyacrylamide gels (6 % for HECTD1 and 10 % for YBX1 and YBX3), transferred onto a PVDF membrane and analysed by Western blotting for the respective proteins. The efficiency of the knockdown was quantified and normalised to the loading control (β-actin).

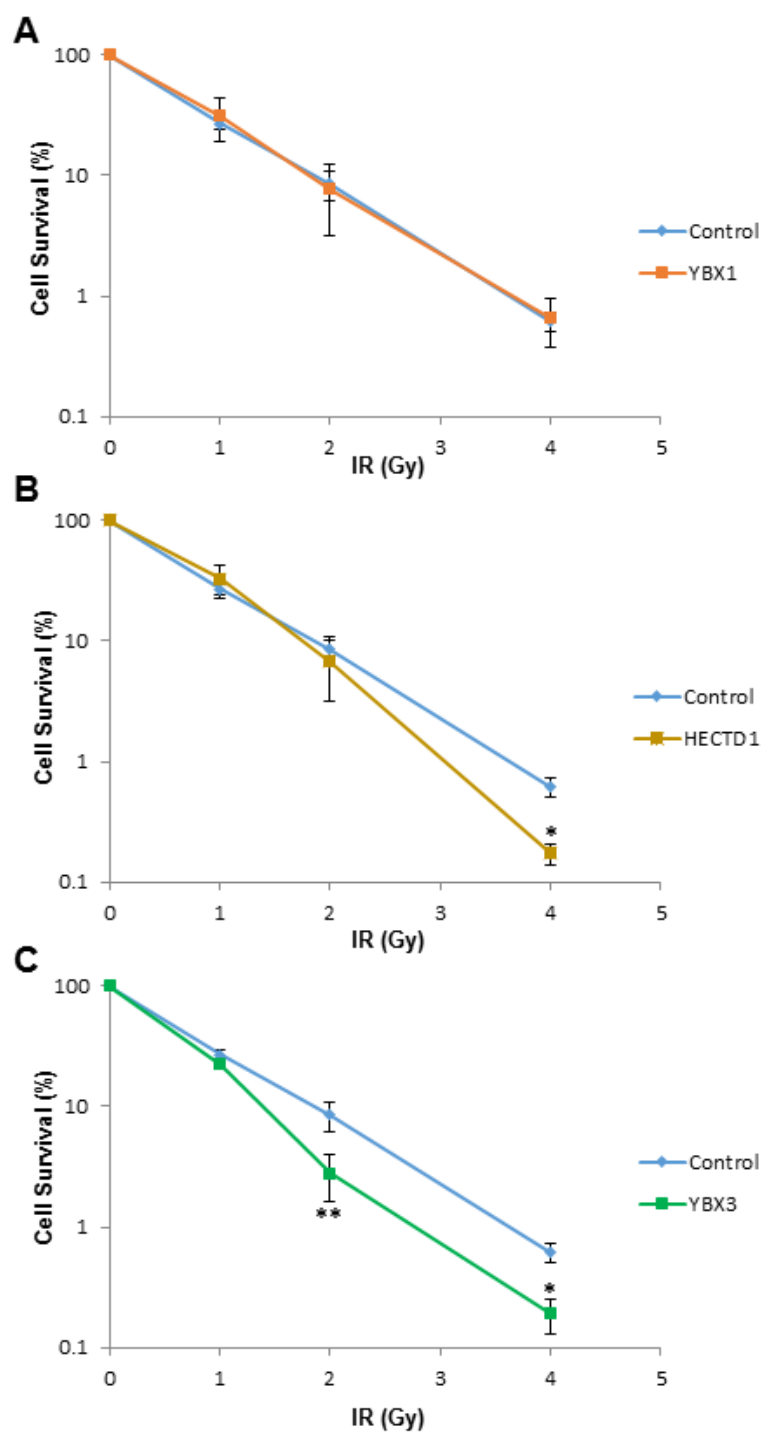


Figure 62: The effect of YBX1, YBX3 and HECTD1 on cellular sensitivity to IR. HeLa cells were grown in 3 cm dishes for 24 h to 30–50% confluency and then treated with Lipofectamine RNAiMAX transfection reagent in the presence of HECTD1 siRNA, YBX1 siRNA, YBX3 siRNA or RNAiMAX alone (as a control) for 48 h. Clonogenic survival of cells was analysed following treatment with increasing doses of ionising radiation (0–4 Gy) (A, B, C). Shown is the surviving fraction with standard error of the mean from at least three independent experiments. SnF is shown as * $p < 0.01$ and ** $p < 0.001$.

It was found that a YBX1 knockdown had no effect on HeLa cell survival compared to the control, suggesting that YBX1 is not essential for the cellular response to IR (Figure 62A). In contrast, YBX3 knockdown did sensitise cells particularly following 2 Gy and 4 Gy x-ray irradiation. Using a one way ANOVA statistical test at 2 Gy compared to the control this was found to be significant (significance factor (SnF) $p = < 0.001$) and a 4 Gy (SnF $p < 0.01$) (Figure 62B). A HECTD1 knockdown also sensitised cells to IR, but was only statistically significant after 4 Gy x-ray irradiation (SnF $p = < 0.01$) (Figure 62C). These results suggest that YBX3 is required for cell survival in response to IR, and predictably this effect is through modulating DNA damage repair. HECTD1 only appears to be controlling cell survival, and thus DNA damage repair, at high doses of radiation, suggesting that it could be having an effect on specific types of DNA damage or that there is a particular threshold for increased radiosensitivity. Therefore IR-induced DNA damage repair kinetics following these protein knockdowns was assessed in HeLa cells, but also normal lung fibroblasts, to see if there was any delay in DNA damage repair using the alkaline comet assay.

5.4.4 Analysing IR-induced cellular DNA damage repair kinetics following knockdown of YBX1, YBX3 and HECTD1

As YBX3 and HECTD1 (to some extent) appear to be required for HeLa cell survival following IR, we analysed whether this was caused by changes in DNA damage repair kinetics by utilising the alkaline single cell gel electrophoresis (comet) assay. The alkaline comet assay measures collectively DNA single strand breaks, double strand breaks and alkali labile sites. This was initially analysed in HeLa cells. In control cells (transfection reagent only), the majority of IR-induced DNA damage was repaired by 60-120 min post-irradiation, with a gradual decrease in % tail DNA observed from 10-60 min post-irradiation (Figure 63; blue bars). Following YBX3 siRNA, there appeared to be a delay in DNA damage repair, particularly at these later time points (60 and 120 min) and indeed after 120 min there a statistically significant difference in DNA damage levels compared to control transfected cells ($p < 0.05$; Figure 63; green bars). Interestingly, there was also a significant increase in the basal levels of DNA damage in unirradiated cells following YBX3 knockdown in comparison to control transfected cells. A significant difference in DNA damage repair kinetics was also seen following HECTD1 siRNA, compared to control transfected cells, and particularly this was statistically significant at 120 min post-irradiation ($p < 0.01$; Figure 63; yellow bars). However in the absence of HECTD1, there was no significant difference in the % tail DNA in unirradiated controls. These data suggest that both YBX3 and HECTD1 appear to play a role, albeit differing roles, in the repair of IR-induced DNA damage in HeLa cells.

Since HeLa cells are cervical cancer cells, it was also interesting to examine whether YBX3 and HECTD1 play a role in normal cells in response to DNA damage. Therefore normal human lung fibroblasts (AG06173) were used in a similar experiment. Similar to that observed with

HeLa cells, in control fibroblasts (transfection reagent only), the majority of IR-induced DNA damage was repaired by 60-120 min post-irradiation, with a gradual decrease observed from 15-60 min post-irradiation (Figure 64; blue bars). Following YBX3 knockdown, there was a significant delay in DNA damage repair at all the time points investigated (15-120 min), suggesting that YBX3 is playing a critical role in the response to IR-induced DNA damage in normal cells (Figure 64; green bars). There was also defective DNA damage repair in the absence of HECTD1 in normal fibroblasts, although this was only significant at 30-120 min post-irradiation (Figure 64; yellow bars). It should also be noted that depletion of HECTD1 or YBX3 also caused a significant accumulation of DNA damage in the unirradiated controls.

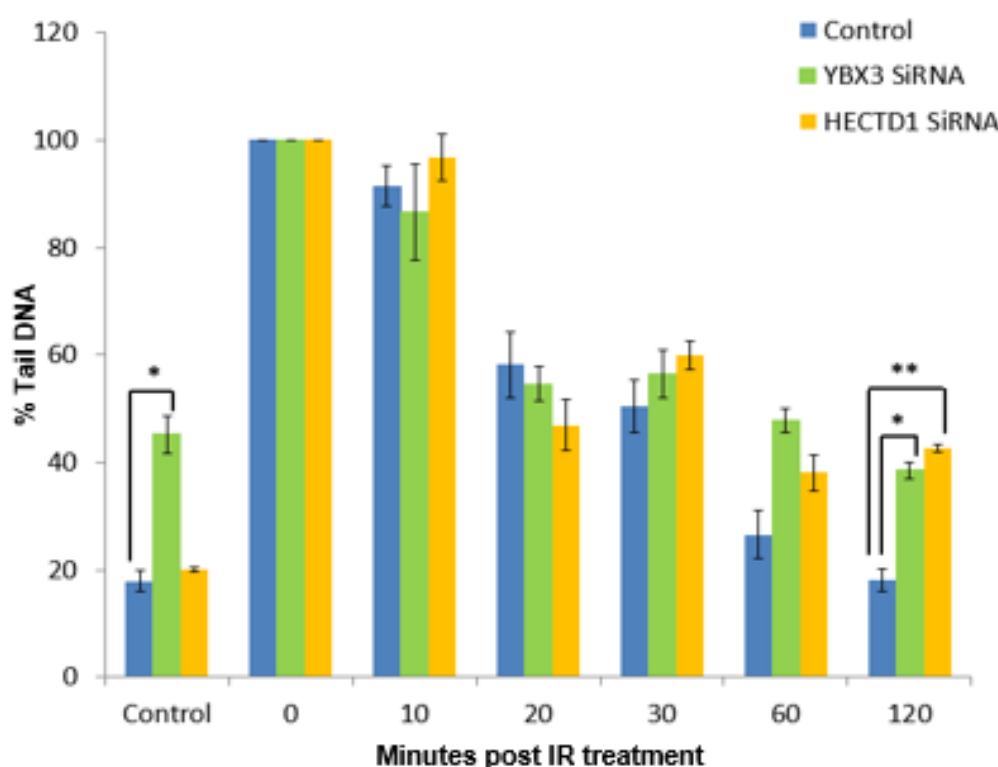


Figure 63; Analysing ionising radiation-induced DNA damage repair kinetics following siRNA knockdown of YBX1, YBX3 and HECTD1 in HeLa cells. HeLa cells were irradiated (1.5 Gy) and DNA single/double strand breaks and alkali labile sites measured at various time points post-irradiation (0-120 min) by the alkaline single cell gel electrophoresis (comet) assay. Shown is the % tail DNA with standard deviations from at least three independent experiments. * $p < 0.05$ and ** $p < 0.01$, as analysed by a one sample t -test.

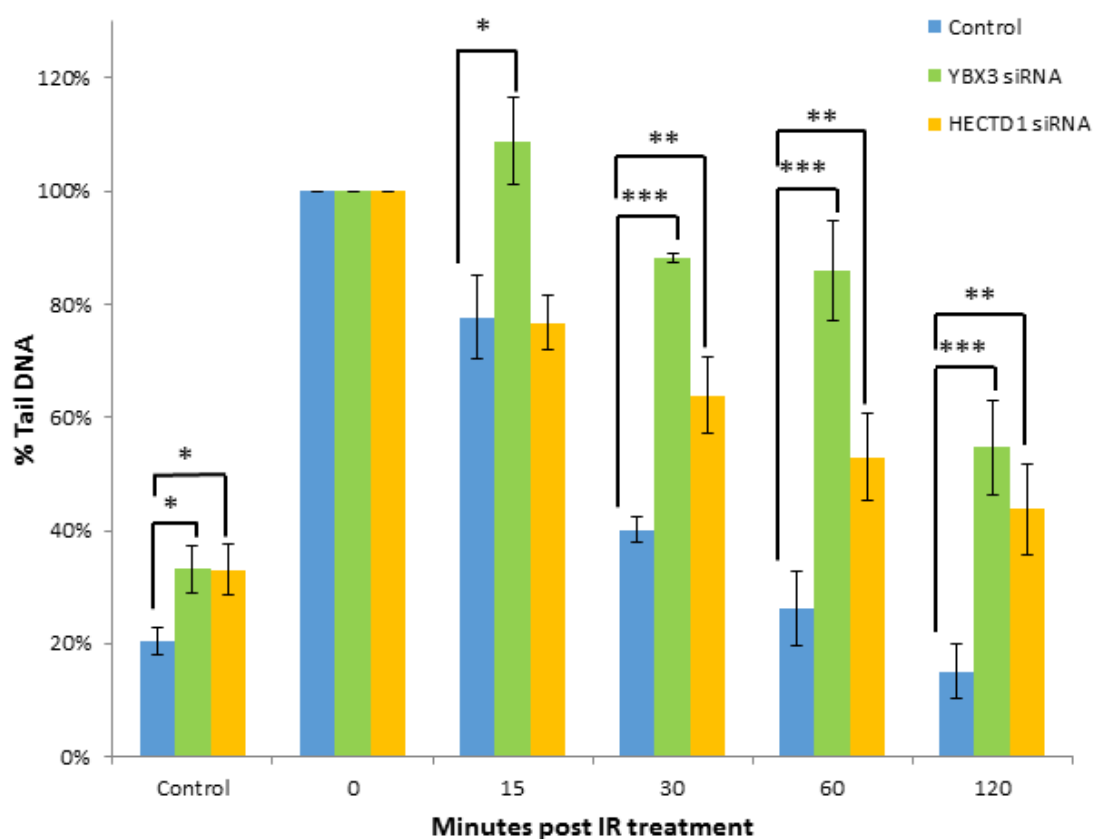


Figure 64; Analysing IR-induced DNA damage repair kinetics following siRNA knockdown of YBX1, YBX3 and HECTD1 in normal lung fibroblasts. Normal lung fibroblast cells (AG06173) were irradiated (1.5 Gy) and DNA single/double strand breaks and alkali labile sites measured at various time points post-irradiation (0-120 min) by the alkaline single cell gel electrophoresis (comet) assay. Shown is the % tail DNA with standard deviations from at least three independent experiments. * $p < 0.05$, ** $p < 0.01$ and *** $p < 0.001$, as analysed by a one sample t -test

5.5 Summary

In Chapter 4, I revealed evidence suggesting that the increase in the activity of APE1 towards the THF-IN mononucleosome substrate caused by WCE was thought to be due to a E3 ubiquitin ligase(s) or PARPs, as when factors were added to stimulate ubiquitination or poly(ADPribosyl)ation in the BER *in vitro* assay, the substrate showed increased incision. Ubiquitination was selected as the primary PTM to follow up due to the expertise of this laboratory and more importantly it's heavy implication in chromatin remodelling during DSB repair and NER. To attempt to discover the potential E3 ubiquitin ligase(s) responsible for the increase of activity of APE1, two approaches were used. Initially a candidate approach was used, screening selected E3 ligases (11 in total) that are known to be involved in different types of DNA damage repair pathways. These E3 ligase(s) were knocked down using siRNA in HeLa cells, and WCE were then used in the BER *in vitro* repair assay with factors to support ubiquitination (and poly(ADP-ribosyl)ation) to assess APE1 activity towards the THF-IN mononucleosome substrate. It was found that there was no dramatic and significant difference in APE1 incision activity between the control and the siRNA knockdowns for MSL2, UBR2, RNF168, RNF20, DZIP3, CUL4A, CUL1, RNF2, RNF8, MULE and BRCA1 using either an extract titration or a reaction time course. Whilst the sensitivity of the assay could be questioned, and there appeared to some candidates that caused a minor reduction in the efficiency of THF incision (eg. UBR2, RNF168, DZIP3 and CUL1), arguably it appears as though these enzymes alone are not absolutely essential for the repair of the THF-IN mononucleosome substrate. Alternatively, there could be multiple overlapping activities which may be able to compensate for the lack of one of these enzymes. Therefore a different approach was used to identify potential E3 ubiquitin ligase(s) and/or chromatin remodellers that were stimulating APE1 incision activity towards the THF-IN mononucleosome substrate.

A fractionation approach was used to purify and ultimately identify novel activities that stimulate APE1 activity towards the THF-IN mononucleosome substrate. This approach has been used successfully in Dr Parsons' laboratory to identify E3 ubiquitin ligases that regulate the cellular levels of BER proteins, although this is the first time that this approach has been used in combination with mononucleosome substrates and the BER *in vitro* assay. This approach involves sequential chromatography of HeLa WCE over four separate chromatography columns. After each fractionation, protein fractions were analysed for APE1 stimulatory activity on the THF-IN substrate which was above the basal activity of recombinant APE1 only, which was added to the BER *in vitro* assay. This sequential approach purifies the protein(s) responsible so that they can be easily identified by mass spectrometry. Firstly a Phosphocellulose column was used to separate HeLa WCE into two protein fractions; PC150 and PC100 that largely contain non-DNA and DNA binding proteins, respectively. APE1 was then immunodepleted from these two fractions, and from the full HeLa WCE, as much as possible in order to remove any endogenous APE1 present that may elevate THF site incision. This was largely successful in the WCE and PC150 fractions, although the PC1000 fraction

still contained substantial amounts of APE1. Nevertheless, these cell extracts were then used in the BER *in vitro* assay with and without added recombinant APE1, which alone caused around ~20 % incision of the THF-IN mononucleosome substrate. This was the baseline value we set for examining any significant increases in THF site incision, therefore any difference above this value indicated that there were factors in the fraction that were stimulating APE1 activity. The PC1000 fraction didn't increase APE1 incision above this baseline value suggesting that this fraction lacked proteins that we have shown to stimulate APE1 incision activity towards the THF-IN mononucleosome substrate. The PC150 fraction however increased APE1 incision by ~40 % above this baseline value, indicating that there were factors in this fraction that made the THF site in THF-IN mononucleosome more accessible to APE1. Predictably these were thought to be E3 ubiquitin ligase(s) and/or chromatin remodellers, that were increasing the incision activity of APE1 towards this substrate, as originally the WCE activity was found to be highly dependent on ubiquitination. As the PC150 fraction contained APE1 stimulating activity this fraction was further separated by sequential chromatography.

In the second chromatography step, which used an ion exchange (Mono Q) column, surprisingly three novel APE1 stimulatory activities were identified which increased APE1 incision of the THF-IN mononucleosome substrate above the baseline value. As previously, the BER *in vitro* assay was used with factors to stimulate ubiquitination and poly(ADP-ribosyl)ation. Residual, endogenous APE1 protein was identified in the fractions from the Mono Q column, however this did overlap with any of the three identified, major activities. Fractions for the three separate activities were pooled and purified over another two columns; gel filtration (Superdex 200) and a final ion exchange (Mono Q) column separately using the same approach as before to identify active fractions. The most active fraction after the final ion exchange fractionation was analysed by mass spectrometry to identify candidate E3 ligases and/or chromatin remodelling complexes that were potentially stimulating APE1 activity by changing the structure of the mononucleosome to make the THF site in THF-IN mononucleosome more accessible to APE1. Mass spectrometry identified several candidate proteins; activity 1 HECTD1 and CHIP, activity 2, MULE and DDB1 and activity 3 YBX1 and YBX3.

For activity 1, the presence of CHIP protein in the fractions did not appear to align well with the initial ion exchange activity profile of APE1 stimulation on THF-IN, however HECTD1 showed a strong alignment and this was shown throughout all activity profiles for each of the chromatography steps. As HECTD1 is an E3 ubiquitin ligase, the most active fraction from the final chromatography step was analysed for its dependence on ubiquitination by removing factors (E1/E2 enzymes) that supported ubiquitination. When these factors were removed, the activity of APE1 incision of the THF-IN mononucleosome substrate decreased, giving more evidence and confidence that this novel APE1 stimulating activity was accomplished by HECTD1. For activity 2, MULE and DDB1 showed only some degree of alignment towards the activity for each of the fractionation steps. CUL4A which is known to be a multiple E3 ligase

complexes with DDB1, was also analysed at the final ion exchange (Mono Q) stage and indeed aligned with DDB1, and again to some degree with the APE1 stimulatory activity profile for THF-IN. However, the most active fraction from the final ion exchange chromatography was found to be not dependent on ubiquitination, suggesting that this novel activity was not caused by MULE or DDB1, so this activity was not analysed further at this stage. For activity 3, the Y-box proteins YBX1 and YBX3 were found in high abundance in the fractions and again these proteins appeared to align, to some degree, with the APE1 stimulatory activity profile for THF-IN all the subsequent chromatography steps. Interestingly this activity was found to be dependent on ubiquitination, and whilst YBX1 and/or YBX3 have no known E3 ubiquitin ligase activity, this suggested that these proteins could be facilitating an E3 ubiquitin ligase present in the fraction to stimulate APE1 activity towards the THF-IN mononucleosome substrate. However, no E3 ubiquitin ligases were discovered to be present in these active fractions by mass spectrometry.

Since HECTD1, YBX3 and YBX1 proteins appeared to be good follow up candidates from the fractionation strategy, it was decided to examine their effect on cell survival and DNA damage repair kinetics in response to IR. If these candidate proteins were stimulating APE1 activity by histone modifications and/or chromatin remodelling, it can be expected that cells would be unable to repair occluded DNA damage sites, and that DNA damage persistence could cause cell sensitivity to IR. Following YBX3 siRNA in HeLa cells, it was discovered that there was significantly reduced cell survival at 2 Gy and 4 Gy doses of IR. HECTD1 siRNA, however, only appeared to significantly affect cell survival at the highest dose used (4 Gy). These data would suggest that both YBX3, and to some extent HECTD1, play roles in controlling cell survival in response to IR. The roles of these proteins specifically in DNA damage repair in HeLa cells was discovered by a delay in IR-induced DNA damage repair as visualised by the comet assay, compared to the untransfected control, largely at later times (60 and 120 min) post-irradiation. This delay in repair would appear to correlate with increased sensitivity of cells in the absence of YBX3 and HECTD1 following irradiation. Lastly since HeLa cells were used for analysis, which are cervical cancer cells, I also acquired exploratory data examining the role of HECTD1 and YBX3 in DNA damage repair in normal human lung fibroblasts. An siRNA knockdown of either YBX3 and HECTD1 also reduced IR-induced DNA damage repair kinetics in normal fibroblasts compared to the untransfected control, at several time points post-irradiation. This suggests that HECTD1 and YBX3 not only play a role in HeLa (cancer) cells, but are also essential proteins in normal cells required in the cellular response to IR-induced DNA damage.

In summary, both HECTD1 and YBX3 identified in this study appear to be strong candidates required for BER, which I predict is catalysed through histone ubiquitination and chromatin remodelling. I propose that these proteins make sterically occluded DNA damage (eg. AP sites) more accessible to BER proteins (eg. APE1) and thus facilitate efficient DNA damage repair.

CHAPTER VI

DISCUSSION

6.1 Overview

Damage to DNA occurs frequently through endogenous sources such as normal cellular metabolism and exogenous sources so it is important that cells repair the damage to maintain genome stability. Indeed it is thought that around 10,000 DNA base lesions are generated in every cell per day from ROS from cellular metabolism. BER is highly conserved and is essential for the repair of the majority of endogenous DNA base damages to maintain genome integrity. If DNA base damages are not repaired the integrity of the genome can be compromised, stalling replication and transcription which can lead to diseases including cancer, premature aging and neurodegeneration (5, 6). This highlights the importance of increasing our understanding of the response and repair of DNA lesions which are processed by BER, as proteins associated with the repair pathway can be potentially harnessed to produce new therapies for diseases such as cancer. A good example of this is the use of inhibitors targeting PARP-1 for the treatment of BRCA-deficient tumours. It is therefore of interest to discover novel proteins involved in chromatin remodelling during BER as it is a source of potential therapeutic targets to treat human diseases.

DNA in cells is packaged tightly into chromatin, generated in a vast array of loops and coils in a co-ordinated manner. Chromatin is arranged and regulated so that DNA can still be accessed by proteins for important biological processes, including transcription, replication and repair. Chromatin at its most basic level is organised of nucleosomes which link together to form nucleosome arrays. Nucleosomes consist of two copies of each of histone H2A, H2B, H3 and H4 forming the histone octamer and approximately 147 bp genomic DNA is wrapped around the octamer (16). Nucleosome arrays are packed together to form the chromatin fibre, which are coiled and looped into increasingly higher orders of chromatin with the assistance chromatin regulator proteins to form chromosomes (106).

Chromatin and nucleosomes form an obstruction to proteins required for important biological processes requiring access to genomic DNA, depending on the DNA to nucleosome interface. This is overcome by the dynamic properties of histones, and are regulated in such a way to either stimulate or repress biological processes. Histones have N-terminal tails which protrude

out of the nucleosome and specific residues can be modified through PTMs including acetylation, poly(ADPribose)ylation, ubiquitination, methylation and phosphorylation. These can alter the chromatin structure in a number of ways including; manipulating the electrostatic interactions between the DNA and the histone octamer, disturbing protein-protein and protein-DNA interactions, histone exchange and causing the recruitment of ATP-dependent chromatin remodelling complexes (106-108, 127). These alterations on histones can ultimately lead to chromatin condensation and so sterically obstructed sequences of DNA can be accessed by proteins in order for biological processes can take place (107). Fluctuations in chromatin structure is essential in the DNA damage response to regulate checkpoint signalling and DNA repair and therefore to maintain genome integrity. DNA repair proteins must be able to access DNA lesions so repair can take place regardless of the location within chromatin. Evidence for chromatin remodelling in DNA repair is increasing, although in contrast to BER, at this time chromatin remodelling has generally been connected to DSB (HR and NHEJ) and NER (174). Histone modifications and chromatin remodelling in response to damaged DNA bases to facilitate BER is poorly understood. Chromatin remodelling is thought to be necessary based on evidence from mononucleosome substrates which have been utilised in several published studies. These substrates have shown that BER enzymes are significantly less efficient at sites where the base lesion is sterically occluded, with the DNA backbone facing towards the core of the histone octamer or located close to the dyad axis of the nucleosome. In contrast, base lesion sites that are away from the dyad axis and the DNA backbone is orientated so it faces outwards are efficiently processed by BER enzymes. To maintain genome integrity, sterically occluded base lesions must be repaired suggesting that chromatin relaxation events need to take place to slide, unwind or remove histones so that base lesions are accessible for repair (16, 242, 252, 254, 256, 257, 284, 285). The precise mechanisms by which these occluded sites are regulated to facilitate BER enzymes are currently largely unknown.

The study presented in this thesis using mononucleosome substrates, aimed to identify specific histone modifiers and/or the chromatin remodellers that are involved in the processing of DNA base damage during BER. The results show that the sterically occluded THF-IN site can be more efficiently processed by APE1 present in HeLa WCE in largely a ubiquitination-dependent event, predictably by a E3 ligase, but not by recombinant APE1 only. This is thought to be by causing a structural change in the mononucleosome through histone PTMs or causing the recruitment of ATP-dependent chromatin remodelling complexes. A sequential chromatography approach of proteins purified from HeLa WCE was used to purify and identify the E3 ubiquitin ligase HECTD1, and the DNA binding protein YBX3, in active fractions that stimulated THF-IN incision by APE1. I found that depletion of these proteins in HeLa cells and in normal human lung fibroblasts (AG06173) delayed DNA damage repair following IR. Furthermore, depletion of HECTD1 and YBX3 in HeLa cells sensitised cells to IR. Therefore I hypothesise that both YBX3 and HECTD1 appear to be strong candidates required for improving the efficiency of BER through histone ubiquitination and/or chromatin remodelling.

6.2 Mononucleosomes as substrates for BER

Several published studies have used mononucleosomes to monitor the repair of differently orientated base lesions and intermediates by purified BER enzymes. It has been well established and documented from these investigations that base lesions located near the dyad axis and/or orientated so the backbone is facing towards the histone core cause a significant decrease in the efficiency of repair by purified BER enzymes (16, 242, 252, 254, 256, 257, 284, 285). However, the efficiency of repair of these substrates by BER proteins present within cell extracts, which contain histone modifiers and chromatin remodellers, has not previously been reported in such detail. Therefore, I uniquely used mononucleosome substrates to examine any possible effect of histone modification enzymes present in WCE in facilitating APE1 activity at sterically occluded THF sites, in comparison to recombinant APE1 only, with the eventual goal of purifying and identifying these enzymes. Two mononucleosome substrates were designed containing THF in two different site-specific regions; THF-OUT at +12 and THF-IN +11 from the nucleosome dyad, in order to investigate this. The orientation of the THF when reconstituted to form the mononucleosome was determined from the crystal structure of the Widom 601 nucleosome positioning sequence and from previously published work (242). The Widom 601 nucleosome sequence was selected for its near identical orientation when reconstituted in a nucleosome compared to human DNA and has strong nucleosome affinity properties (247). This is a standard sequence for use when reconstituting nucleosomes and has been used by previous studies examining BER enzymes in mononucleosomes (242, 257, 271). A THF was used as an alternative to an AP-site as it is significantly more stable, and exhibits virtually no difference in APE1 activity compared to AP-sites generated by glycosylases (254). The method in which the two site specific THFs were introduced into the Widom 601 nucleosome positioning has been previously reported (257), involving cloning of duplex oligonucleotides containing THF into the 601 sequence. However, we modified this methodology by utilising IRDye700 or IRDye800 primers to generate fluorescently labelled DNA which could be accurately detected and quantified using the Odyssey Image Analysis System. Other similar studies utilise radiolabelling to visualise DNA in this context, and so this is the first study to use fluorescently tagged primers to study BER enzyme activities in a mononucleosome context, providing a safer alternative which can be easily and reliably quantified. Following PCR cloning, the substrates were bound with *Xenopus Laevis* recombinant histone octamer, which are commonly used as they can be easily expressed in bacterial systems to high purity and are highly homologous to human histones (245, 246). Each histone was firstly overexpressed in *E.coli*, purified from inclusion bodies by gel filtration and ion exchange chromatography (under denaturing conditions) and refolded to form the histone octamer, as previously shown (246). The THF-OUT and THF-IN mononucleosome substrates were prepared using a 1:1 ratio of substrate DNA and histone octamer to achieve optimum reconstitution. The optimised methodology described in this thesis can be used in the future to study a variety of different BER steps (eg. DNA glycosylase excision of damaged DNA bases and Pol β gap filling activity) and so has the potential to

investigate if there are different chromatin modifications taking place to facilitate independent activities of BER enzymes.

Before analysing the incision of the THF mononucleosome substrates by recombinant APE1 versus WCE, it was important to examine whether there was any sequence bias towards the two different THF-sites in free DNA. There was a slight bias towards free DNA of THF-OUT compared to THF-IN, the difference however was very minimal. This bias was thought to be because of the sequence context of THF-site. The THF-site for THF-IN has C→G either side, whereas THF-OUT has C→G and T→A either side. C→G rich regions because of the presence of three hydrogen bonds are more stable than A→T regions which have two and so this maybe having an impact on the slight bias towards to THF-OUT in free DNA. This minimal difference in sequence bias by APE1 has been reported previously (286). The same BER *in vitro* assay was expanded to incorporate the THF-OUT and THF-IN mononucleosome substrates. As previously mentioned, mononucleosome substrates have been used successfully in number of published studies to analyse the activity of BER enzymes to numerous lesions at different translational and rotational positions (242, 254, 257). Using mononucleosome substrates do have their limitations as they are just a single nucleosome and so lack the full chromatin structure which may produce different histone dynamics and chromatin remodelling activity. They are however a much better substrate than just using free DNA alone, which would not give any insight into nucleosome dynamics during DNA repair. There has been progression of the mononucleosome to dinucleosomes containing linker DNA and H1 in a recent study examining 8-oxo-G removal (252). Furthermore in the future, there could be more complex chromatin structures created, such as vast nucleosome arrays or chromatin fibres, however at this stage mononucleosome substrates appear to be the best models for investigating nucleosome dynamics during BER.

6.3 APE1 in HeLa WCE can efficiently incise THF-IN

I discovered that recombinant APE1 activity was significantly impeded to the sterically occluded THF site in THF-IN compared the THF site in THF-OUT which (as expected) was efficiently processed by APE1 (~3-fold difference in incision) as seen in previous studies (254). The same was result was initially found using HeLa WCE, which we hypothesised that histone modifiers and/or chromatin remodellers would make this site more accessible to APE1, facilitating its activity. However, largely because of the short amount of time THF-IN was incubated with HeLa WCE (10 mins) but also the requirement of additional factors necessary to stimulate any possible remodelling event due to very low concentration of HeLa WCE used, it was decided that the BER *in vitro* assay would be revised. Initially by increasing the length of time THF-IN was incubated with HeLa WCE, this had no dramatic effect on APE1 activity, suggesting that time (partially) was not a contributing factor to the lack of any potential chromatin remodelling activity. Ubiquitination is a strong area of interest in this laboratory, but

more importantly ubiquitination of histones has been shown to be a vital event in the DDR in DSB repair and NER further strengthening the interest to investigate this PTM event (196, 204, 273, 287, 288). I discovered that the presence of supplementary ubiquitin in the BER *in vitro* reaction using a time course experiment significantly increased APE1 activity in HeLa WCE towards THF-IN. This indicated that a ubiquitination-dependent process could be taking place which is increasing the accessibility of the THF site to APE1. This was thought to be due to a partial unwrapping event as the mononucleosome structure itself was found to remain intact following gel analysis. Additional ubiquitin had no effect on the activity of recombinant APE1 alone towards the free DNA substrates, or of WCE for the THF site in THF-OUT, suggesting that this stimulatory effect is specifically required for accessing THF-IN. It also rules out the possibility that APE1 itself was undergoing ubiquitination thus increasing its activity, and the specificity to increase APE1 activity in HeLa WCE towards THF-IN and not THF-OUT suggested that histones were being ubiquitinated facilitating access of APE1 to THF-IN. A trial experiment was performed to analyse the optimum conditions for the BER *in vitro* assay, maximising THF-IN incision. I discovered that the combined addition of NAD required for poly(ADP-ribosyl)ation and all factors required for ubiquitination (ubiquitin, E1/E2 enzymes) produce a significant increase in incision by APE1 in HeLa WCE in the THF-IN mononucleosome substrate. Of note, although ATP supporting phosphorylation events with the addition of PC and PCK to regenerate ATP had no additive effect on APE1 activity in combination with ubiquitination supporting factors, these factors alone did produce a mild increase in THF-IN mononucleosome incision. This suggested that a phosphorylation event may play a minor role in facilitating APE1 activity. Subsequently in a full time course experiment using the BER *in vitro* assay with factors added to stimulate ubiquitination (ubiquitin, E1/E2 enzymes), the degree of THF-IN incision by APE1 present in HeLa WCE increased to almost the same efficiency as cleavage of the THF-OUT mononucleosome substrate. On comparison of recombinant APE1 alone and in HeLa WCE, these additional factors caused an approximate 4-fold increase in incision of THF-IN by APE1 in HeLa WCE. On the other hand THF-OUT was incised to a similar degree using the same concentrations of APE1 alone and in HeLa WCE.

My data therefore strongly indicate novel evidence that additional supporting factors stimulating ubiquitination and poly(ADP-ribosyl)ation events cause the THF site in THF-IN to become more accessible to APE1 in HeLa WCE. Whilst the importance of poly(ADP-ribosyl)ation (predictably via PARP-1) cannot be dismissed, the fact that stimulatory activity was largely observed with ubiquitin only suggested that potentially an E3 ubiquitin ligase is capable of ubiquitinating histones and either causing a structural change in the mononucleosome structure or is actively recruiting an ATP-dependent chromatin remodeller making the THF site in THF-IN more accessible to APE1. As mentioned above, I found no evidence that a total unwrapping of DNA from the histone octamer was being induced since the mononucleosome structure remained intact following gel analysis, and would appear to

suggest that a partial unwrapping event is taking place. Nevertheless, to our knowledge, this is the first evidence suggesting that BER of sterically occluded DNA damage sites in a chromatin model are stimulated by ubiquitination.

This finding that BER can be stimulated to sterically occluded site by ubiquitination relates to other work in the DNA repair field, particularly related to DSB repair and NER. For example, H2AK119 and H2AK120 monoubiquitylation by the Polycomb E3 ligase complex BMI1–RING1B has been shown to be important for efficient DSB repair (273). RNF8, which accumulates at DSBs, monoubiquitinates H2A and H2AX which then catalyses the K63-linked ubiquitin chains with UBC1, that interact with MDC1 to recruit this protein to DNA damage sites (198). This monoubiquitination of histones causes the recruitment of RNF168 to initiate H2A/H2AX K13 and K15-dependent polyubiquitination. The ubiquitination of histones allows the recruitment of 53BP1 and BRCA1 by altering chromatin accessibility, so facilitating 53BP1 loading (199). In NER although the exact ubiquitination sites of H2A, H3 and H4 have yet to be identified, their ubiquitination by CUL4-DDB-ROC1 ubiquitin ligase destabilises nucleosomes, facilitating the release of DDB2/XPE and may also enable NER proteins to access lesions (289, 290). In this context, BER stimulation at occluded DNA damage sites by ubiquitination could be increasing the accessibility of BER proteins to the lesions, and so increasing their activity (241). To examine this in more detail, we could study histone ubiquitination directly by using mononucleosome substrates in the *in vitro* BER assay and examining common histone ubiquitination sites (e.g. H2A K13, K15 or K119 and H2B K120) by western blotting. We could mutate specific residues in histones which form mononucleosomes such as a K to R to observe if there is any observed lack of stimulation of APE1 activity to incise the THF-site in THF-IN which would show that if this site specific ubiquitination is required.

There is evidence for nucleosome unwrapping during DNA repair, particularly during NER and DSB repair. A study has shown that UV photoproducts enhanced the unwrapping of the DNA from histones increasing the exposure of DNA lesions to NER proteins (291). To allow protein access to DSBs, it has been suggested that the p400 SWI/SNF ATPase and histone acetylation by Tip60 destabilises nucleosomes causing a reduction in nucleosome array packing causing a more open conformation (292). RAD51 nucleoprotein filament during HR has also been shown to cause the unwrapping of DNA from core histones through ATP-hydrolysis (293). Specifically related to BER it has been suggested, although not proven in detail, that the repair of 8-oxo-G lesions by OGG1 in BER is stimulated by SWI/SNF by either chromatin remodelling or sliding to allow for efficient repair (259). Another study analysing the same lesion in a dinucleosome found that removal of H1 by NAP-1 allowed for the complete remodelling of dinucleosomes by RSC for efficient removal of 8-oxo-G (252). FACT and RSC are also thought to act in concert to facilitate BER, their presence increased nucleosome mobility (sliding) to increase excision of DNA lesions. In this study nucleosome mobility was

measured using native PAGE to measure centrally and end-positioned nucleosomes (241). Therefore it would be interesting to use a similar approach to examine whether there is any nucleosome sliding in our experimental system utilising THF-IN and HeLa WCE.

6.4 HECTD1 and YBX3 are possible candidates for chromatin modelling activity to facilitate BER

Since I discovered that the activity of APE1 in HeLa WCE towards the THF-IN mononucleosome substrate was being stimulated by ubiquitination, I began the search for an E3 ubiquitin ligase capable of performing this role. Initially, an siRNA screening approach was utilised whereby eleven E3 ubiquitin ligase enzymes known to catalyse histone ubiquitination were individually depleted in HeLa cells and WCE prepared. These WCE were then analysed in the presence of ubiquitination and poly(ADP-ribosyl)ation stimulating factors for their ability to efficiently process THF-IN. Predictably, depletion of the specific E3 ubiquitin ligase for this substrate would reduce the ability of APE1 to incise THF-IN, however this candidate approach showed no difference in THF-IN incision by APE1. This could mean either two results. Either these specific E3 ubiquitin ligases are not implicated in chromatin remodelling of THF-IN and necessary for APE1 activity, or that there are many overlapping activities to compensate for the lack of one of these enzymes. Therefore a different strategy was employed using a fractionation approach that has been successfully utilised on a number of occasions to identify E3 ubiquitin ligases that regulate cellular levels of BER enzymes in this laboratory (267, 272, 282, 283). However, for the first time, this approach was used in combination with mononucleosomes and the BER *in vitro* assay. Therefore proteins from HeLa WCE were sequentially fractionated over four separate chromatography columns, and after each fractionation step, fractions were individually analysed using the BER *in vitro* assay incorporating THF-IN to identify activities stimulating the basal activity of recombinant APE1 only (which was added to all fractions). As in the siRNA screening above, factors supporting ubiquitination and poly(ADP-ribosyl)ation were added in order to maximise THF-IN incision. The PC150 fraction, containing largely non-DNA binding proteins, was able to increase the basal level of incision activity of recombinant APE1 against the THF-IN mononucleosome using the BER *in vitro* assay. The PC150 fraction was further fractionated by ion-exchange chromatography which identified three separate activities stimulating APE1 incision of THF-IN, above the basal level of recombinant APE1 only. These three activities were individually purified over two further chromatography columns (gel filtration and ion exchange) again to identify active fractions towards THF-IN. Following completion of this process, mass spectrometry analysis of the most active fraction from each of the purifications the last stage of the fractionation was performed and a list of proteins present were generated. Since activity of APE1 in HeLa WCE towards THF-IN was largely ubiquitin-dependent, we particularly focussed on known E3 ubiquitin ligases with high mascot scores present in the respective activities. Active fractions were then probed by Western blotting using antibodies against the

candidate proteins, to examine their alignment with the activity profiles for each of the fractionation stages. The E3 ubiquitin ligase scaffold proteins CUL4A and DDB1 showed some degree of alignment to the activity profiles of APE1 activity towards THF-IN from activity 2. However, it was discovered that the stimulatory activity of APE1 towards THF-IN using purified fractions from this activity was actually not dependent on the presence of ubiquitination factors, suggesting another mechanism was taking place to make THF-IN more accessible. At this point, this particular activity was not followed any further. The E3 ubiquitin ligase HECTD1 showed a strong alignment to activity 1 profiles for each fractionation step, and furthermore the most active fraction from the final chromatography step was found to be dependent on ubiquitination factors in simulating APE1 activity towards the THF-IN mononucleosome. The mass spectrometry results for activity three did not identify any E3 ligases. However, Y-Box proteins YBX1 and YBX3 were found to be in high abundance and the proteins aligned to some degree to the activity 3 profiles of APE1 stimulatory activity in all chromatography steps. Surprisingly, this activity was also found to be dependent on ubiquitination, although YBX1 and YBX3 have no known E3 ligase activity.

HECTD1, YBX1 and YBX3 proteins were therefore examined further for their effect on cellular survival and DNA damage repair kinetics using clonogenic assays and alkaline comet assays, respectively. If these proteins were stimulating APE1 accessibility to AP sites by histone modifications and/or chromatin remodelling, it can be expected that cells would not be able to repair particularly sterically occluded DNA damage sites, and that their persistence may cause sensitivity to DNA damaging agents. These proteins were therefore depleted using siRNA in HeLa cells but also in normal lung fibroblasts (AG06173). An siRNA knockdown of either HECTD1 and YBX3 (but not YBX1) in normal lung fibroblasts caused a significant delay in the repair of SSB and alkali-labile sites following ionising radiation. Interestingly in HeLa cells, a lack of HECTD1 and YBX3 only caused a significant difference in the levels of SSB and alkali labile sites at later time points post-irradiation compared to the control. I also demonstrated that siRNA knockdown of HECTD1, and more so YBX3, caused reduced survival of HeLa cells following IR treatment, whereas YBX1 knockdown however had no effect on cell survival following IR. Whilst the observed differences in responses between cancer cells and normal cells are interesting but require further investigation, but indicates that there are either AP sites being formed directly, or formed during the processing of damaged DNA bases, that are persistent in cells that don't contain HECTD1 or YBX3. However whether there are still residual damaged DNA bases in more sterically occluded sites within the chromatin that haven't been processed at the later time points, and which are not revealed by the alkaline comet assay, is at this stage unknown. This could be investigated using enzyme modified comet assays, whereby following cell lysis, the DNA is treated with recombinant DNA repair enzymes that incises any residual DNA damage thus creating additional strand breaks that can be observed following electrophoresis. Consequently, our data would suggest that HECTD1 and YBX3 play an important role in the cellular response to DNA damage following

IR induced DNA damage, through modulating the efficiency of BER. I predict that these proteins play a role in catalysing BER through histone ubiquitination and chromatin remodelling causing sterically occluded sites to become more assessable to BER proteins to facilitate efficient DNA damage repair.

YBX1 and YBX3 are Y-box proteins of the cold shock family which are involved in transcriptional and translational control. They are predominantly located in the cytoplasm, but are expected to localise to the nucleus due to their role in transcription. YBX1 has been the most extensively studied and has been found to be involved in the transcription of several important genes involved in tumour development (294, 295). YBX1 has also been found to protect cells against DNA damaging agents and may have an additional function in DNA repair as its truncated form complexes with the MRN complex proteins Mre11 and RAD50 following genotoxic stress (296). APE1 specifically has been shown to stably interact with YBX1 to increase drug resistance via the regulatory function of acetylated APE1 causing multidrug resistance gene (MDR1)-mediated drug resistance. YBX1 has also been shown inhibit AP site incision by NEIL1 and APE1 on single stranded DNA, suggesting YBX1 has a direct interaction with AP sites (297, 298). The association of YBX1 with APE1, NEIL1 and DNA repair suggests that it may be a promising candidate in facilitating APE1 activity towards the THF-IN mononucleosome. However, I observed that a YBX1 knockdown did not affect cell survival following IR, which would appear to suggest that YBX1 is not involved in increasing accessibility to AP sites by histone modifications and/or chromatin remodelling. Nevertheless, the role of YBX1 in BER does require further experimentation.

YBX3 has been shown to be a repressor of some growth factors promoter, such as the GM PSF promoter and is important for metazoan development and fertility (294, 299). I propose that YBX3 is either directly or indirectly affecting the accessibility of BER proteins to occluded DNA lesions processed by BER. YBX3 knockdown sensitised cells to IR and delayed repair kinetics suggesting its involvement in facilitating BER through histone modifications and/or chromatin remodelling. YBX3 has no known E3 ubiquitin ligase activity so it is unlikely that YBX3 is ubiquitinating histones alone, but as it is a known transcription factor, it may be upregulating the expression of an unknown E3 ubiquitin ligase. YBX3 could also be a novel chromatin remodeller, binding to DNA associated with the nucleosome and increasing AP site accessibility to APE1. Therefore further studies to establish the impact of YBX3 on mononucleosome structure and function during BER are necessary.

The E3 ubiquitin ligase HECTD1 has not been associated with any DNA repair pathway in published studies and doesn't appear to be extensively studied. HECTD1 is required for the development of head mesenchyme and neural tube closure and is involved in the polyubiquitination of adenomatous polyposis coli (APC) to promote APC-Axin interaction to down regulate the Wnt signalling pathway (300, 301). As an active E3 ubiquitin ligase, I now

propose that HECTD1 may also ubiquitinate histones required for increasing accessibility of DNA base damage during BER. As HECTD1 knockdown both increased cell sensitivity towards IR and delayed repair kinetics this makes it a promising candidate for involvement in increasing the accessibility of AP sites to APE1, and possibly other BER lesions which have not been analysed. If HECTD1 is ubiquitinating histones directly, then this change itself may influence histone-histone and/or histone-DNA interactions, making occluded sites more accessible. It is also conceivable that HECTD1 may be in association with a chromatin remodeller, and therefore ubiquitination of histones could be allowing binding and stimulating activity of a chromatin remodeller. However, a chromatin remodeller was not identified in active protein fractions purified from HeLa extracts by mass spectrometry.

It is important to highlight that HECTD1 is frequently mutated, deleted and amplified in a wide range of cancers. For example it is commonly mutated in prostate cancer, bladder cancer and small lung cell carcinoma and amplified in lung adenocarcinoma. YBX3 is also mutated, deleted and amplified in a range of cancers, including lung adenocarcinoma and ovarian cancers. This suggests that both HECTD1 and YBX3 are important for genome stability and thus in the prevention of disease, and I now predict that this could be through controlling BER. Whilst there is obviously a large amount of research which needs to be completed to support our work, this also further supports the advantage of targeting HECTD1 and YBX3 as a therapy for cancer treatment in conjunction with IR (302, 303).

6.5 Future Work

The identification of HECTD1 and YBX3 as candidates for histone modifiers and chromatin remodellers to facilitate BER at occluded base damage sites needs further confirmation but also that the precise mechanism that they achieve this is currently unknown. In order to validate this observation, HECTD1 and YBX3 could be overexpressed and purified from *E.coli* and then the proteins examined in the *in vitro* BER assay with the THF-IN substrate to confirm that they are able to stimulate incision by APE1. It would be interesting to see whether these proteins, or active fractions containing these two proteins, also affected incision of THF-OUT by APE1. We would expect that the incision of the site would remain similar as histone modification or chromatin remodelling activity at this site is not needed for effective APE1 activity. If processing of this site by APE1 increased then this may suggest that these proteins were increasing activity another way, possibly through altered regulation of APE1, but may also indicate that these proteins may have an impact on APE1 activity globally throughout the genome. However this would seem unlikely based on the observed lack of difference of HeLa WCE with and without the ubiquitination and poly(ADP-ribosyl)ation supporting factors have on APE1 activity on THF-OUT. I have further shown that knockdown of HECTD1 and YBX3 delays IR-induced DNA damage repair kinetics in HeLa and AG06173 cells, presumably through decreased processing of occluded DNA damage sites, and also lead to increased

radiosensitivity of HeLa cells. It would be interesting to establish if these proteins when overexpressed in cells cause the opposite effect by increasing DNA damage repair kinetics and increasing resistance to IR, which would further validate their role in modulating BER in cultured cells. Therefore HECTD1 and YBX3 require cloning into mammalian expression plasmids in order to be able to achieve these experiments. As an extension of these experiments, it would be interesting to examine by immunofluorescence microscopy whether HECTD1 and YBX3 localise to the nucleus following IR- induced DNA damage, as these proteins are thought to reside in the cytoplasm, and potentially whether they form discrete foci in the nucleus would be an indicator that they were interacting with DNA damage sites in histones.

The mechanism in which HECTD1 and YBX3 are functioning needs to be identified. As indicated above, recombinant HECTD1 and YBX3 could be overexpressed in *E.Coli* and then added to the BER *in vitro* assays with THF-IN to confirm increased activity of recombinant APE1 on this site, but also the histones themselves could be examined in detail. Firstly the histones could be extracted and then analysed by Western blotting to determine whether they are ubiquitinated directly, particularly by HECTD1. This could be achieved by either using antibodies against specific histone ubiquitination sites (eg. H2B lysine 120, H2A lysine K13, K15, 119) or by using antibodies against the unmodified histones and examining whether there is any protein shift (eg. 8 kDa) equivalent to ubiquitination. Secondly, and as highlighted above, a recent study has looked at nucleosome mobilisation efficiency to quantify nucleosome sliding (241). It would therefore also be interesting to see if these two candidate proteins, YBX3 and HECTD1, in active fractions or as purified proteins are able to induce nucleosome sliding as determined by gel analysis which is then providing increased accessibility of recombinant APE1 to THF-IN. If recombinant HECTD1 and YBX3 are unable to recapitulate our findings of stimulating APE1 to THF-IN *in vitro*, then further investigations into these proteins will have to be undertaken. It is possible that these proteins may require post-translational modifications or accessory proteins for histone modification and/or chromatin remodelling activity. If this is the case, then the proteins could be overexpressed and purified from cultured human cells (or insect cells) and then their activity re-examined, but also the interactions of these with other cellular proteins could be determined by mass spectrometry analysis. One final point to examine is the possible specificity of HECTD1 and YBX3 for stimulating BER *in vitro*. Whilst I have demonstrated that active fractions containing these proteins stimulate APE1 activity on a THF site, it would be interesting to test whether this is similarly observed using other BER substrate and protein combinations. For example, the activity of specific DNA glycosylases on DNA base damage (eg. OGG1 on 8-oxoG; NTH1 on thymine glycol), Pol β activity on a single nucleotide gap, and XRCC1-Lig III α activity on a nicked mononucleosome substrate could be determined.

6.6 Concluding remarks

A method was successfully developed and established to produce mononucleosome substrates with differently orientated THF sites. I demonstrated that recombinant APE1 activity is significantly impeded to the THF site in THF-IN, but efficiently processed the THF-OUT, but that APE1 in HeLa WCE with factors supporting ubiquitination and poly(ADP-ribosyl)ation was able to efficiently process the THF site in both THF-IN and THF-OUT. Using a fractionation approach, I discovered three novel activities to stimulate THF incision of THF-IN through what we predicted to be a histone modification and/or chromatin remodelling event. Two candidate proteins, HECTD1 and YBX3, were identified in these activity fractions by mass spectrometry and further shown to control cellular DNA damage repair kinetics and cell survival following ionising radiation. Collectively, the data presented in this thesis strongly suggest that HECTD1 and YBX3 are novel proteins which are important for facilitating BER by altering chromatin structure to make occluded site more accessible. This work provides a solid foundation for further analysis of the roles of HECTD1 and YBX3 in BER, but also once validated, these proteins could potentially be novel targets for drugs or small molecule inhibitors that can be used to increase cancer cell sensitivity to IR. HECTD1 is frequently mutated in prostate cancer, bladder cancer and small lung cell carcinoma and amplified in several others, for example lung adenocarcinoma. YBX3 is also mutated, deleted and amplified in a range of cancers such as lung adenocarcinoma and ovarian cancers. Therefore targeting HECTD1 and YBX3, in the future, may provide a novel mode of therapy for cancer treatment in conjunction with IR.

References

1. Watson JD, Crick FH. Molecular structure of nucleic acids; a structure for deoxyribose nucleic acid. *Nature*. 1953;171(4356):737-8.
2. Pray LA. Discovery of DNA Structure and Function: Watson and Crick. *Nature Education*. 2008;1(1):100.
3. Hoeijmakers JHJ. DNA Damage, Aging, and Cancer. *New England Journal of Medicine*. 2009;361(15):1475-85.
4. Lindahl T. Instability and decay of the primary structure of DNA. *Nature*. 1993;362(6422):709-15.
5. Wilson DM, 3rd, Bohr VA. The mechanics of base excision repair, and its relationship to aging and disease. *DNA Repair (Amst)*. 2007;6(4):544-59.
6. Maynard S, Schurman SH, Harboe C, de Souza-Pinto NC, Bohr VA. Base excision repair of oxidative DNA damage and association with cancer and aging. *Carcinogenesis*. 2009;30(1):2-10.
7. De Bont R, van Larebeke N. Endogenous DNA damage in humans: a review of quantitative data. *Mutagenesis*. 2004;19(3):169-85.
8. Tudek B, Winczura A, Janik J, Siomek A, Foksinski M, Olinski R. Involvement of oxidatively damaged DNA and repair in cancer development and aging. *Am J Transl Res*. 2010;2(3):254-84.
9. McCulloch SD, Kunkel TA. The fidelity of DNA synthesis by eukaryotic replicative and translesion synthesis polymerases. *Cell Res*. 2008;18(1):148-61.
10. Sugiyama H, Fujiwara T, Ura A, Tashiro T, Yamamoto K, Kawanishi S, et al. Chemistry of thermal degradation of abasic sites in DNA. Mechanistic investigation on thermal DNA strand cleavage of alkylated DNA. *Chem Res Toxicol*. 1994;7(5):673-83.
11. Lawrence CW, Borden A, Banerjee SK, LeClerc JE. Mutation frequency and spectrum resulting from a single abasic site in a single-stranded vector. *Nucleic Acids Res*. 1990;18(8):2153-7.
12. Yonekura S, Nakamura N, Yonei S, Zhang-Akiyama QM. Generation, biological consequences and repair mechanisms of cytosine deamination in DNA. *J Radiat Res*. 2009;50(1):19-26.
13. Jackson AL, Chen R, Loeb LA. Induction of microsatellite instability by oxidative DNA damage. *Proc Natl Acad Sci U S A*. 1998;95(21):12468-73.
14. Cooper DN, Youssoufian H. The CpG dinucleotide and human genetic disease. *Hum Genet*. 1988;78(2):151-5.
15. Seeberg E, Eide L, Bjoras M. The base excision repair pathway. *Trends Biochem Sci*. 1995;20(10):391-7.
16. Odell ID, Wallace SS, Pederson DS. Rules of engagement for base excision repair in chromatin. *J Cell Physiol*. 2013;228(2):258-66.
17. Cadet J, Berger M, Douki T, Ravanat JL. Oxidative damage to DNA: formation, measurement, and biological significance. *Rev Physiol Biochem Pharmacol*. 1997;131:1-87.
18. Roszkowski K, Jozwicki W, Blaszczyk P, Mucha-Malecka A, Siomek A. Oxidative damage DNA: 8-oxoGua and 8-oxodG as molecular markers of cancer. *Med Sci Monit*. 2011;17(6):CR329-33.
19. Burney S, Caulfield JL, Niles JC, Wishnok JS, Tannenbaum SR. The chemistry of DNA damage from nitric oxide and peroxynitrite. *Mutat Res*. 1999;424(1-2):37-49.
20. Major GN, Collier JD. Repair of DNA lesion O6-methylguanine in hepatocellular carcinogenesis. *J Hepatobiliary Pancreat Surg*. 1998;5(4):355-66.

21. Parsons JL, Nicolay NH, Sharma RA. Biological and therapeutic relevance of nonreplicative DNA polymerases to cancer. *Antioxid Redox Signal*. 2013;18(8):851-73.
22. Brown JA, Pack LR, Sanman LE, Suo Z. Efficiency and fidelity of human DNA polymerases lambda and beta during gap-filling DNA synthesis. *DNA Repair (Amst)*. 2011;10(1):24-33.
23. Shimizu M, Gruz P, Kamiya H, Kim SR, Pisani FM, Masutani C, et al. Erroneous incorporation of oxidized DNA precursors by Y-family DNA polymerases. *EMBO Rep*. 2003;4(3):269-73.
24. McClendon AK, Osheroff N. DNA topoisomerase II, genotoxicity, and cancer. *Mutat Res*. 2007;623(1-2):83-97.
25. Rodgers K, McVey M. Error-Prone Repair of DNA Double-Strand Breaks. *J Cell Physiol*. 2016;231(1):15-24.
26. Helleday T, Eshtad S, Nik-Zainal S. Mechanisms underlying mutational signatures in human cancers. *Nat Rev Genet*. 2014;15(9):585-98.
27. Gupta RC, Lutz WK. Background DNA damage for endogenous and unavoidable exogenous carcinogens: a basis for spontaneous cancer incidence? *Mutat Res*. 1999;424(1-2):1-8.
28. Ravanat JL, Douki T, Cadet J. Direct and indirect effects of UV radiation on DNA and its components. *J Photochem Photobiol B*. 2001;63(1-3):88-102.
29. Rastogi RP, Richa, Kumar A, Tyagi MB, Sinha RP. Molecular mechanisms of ultraviolet radiation-induced DNA damage and repair. *J Nucleic Acids*. 2010;2010:592980.
30. Sinha RP, Hader DP. UV-induced DNA damage and repair: a review. *Photochem Photobiol Sci*. 2002;1(4):225-36.
31. Ward JF. DNA damage produced by ionizing radiation in mammalian cells: identities, mechanisms of formation, and reparability. *Prog Nucleic Acid Res Mol Biol*. 1988;35:95-125.
32. Santivasi WL, Xia F. Ionizing radiation-induced DNA damage, response, and repair. *Antioxid Redox Signal*. 2014;21(2):251-9.
33. Lomax ME, Folkes LK, O'Neill P. Biological consequences of radiation-induced DNA damage: relevance to radiotherapy. *Clin Oncol (R Coll Radiol)*. 2013;25(10):578-85.
34. Cadet J, Douki T, Ravanat JL. Oxidatively generated damage to the guanine moiety of DNA: mechanistic aspects and formation in cells. *Acc Chem Res*. 2008;41(8):1075-83.
35. Fu D, Calvo JA, Samson LD. Balancing repair and tolerance of DNA damage caused by alkylating agents. *Nat Rev Cancer*. 2012;12(2):104-20.
36. Drablos F, Feyzi E, Aas PA, Vaagbo CB, Kavli B, Bratlie MS, et al. Alkylation damage in DNA and RNA--repair mechanisms and medical significance. *DNA Repair (Amst)*. 2004;3(11):1389-407.
37. Johnson RE, Yu SL, Prakash S, Prakash L. A role for yeast and human translesion synthesis DNA polymerases in promoting replication through 3-methyl adenine. *Mol Cell Biol*. 2007;27(20):7198-205.
38. Noll DM, Mason TM, Miller PS. Formation and repair of interstrand cross-links in DNA. *Chem Rev*. 2006;106(2):277-301.
39. Khanna KK, Jackson SP. DNA double-strand breaks: signaling, repair and the cancer connection. *Nat Genet*. 2001;27(3):247-54.
40. Jackson SP. Sensing and repairing DNA double-strand breaks. *Carcinogenesis*. 2002;23(5):687-96.
41. Lorat Y, Timm S, Jakob B, Taucher-Scholz G, Rube CE. Clustered double-strand breaks in heterochromatin perturb DNA repair after high linear energy transfer irradiation. *Radiother Oncol*. 2016;121(1):154-61.
42. Caldecott KW. Single-strand break repair and genetic disease. *Nat Rev Genet*. 2008;9(8):619-31.

43. Lindahl T, Nyberg B. Rate of depurination of native deoxyribonucleic acid. *Biochemistry*. 1972;11(19):3610-8.
44. Boiteux S, Guillet M. Abasic sites in DNA: repair and biological consequences in *Saccharomyces cerevisiae*. *DNA Repair (Amst)*. 2004;3(1):1-12.
45. Cheng KC, Cahill DS, Kasai H, Nishimura S, Loeb LA. 8-Hydroxyguanine, an abundant form of oxidative DNA damage, causes G----T and A----C substitutions. *J Biol Chem*. 1992;267(1):166-72.
46. Dolinnaya NG, Kubareva EA, Romanova EA, Trikin RM, Oretskaya TS. Thymidine glycol: the effect on DNA molecular structure and enzymatic processing. *Biochimie*. 2013;95(2):134-47.
47. Wyman C, Kanaar R. DNA double-strand break repair: all's well that ends well. *Annu Rev Genet*. 2006;40:363-83.
48. Symington LS, Gautier J. Double-strand break end resection and repair pathway choice. *Annu Rev Genet*. 2011;45:247-71.
49. Dudas A, Chovanec M. DNA double-strand break repair by homologous recombination. *Mutat Res*. 2004;566(2):131-67.
50. Li X, Heyer WD. Homologous recombination in DNA repair and DNA damage tolerance. *Cell Res*. 2008;18(1):99-113.
51. Yu Z, Chen J, Ford BN, Brackley ME, Glickman BW. Human DNA repair systems: an overview. *Environ Mol Mutagen*. 1999;33(1):3-20.
52. Davis AJ, Chen DJ. DNA double strand break repair via non-homologous end-joining. *Transl Cancer Res*. 2013;2(3):130-43.
53. Weterings E, Chen DJ. The endless tale of non-homologous end-joining. *Cell Res*. 2008;18(1):114-24.
54. Marteijn JA, Lans H, Vermeulen W, Hoeijmakers JH. Understanding nucleotide excision repair and its roles in cancer and ageing. *Nat Rev Mol Cell Biol*. 2014;15(7):465-81.
55. Scharer OD. Nucleotide excision repair in eukaryotes. *Cold Spring Harb Perspect Biol*. 2013;5(10):a012609.
56. Spivak G. Nucleotide excision repair in humans. *DNA Repair (Amst)*. 2015;36:13-8.
57. de Boer J, Hoeijmakers JH. Nucleotide excision repair and human syndromes. *Carcinogenesis*. 2000;21(3):453-60.
58. Kim YJ, Wilson DM, 3rd. Overview of base excision repair biochemistry. *Curr Mol Pharmacol*. 2012;5(1):3-13.
59. Parsons JL, Dianov GL. Co-ordination of base excision repair and genome stability. *DNA Repair (Amst)*. 2013;12(5):326-33.
60. Wallace SS. Base excision repair: a critical player in many games. *DNA Repair (Amst)*. 2014;19:14-26.
61. Krokan HE, Bjoras M. Base excision repair. *Cold Spring Harb Perspect Biol*. 2013;5(4):a012583.
62. Parsons JL, Edmonds MJ. The Base Excision Repair Pathway. *Encyclopedia of Cell Biology*. Waltham: Academic Press; 2016. p. 442-50.
63. Wilson DM, 3rd, Barsky D. The major human abasic endonuclease: formation, consequences and repair of abasic lesions in DNA. *Mutat Res*. 2001;485(4):283-307.
64. Mol CD, Izumi T, Mitra S, Tainer JA. DNA-bound structures and mutants reveal abasic DNA binding by APE1 and DNA repair coordination [corrected]. *Nature*. 2000;403(6768):451-6.
65. Gorman MA, Morera S, Rothwell DG, de La Fortelle E, Mol CD, Tainer JA, et al. The crystal structure of the human DNA repair endonuclease HAP1 suggests the recognition of extra-helical deoxyribose at DNA abasic sites. *EMBO J*. 1997;16(21):6548-58.
66. Chou KM, Cheng YC. An exonucleolytic activity of human apurinic/apyrimidinic endonuclease on 3' mispaired DNA. *Nature*. 2002;415(6872):655-9.

67. Lavrik OI, Prasad R, Sobol RW, Horton JK, Ackerman EJ, Wilson SH. Photoaffinity labeling of mouse fibroblast enzymes by a base excision repair intermediate. Evidence for the role of poly(ADP-ribose) polymerase-1 in DNA repair. *J Biol Chem.* 2001;276(27):25541-8.
68. Parsons JL, Dianova, II, Allinson SL, Dianov GL. Poly(ADP-ribose) polymerase-1 protects excessive DNA strand breaks from deterioration during repair in human cell extracts. *FEBS J.* 2005;272(8):2012-21.
69. Brem R, Hall J. XRCC1 is required for DNA single-strand break repair in human cells. *Nucleic Acids Res.* 2005;33(8):2512-20.
70. Dianov GL, Parsons JL. Co-ordination of DNA single strand break repair. *DNA Repair (Amst).* 2007;6(4):454-60.
71. Parsons JL, Dianova, II, Dianov GL. APE1 is the major 3'-phosphoglycolate activity in human cell extracts. *Nucleic Acids Res.* 2004;32(12):3531-6.
72. Wilson DM, 3rd. Processing of nonconventional DNA strand break ends. *Environ Mol Mutagen.* 2007;48(9):772-82.
73. Beard WA, Prasad R, Wilson SH. Activities and mechanism of DNA polymerase beta. *Methods Enzymol.* 2006;408:91-107.
74. Bebenek K, Tissier A, Frank EG, McDonald JP, Prasad R, Wilson SH, et al. 5'-Deoxyribose phosphate lyase activity of human DNA polymerase iota in vitro. *Science.* 2001;291(5511):2156-9.
75. Bernstein NK, Williams RS, Rakovszky ML, Cui D, Green R, Karimi-Busheri F, et al. The molecular architecture of the mammalian DNA repair enzyme, polynucleotide kinase. *Mol Cell.* 2005;17(5):657-70.
76. Loeb LA, Monnat RJ, Jr. DNA polymerases and human disease. *Nat Rev Genet.* 2008;9(8):594-604.
77. Chan KK, Zhang QM, Dianov GL. Base excision repair fidelity in normal and cancer cells. *Mutagenesis.* 2006;21(3):173-8.
78. Pelletier H, Sawaya MR, Wolfle W, Wilson SH, Kraut J. Crystal structures of human DNA polymerase beta complexed with DNA: implications for catalytic mechanism, processivity, and fidelity. *Biochemistry.* 1996;35(39):12742-61.
79. Dantzer F, de La Rubia G, Menissier-De Murcia J, Hostomsky Z, de Murcia G, Schreiber V. Base excision repair is impaired in mammalian cells lacking Poly(ADP-ribose) polymerase-1. *Biochemistry.* 2000;39(25):7559-69.
80. Bennett RA, Wilson DM, 3rd, Wong D, Demple B. Interaction of human apurinic endonuclease and DNA polymerase beta in the base excision repair pathway. *Proc Natl Acad Sci U S A.* 1997;94(14):7166-9.
81. Braithwaite EK, Prasad R, Shock DD, Hou EW, Beard WA, Wilson SH. DNA polymerase lambda mediates a back-up base excision repair activity in extracts of mouse embryonic fibroblasts. *J Biol Chem.* 2005;280(18):18469-75.
82. Podlutzky AJ, Dianova, II, Podust VN, Bohr VA, Dianov GL. Human DNA polymerase beta initiates DNA synthesis during long-patch repair of reduced AP sites in DNA. *EMBO J.* 2001;20(6):1477-82.
83. Sung JS, Demple B. Roles of base excision repair subpathways in correcting oxidized abasic sites in DNA. *FEBS J.* 2006;273(8):1620-9.
84. Petermann E, Ziegler M, Oei SL. ATP-dependent selection between single nucleotide and long patch base excision repair. *DNA Repair (Amst).* 2003;2(10):1101-14.
85. Storici F, Henneke G, Ferrari E, Gordenin DA, Hubscher U, Resnick MA. The flexible loop of human FEN1 endonuclease is required for flap cleavage during DNA replication and repair. *EMBO J.* 2002;21(21):5930-42.

86. Haracska L, Prakash L, Prakash S. A mechanism for the exclusion of low-fidelity human Y-family DNA polymerases from base excision repair. *Genes Dev.* 2003;17(22):2777-85.
87. Tomkinson AE, Vijayakumar S, Pascal JM, Ellenberger T. DNA ligases: structure, reaction mechanism, and function. *Chem Rev.* 2006;106(2):687-99.
88. Cappelli E, Taylor R, Cevasco M, Abbondandolo A, Caldecott K, Frosina G. Involvement of XRCC1 and DNA ligase III gene products in DNA base excision repair. *J Biol Chem.* 1997;272(38):23970-5.
89. Caldecott KW, Tucker JD, Stanker LH, Thompson LH. Characterization of the XRCC1-DNA ligase III complex in vitro and its absence from mutant hamster cells. *Nucleic Acids Res.* 1995;23(23):4836-43.
90. Caldecott KW, McKeown CK, Tucker JD, Ljungquist S, Thompson LH. An interaction between the mammalian DNA repair protein XRCC1 and DNA ligase III. *Mol Cell Biol.* 1994;14(1):68-76.
91. Caldecott KW. Mammalian DNA single-strand break repair: an X-ra(y)ted affair. *Bioessays.* 2001;23(5):447-55.
92. Parsons JL, Dianova, II, Allinson SL, Dianov GL. DNA polymerase beta promotes recruitment of DNA ligase III alpha-XRCC1 to sites of base excision repair. *Biochemistry.* 2005;44(31):10613-9.
93. Caldecott KW, Aoufouchi S, Johnson P, Shall S. XRCC1 polypeptide interacts with DNA polymerase beta and possibly poly (ADP-ribose) polymerase, and DNA ligase III is a novel molecular 'nick-sensor' in vitro. *Nucleic Acids Res.* 1996;24(22):4387-94.
94. Dianova, II, Sleeth KM, Allinson SL, Parsons JL, Breslin C, Caldecott KW, et al. XRCC1-DNA polymerase beta interaction is required for efficient base excision repair. *Nucleic Acids Res.* 2004;32(8):2550-5.
95. Vascotto C, Fishel ML. Chapter 3 - Blockade of Base Excision Repair: Inhibition of Small Lesions Results in Big Consequences to Cancer Cells A2 - Kelley, Mark R. *DNA Repair in Cancer Therapy.* San Diego: Academic Press; 2012. p. 29-53.
96. Dianov GL. Base excision repair targets for cancer therapy. *Am J Cancer Res.* 2011;1(7):845-51.
97. Paz-Elizur T, Sevilya Z, Leitner-Dagan Y, Elinger D, Roisman LC, Livneh Z. DNA repair of oxidative DNA damage in human carcinogenesis: potential application for cancer risk assessment and prevention. *Cancer Lett.* 2008;266(1):60-72.
98. Nemec AA, Wallace SS, Sweasy JB. Variant base excision repair proteins: contributors to genomic instability. *Semin Cancer Biol.* 2010;20(5):320-8.
99. Wallace SS, Murphy DL, Sweasy JB. Base excision repair and cancer. *Cancer Lett.* 2012;327(1-2):73-89.
100. Starcevic D, Dalal S, Sweasy JB. Is there a link between DNA polymerase beta and cancer? *Cell cycle (Georgetown, Tex).* 2004;3(8):998-1001.
101. Kumar A, Pant MC, Singh HS, Khandelwal S. Reduced expression of DNA repair genes (XRCC1, XPD, and OGG1) in squamous cell carcinoma of head and neck in North India. *Tumour Biol.* 2012;33(1):111-9.
102. Wen X, Lu R, Xie S, Zheng H, Wang H, Wang Y, et al. APE1 overexpression promotes the progression of ovarian cancer and serves as a potential therapeutic target. *Cancer Biomark.* 2016;17(3):313-22.
103. Ang MK, Patel MR, Yin XY, Sundaram S, Fritchie K, Zhao N, et al. High XRCC1 protein expression is associated with poorer survival in patients with head and neck squamous cell carcinoma. *Clin Cancer Res.* 2011;17(20):6542-52.
104. Albertella MR, Lau A, O'Connor MJ. The overexpression of specialized DNA polymerases in cancer. *DNA Repair (Amst).* 2005;4(5):583-93.

105. Price Brendan D, D'Andrea Alan D. Chromatin Remodeling at DNA Double-Strand Breaks. *Cell*. 2013;152(6):1344-54.
106. Luger K, Dechassa ML, Tremethick DJ. New insights into nucleosome and chromatin structure: an ordered state or a disordered affair? *Nat Rev Mol Cell Biol*. 2012;13(7):436-47.
107. Soria G, Polo SE, Almouzni G. Prime, repair, restore: the active role of chromatin in the DNA damage response. *Mol Cell*. 2012;46(6):722-34.
108. Cruickshank MN, Besant P, Ulgiati D. The impact of histone post-translational modifications on developmental gene regulation. *Amino Acids*. 2010;39(5):1087-105.
109. Luger K, Mader AW, Richmond RK, Sargent DF, Richmond TJ. Crystal structure of the nucleosome core particle at 2.8 Å resolution. *Nature*. 1997;389(6648):251-60.
110. Smith S, Stillman B. Stepwise assembly of chromatin during DNA replication in vitro. *EMBO J*. 1991;10(4):971-80.
111. Kulaeva OI, Hsieh FK, Studitsky VM. RNA polymerase complexes cooperate to relieve the nucleosomal barrier and evict histones. *Proc Natl Acad Sci U S A*. 2010;107(25):11325-30.
112. Jonkers I, Lis JT. Getting up to speed with transcription elongation by RNA polymerase II. *Nat Rev Mol Cell Biol*. 2015;16(3):167-77.
113. Ahmad K, Henikoff S. The histone variant H3.3 marks active chromatin by replication-independent nucleosome assembly. *Mol Cell*. 2002;9(6):1191-200.
114. Weber CM, Henikoff S. Histone variants: dynamic punctuation in transcription. *Genes Dev*. 2014;28(7):672-82.
115. Tagami H, Ray-Gallet D, Almouzni G, Nakatani Y. Histone H3.1 and H3.3 complexes mediate nucleosome assembly pathways dependent or independent of DNA synthesis. *Cell*. 2004;116(1):51-61.
116. Stoler S, Keith KC, Curnick KE, Fitzgerald-Hayes M. A mutation in CSE4, an essential gene encoding a novel chromatin-associated protein in yeast, causes chromosome nondisjunction and cell cycle arrest at mitosis. *Genes Dev*. 1995;9(5):573-86.
117. Henikoff S, Furuyama T, Ahmad K. Histone variants, nucleosome assembly and epigenetic inheritance. *Trends Genet*. 2004;20(7):320-6.
118. Tachiwana H, Osakabe A, Shiga T, Miya Y, Kimura H, Kagawa W, et al. Structures of human nucleosomes containing major histone H3 variants. *Acta Crystallogr D Biol Crystallogr*. 2011;67(Pt 6):578-83.
119. Liu CP, Xiong C, Wang M, Yu Z, Yang N, Chen P, et al. Structure of the variant histone H3.3-H4 heterodimer in complex with its chaperone DAXX. *Nature structural & molecular biology*. 2012;19(12):1287-92.
120. Mito Y, Henikoff JG, Henikoff S. Genome-scale profiling of histone H3.3 replacement patterns. *Nat Genet*. 2005;37(10):1090-7.
121. Wirbelauer C, Bell O, Schubeler D. Variant histone H3.3 is deposited at sites of nucleosomal displacement throughout transcribed genes while active histone modifications show a promoter-proximal bias. *Genes Dev*. 2005;19(15):1761-6.
122. Henikoff S. Nucleosome destabilization in the epigenetic regulation of gene expression. *Nat Rev Genet*. 2008;9(1):15-26.
123. Chow CM, Georgiou A, Szutorisz H, Maia e Silva A, Pombo A, Barahona I, et al. Variant histone H3.3 marks promoters of transcriptionally active genes during mammalian cell division. *EMBO Rep*. 2005;6(4):354-60.
124. Talbert PB, Henikoff S. Histone variants--ancient wrap artists of the epigenome. *Nat Rev Mol Cell Biol*. 2010;11(4):264-75.
125. Suto RK, Clarkson MJ, Tremethick DJ, Luger K. Crystal structure of a nucleosome core particle containing the variant histone H2A.Z. *Nat Struct Biol*. 2000;7(12):1121-4.
126. Meneghini MD, Wu M, Madhani HD. Conserved histone variant H2A.Z protects euchromatin from the ectopic spread of silent heterochromatin. *Cell*. 2003;112(5):725-36.

127. Andrews AJ, Luger K. Nucleosome structure(s) and stability: variations on a theme. *Annu Rev Biophys.* 2011;40:99-117.
128. van Holde KE. The Nucleosome. *Chromatin*. New York, NY: Springer New York; 1989. p. 219-88.
129. Polach KJ, Widom J. Mechanism of protein access to specific DNA sequences in chromatin: a dynamic equilibrium model for gene regulation. *J Mol Biol.* 1995;254(2):130-49.
130. Geraghty DS, Sucic HB, Chen J, Pederson DS. Evidence that partial unwrapping of DNA from nucleosomes facilitates the binding of heat shock factor following DNA replication in yeast. *The Journal of biological chemistry.* 1998;273(32):20463-72.
131. Li G, Widom J. Nucleosomes facilitate their own invasion. *Nature structural & molecular biology.* 2004;11(8):763-9.
132. Neumann H, Hancock SM, Buning R, Routh A, Chapman L, Somers J, et al. A method for genetically installing site-specific acetylation in recombinant histones defines the effects of H3 K56 acetylation. *Mol Cell.* 2009;36(1):153-63.
133. Poirier MG, Bussiek M, Langowski J, Widom J. Spontaneous access to DNA target sites in folded chromatin fibers. *J Mol Biol.* 2008;379(4):772-86.
134. Harshman SW, Young NL, Parthun MR, Freitas MA. H1 histones: current perspectives and challenges. *Nucleic Acids Res.* 2013;41(21):9593-609.
135. Li G, Reinberg D. Chromatin higher-order structures and gene regulation. *Current opinion in genetics & development.* 2011;21(2):175-86.
136. Khoury GA, Baliban RC, Floudas CA. Proteome-wide post-translational modification statistics: frequency analysis and curation of the swiss-prot database. *Sci Rep.* 2011;1.
137. North JA, Simon M, Ferdinand MB, Shoffner MA, Picking JW, Howard CJ, et al. Histone H3 phosphorylation near the nucleosome dyad alters chromatin structure. *Nucleic Acids Res.* 2014;42(8):4922-33.
138. Petruk S, Sedkov Y, Johnston DM, Hodgson JW, Black KL, Kovermann SK, et al. TrxG and PcG proteins but not methylated histones remain associated with DNA through replication. *Cell.* 2012;150(5):922-33.
139. Williams SK, Truong D, Tyler JK. Acetylation in the globular core of histone H3 on lysine-56 promotes chromatin disassembly during transcriptional activation. *Proc Natl Acad Sci U S A.* 2008;105(26):9000-5.
140. Lee JS, Shukla A, Schneider J, Swanson SK, Washburn MP, Florens L, et al. Histone crosstalk between H2B monoubiquitination and H3 methylation mediated by COMPASS. *Cell.* 2007;131(6):1084-96.
141. Venkatesh S, Smolle M, Li H, Gogol MM, Saint M, Kumar S, et al. Set2 methylation of histone H3 lysine 36 suppresses histone exchange on transcribed genes. *Nature.* 2012;489(7416):452-5.
142. Bannister AJ, Kouzarides T. Regulation of chromatin by histone modifications. *Cell Res.* 2011;21(3):381-95.
143. Rodriguez-Paredes M, Esteller M. Cancer epigenetics reaches mainstream oncology. *Nat Med.* 2011;17(3):330-9.
144. Ubersax JA, Ferrell JE, Jr. Mechanisms of specificity in protein phosphorylation. *Nat Rev Mol Cell Biol.* 2007;8(7):530-41.
145. Graff J, Tsai LH. Histone acetylation: molecular mnemonics on the chromatin. *Nat Rev Neurosci.* 2013;14(2):97-111.
146. Manohar M, Mooney AM, North JA, Nakkula RJ, Picking JW, Edon A, et al. Acetylation of histone H3 at the nucleosome dyad alters DNA-histone binding. *J Biol Chem.* 2009;284(35):23312-21.
147. Hasan S, Hottiger MO. Histone acetyl transferases: a role in DNA repair and DNA replication. *J Mol Med (Berl).* 2002;80(8):463-74.

148. Shilatifard A. Chromatin modifications by methylation and ubiquitination: implications in the regulation of gene expression. *Annu Rev Biochem.* 2006;75:243-69.
149. Weissman AM. Themes and variations on ubiquitylation. *Nat Rev Mol Cell Biol.* 2001;2(3):169-78.
150. Ye Y, Rape M. Building ubiquitin chains: E2 enzymes at work. *Nat Rev Mol Cell Biol.* 2009;10(11):755-64.
151. Metzger MB, Hristova VA, Weissman AM. HECT and RING finger families of E3 ubiquitin ligases at a glance. *J Cell Sci.* 2012;125(Pt 3):531-7.
152. Ardley HC, Robinson PA. E3 ubiquitin ligases. *Essays Biochem.* 2005;41:15-30.
153. Varshavsky A. The N-end rule pathway and regulation by proteolysis. *Protein Sci.* 2011;20(8):1298-345.
154. Han J, Zhang H, Zhang H, Wang Z, Zhou H, Zhang Z. A Cul4 E3 ubiquitin ligase regulates histone hand-off during nucleosome assembly. *Cell.* 2013;155(4):817-29.
155. Reyes-Turcu FE, Ventii KH, Wilkinson KD. Regulation and cellular roles of ubiquitin-specific deubiquitinating enzymes. *Annu Rev Biochem.* 2009;78:363-97.
156. Zhang Y. Transcriptional regulation by histone ubiquitination and deubiquitination. *Genes Dev.* 2003;17(22):2733-40.
157. Cao J, Yan Q. Histone ubiquitination and deubiquitination in transcription, DNA damage response, and cancer. *Front Oncol.* 2012;2:26.
158. Ray Chaudhuri A, Nussenzweig A. The multifaceted roles of PARP1 in DNA repair and chromatin remodelling. *Nat Rev Mol Cell Biol.* 2017;18(10):610-21.
159. Morales J, Li L, Fattah FJ, Dong Y, Bey EA, Patel M, et al. Review of poly (ADP-ribose) polymerase (PARP) mechanisms of action and rationale for targeting in cancer and other diseases. *Crit Rev Eukaryot Gene Expr.* 2014;24(1):15-28.
160. Gibson BA, Kraus WL. New insights into the molecular and cellular functions of poly(ADP-ribose) and PARPs. *Nat Rev Mol Cell Biol.* 2012;13(7):411-24.
161. Quenet D, El Ramy R, Schreiber V, Dantzer F. The role of poly(ADP-ribosyl)ation in epigenetic events. *Int J Biochem Cell Biol.* 2009;41(1):60-5.
162. Krishnakumar R, Kraus WL. PARP-1 regulates chromatin structure and transcription through a KDM5B-dependent pathway. *Mol Cell.* 2010;39(5):736-49.
163. Martinez-Zamudio R, Ha HC. Histone ADP-ribosylation facilitates gene transcription by directly remodeling nucleosomes. *Mol Cell Biol.* 2012;32(13):2490-502.
164. Bowman GD, Poirier MG. Post-translational modifications of histones that influence nucleosome dynamics. *Chem Rev.* 2015;115(6):2274-95.
165. Das C, Tyler JK, Churchill ME. The histone shuffle: histone chaperones in an energetic dance. *Trends Biochem Sci.* 2010;35(9):476-89.
166. Burgess RJ, Zhang Z. Histone chaperones in nucleosome assembly and human disease. *Nat Struct Mol Biol.* 2013;20(1):14-22.
167. Clapier CR, Cairns BR. The biology of chromatin remodeling complexes. *Annu Rev Biochem.* 2009;78:273-304.
168. Rogakou EP, Boon C, Redon C, Bonner WM. Megabase chromatin domains involved in DNA double-strand breaks in vivo. *J Cell Biol.* 1999;146(5):905-16.
169. Jackson SP, Bartek J. The DNA-damage response in human biology and disease. *Nature.* 2009;461(7267):1071-8.
170. Kinner A, Wu W, Staudt C, Iliakis G. Gamma-H2AX in recognition and signaling of DNA double-strand breaks in the context of chromatin. *Nucleic Acids Res.* 2008;36(17):5678-94.
171. Lukas C, Melander F, Stucki M, Falck J, Bekker-Jensen S, Goldberg M, et al. Mdc1 couples DNA double-strand break recognition by Nbs1 with its H2AX-dependent chromatin retention. *EMBO J.* 2004;23(13):2674-83.

172. You Z, Chahwan C, Bailis J, Hunter T, Russell P. ATM activation and its recruitment to damaged DNA require binding to the C terminus of Nbs1. *Mol Cell Biol.* 2005;25(13):5363-79.
173. Jungmichel S, Stucki M. MDC1: The art of keeping things in focus. *Chromosoma.* 2010;119(4):337-49.
174. Dinant C, Houtsmuller AB, Vermeulen W. Chromatin structure and DNA damage repair. *Epigenetics Chromatin.* 2008;1(1):9.
175. Fernandez-Capetillo O, Allis CD, Nussenzweig A. Phosphorylation of histone H2B at DNA double-strand breaks. *J Exp Med.* 2004;199(12):1671-7.
176. Harvey AC, Jackson SP, Downs JA. *Saccharomyces cerevisiae* histone H2A Ser122 facilitates DNA repair. *Genetics.* 2005;170(2):543-53.
177. Utley RT, Lacoste N, Jobin-Robitaille O, Allard S, Cote J. Regulation of NuA4 histone acetyltransferase activity in transcription and DNA repair by phosphorylation of histone H4. *Mol Cell Biol.* 2005;25(18):8179-90.
178. Bird AW, Yu DY, Pray-Grant MG, Qiu Q, Harmon KE, Megee PC, et al. Acetylation of histone H4 by Esa1 is required for DNA double-strand break repair. *Nature.* 2002;419(6905):411-5.
179. Ikura T, Ogryzko VV, Grigoriev M, Groisman R, Wang J, Horikoshi M, et al. Involvement of the TIP60 histone acetylase complex in DNA repair and apoptosis. *Cell.* 2000;102(4):463-73.
180. Murr R, Loizou JI, Yang YG, Cuenin C, Li H, Wang ZQ, et al. Histone acetylation by Trrap-Tip60 modulates loading of repair proteins and repair of DNA double-strand breaks. *Nat Cell Biol.* 2006;8(1):91-9.
181. Gospodinov A, Tsaneva I, Anachkova B. RAD51 foci formation in response to DNA damage is modulated by TIP49. *Int J Biochem Cell Biol.* 2009;41(4):925-33.
182. Tjeertes JV, Miller KM, Jackson SP. Screen for DNA-damage-responsive histone modifications identifies H3K9Ac and H3K56Ac in human cells. *EMBO J.* 2009;28(13):1878-89.
183. Ogiwara H, Ui A, Otsuka A, Satoh H, Yokomi I, Nakajima S, et al. Histone acetylation by CBP and p300 at double-strand break sites facilitates SWI/SNF chromatin remodeling and the recruitment of non-homologous end joining factors. *Oncogene.* 2011;30(18):2135-46.
184. Sharma GG, So S, Gupta A, Kumar R, Cayrou C, Avvakumov N, et al. MOF and histone H4 acetylation at lysine 16 are critical for DNA damage response and double-strand break repair. *Mol Cell Biol.* 2010;30(14):3582-95.
185. Li X, Corsa CA, Pan PW, Wu L, Ferguson D, Yu X, et al. MOF and H4 K16 acetylation play important roles in DNA damage repair by modulating recruitment of DNA damage repair protein Mdc1. *Mol Cell Biol.* 2010;30(22):5335-47.
186. Tamburini BA, Tyler JK. Localized histone acetylation and deacetylation triggered by the homologous recombination pathway of double-strand DNA repair. *Mol Cell Biol.* 2005;25(12):4903-13.
187. Miller KM, Tjeertes JV, Coates J, Legube G, Polo SE, Britton S, et al. Human HDAC1 and HDAC2 function in the DNA-damage response to promote DNA nonhomologous end-joining. *Nat Struct Mol Biol.* 2010;17(9):1144-51.
188. Ramanathan B, Smerdon MJ. Changes in nuclear protein acetylation in u.v.-damaged human cells. *Carcinogenesis.* 1986;7(7):1087-94.
189. Ramanathan B, Smerdon MJ. Enhanced DNA repair synthesis in hyperacetylated nucleosomes. *J Biol Chem.* 1989;264(19):11026-34.
190. Yu Y, Waters R. Histone acetylation, chromatin remodelling and nucleotide excision repair: hint from the study on MFA2 in *Saccharomyces cerevisiae*. *Cell Cycle.* 2005;4(8):1043-5.

191. Guo R, Chen J, Mitchell DL, Johnson DG. GCN5 and E2F1 stimulate nucleotide excision repair by promoting H3K9 acetylation at sites of damage. *Nucleic Acids Res.* 2011;39(4):1390-7.
192. Rubbi CP, Milner J. p53 is a chromatin accessibility factor for nucleotide excision repair of DNA damage. *EMBO J.* 2003;22(4):975-86.
193. Allison SJ, Milner J. Remodelling chromatin on a global scale: a novel protective function of p53. *Carcinogenesis.* 2004;25(9):1551-7.
194. Cheung KJ, Jr., Mitchell D, Lin P, Li G. The tumor suppressor candidate p33(ING1) mediates repair of UV-damaged DNA. *Cancer Res.* 2001;61(13):4974-7.
195. Kuo WH, Wang Y, Wong RP, Campos EI, Li G. The ING1b tumor suppressor facilitates nucleotide excision repair by promoting chromatin accessibility to XPA. *Exp Cell Res.* 2007;313(8):1628-38.
196. Huen MS, Grant R, Manke I, Minn K, Yu X, Yaffe MB, et al. RNF8 transduces the DNA-damage signal via histone ubiquitylation and checkpoint protein assembly. *Cell.* 2007;131(5):901-14.
197. Kolas NK, Chapman JR, Nakada S, Ylanko J, Chahwan R, Sweeney FD, et al. Orchestration of the DNA-damage response by the RNF8 ubiquitin ligase. *Science.* 2007;318(5856):1637-40.
198. Plans V, Scheper J, Soler M, Loukili N, Okano Y, Thomson TM. The RING finger protein RNF8 recruits UBC13 for lysine 63-based self polyubiquitylation. *J Cell Biochem.* 2006;97(3):572-82.
199. Doil C, Mailand N, Bekker-Jensen S, Menard P, Larsen DH, Pepperkok R, et al. RNF168 binds and amplifies ubiquitin conjugates on damaged chromosomes to allow accumulation of repair proteins. *Cell.* 2009;136(3):435-46.
200. Stewart GS, Panier S, Townsend K, Al-Hakim AK, Kolas NK, Miller ES, et al. The RIDDLE syndrome protein mediates a ubiquitin-dependent signaling cascade at sites of DNA damage. *Cell.* 2009;136(3):420-34.
201. Bekker-Jensen S, Rendtlew Danielsen J, Fugger K, Gromova I, Nerstedt A, Lukas C, et al. HERC2 coordinates ubiquitin-dependent assembly of DNA repair factors on damaged chromosomes. *Nat Cell Biol.* 2010;12(1):80-6; sup pp 1-12.
202. Moyal L, Lerenthal Y, Gana-Weisz M, Mass G, So S, Wang SY, et al. Requirement of ATM-dependent monoubiquitylation of histone H2B for timely repair of DNA double-strand breaks. *Mol Cell.* 2011;41(5):529-42.
203. Nakamura K, Kato A, Kobayashi J, Yanagihara H, Sakamoto S, Oliveira DV, et al. Regulation of homologous recombination by RNF20-dependent H2B ubiquitination. *Mol Cell.* 2011;41(5):515-28.
204. Bergink S, Salomons FA, Hoogstraten D, Groothuis TA, de Waard H, Wu J, et al. DNA damage triggers nucleotide excision repair-dependent monoubiquitylation of histone H2A. *Genes Dev.* 2006;20(10):1343-52.
205. Kapetanaki MG, Guerrero-Santoro J, Bisi DC, Hsieh CL, Rapic-Otrin V, Levine AS. The DDB1-CUL4A-DDB2 ubiquitin ligase is deficient in xeroderma pigmentosum group E and targets histone H2A at UV-damaged DNA sites. *Proceedings of the National Academy of Sciences of the United States of America.* 2006;103(8):2588-93.
206. Zhu Q, Wani G, Arab HH, El-Mahdy MA, Ray A, Wani AA. Chromatin restoration following nucleotide excision repair involves the incorporation of ubiquitinated H2A at damaged genomic sites. *DNA Repair (Amst).* 2009;8(2):262-73.
207. Marteijn JA, Bekker-Jensen S, Mailand N, Lans H, Schwertman P, Gourdin AM, et al. Nucleotide excision repair-induced H2A ubiquitination is dependent on MDC1 and RNF8 and reveals a universal DNA damage response. *J Cell Biol.* 2009;186(6):835-47.
208. Kouzarides T. SnapShot: Histone-modifying enzymes. *Cell.* 2007;128(4):802.

209. Shukla A, Chaurasia P, Bhaumik SR. Histone methylation and ubiquitination with their cross-talk and roles in gene expression and stability. *Cellular and molecular life sciences* : CMLS. 2009;66(8):1419-33.
210. Huyen Y, Zgheib O, Ditullio RA, Jr., Gorgoulis VG, Zacharatos P, Petty TJ, et al. Methylated lysine 79 of histone H3 targets 53BP1 to DNA double-strand breaks. *Nature*. 2004;432(7015):406-11.
211. Wysocki R, Javaheri A, Allard S, Sha F, Cote J, Kron SJ. Role of Dot1-dependent histone H3 methylation in G1 and S phase DNA damage checkpoint functions of Rad9. *Mol Cell Biol*. 2005;25(19):8430-43.
212. Sanders SL, Portoso M, Mata J, Bahler J, Allshire RC, Kouzarides T. Methylation of histone H4 lysine 20 controls recruitment of Crb2 to sites of DNA damage. *Cell*. 2004;119(5):603-14.
213. Schotta G, Sengupta R, Kubicek S, Malin S, Kauer M, Callen E, et al. A chromatin-wide transition to H4K20 monomethylation impairs genome integrity and programmed DNA rearrangements in the mouse. *Genes Dev*. 2008;22(15):2048-61.
214. Pei H, Zhang L, Luo K, Qin Y, Chesi M, Fei F, et al. MMSET regulates histone H4K20 methylation and 53BP1 accumulation at DNA damage sites. *Nature*. 2011;470(7332):124-8.
215. Messner S, Hottiger MO. Histone ADP-ribosylation in DNA repair, replication and transcription. *Trends Cell Biol*. 2011;21(9):534-42.
216. Rakhimova A, Ura S, Hsu DW, Wang HY, Pears CJ, Lakin ND. Site-specific ADP-ribosylation of histone H2B in response to DNA double strand breaks. *Sci Rep*. 2017;7:43750.
217. Robu M, Shah RG, Petitclerc N, Brind'Amour J, Kandan-Kulangara F, Shah GM. Role of poly(ADP-ribose) polymerase-1 in the removal of UV-induced DNA lesions by nucleotide excision repair. *Proc Natl Acad Sci U S A*. 2013;110(5):1658-63.
218. Grundy GJ, Polo LM, Zeng Z, Rulten SL, Hoch NC, Paomephan P, et al. PARP3 is a sensor of nicked nucleosomes and monoribosylates histone H2B(Glu2). *Nat Commun*. 2016;7:12404.
219. Tini M, Benecke A, Um SJ, Torchia J, Evans RM, Chambon P. Association of CBP/p300 acetylase and thymine DNA glycosylase links DNA repair and transcription. *Mol Cell*. 2002;9(2):265-77.
220. Khoronenkova SV, Dianova II, Parsons JL, Dianov GL. USP7/HAUSP stimulates repair of oxidative DNA lesions. *Nucleic Acids Res*. 2011;39(7):2604-9.
221. Rodriguez Y, Hinz JM, Laughery MF, Wyrick JJ, Smerdon MJ. Site-specific Acetylation of Histone H3 Decreases Polymerase beta Activity on Nucleosome Core Particles in Vitro. *The Journal of biological chemistry*. 2016;291(21):11434-45.
222. van Attikum H, Fritsch O, Hohn B, Gasser SM. Recruitment of the INO80 complex by H2A phosphorylation links ATP-dependent chromatin remodeling with DNA double-strand break repair. *Cell*. 2004;119(6):777-88.
223. Kitayama K, Kamo M, Oma Y, Matsuda R, Uchida T, Ikura T, et al. The human actin-related protein hArp5: nucleo-cytoplasmic shuttling and involvement in DNA repair. *Exp Cell Res*. 2009;315(2):206-17.
224. Tsukuda T, Fleming AB, Nickoloff JA, Osley MA. Chromatin remodelling at a DNA double-strand break site in *Saccharomyces cerevisiae*. *Nature*. 2005;438(7066):379-83.
225. Park EJ, Hur SK, Kwon J. Human INO80 chromatin-remodelling complex contributes to DNA double-strand break repair via the expression of Rad54B and XRCC3 genes. *Biochem J*. 2010;431(2):179-87.
226. Gospodinov A, Vaissiere T, Krastev DB, Legube G, Anachkova B, Herceg Z. Mammalian Ino80 mediates double-strand break repair through its role in DNA end strand resection. *Mol Cell Biol*. 2011;31(23):4735-45.

227. van Attikum H, Fritsch O, Gasser SM. Distinct roles for SWR1 and INO80 chromatin remodeling complexes at chromosomal double-strand breaks. *EMBO J.* 2007;26(18):4113-25.
228. Lee HS, Park JH, Kim SJ, Kwon SJ, Kwon J. A cooperative activation loop among SWI/SNF, gamma-H2AX and H3 acetylation for DNA double-strand break repair. *Embo j.* 2010;29(8):1434-45.
229. Bochar DA, Wang L, Beniya H, Kinev A, Xue Y, Lane WS, et al. BRCA1 is associated with a human SWI/SNF-related complex: linking chromatin remodeling to breast cancer. *Cell.* 2000;102(2):257-65.
230. Ura K, Araki M, Saeki H, Masutani C, Ito T, Iwai S, et al. ATP-dependent chromatin remodeling facilitates nucleotide excision repair of UV-induced DNA lesions in synthetic dinucleosomes. *EMBO J.* 2001;20(8):2004-14.
231. Lake RJ, Geyko A, Hemashettar G, Zhao Y, Fan HY. UV-induced association of the CSB remodeling protein with chromatin requires ATP-dependent relief of N-terminal autorepression. *Mol Cell.* 2010;37(2):235-46.
232. Hara R, Sancar A. The SWI/SNF chromatin-remodeling factor stimulates repair by human excision nuclease in the mononucleosome core particle. *Mol Cell Biol.* 2002;22(19):6779-87.
233. Hara R, Sancar A. Effect of damage type on stimulation of human excision nuclease by SWI/SNF chromatin remodeling factor. *Mol Cell Biol.* 2003;23(12):4121-5.
234. Zhao Q, Wang QE, Ray A, Wani G, Han C, Milum K, et al. Modulation of nucleotide excision repair by mammalian SWI/SNF chromatin-remodeling complex. *J Biol Chem.* 2009;284(44):30424-32.
235. Gong F, Fahy D, Liu H, Wang W, Smerdon MJ. Role of the mammalian SWI/SNF chromatin remodeling complex in the cellular response to UV damage. *Cell Cycle.* 2008;7(8):1067-74.
236. Gong F, Fahy D, Smerdon MJ. Rad4-Rad23 interaction with SWI/SNF links ATP-dependent chromatin remodeling with nucleotide excision repair. *Nat Struct Mol Biol.* 2006;13(10):902-7.
237. Jiang Y, Wang X, Bao S, Guo R, Johnson DG, Shen X, et al. INO80 chromatin remodeling complex promotes the removal of UV lesions by the nucleotide excision repair pathway. *Proceedings of the National Academy of Sciences of the United States of America.* 2010;107(40):17274-9.
238. Cho I, Tsai PF, Lake RJ, Basheer A, Fan HY. ATP-dependent chromatin remodeling by Cockayne syndrome protein B and NAP1-like histone chaperones is required for efficient transcription-coupled DNA repair. *PLoS Genet.* 2013;9(4):e1003407.
239. Roberts SA, Ramsden DA. Loading of the nonhomologous end joining factor, Ku, on protein-occluded DNA ends. *J Biol Chem.* 2007;282(14):10605-13.
240. Hara R, Mo J, Sancar A. DNA damage in the nucleosome core is refractory to repair by human excision nuclease. *Mol Cell Biol.* 2000;20(24):9173-81.
241. Charles Richard JL, Shukla MS, Menoni H, Ouararhni K, Lone IN, Roulland Y, et al. FACT Assists Base Excision Repair by Boosting the Remodeling Activity of RSC. *PLoS genetics.* 2016;12(7):e1006221.
242. Rodriguez Y, Smerdon MJ. The structural location of DNA lesions in nucleosome core particles determines accessibility by base excision repair enzymes. *The Journal of biological chemistry.* 2013;288(19):13863-75.
243. Hayes JJ, Lee KM. In vitro reconstitution and analysis of mononucleosomes containing defined DNAs and proteins. *Methods.* 1997;12(1):2-9.
244. Shechter DD, H. Allis, C. Hake, S. Extraction, purification and analysis of histones. *Nature Protocols.* 2007;2:1445-57.

245. Lowary PT, Widom J. New DNA sequence rules for high affinity binding to histone octamer and sequence-directed nucleosome positioning. *J Mol Biol.* 1998;276(1):19-42.
246. Luger K, Rechsteiner TJ, Richmond TJ. Preparation of nucleosome core particle from recombinant histones. *Methods Enzymol.* 1999;304:3-19.
247. Makde RD, England JR, Yennawar HP, Tan S. Structure of RCC1 chromatin factor bound to the nucleosome core particle. *Nature.* 2010;467(7315):562-6.
248. Parikh SS, Mol CD, Slupphaug G, Bharati S, Krokan HE, Tainer JA. Base excision repair initiation revealed by crystal structures and binding kinetics of human uracil-DNA glycosylase with DNA. *EMBO J.* 1998;17(17):5214-26.
249. Slupphaug G, Mol CD, Kavli B, Arvai AS, Krokan HE, Tainer JA. A nucleotide-flipping mechanism from the structure of human uracil-DNA glycosylase bound to DNA. *Nature.* 1996;384(6604):87-92.
250. Prasad A, Wallace SS, Pederson DS. Initiation of base excision repair of oxidative lesions in nucleosomes by the human, bifunctional DNA glycosylase NTH1. *Mol Cell Biol.* 2007;27(24):8442-53.
251. Odell ID, Newick K, Heintz NH, Wallace SS, Pederson DS. Non-specific DNA binding interferes with the efficient excision of oxidative lesions from chromatin by the human DNA glycosylase, NEIL1. *DNA Repair (Amst).* 2010;9(2):134-43.
252. Menoni H, Shukla MS, Gerson V, Dimitrov S, Angelov D. Base excision repair of 8-oxoG in dinucleosomes. *Nucleic Acids Res.* 2012;40(2):692-700.
253. Beard BC, Wilson SH, Smerdon MJ. Suppressed catalytic activity of base excision repair enzymes on rotationally positioned uracil in nucleosomes. *Proc Natl Acad Sci U S A.* 2003;100(13):7465-70.
254. Hinz JM. Impact of abasic site orientation within nucleosomes on human APE1 endonuclease activity. *Mutat Res.* 2014;766-767:19-24.
255. Odell ID, Barbour JE, Murphy DL, Della-Maria JA, Sweasy JB, Tomkinson AE, et al. Nucleosome disruption by DNA ligase III-XRCC1 promotes efficient base excision repair. *Mol Cell Biol.* 2011;31(22):4623-32.
256. Bruner SD, Norman DP, Verdine GL. Structural basis for recognition and repair of the endogenous mutagen 8-oxoguanine in DNA. *Nature.* 2000;403(6772):859-66.
257. Eccles LJ, Menoni H, Angelov D, Lomax ME, O'Neill P. Efficient cleavage of single and clustered AP site lesions within mono-nucleosome templates by CHO-K1 nuclear extract contrasts with retardation of incision by purified APE1. *DNA Repair (Amst).* 2015;35:27-36.
258. Nakanishi S, Prasad R, Wilson SH, Smerdon M. Different structural states in oligonucleosomes are required for early versus late steps of base excision repair. *Nucleic Acids Res.* 2007;35(13):4313-21.
259. Menoni H, Gasparutto D, Hamiche A, Cadet J, Dimitrov S, Bouvet P, et al. ATP-dependent chromatin remodeling is required for base excision repair in conventional but not in variant H2A.Bbd nucleosomes. *Mol Cell Biol.* 2007;27(17):5949-56.
260. Chai B, Huang J, Cairns BR, Laurent BC. Distinct roles for the RSC and Swi/Snf ATP-dependent chromatin remodelers in DNA double-strand break repair. *Genes Dev.* 2005;19(14):1656-61.
261. Koyama H, Itoh M, Miyahara K, Tsuchiya E. Abundance of the RSC nucleosome-remodeling complex is important for the cells to tolerate DNA damage in *Saccharomyces cerevisiae*. *FEBS Lett.* 2002;531(2):215-21.
262. Czaja W, Bespalov VA, Hinz JM, Smerdon MJ. Proficient repair in chromatin remodeling defective ino80 mutants of *Saccharomyces cerevisiae* highlights replication defects as the main contributor to DNA damage sensitivity. *DNA Repair (Amst).* 2010;9(9):976-84.

263. Czaja W, Mao P, Smerdon MJ. Chromatin remodelling complex RSC promotes base excision repair in chromatin of *Saccharomyces cerevisiae*. *DNA Repair (Amst)*. 2014;16:35-43.
264. Rouleau M, Aubin RA, Poirier GG. Poly(ADP-ribosyl)ated chromatin domains: access granted. *J Cell Sci*. 2004;117(Pt 6):815-25.
265. Kim MY, Mauro S, Gevry N, Lis JT, Kraus WL. NAD⁺-dependent modulation of chromatin structure and transcription by nucleosome binding properties of PARP-1. *Cell*. 2004;119(6):803-14.
266. Ko HL, Ren EC. Functional Aspects of PARP1 in DNA Repair and Transcription. *Biomolecules*. 2012;2(4):524-48.
267. Edmonds MJ, Carter RJ, Nickson CM, Williams SC, Parsons JL. Ubiquitylation-dependent regulation of NEIL1 by Mule and TRIM26 is required for the cellular DNA damage response. *Nucleic Acids Res*. 2017;45(2):726-38.
268. Thuring RW, Sanders JP, Borst P. A freeze-squeeze method for recovering long DNA from agarose gels. *Anal Biochem*. 1975;66(1):213-20.
269. Nickson CM, Parsons JL. Monitoring regulation of DNA repair activities of cultured cells in-gel using the comet assay. *Front Genet*. 2014;5:232.
270. Vasudevan D, Chua EY, Davey CA. Crystal structures of nucleosome core particles containing the '601' strong positioning sequence. *J Mol Biol*. 2010;403(1):1-10.
271. Hinz JM, Rodriguez Y, Smerdon MJ. Rotational dynamics of DNA on the nucleosome surface markedly impact accessibility to a DNA repair enzyme. *Proc Natl Acad Sci U S A*. 2010;107(10):4646-51.
272. Parsons JL, Tait PS, Finch D, Dianova, II, Edelmann MJ, Khoronenkova SV, et al. Ubiquitin ligase ARF-BP1/Mule modulates base excision repair. *EMBO J*. 2009;28(20):3207-15.
273. Schwertman P, Bekker-Jensen S, Mailand N. Regulation of DNA double-strand break repair by ubiquitin and ubiquitin-like modifiers. *Nat Rev Mol Cell Biol*. 2016;17(6):379-94.
274. Van Rechem C, Black JC, Abbas T, Allen A, Rinehart CA, Yuan GC, et al. The SKP1-Cul1-F-box and leucine-rich repeat protein 4 (SCF-FbxL4) ubiquitin ligase regulates lysine demethylase 4A (KDM4A)/Jumonji domain-containing 2A (JMJD2A) protein. *J Biol Chem*. 2011;286(35):30462-70.
275. Hannah J, Zhou P. Regulation of DNA damage response pathways by the cullin-RING ubiquitin ligases. *DNA Repair (Amst)*. 2009;8(4):536-43.
276. Zhou W, Zhu P, Wang J, Pascual G, Ohgi KA, Lozach J, et al. Histone H2A monoubiquitination represses transcription by inhibiting RNA polymerase II transcriptional elongation. *Mol Cell*. 2008;29(1):69-80.
277. Wyrick JJ, Kyriss MN, Davis WB. Ascending the nucleosome face: recognition and function of structured domains in the histone H2A-H2B dimer. *Biochim Biophys Acta*. 2012;1819(8):892-901.
278. Liu Z, Oughtred R, Wing SS. Characterization of E3Histone, a novel testis ubiquitin protein ligase which ubiquitinates histones. *Mol Cell Biol*. 2005;25(7):2819-31.
279. Khoronenkova SV, Dianov GL. The emerging role of Mule and ARF in the regulation of base excision repair. *FEBS Lett*. 2011;585(18):2831-5.
280. Pan MR, Peng G, Hung WC, Lin SY. Monoubiquitination of H2AX protein regulates DNA damage response signaling. *J Biol Chem*. 2011;286(32):28599-607.
281. An JY, Kim E, Zakrzewska A, Yoo YD, Jang JM, Han DH, et al. UBR2 of the N-end rule pathway is required for chromosome stability via histone ubiquitylation in spermatocytes and somatic cells. *PLoS One*. 2012;7(5):e37414.
282. Meisenberg C, Tait PS, Dianova, II, Wright K, Edelmann MJ, Ternette N, et al. Ubiquitin ligase UBR3 regulates cellular levels of the essential DNA repair protein APE1 and is required for genome stability. *Nucleic Acids Res*. 2012;40(2):701-11.

283. Parsons JL, Tait PS, Finch D, Dianova II, Allinson SL, Dianov GL. CHIP-mediated degradation and DNA damage-dependent stabilization regulate base excision repair proteins. *Mol Cell*. 2008;29(4):477-87.
284. Rodriguez Y, Hinz JM, Smerdon MJ. Accessing DNA damage in chromatin: Preparing the chromatin landscape for base excision repair. *DNA Repair (Amst)*. 2015;32:113-9.
285. Hinz JM, Czaja W. Facilitation of base excision repair by chromatin remodeling. *DNA Repair (Amst)*. 2015;36:91-7.
286. Berquist BR, McNeill DR, Wilson DM, 3rd. Characterization of abasic endonuclease activity of human Ape1 on alternative substrates, as well as effects of ATP and sequence context on AP site incision. *J Mol Biol*. 2008;379(1):17-27.
287. Lukas J, Lukas C, Bartek J. More than just a focus: The chromatin response to DNA damage and its role in genome integrity maintenance. *Nat Cell Biol*. 2011;13(10):1161-9.
288. Polo SE, Jackson SP. Dynamics of DNA damage response proteins at DNA breaks: a focus on protein modifications. *Genes Dev*. 2011;25(5):409-33.
289. Wang H, Zhai L, Xu J, Joo HY, Jackson S, Erdjument-Bromage H, et al. Histone H3 and H4 ubiquitylation by the CUL4-DDB-ROC1 ubiquitin ligase facilitates cellular response to DNA damage. *Mol Cell*. 2006;22(3):383-94.
290. Lan L, Nakajima S, Kapetanaki MG, Hsieh CL, Fagerburg M, Thickman K, et al. Monoubiquitinated histone H2A destabilizes photolesion-containing nucleosomes with concomitant release of UV-damaged DNA-binding protein E3 ligase. *The Journal of biological chemistry*. 2012;287(15):12036-49.
291. Duan MR, Smerdon MJ. UV damage in DNA promotes nucleosome unwrapping. *The Journal of biological chemistry*. 2010;285(34):26295-303.
292. Xu Y, Sun Y, Jiang X, Ayrapetov MK, Moskwa P, Yang S, et al. The p400 ATPase regulates nucleosome stability and chromatin ubiquitination during DNA repair. *J Cell Biol*. 2010;191(1):31-43.
293. North JA, Amunugama R, Klajner M, Bruns AN, Poirier MG, Fishel R. ATP-dependent nucleosome unwrapping catalyzed by human RAD51. *Nucleic Acids Res*. 2013;41(15):7302-12.
294. Prachu L HA, Martin M, Warsome F, Sun E, Lu T. Role of post-translational modification of the Y box binding protein in human cancers. *Genes and Diseases*. 2015;2(3):240-6.
295. Matsumoto K, Bay BH. Significance of the Y-box proteins in human cancers. *J Mol Genet Med*. 2005;1(1):11-7.
296. Kim ER, Selyutina AA, Buldakov IA, Evdokimova V, Ovchinnikov LP, Sorokin AV. The proteolytic YB-1 fragment interacts with DNA repair machinery and enhances survival during DNA damaging stress. *Cell Cycle*. 2013;12(24):3791-803.
297. Fomina EE, Pestryakov PE, Kretov DA, Zharkov DO, Ovchinnikov LP, Curmi PA, et al. Inhibition of abasic site cleavage in bubble DNA by multifunctional protein YB-1. *J Mol Recognit*. 2015;28(2):117-23.
298. Pestryakov P, Zharkov DO, Grin I, Fomina EE, Kim ER, Hamon L, et al. Effect of the multifunctional proteins RPA, YB-1, and XPC repair factor on AP site cleavage by DNA glycosylase NEIL1. *J Mol Recognit*. 2012;25(4):224-33.
299. Synder E RS, M Sharma, A Dearth, B Smoth, E Braun. Compound Heterozygosity for Y box Proteins Causes Sterility Due to Loss of Translational Repression. *PLOS Genetics*. 2015.
300. Zohn IE, Anderson KV, Niswander L. The Hectd1 ubiquitin ligase is required for development of the head mesenchyme and neural tube closure. *Dev Biol*. 2007;306(1):208-21.
301. Tran H, Bustos D, Yeh R, Rubinfeld B, Lam C, Shriver S, et al. HectD1 E3 ligase modifies adenomatous polyposis coli (APC) with polyubiquitin to promote the APC-axin interaction. *J Biol Chem*. 2013;288(6):3753-67.

302. Geo J AB, Dogrusoz U, Dresdner G, Gross B, Sumer S, Sun Y, Jacobsen A, Sinha R, E Larsson, E Cerami, C Sander, N Schultz. Integrative Analysis of Complex Cancer Genomics ad Clinical Profiles Using the cBioPortal. *Science Signalling*. 2013;6(269).
303. Cerami E, Gao J, Dogrusoz U, Gross BE, Sumer SO, Aksoy BA, et al. The cBio cancer genomics portal: an open platform for exploring multidimensional cancer genomics data. *Cancer Discov*. 2012;2(5):401-4.

Appendix I

Mass spectrometry analysis results for activity 1

The most active fraction from the final ion exchange (Mono Q) chromatography step, fraction 16 (5.3.3.1.2) for activity 1, was analysed by mass spectrometry by Dr Deborah M Simpson (Centre for Proteasome Research, University of Liverpool) to identify candidate E3 ubiquitin ligases and/or chromatin remodellers. The full list of proteins identified is shown below in descending order of mascot score.

Accession	Description	Mascot
P07900	Heat shock protein HSP 90-alpha OS=Homo sapiens GN=HSP90AA1 PE=1 SV=5 - [HS90A_HUMAN]	3426.13
P08238	Heat shock protein HSP 90-beta OS=Homo sapiens GN=HSP90AB1 PE=1 SV=4 - [HS90B_HUMAN]	3379.29
P11021	78 kDa glucose-regulated protein OS=Homo sapiens GN=HSPA5 PE=1 SV=2 - [GRP78_HUMAN]	889
P31327	Carbamoyl-phosphate synthase [ammonia], mitochondrial OS=Homo sapiens GN=CPS1 PE=1 SV=2 - [CPSM_HUMAN]	879.55
P13667	Protein disulfide-isomerase A4 OS=Homo sapiens GN=PDIA4 PE=1 SV=2 - [PDIA4_HUMAN]	773.18
Q16543	Hsp90 co-chaperone Cdc37 OS=Homo sapiens GN=CDC37 PE=1 SV=1 - [CDC37_HUMAN]	668.43
P49736	DNA replication licensing factor MCM2 OS=Homo sapiens GN=MCM2 PE=1 SV=4 - [MCM2_HUMAN]	652.36
P33993	DNA replication licensing factor MCM7 OS=Homo sapiens GN=MCM7 PE=1 SV=4 - [MCM7_HUMAN]	645.29
Q15042	Rab3 GTPase-activating protein catalytic subunit OS=Homo sapiens GN=RAB3GAP1 PE=1 SV=3 - [RB3GP_HUMAN]	618.74
P25786	Proteasome subunit alpha type-1 OS=Homo sapiens GN=PSMA1 PE=1 SV=1 - [PSA1_HUMAN]	615.49
P11142	Heat shock cognate 71 kDa protein OS=Homo sapiens GN=HSPA8 PE=1 SV=1 - [HSP7C_HUMAN]	597.47
Q9ULT8	E3 ubiquitin-protein ligase HECTD1 OS=Homo sapiens GN=HECTD1 PE=1 SV=3 - [HECD1_HUMAN]	591.28
P28074	Proteasome subunit beta type-5 OS=Homo sapiens GN=PSMB5 PE=1 SV=3 - [PSB5_HUMAN]	589.67
P60900	Proteasome subunit alpha type-6 OS=Homo sapiens GN=PSMA6 PE=1 SV=1 - [PSA6_HUMAN]	563.09
Q9UNE7	E3 ubiquitin-protein ligase CHIP OS=Homo sapiens GN=STUB1 PE=1 SV=2 - [CHIP_HUMAN]	536.44
O60763	General vesicular transport factor p115 OS=Homo sapiens GN=USO1 PE=1 SV=2 - [USO1_HUMAN]	534.52
Q14566	DNA replication licensing factor MCM6 OS=Homo sapiens GN=MCM6 PE=1 SV=1 - [MCM6_HUMAN]	534.2

Accession	Description	Mascot
P34932	Heat shock 70 kDa protein 4 OS=Homo sapiens GN=HSPA4 PE=1 SV=4 - [HSP74_HUMAN]	533.78
P33991	DNA replication licensing factor MCM4 OS=Homo sapiens GN=MCM4 PE=1 SV=5 - [MCM4_HUMAN]	502.65
P53621	Coatomer subunit alpha OS=Homo sapiens GN=COPA PE=1 SV=2 - [COPA_HUMAN]	483.73
P49411	Elongation factor Tu, mitochondrial OS=Homo sapiens GN=TUFM PE=1 SV=2 - [EFTU_HUMAN]	465.39
P0DMV9	Heat shock 70 kDa protein 1B OS=Homo sapiens GN=HSPA1B PE=1 SV=1 - [HS71B_HUMAN]	464.13
P07951	Tropomyosin beta chain OS=Homo sapiens GN=TPM2 PE=1 SV=1 - [TPM2_HUMAN]	462.39
P06733	Alpha-enolase OS=Homo sapiens GN=ENO1 PE=1 SV=2 - [ENOA_HUMAN]	454.77
Q15084	Protein disulfide-isomerase A6 OS=Homo sapiens GN=PDIA6 PE=1 SV=1 - [PDIA6_HUMAN]	454.07
Q13409	Cytoplasmic dynein 1 intermediate chain 2 OS=Homo sapiens GN=DYNC1I2 PE=1 SV=3 - [DC1I2_HUMAN]	441.56
P35998	26S protease regulatory subunit 7 OS=Homo sapiens GN=PSMC2 PE=1 SV=3 - [PRS7_HUMAN]	433.07
P60709	Actin, cytoplasmic 1 OS=Homo sapiens GN=ACTB PE=1 SV=1 - [ACTB_HUMAN]	426.45
O14818	Proteasome subunit alpha type-7 OS=Homo sapiens GN=PSMA7 PE=1 SV=1 - [PSA7_HUMAN]	421.41
Q58FG1	Putative heat shock protein HSP 90-alpha A4 OS=Homo sapiens GN=HSP90AA4P PE=5 SV=1 - [HS904_HUMAN]	420.1
P35606	Coatomer subunit beta' OS=Homo sapiens GN=COPB2 PE=1 SV=2 - [COPB2_HUMAN]	416.29
Q9H3U1	Protein unc-45 homolog A OS=Homo sapiens GN=UNC45A PE=1 SV=1 - [UN45A_HUMAN]	413.96
P02786	Transferrin receptor protein 1 OS=Homo sapiens GN=TFRC PE=1 SV=2 - [TFR1_HUMAN]	405.71
Q9H2M9	Rab3 GTPase-activating protein non-catalytic subunit OS=Homo sapiens GN=RAB3GAP2 PE=1 SV=1 - [RBGPR_HUMAN]	398.18
Q9Y4E8	Ubiquitin carboxyl-terminal hydrolase 15 OS=Homo sapiens GN=USP15 PE=1 SV=3 - [UBP15_HUMAN]	392.58
P62195	26S protease regulatory subunit 8 OS=Homo sapiens GN=PSMC5 PE=1 SV=1 - [PRS8_HUMAN]	374.86
P28066	Proteasome subunit alpha type-5 OS=Homo sapiens GN=PSMA5 PE=1 SV=3 - [PSA5_HUMAN]	374.57
Q9Y230	RuvB-like 2 OS=Homo sapiens GN=RUVBL2 PE=1 SV=3 - [RUVB2_HUMAN]	363.07
P07437	Tubulin beta chain OS=Homo sapiens GN=TUBB PE=1 SV=2 - [TBB5_HUMAN]	362.22
P38646	Stress-70 protein, mitochondrial OS=Homo sapiens GN=HSPA9 PE=1 SV=2 - [GRP75_HUMAN]	346.75
P68371	Tubulin beta-4B chain OS=Homo sapiens GN=TUBB4B PE=1 SV=1 - [TBB4B_HUMAN]	340.27
Q9BQE3	Tubulin alpha-1C chain OS=Homo sapiens GN=TUBA1C PE=1 SV=1 - [TBA1C_HUMAN]	332.82
P20618	Proteasome subunit beta type-1 OS=Homo sapiens GN=PSMB1 PE=1 SV=2 - [PSB1_HUMAN]	322.96
P28070	Proteasome subunit beta type-4 OS=Homo sapiens GN=PSMB4 PE=1 SV=4 - [PSB4_HUMAN]	313.83
P55786	Puromycin-sensitive aminopeptidase OS=Homo sapiens GN=NPEPPS PE=1 SV=2 - [PSA_HUMAN]	312.05

Accession	Description	Mascot
Q9BT78	COP9 signalosome complex subunit 4 OS=Homo sapiens GN=COPS4 PE=1 SV=1 - [CSN4_HUMAN]	301.48
P25788	Proteasome subunit alpha type-3 OS=Homo sapiens GN=PSMA3 PE=1 SV=2 - [PSA3_HUMAN]	301.2
Q9UBW8	COP9 signalosome complex subunit 7a OS=Homo sapiens GN=COPS7A PE=1 SV=1 - [CSN7A_HUMAN]	290.59
P07237	Protein disulfide-isomerase OS=Homo sapiens GN=P4HB PE=1 SV=3 - [PDIA1_HUMAN]	289.08
Q13200	26S proteasome non-ATPase regulatory subunit 2 OS=Homo sapiens GN=PSMD2 PE=1 SV=3 - [PSMD2_HUMAN]	288.25
P35527	Keratin, type I cytoskeletal 9 OS=Homo sapiens GN=KRT9 PE=1 SV=3 - [K1C9_HUMAN]	286.19
Q99436	Proteasome subunit beta type-7 OS=Homo sapiens GN=PSMB7 PE=1 SV=1 - [PSB7_HUMAN]	273.68
P49327	Fatty acid synthase OS=Homo sapiens GN=FASN PE=1 SV=3 - [FAS_HUMAN]	271.23
Q6IN85	Serine/threonine-protein phosphatase 4 regulatory subunit 3A OS=Homo sapiens GN=PPP4R3A PE=1 SV=1 - [P4R3A_HUMAN]	266.2
P08195	4F2 cell-surface antigen heavy chain OS=Homo sapiens GN=SLC3A2 PE=1 SV=3 - [4F2_HUMAN]	264.7
Q00839	Heterogeneous nuclear ribonucleoprotein U OS=Homo sapiens GN=HNRNPU PE=1 SV=6 - [HNRPU_HUMAN]	264.37
P04264	Keratin, type II cytoskeletal 1 OS=Homo sapiens GN=KRT1 PE=1 SV=6 - [K2C1_HUMAN]	262.13
Q14203	Dynactin subunit 1 OS=Homo sapiens GN=DCTN1 PE=1 SV=3 - [DCTN1_HUMAN]	258.74
Q99961	Endophilin-A2 OS=Homo sapiens GN=SH3GL1 PE=1 SV=1 - [SH3G1_HUMAN]	258.07
Q96K76	Ubiquitin carboxyl-terminal hydrolase 47 OS=Homo sapiens GN=USP47 PE=1 SV=3 - [UBP47_HUMAN]	257.57
Q93008	Probable ubiquitin carboxyl-terminal hydrolase FAF-X OS=Homo sapiens GN=USP9X PE=1 SV=3 - [USP9X_HUMAN]	255.84
P61201	COP9 signalosome complex subunit 2 OS=Homo sapiens GN=COPS2 PE=1 SV=1 - [CSN2_HUMAN]	249.14
P28072	Proteasome subunit beta type-6 OS=Homo sapiens GN=PSMB6 PE=1 SV=4 - [PSB6_HUMAN]	228.7
Q92905	COP9 signalosome complex subunit 5 OS=Homo sapiens GN=COPS5 PE=1 SV=4 - [CSN5_HUMAN]	224.59
P25705	ATP synthase subunit alpha, mitochondrial OS=Homo sapiens GN=ATP5A1 PE=1 SV=1 - [ATPA_HUMAN]	222.15
Q99460	26S proteasome non-ATPase regulatory subunit 1 OS=Homo sapiens GN=PSMD1 PE=1 SV=2 - [PSMD1_HUMAN]	221.5
P68366	Tubulin alpha-4A chain OS=Homo sapiens GN=TUBA4A PE=1 SV=1 - [TBA4A_HUMAN]	220.41
P48444	Coatamer subunit delta OS=Homo sapiens GN=ARCN1 PE=1 SV=1 - [COPD_HUMAN]	212.07
O60664	Perilipin-3 OS=Homo sapiens GN=PLIN3 PE=1 SV=3 - [PLIN3_HUMAN]	210.73
P14324	Farnesyl pyrophosphate synthase OS=Homo sapiens GN=FDPS PE=1 SV=4 - [FPPS_HUMAN]	209.83
P17980	26S protease regulatory subunit 6A OS=Homo sapiens GN=PSMC3 PE=1 SV=3 - [PRS6A_HUMAN]	207.88
P49721	Proteasome subunit beta type-2 OS=Homo sapiens GN=PSMB2 PE=1 SV=1 - [PSB2_HUMAN]	206.68

Accession	Description	Mascot
P17812	CTP synthase 1 OS=Homo sapiens GN=CTPS1 PE=1 SV=2 - [PYRG1_HUMAN]	206.63
P62191	26S protease regulatory subunit 4 OS=Homo sapiens GN=PSMC1 PE=1 SV=1 - [PRS4_HUMAN]	206.39
P52292	Importin subunit alpha-1 OS=Homo sapiens GN=KPNA2 PE=1 SV=1 - [IMA1_HUMAN]	203.75
P10809	60 kDa heat shock protein, mitochondrial OS=Homo sapiens GN=HSPD1 PE=1 SV=2 - [CH60_HUMAN]	199.73
P48449	Lanosterol synthase OS=Homo sapiens GN=LSS PE=1 SV=1 - [ERG7_HUMAN]	196.75
P31153	S-adenosylmethionine synthase isoform type-2 OS=Homo sapiens GN=MAT2A PE=1 SV=1 - [METK2_HUMAN]	191.43
Q9BR76	Coronin-1B OS=Homo sapiens GN=CORO1B PE=1 SV=1 - [COR1B_HUMAN]	189.39
P28062	Proteasome subunit beta type-8 OS=Homo sapiens GN=PSMB8 PE=1 SV=3 - [PSB8_HUMAN]	187.48
P17655	Calpain-2 catalytic subunit OS=Homo sapiens GN=CAPN2 PE=1 SV=6 - [CAN2_HUMAN]	185.86
Q9UJU6	Drebrin-like protein OS=Homo sapiens GN=DBNL PE=1 SV=1 - [DBNL_HUMAN]	183.42
Q9Y265	RuvB-like 1 OS=Homo sapiens GN=RUVBL1 PE=1 SV=1 - [RUVB1_HUMAN]	182.18
O00148	ATP-dependent RNA helicase DDX39A OS=Homo sapiens GN=DDX39A PE=1 SV=2 - [DX39A_HUMAN]	180.68
Q14974	Importin subunit beta-1 OS=Homo sapiens GN=KPNB1 PE=1 SV=2 - [IMB1_HUMAN]	180.54
P63104	14-3-3 protein zeta/delta OS=Homo sapiens GN=YWHAZ PE=1 SV=1 - [1433Z_HUMAN]	169.65
Q7L3B6	Hsp90 co-chaperone Cdc37-like 1 OS=Homo sapiens GN=CDC37L1 PE=1 SV=1 - [CD37L_HUMAN]	166.93
P49321	Nuclear autoantigenic sperm protein OS=Homo sapiens GN=NASP PE=1 SV=2 - [NASP_HUMAN]	162.66
P30453	HLA class I histocompatibility antigen, A-34 alpha chain OS=Homo sapiens GN=HLA-A PE=1 SV=1 - [1A34_HUMAN]	159.74
P23396	40S ribosomal protein S3 OS=Homo sapiens GN=RPS3 PE=1 SV=2 - [RS3_HUMAN]	158.36
Q01813	ATP-dependent 6-phosphofructokinase, platelet type OS=Homo sapiens GN=PFBP PE=1 SV=2 - [PFBP_HUMAN]	157.66
P31689	DnaJ homolog subfamily A member 1 OS=Homo sapiens GN=DNAJA1 PE=1 SV=2 - [DNJA1_HUMAN]	155.24
Q92598	Heat shock protein 105 kDa OS=Homo sapiens GN=HSPH1 PE=1 SV=1 - [HS105_HUMAN]	151.98
O75179	Ankyrin repeat domain-containing protein 17 OS=Homo sapiens GN=ANKRD17 PE=1 SV=3 - [ANR17_HUMAN]	151.76
P25787	Proteasome subunit alpha type-2 OS=Homo sapiens GN=PSMA2 PE=1 SV=2 - [PSA2_HUMAN]	150.7
P30153	Serine/threonine-protein phosphatase 2A 65 kDa regulatory subunit A alpha isoform OS=Homo sapiens GN=PPP2R1A PE=1 SV=4 - [2AAA_HUMAN]	150.46
O95757	Heat shock 70 kDa protein 4L OS=Homo sapiens GN=HSPA4L PE=1 SV=3 - [HS74L_HUMAN]	147.05
Q9H9Q2	COP9 signalosome complex subunit 7b OS=Homo sapiens GN=COPS7B PE=1 SV=1 - [CSN7B_HUMAN]	143.38
P13489	Ribonuclease inhibitor OS=Homo sapiens GN=RNH1 PE=1 SV=2 - [RINI_HUMAN]	142.72
P25789	Proteasome subunit alpha type-4 OS=Homo sapiens GN=PSMA4 PE=1 SV=1 - [PSA4_HUMAN]	142.57

Accession	Description	Mascot
P01891	HLA class I histocompatibility antigen, A-68 alpha chain OS=Homo sapiens GN=HLA-A PE=1 SV=4 - [1A68_HUMAN]	140.4
Q13098	COP9 signalosome complex subunit 1 OS=Homo sapiens GN=GPS1 PE=1 SV=4 - [CSN1_HUMAN]	140.15
P24534	Elongation factor 1-beta OS=Homo sapiens GN=EEF1B2 PE=1 SV=3 - [EF1B_HUMAN]	135.37
Q9BQA1	Methylosome protein 50 OS=Homo sapiens GN=WDR77 PE=1 SV=1 - [MEP50_HUMAN]	132.54
P47712	Cytosolic phospholipase A2 OS=Homo sapiens GN=PLA2G4A PE=1 SV=2 - [PA24A_HUMAN]	132.11
O60443	Non-syndromic hearing impairment protein 5 OS=Homo sapiens GN=DFNA5 PE=1 SV=2 - [DFNA5_HUMAN]	131.87
P10155	60 kDa SS-A/Ro ribonucleoprotein OS=Homo sapiens GN=TROVE2 PE=1 SV=2 - [RO60_HUMAN]	130.34
O95831	Apoptosis-inducing factor 1, mitochondrial OS=Homo sapiens GN=AIFM1 PE=1 SV=1 - [AIFM1_HUMAN]	130.14
P68104	Elongation factor 1-alpha 1 OS=Homo sapiens GN=EEF1A1 PE=1 SV=1 - [EF1A1_HUMAN]	129.43
Q99832	T-complex protein 1 subunit eta OS=Homo sapiens GN=CCT7 PE=1 SV=2 - [TCPH_HUMAN]	127.16
Q99536	Synaptic vesicle membrane protein VAT-1 homolog OS=Homo sapiens GN=VAT1 PE=1 SV=2 - [VAT1_HUMAN]	123.87
Q9UNS2	COP9 signalosome complex subunit 3 OS=Homo sapiens GN=COPS3 PE=1 SV=3 - [CSN3_HUMAN]	123.46
P40939	Trifunctional enzyme subunit alpha, mitochondrial OS=Homo sapiens GN=HADHA PE=1 SV=2 - [ECHA_HUMAN]	123.37
Q9UBE0	SUMO-activating enzyme subunit 1 OS=Homo sapiens GN=SAE1 PE=1 SV=1 - [SAE1_HUMAN]	121.68
P13639	Elongation factor 2 OS=Homo sapiens GN=EEF2 PE=1 SV=4 - [EF2_HUMAN]	120.59
P30464	HLA class I histocompatibility antigen, B-15 alpha chain OS=Homo sapiens GN=HLA-B PE=1 SV=2 - [1B15_HUMAN]	118.58
Q14247	Src substrate cortactin OS=Homo sapiens GN=CTTN PE=1 SV=2 - [SRC8_HUMAN]	116.07
O95816	BAG family molecular chaperone regulator 2 OS=Homo sapiens GN=BAG2 PE=1 SV=1 - [BAG2_HUMAN]	115.37
P08134	Rho-related GTP-binding protein RhoC OS=Homo sapiens GN=RHOC PE=1 SV=1 - [RHOC_HUMAN]	114.63
P55072	Transitional endoplasmic reticulum ATPase OS=Homo sapiens GN=VCP PE=1 SV=4 - [TERA_HUMAN]	113.64
P55060	Exportin-2 OS=Homo sapiens GN=CSE1L PE=1 SV=3 - [XPO2_HUMAN]	113.4
O60232	Sjogren syndrome/scleroderma autoantigen 1 OS=Homo sapiens GN=SSSCA1 PE=1 SV=1 - [SSA27_HUMAN]	111.7
P04792	Heat shock protein beta-1 OS=Homo sapiens GN=HSPB1 PE=1 SV=2 - [HSPB1_HUMAN]	111.62
P62826	GTP-binding nuclear protein Ran OS=Homo sapiens GN=RAN PE=1 SV=3 - [RAN_HUMAN]	111.19
Q99614	Tetratricopeptide repeat protein 1 OS=Homo sapiens GN=TTC1 PE=1 SV=1 - [TTC1_HUMAN]	110.89
P21980	Protein-glutamine gamma-glutamyltransferase 2 OS=Homo sapiens GN=TGM2 PE=1 SV=2 - [TGM2_HUMAN]	109.86
O60884	DnaJ homolog subfamily A member 2 OS=Homo sapiens GN=DNAJA2 PE=1 SV=1 - [DNJA2_HUMAN]	107.05
P14618	Pyruvate kinase PKM OS=Homo sapiens GN=PKM PE=1 SV=4 - [KPYM_HUMAN]	106.33

Accession	Description	Mascot
Q9Y5P4	Collagen type IV alpha-3-binding protein OS=Homo sapiens GN=COL4A3BP PE=1 SV=1 - [C43BP_HUMAN]	105.99
P62258	14-3-3 protein epsilon OS=Homo sapiens GN=YWHAE PE=1 SV=1 - [1433E_HUMAN]	104.21
P12004	Proliferating cell nuclear antigen OS=Homo sapiens GN=PCNA PE=1 SV=1 - [PCNA_HUMAN]	104.21
O15460	Prolyl 4-hydroxylase subunit alpha-2 OS=Homo sapiens GN=P4HA2 PE=1 SV=1 - [P4HA2_HUMAN]	101.42
P51784	Ubiquitin carboxyl-terminal hydrolase 11 OS=Homo sapiens GN=USP11 PE=1 SV=3 - [UBP11_HUMAN]	101.03
P41250	Glycine--tRNA ligase OS=Homo sapiens GN=GARS PE=1 SV=3 - [SYG_HUMAN]	100.78
Q15029	116 kDa U5 small nuclear ribonucleoprotein component OS=Homo sapiens GN=EFTUD2 PE=1 SV=1 - [U5S1_HUMAN]	100.23
P46459	Vesicle-fusing ATPase OS=Homo sapiens GN=NSF PE=1 SV=3 - [NSF_HUMAN]	99.01
P61163	Alpha-centractin OS=Homo sapiens GN=ACTR1A PE=1 SV=1 - [ACTZ_HUMAN]	98.11
O43242	26S proteasome non-ATPase regulatory subunit 3 OS=Homo sapiens GN=PSMD3 PE=1 SV=2 - [PSMD3_HUMAN]	98.08
Q99627	COP9 signalosome complex subunit 8 OS=Homo sapiens GN=COPS8 PE=1 SV=1 - [CSN8_HUMAN]	97.62
P27348	14-3-3 protein theta OS=Homo sapiens GN=YWHAQ PE=1 SV=1 - [1433T_HUMAN]	97.16
Q15018	BRISC complex subunit Abro1 OS=Homo sapiens GN=FAM175B PE=1 SV=2 - [F175B_HUMAN]	96.52
P43686	26S protease regulatory subunit 6B OS=Homo sapiens GN=PSMC4 PE=1 SV=2 - [PRS6B_HUMAN]	95.59
P13798	Acylamino-acid-releasing enzyme OS=Homo sapiens GN=APEH PE=1 SV=4 - [ACPH_HUMAN]	95.43
O00233	26S proteasome non-ATPase regulatory subunit 9 OS=Homo sapiens GN=PSMD9 PE=1 SV=3 - [PSMD9_HUMAN]	94.05
P31946	14-3-3 protein beta/alpha OS=Homo sapiens GN=YWHAB PE=1 SV=3 - [1433B_HUMAN]	92.62
Q14160	Protein scribble homolog OS=Homo sapiens GN=SCRIB PE=1 SV=4 - [SCRIB_HUMAN]	91.33
Q9P289	Serine/threonine-protein kinase 26 OS=Homo sapiens GN=STK26 PE=1 SV=2 - [STK26_HUMAN]	91.04
Q13428	Treacle protein OS=Homo sapiens GN=TCOF1 PE=1 SV=3 - [TCOF_HUMAN]	90.39
P61981	14-3-3 protein gamma OS=Homo sapiens GN=YWHAG PE=1 SV=2 - [1433G_HUMAN]	90.1
P51570	Galactokinase OS=Homo sapiens GN=GALK1 PE=1 SV=1 - [GALK1_HUMAN]	90.04
Q15645	Pachytene checkpoint protein 2 homolog OS=Homo sapiens GN=TRIP13 PE=1 SV=2 - [PCH2_HUMAN]	88.71
P61586	Transforming protein RhoA OS=Homo sapiens GN=RHOA PE=1 SV=1 - [RHOA_HUMAN]	88.18
P78344	Eukaryotic translation initiation factor 4 gamma 2 OS=Homo sapiens GN=EIF4G2 PE=1 SV=1 - [IF4G2_HUMAN]	87.77
P12268	Inosine-5'-monophosphate dehydrogenase 2 OS=Homo sapiens GN=IMPDH2 PE=1 SV=2 - [IMDH2_HUMAN]	87.67
O95218	Zinc finger Ran-binding domain-containing protein 2 OS=Homo sapiens GN=ZRANB2 PE=1 SV=2 - [ZRAB2_HUMAN]	87.41
Q8N163	Cell cycle and apoptosis regulator protein 2 OS=Homo sapiens GN=CCAR2 PE=1 SV=2 - [CCAR2_HUMAN]	87.08

Accession	Description	Mascot
Q86VP6	Cullin-associated NEDD8-dissociated protein 1 OS=Homo sapiens GN=CAND1 PE=1 SV=2 - [CAND1_HUMAN]	86.97
P62491	Ras-related protein Rab-11A OS=Homo sapiens GN=RAB11A PE=1 SV=3 - [RB11A_HUMAN]	86.9
P52294	Importin subunit alpha-5 OS=Homo sapiens GN=KPNA1 PE=1 SV=3 - [IMA5_HUMAN]	86.74
P62495	Eukaryotic peptide chain release factor subunit 1 OS=Homo sapiens GN=ETF1 PE=1 SV=3 - [ERF1_HUMAN]	85.88
P35613	Basigin OS=Homo sapiens GN=BSG PE=1 SV=2 - [BASI_HUMAN]	84.47
P46782	40S ribosomal protein S5 OS=Homo sapiens GN=RPS5 PE=1 SV=4 - [RS5_HUMAN]	84.31
Q92928	Putative Ras-related protein Rab-1C OS=Homo sapiens GN=RAB1C PE=5 SV=2 - [RAB1C_HUMAN]	81.29
Q7L5N1	COP9 signalosome complex subunit 6 OS=Homo sapiens GN=COPS6 PE=1 SV=1 - [CSN6_HUMAN]	80.64
Q9UNZ2	NSFL1 cofactor p47 OS=Homo sapiens GN=NSFL1C PE=1 SV=2 - [NSF1C_HUMAN]	80.11
P52298	Nuclear cap-binding protein subunit 2 OS=Homo sapiens GN=NCBP2 PE=1 SV=1 - [NCBP2_HUMAN]	78.79
O14732	Inositol monophosphatase 2 OS=Homo sapiens GN=IMPA2 PE=1 SV=1 - [IMPA2_HUMAN]	78.2
O75832	26S proteasome non-ATPase regulatory subunit 10 OS=Homo sapiens GN=PSMD10 PE=1 SV=1 - [PSD10_HUMAN]	78.16
P08754	Guanine nucleotide-binding protein G(k) subunit alpha OS=Homo sapiens GN=GNAI3 PE=1 SV=3 - [GNAI3_HUMAN]	77.71
Q8IZP2	Putative protein FAM10A4 OS=Homo sapiens GN=ST13P4 PE=5 SV=1 - [ST134_HUMAN]	77.57
P26641	Elongation factor 1-gamma OS=Homo sapiens GN=EEF1G PE=1 SV=3 - [EF1G_HUMAN]	77.37
P04843	Dolichyl-diphosphooligosaccharide--protein glycosyltransferase subunit 1 OS=Homo sapiens GN=RPN1 PE=1 SV=1 - [RPN1_HUMAN]	77.35
Q9UBT2	SUMO-activating enzyme subunit 2 OS=Homo sapiens GN=UBA2 PE=1 SV=2 - [SAE2_HUMAN]	77.21
Q8TF09	Dynein light chain roadblock-type 2 OS=Homo sapiens GN=DYNLRB2 PE=1 SV=1 - [DLRB2_HUMAN]	76.82
O95433	Activator of 90 kDa heat shock protein ATPase homolog 1 OS=Homo sapiens GN=AHSA1 PE=1 SV=1 - [AHSA1_HUMAN]	76.28
P13645	Keratin, type I cytoskeletal 10 OS=Homo sapiens GN=KRT10 PE=1 SV=6 - [K1C10_HUMAN]	75.66
P60842	Eukaryotic initiation factor 4A-I OS=Homo sapiens GN=EIF4A1 PE=1 SV=1 - [IF4A1_HUMAN]	75.45
P49720	Proteasome subunit beta type-3 OS=Homo sapiens GN=PSMB3 PE=1 SV=2 - [PSB3_HUMAN]	75.43
Q9UHG3	Prenylcysteine oxidase 1 OS=Homo sapiens GN=PCYOX1 PE=1 SV=3 - [PCYOX_HUMAN]	75.27
P78318	Immunoglobulin-binding protein 1 OS=Homo sapiens GN=IGBP1 PE=1 SV=1 - [IGBP1_HUMAN]	74.69
P38606	V-type proton ATPase catalytic subunit A OS=Homo sapiens GN=ATP6V1A PE=1 SV=2 - [VATA_HUMAN]	73.53
Q13561	Dynactin subunit 2 OS=Homo sapiens GN=DCTN2 PE=1 SV=4 - [DCTN2_HUMAN]	73.11
O14980	Exportin-1 OS=Homo sapiens GN=XPO1 PE=1 SV=1 - [XPO1_HUMAN]	72.48

Accession	Description	Mascot
P47755	F-actin-capping protein subunit alpha-2 OS=Homo sapiens GN=CAPZA2 PE=1 SV=3 - [CAZA2_HUMAN]	72.26
Q9H4A6	Golgi phosphoprotein 3 OS=Homo sapiens GN=GOLPH3 PE=1 SV=1 - [GOLP3_HUMAN]	71.88
P11279	Lysosome-associated membrane glycoprotein 1 OS=Homo sapiens GN=LAMP1 PE=1 SV=3 - [LAMP1_HUMAN]	71.59
Q5JVF3	PCI domain-containing protein 2 OS=Homo sapiens GN=PCID2 PE=1 SV=2 - [PCID2_HUMAN]	71.34
P55084	Trifunctional enzyme subunit beta, mitochondrial OS=Homo sapiens GN=HADHB PE=1 SV=3 - [ECHB_HUMAN]	71.33
Q04917	14-3-3 protein eta OS=Homo sapiens GN=YWHAH PE=1 SV=4 - [1433F_HUMAN]	70.07
Q14697	Neutral alpha-glucosidase AB OS=Homo sapiens GN=GANAB PE=1 SV=3 - [GANAB_HUMAN]	68.55
P06576	ATP synthase subunit beta, mitochondrial OS=Homo sapiens GN=ATP5B PE=1 SV=3 - [ATPB_HUMAN]	68.41
P11586	C-1-tetrahydrofolate synthase, cytoplasmic OS=Homo sapiens GN=MTHFD1 PE=1 SV=3 - [C1TC_HUMAN]	68.37
O00231	26S proteasome non-ATPase regulatory subunit 11 OS=Homo sapiens GN=PSMD11 PE=1 SV=3 - [PSD11_HUMAN]	68.22
P55884	Eukaryotic translation initiation factor 3 subunit B OS=Homo sapiens GN=EIF3B PE=1 SV=3 - [EIF3B_HUMAN]	68.15
P60953	Cell division control protein 42 homolog OS=Homo sapiens GN=CDC42 PE=1 SV=2 - [CDC42_HUMAN]	68.01
P12109	Collagen alpha-1(VI) chain OS=Homo sapiens GN=COL6A1 PE=1 SV=3 - [CO6A1_HUMAN]	66.72
P08727	Keratin, type I cytoskeletal 19 OS=Homo sapiens GN=KRT19 PE=1 SV=4 - [K1C19_HUMAN]	66.45
O60547	GDP-mannose 4,6 dehydratase OS=Homo sapiens GN=GMDS PE=1 SV=1 - [GMDS_HUMAN]	66.1
P01130	Low-density lipoprotein receptor OS=Homo sapiens GN=LDLR PE=1 SV=1 - [LDLR_HUMAN]	65.13
P43358	Melanoma-associated antigen 4 OS=Homo sapiens GN=MAGEA4 PE=1 SV=2 - [MAGA4_HUMAN]	64.05
A4D1P6	WD repeat-containing protein 91 OS=Homo sapiens GN=WDR91 PE=1 SV=2 - [WDR91_HUMAN]	63.97
Q16186	Proteasomal ubiquitin receptor ADRM1 OS=Homo sapiens GN=ADRM1 PE=1 SV=2 - [ADRM1_HUMAN]	63.88
P60510	Serine/threonine-protein phosphatase 4 catalytic subunit OS=Homo sapiens GN=PPP4C PE=1 SV=1 - [PP4C_HUMAN]	63.44
Q15185	Prostaglandin E synthase 3 OS=Homo sapiens GN=PTGES3 PE=1 SV=1 - [TEBP_HUMAN]	63.26
Q9H269	Vacuolar protein sorting-associated protein 16 homolog OS=Homo sapiens GN=VPS16 PE=1 SV=2 - [VPS16_HUMAN]	63.14
Q9UPY3	Endoribonuclease Dicer OS=Homo sapiens GN=DICER1 PE=1 SV=3 - [DICER_HUMAN]	62.67
P35908	Keratin, type II cytoskeletal 2 epidermal OS=Homo sapiens GN=KRT2 PE=1 SV=2 - [K22E_HUMAN]	62.54
Q04837	Single-stranded DNA-binding protein, mitochondrial OS=Homo sapiens GN=SSBP1 PE=1 SV=1 - [SSBP_HUMAN]	62.44
P62333	26S protease regulatory subunit 10B OS=Homo sapiens GN=PSMC6 PE=1 SV=1 - [PRS10_HUMAN]	62.07
P08237	ATP-dependent 6-phosphofructokinase, muscle type OS=Homo sapiens GN=PFKM PE=1 SV=2 - [PFKAM_HUMAN]	61.98
Q15393	Splicing factor 3B subunit 3 OS=Homo sapiens GN=SF3B3 PE=1 SV=4 - [SF3B3_HUMAN]	61.93

Accession	Description	Mascot
P36404	ADP-ribosylation factor-like protein 2 OS=Homo sapiens GN=ARL2 PE=1 SV=4 - [ARL2_HUMAN]	61.69
P49593	Protein phosphatase 1F OS=Homo sapiens GN=PPM1F PE=1 SV=3 - [PPM1F_HUMAN]	61.01
Q13572	Inositol-tetrakisphosphate 1-kinase OS=Homo sapiens GN=ITPK1 PE=1 SV=2 - [ITPK1_HUMAN]	57.59
Q9UK59	Lariat debranching enzyme OS=Homo sapiens GN=DBR1 PE=1 SV=2 - [DBR1_HUMAN]	56.75
P04632	Calpain small subunit 1 OS=Homo sapiens GN=CAPNS1 PE=1 SV=1 - [CPNS1_HUMAN]	55.9
P62316	Small nuclear ribonucleoprotein Sm D2 OS=Homo sapiens GN=SNRPD2 PE=1 SV=1 - [SMD2_HUMAN]	55.83
O43399	Tumor protein D54 OS=Homo sapiens GN=TPD52L2 PE=1 SV=2 - [TPD54_HUMAN]	55.74
P62829	60S ribosomal protein L23 OS=Homo sapiens GN=RPL23 PE=1 SV=1 - [RL23_HUMAN]	55.33
Q9HAV4	Exportin-5 OS=Homo sapiens GN=XPO5 PE=1 SV=1 - [XPO5_HUMAN]	54.67
Q9H4I3	TraB domain-containing protein OS=Homo sapiens GN=TRABD PE=1 SV=1 - [TRABD_HUMAN]	53.83
Q9NQC3	Reticulon-4 OS=Homo sapiens GN=RTN4 PE=1 SV=2 - [RTN4_HUMAN]	53.35
P62805	Histone H4 OS=Homo sapiens GN=HIST1H4A PE=1 SV=2 - [H4_HUMAN]	53.06
Q16531	DNA damage-binding protein 1 OS=Homo sapiens GN=DDB1 PE=1 SV=1 - [DDB1_HUMAN]	53
P62633	Cellular nucleic acid-binding protein OS=Homo sapiens GN=CNBP PE=1 SV=1 - [CNBP_HUMAN]	52.46
P42677	40S ribosomal protein S27 OS=Homo sapiens GN=RPS27 PE=1 SV=3 - [RS27_HUMAN]	52.34
O00487	26S proteasome non-ATPase regulatory subunit 14 OS=Homo sapiens GN=PSMD14 PE=1 SV=1 - [PSDE_HUMAN]	51.67
P49368	T-complex protein 1 subunit gamma OS=Homo sapiens GN=CCT3 PE=1 SV=4 - [TCPG_HUMAN]	51.53
P63010	AP-2 complex subunit beta OS=Homo sapiens GN=AP2B1 PE=1 SV=1 - [AP2B1_HUMAN]	50.85
P51149	Ras-related protein Rab-7a OS=Homo sapiens GN=RAB7A PE=1 SV=1 - [RAB7A_HUMAN]	50.71
O14579	Coatamer subunit epsilon OS=Homo sapiens GN=COPE PE=1 SV=3 - [COPE_HUMAN]	50.49
Q00610	Clathrin heavy chain 1 OS=Homo sapiens GN=CLTC PE=1 SV=5 - [CLH1_HUMAN]	50.31
P27708	CAD protein OS=Homo sapiens GN=CAD PE=1 SV=3 - [PYR1_HUMAN]	49.76
P41091	Eukaryotic translation initiation factor 2 subunit 3 OS=Homo sapiens GN=EIF2S3 PE=1 SV=3 - [IF2G_HUMAN]	49.67
P61221	ATP-binding cassette sub-family E member 1 OS=Homo sapiens GN=ABCE1 PE=1 SV=1 - [ABCE1_HUMAN]	49.51
O60313	Dynamin-like 120 kDa protein, mitochondrial OS=Homo sapiens GN=OPA1 PE=1 SV=3 - [OPA1_HUMAN]	49.33
Q9Y678	Coatamer subunit gamma-1 OS=Homo sapiens GN=COPG1 PE=1 SV=1 - [COPG1_HUMAN]	48.85
Q9NR31	GTP-binding protein SAR1a OS=Homo sapiens GN=SAR1A PE=1 SV=1 - [SAR1A_HUMAN]	48.84
P19623	Spermidine synthase OS=Homo sapiens GN=SRM PE=1 SV=1 - [SPEE_HUMAN]	48.32

Accession	Description	Mascot
Q9NSD9	Phenylalanine--tRNA ligase beta subunit OS=Homo sapiens GN=FARSB PE=1 SV=3 - [SYFB_HUMAN]	47.92
Q13162	Peroxisredoxin-4 OS=Homo sapiens GN=PRDX4 PE=1 SV=1 - [PRDX4_HUMAN]	46.23
P40227	T-complex protein 1 subunit zeta OS=Homo sapiens GN=CCT6A PE=1 SV=3 - [TCPZ_HUMAN]	46.16
P53618	Coatomer subunit beta OS=Homo sapiens GN=COPB1 PE=1 SV=3 - [COPB_HUMAN]	45.37
P42704	Leucine-rich PPR motif-containing protein, mitochondrial OS=Homo sapiens GN=LRPPRC PE=1 SV=3 - [LPPRC_HUMAN]	45.37
P11172	Uridine 5'-monophosphate synthase OS=Homo sapiens GN=UMPS PE=1 SV=1 - [UMPS_HUMAN]	44.93
P60866	40S ribosomal protein S20 OS=Homo sapiens GN=RPS20 PE=1 SV=1 - [RS20_HUMAN]	44.89
O00629	Importin subunit alpha-3 OS=Homo sapiens GN=KPNA4 PE=1 SV=1 - [IMA3_HUMAN]	44.62
Q5VYK3	Proteasome-associated protein ECM29 homolog OS=Homo sapiens GN=ECM29 PE=1 SV=2 - [ECM29_HUMAN]	44.35
P31350	Ribonucleoside-diphosphate reductase subunit M2 OS=Homo sapiens GN=RRM2 PE=1 SV=1 - [RIR2_HUMAN]	44.34
Q9NR19	Acetyl-coenzyme A synthetase, cytoplasmic OS=Homo sapiens GN=ACSS2 PE=1 SV=1 - [ACSA_HUMAN]	44.19
Q9UKV3	Apoptotic chromatin condensation inducer in the nucleus OS=Homo sapiens GN=ACIN1 PE=1 SV=2 - [ACINU_HUMAN]	43.99
Q9Y223	Bifunctional UDP-N-acetylglucosamine 2-epimerase/N-acetylmannosamine kinase OS=Homo sapiens GN=GNE PE=1 SV=1 - [GLCNE_HUMAN]	43.61
Q13263	Transcription intermediary factor 1-beta OS=Homo sapiens GN=TRIM28 PE=1 SV=5 - [TIF1B_HUMAN]	43.47
P62917	60S ribosomal protein L8 OS=Homo sapiens GN=RPL8 PE=1 SV=2 - [RL8_HUMAN]	43.28
Q9NSE4	Isoleucine--tRNA ligase, mitochondrial OS=Homo sapiens GN=IARS2 PE=1 SV=2 - [SYIM_HUMAN]	43.14
P25205	DNA replication licensing factor MCM3 OS=Homo sapiens GN=MCM3 PE=1 SV=3 - [MCM3_HUMAN]	42.94
P13637	Sodium/potassium-transporting ATPase subunit alpha-3 OS=Homo sapiens GN=ATP1A3 PE=1 SV=3 - [AT1A3_HUMAN]	42.8
Q9Y5K5	Ubiquitin carboxyl-terminal hydrolase isozyme L5 OS=Homo sapiens GN=UCHL5 PE=1 SV=3 - [UCHL5_HUMAN]	42.71
Q05655	Protein kinase C delta type OS=Homo sapiens GN=PRKCD PE=1 SV=2 - [KPCD_HUMAN]	42.49
P55036	26S proteasome non-ATPase regulatory subunit 4 OS=Homo sapiens GN=PSMD4 PE=1 SV=1 - [PSMD4_HUMAN]	42.4
P49588	Alanine--tRNA ligase, cytoplasmic OS=Homo sapiens GN=AARS PE=1 SV=2 - [SYAC_HUMAN]	42.12
Q8IYS1	Peptidase M20 domain-containing protein 2 OS=Homo sapiens GN=PM20D2 PE=1 SV=2 - [P20D2_HUMAN]	42.06
O00410	Importin-5 OS=Homo sapiens GN=IPO5 PE=1 SV=4 - [IPO5_HUMAN]	41.67
P98170	E3 ubiquitin-protein ligase XIAP OS=Homo sapiens GN=XIAP PE=1 SV=2 - [XIAP_HUMAN]	41.63
O75436	Vacuolar protein sorting-associated protein 26A OS=Homo sapiens GN=VPS26A PE=1 SV=2 - [VP26A_HUMAN]	41.6
Q13907	Isopentenyl-diphosphate Delta-isomerase 1 OS=Homo sapiens GN=IDI1 PE=1 SV=2 - [IDI1_HUMAN]	41.34

Accession	Description	Mascot
P48556	26S proteasome non-ATPase regulatory subunit 8 OS=Homo sapiens GN=PSMD8 PE=1 SV=2 - [PSMD8_HUMAN]	41.31
Q9BRP4	Proteasomal ATPase-associated factor 1 OS=Homo sapiens GN=PAAF1 PE=1 SV=2 - [PAAF1_HUMAN]	41.19
Q14204	Cytoplasmic dynein 1 heavy chain 1 OS=Homo sapiens GN=DYNC1H1 PE=1 SV=5 - [DYHC1_HUMAN]	40.95
P50416	Carnitine O-palmitoyltransferase 1, liver isoform OS=Homo sapiens GN=CPT1A PE=1 SV=2 - [CPT1A_HUMAN]	40.93
O00505	Importin subunit alpha-4 OS=Homo sapiens GN=KPNA3 PE=1 SV=2 - [IMA4_HUMAN]	40.32
P61923	Coatomer subunit zeta-1 OS=Homo sapiens GN=COPZ1 PE=1 SV=1 - [COPZ1_HUMAN]	40.26
O94808	Glutamine--fructose-6-phosphate aminotransferase [isomerizing] 2 OS=Homo sapiens GN=GFPT2 PE=1 SV=3 - [GFPT2_HUMAN]	40.24
Q8I WV8	E3 ubiquitin-protein ligase UBR2 OS=Homo sapiens GN=UBR2 PE=1 SV=1 - [UBR2_HUMAN]	39.83
O95777	U6 snRNA-associated Sm-like protein LSm8 OS=Homo sapiens GN=LSM8 PE=1 SV=3 - [LSM8_HUMAN]	39.57
Q6NXT2	Histone H3.3C OS=Homo sapiens GN=H3F3C PE=1 SV=3 - [H3C_HUMAN]	39.03
O00232	26S proteasome non-ATPase regulatory subunit 12 OS=Homo sapiens GN=PSMD12 PE=1 SV=3 - [PSD12_HUMAN]	38.99
P09496	Clathrin light chain A OS=Homo sapiens GN=CLTA PE=1 SV=1 - [CLCA_HUMAN]	38.79
Q15738	Sterol-4-alpha-carboxylate 3-dehydrogenase, decarboxylating OS=Homo sapiens GN=NSDHL PE=1 SV=2 - [NSDHL_HUMAN]	38.08
P67775	Serine/threonine-protein phosphatase 2A catalytic subunit alpha isoform OS=Homo sapiens GN=PPP2CA PE=1 SV=1 - [PP2AA_HUMAN]	37.64
Q9UBI6	Guanine nucleotide-binding protein G(I)/G(S)/G(O) subunit gamma-12 OS=Homo sapiens GN=GNG12 PE=1 SV=3 - [GBG12_HUMAN]	37.29
P12110	Collagen alpha-2(VI) chain OS=Homo sapiens GN=COL6A2 PE=1 SV=4 - [CO6A2_HUMAN]	36.98
Q9H7Z7	Prostaglandin E synthase 2 OS=Homo sapiens GN=PTGES2 PE=1 SV=1 - [PGES2_HUMAN]	36.78
O95817	BAG family molecular chaperone regulator 3 OS=Homo sapiens GN=BAG3 PE=1 SV=3 - [BAG3_HUMAN]	36.74
P50570	Dynamin-2 OS=Homo sapiens GN=DNM2 PE=1 SV=2 - [DYN2_HUMAN]	36.69
P48643	T-complex protein 1 subunit epsilon OS=Homo sapiens GN=CCT5 PE=1 SV=1 - [TCPE_HUMAN]	36.57
P47756	F-actin-capping protein subunit beta OS=Homo sapiens GN=CAPZB PE=1 SV=4 - [CAPZB_HUMAN]	36.24
P27824	Calnexin OS=Homo sapiens GN=CANX PE=1 SV=2 - [CALX_HUMAN]	36.14
P14209	CD99 antigen OS=Homo sapiens GN=CD99 PE=1 SV=1 - [CD99_HUMAN]	35.75
Q9NY27	Serine/threonine-protein phosphatase 4 regulatory subunit 2 OS=Homo sapiens GN=PPP4R2 PE=1 SV=3 - [PP4R2_HUMAN]	35.67
Q2TAZ0	Autophagy-related protein 2 homolog A OS=Homo sapiens GN=ATG2A PE=1 SV=3 - [ATG2A_HUMAN]	35.47
Q9UBB4	Ataxin-10 OS=Homo sapiens GN=ATXN10 PE=1 SV=1 - [ATX10_HUMAN]	35.16

Accession	Description	Mascot
P06737	Glycogen phosphorylase, liver form OS=Homo sapiens GN=PYGL PE=1 SV=4 - [PYGL_HUMAN]	35.08
Q32P28	Prolyl 3-hydroxylase 1 OS=Homo sapiens GN=P3H1 PE=1 SV=2 - [P3H1_HUMAN]	35
Q9NZR2	Low-density lipoprotein receptor-related protein 1B OS=Homo sapiens GN=LRP1B PE=1 SV=2 - [LRP1B_HUMAN]	34.98
Q6PIU2	Neutral cholesterol ester hydrolase 1 OS=Homo sapiens GN=NCEH1 PE=1 SV=3 - [NCEH1_HUMAN]	34.83
P05362	Intercellular adhesion molecule 1 OS=Homo sapiens GN=ICAM1 PE=1 SV=2 - [ICAM1_HUMAN]	34.76
O75306	NADH dehydrogenase [ubiquinone] iron-sulfur protein 2, mitochondrial OS=Homo sapiens GN=NDUFS2 PE=1 SV=2 - [NDUS2_HUMAN]	34.66
P32004	Neural cell adhesion molecule L1 OS=Homo sapiens GN=L1CAM PE=1 SV=2 - [L1CAM_HUMAN]	34.32
Q8TC07	TBC1 domain family member 15 OS=Homo sapiens GN=TBC1D15 PE=1 SV=2 - [TBC15_HUMAN]	33.96
Q16850	Lanosterol 14-alpha demethylase OS=Homo sapiens GN=CYP51A1 PE=1 SV=3 - [CP51A_HUMAN]	33.93
Q7L1Q6	Basic leucine zipper and W2 domain-containing protein 1 OS=Homo sapiens GN=BZW1 PE=1 SV=1 - [BZW1_HUMAN]	33.87
Q8TC12	Retinol dehydrogenase 11 OS=Homo sapiens GN=RDH11 PE=1 SV=2 - [RDH11_HUMAN]	33.33
Q9UNH7	Sorting nexin-6 OS=Homo sapiens GN=SNX6 PE=1 SV=1 - [SNX6_HUMAN]	33.09
Q92616	Translational activator GCN1 OS=Homo sapiens GN=GCN1L1 PE=1 SV=6 - [GCN1L_HUMAN]	32.94
Q9NXR7	BRCA1-A complex subunit BRE OS=Homo sapiens GN=BRE PE=1 SV=2 - [BRE_HUMAN]	32.6
P12111	Collagen alpha-3(VI) chain OS=Homo sapiens GN=COL6A3 PE=1 SV=5 - [CO6A3_HUMAN]	32.58
P15880	40S ribosomal protein S2 OS=Homo sapiens GN=RPS2 PE=1 SV=2 - [RS2_HUMAN]	32.42
O43852	Calumenin OS=Homo sapiens GN=CALU PE=1 SV=2 - [CALU_HUMAN]	32.38
Q969Z0	Protein TBRG4 OS=Homo sapiens GN=TBRG4 PE=1 SV=1 - [TBRG4_HUMAN]	32.05
O75496	Geminin OS=Homo sapiens GN=GMNN PE=1 SV=1 - [GEMI_HUMAN]	30.96
Q9BPW8	Protein NipSnap homolog 1 OS=Homo sapiens GN=NIPSNAP1 PE=1 SV=1 - [NIPS1_HUMAN]	30.87
O43681	ATPase ASNA1 OS=Homo sapiens GN=ASNA1 PE=1 SV=2 - [ASNA_HUMAN]	30.82
Q8WY22	BRI3-binding protein OS=Homo sapiens GN=BRI3BP PE=1 SV=1 - [BRI3B_HUMAN]	30.71
Q13085	Acetyl-CoA carboxylase 1 OS=Homo sapiens GN=ACACA PE=1 SV=2 - [ACACA_HUMAN]	30.5
P01374	Lymphotoxin-alpha OS=Homo sapiens GN=LTA PE=1 SV=2 - [TNFB_HUMAN]	30.08
P31943	Heterogeneous nuclear ribonucleoprotein H OS=Homo sapiens GN=HNRNPH1 PE=1 SV=4 - [HNRH1_HUMAN]	30.07
Q9Y333	U6 snRNA-associated Sm-like protein LSm2 OS=Homo sapiens GN=LSM2 PE=1 SV=1 - [LSM2_HUMAN]	30.01
Q15008	26S proteasome non-ATPase regulatory subunit 6 OS=Homo sapiens GN=PSMD6 PE=1 SV=1 - [PSMD6_HUMAN]	29.85
P62249	40S ribosomal protein S16 OS=Homo sapiens GN=RPS16 PE=1 SV=2 - [RS16_HUMAN]	29.62

Accession	Description	Mascot
P11498	Pyruvate carboxylase, mitochondrial OS=Homo sapiens GN=PC PE=1 SV=2 - [PYC_HUMAN]	29.61
P50990	T-complex protein 1 subunit theta OS=Homo sapiens GN=CCT8 PE=1 SV=4 - [TCPQ_HUMAN]	29.5
Q9H3P7	Golgi resident protein GCP60 OS=Homo sapiens GN=ACBD3 PE=1 SV=4 - [GCP60_HUMAN]	29.39
Q8TF72	Protein Shroom3 OS=Homo sapiens GN=SHROOM3 PE=1 SV=2 - [SHRM3_HUMAN]	29.33
Q9Y243	RAC-gamma serine/threonine-protein kinase OS=Homo sapiens GN=AKT3 PE=1 SV=1 - [AKT3_HUMAN]	29.26
Q8WTV0	Scavenger receptor class B member 1 OS=Homo sapiens GN=SCARB1 PE=1 SV=1 - [SCRB1_HUMAN]	29.05
P51808	Dynein light chain Tctex-type 3 OS=Homo sapiens GN=DYNLT3 PE=1 SV=1 - [DYLT3_HUMAN]	28.93
Q9Y6E2	Basic leucine zipper and W2 domain-containing protein 2 OS=Homo sapiens GN=BZW2 PE=1 SV=1 - [BZW2_HUMAN]	28.92
Q17RC7	Exocyst complex component 3-like protein 4 OS=Homo sapiens GN=EXOC3L4 PE=1 SV=2 - [EX3L4_HUMAN]	28.28
Q15181	Inorganic pyrophosphatase OS=Homo sapiens GN=PPA1 PE=1 SV=2 - [IPYR_HUMAN]	28.14
Q9UNM6	26S proteasome non-ATPase regulatory subunit 13 OS=Homo sapiens GN=PSMD13 PE=1 SV=2 - [PSD13_HUMAN]	28.12
O60814	Histone H2B type 1-K OS=Homo sapiens GN=HIST1H2BK PE=1 SV=3 - [H2B1K_HUMAN]	27.84
O95394	Phosphoacetylglucosamine mutase OS=Homo sapiens GN=PGM3 PE=1 SV=1 - [AGM1_HUMAN]	27.8
Q15365	Poly(rC)-binding protein 1 OS=Homo sapiens GN=PCBP1 PE=1 SV=2 - [PCBP1_HUMAN]	27.1
P63173	60S ribosomal protein L38 OS=Homo sapiens GN=RPL38 PE=1 SV=2 - [RL38_HUMAN]	26.88
Q9HDC9	Adipocyte plasma membrane-associated protein OS=Homo sapiens GN=APMAP PE=1 SV=2 - [APMAP_HUMAN]	26.77
P55039	Developmentally-regulated GTP-binding protein 2 OS=Homo sapiens GN=DRG2 PE=1 SV=1 - [DRG2_HUMAN]	26.72
O60437	Periplakin OS=Homo sapiens GN=PPL PE=1 SV=4 - [PEPL_HUMAN]	26.56
O75915	PRA1 family protein 3 OS=Homo sapiens GN=ARL6IP5 PE=1 SV=1 - [PRAF3_HUMAN]	26.42
P62877	E3 ubiquitin-protein ligase RBX1 OS=Homo sapiens GN=RBX1 PE=1 SV=1 - [RBX1_HUMAN]	26
O75052	Carboxyl-terminal PDZ ligand of neuronal nitric oxide synthase protein OS=Homo sapiens GN=NOS1AP PE=1 SV=3 - [CAPON_HUMAN]	25.91
Q2KHT3	Protein CLEC16A OS=Homo sapiens GN=CLEC16A PE=2 SV=2 - [CL16A_HUMAN]	25.44
Q9UJY1	Heat shock protein beta-8 OS=Homo sapiens GN=HSPB8 PE=1 SV=1 - [HSPB8_HUMAN]	24.14
O14744	Protein arginine N-methyltransferase 5 OS=Homo sapiens GN=PRMT5 PE=1 SV=4 - [ANM5_HUMAN]	24.03
P43246	DNA mismatch repair protein Msh2 OS=Homo sapiens GN=MSH2 PE=1 SV=1 - [MSH2_HUMAN]	24.02
P13984	General transcription factor IIF subunit 2 OS=Homo sapiens GN=GTF2F2 PE=1 SV=2 - [T2FB_HUMAN]	23.27
Q86WU2	Probable D-lactate dehydrogenase, mitochondrial OS=Homo sapiens GN=LDHD PE=1 SV=1 - [LDHD_HUMAN]	22.54
P30622	CAP-Gly domain-containing linker protein 1 OS=Homo sapiens GN=CLIP1 PE=1 SV=2 - [CLIP1_HUMAN]	22.52

Accession	Description	Mascot
P28065	Proteasome subunit beta type-9 OS=Homo sapiens GN=PSMB9 PE=1 SV=2 - [PSB9_HUMAN]	22.2
Q9BVC6	Transmembrane protein 109 OS=Homo sapiens GN=TMEM109 PE=1 SV=1 - [TM109_HUMAN]	22.03
Q96BN8	Ubiquitin thioesterase otulin OS=Homo sapiens GN=OTULIN PE=1 SV=3 - [OTUL_HUMAN]	20.15
Q96B36	Proline-rich AKT1 substrate 1 OS=Homo sapiens GN=AKT1S1 PE=1 SV=1 - [AKTS1_HUMAN]	18.9

Appendix II

Mass spectrometry analysis results for activity 2

The most active fraction from the final ion exchange (Mono Q) chromatography step, fraction 21 (5.3.3.2.2) for activity 2, was analysed by mass spectrometry by Dr Deborah M Simpson (Centre for Proteasome Research, University of Liverpool) to identify candidate E3 ubiquitin ligases and/or chromatin remodellers. The full list of proteins identified is shown below in descending order of mascot score.

Accession	Description	Mascot
P19338	Nucleolin OS=Homo sapiens GN=NCL PE=1 SV=3 - [NUCL_HUMAN]	2355.74
O00267	Transcription elongation factor SPT5 OS=Homo sapiens GN=SUPT5H PE=1 SV=1 - [SPT5H_HUMAN]	1699.3
O15355	Protein phosphatase 1G OS=Homo sapiens GN=PPM1G PE=1 SV=1 - [PPM1G_HUMAN]	1581.25
Q7KZ85	Transcription elongation factor SPT6 OS=Homo sapiens GN=SUPT6H PE=1 SV=2 - [SPT6H_HUMAN]	1445.85
P49792	E3 SUMO-protein ligase RanBP2 OS=Homo sapiens GN=RANBP2 PE=1 SV=2 - [RBP2_HUMAN]	1138.41
Q7Z6Z7	E3 ubiquitin-protein ligase HUWE1 OS=Homo sapiens GN=HUWE1 PE=1 SV=3 - [HUWE1_HUMAN]	1040.56
P31327	Carbamoyl-phosphate synthase [ammonia], mitochondrial OS=Homo sapiens GN=CPS1 PE=1 SV=2 - [CPSM_HUMAN]	891.5
P07437	Tubulin beta chain OS=Homo sapiens GN=TUBB PE=1 SV=2 - [TBB5_HUMAN]	831.35
P68371	Tubulin beta-4B chain OS=Homo sapiens GN=TUBB4B PE=1 SV=1 - [TBB4B_HUMAN]	760.53
O43847	Nardilysin OS=Homo sapiens GN=NRD1 PE=1 SV=2 - [NRDC_HUMAN]	739.28
P55072	Transitional endoplasmic reticulum ATPase OS=Homo sapiens GN=VCP PE=1 SV=4 - [TERA_HUMAN]	736.18
Q9UNZ2	NSFL1 cofactor p47 OS=Homo sapiens GN=NSFL1C PE=1 SV=2 - [NSF1C_HUMAN]	728.8
P11021	78 kDa glucose-regulated protein OS=Homo sapiens GN=HSPA5 PE=1 SV=2 - [GRP78_HUMAN]	716.35
O43719	HIV Tat-specific factor 1 OS=Homo sapiens GN=HTATSF1 PE=1 SV=1 - [HTSF1_HUMAN]	702.56
P53621	Coatomer subunit alpha OS=Homo sapiens GN=COPA PE=1 SV=2 - [COPA_HUMAN]	688.71
Q13885	Tubulin beta-2A chain OS=Homo sapiens GN=TUBB2A PE=1 SV=1 - [TBB2A_HUMAN]	664.12
P29692	Elongation factor 1-delta OS=Homo sapiens GN=EEF1D PE=1 SV=5 - [EF1D_HUMAN]	645.89

Accession	Description	Mascot
Q9Y230	RuvB-like 2 OS=Homo sapiens GN=RUVBL2 PE=1 SV=3 - [RUVB2_HUMAN]	636.63
Q9Y4B6	Protein VPRBP OS=Homo sapiens GN=VPRBP PE=1 SV=3 - [VPRBP_HUMAN]	592.64
P11142	Heat shock cognate 71 kDa protein OS=Homo sapiens GN=HSPA8 PE=1 SV=1 - [HSP7C_HUMAN]	561
P26641	Elongation factor 1-gamma OS=Homo sapiens GN=EEF1G PE=1 SV=3 - [EF1G_HUMAN]	550.42
P0DMV9	Heat shock 70 kDa protein 1B OS=Homo sapiens GN=HSPA1B PE=1 SV=1 - [HS71B_HUMAN]	550.38
P46060	Ran GTPase-activating protein 1 OS=Homo sapiens GN=RANGAP1 PE=1 SV=1 - [RAGP1_HUMAN]	548.77
Q07021	Complement component 1 Q subcomponent-binding protein, mitochondrial OS=Homo sapiens GN=C1QBP PE=1 SV=1 - [C1QBP_HUMAN]	547.78
P35606	Coatomer subunit beta' OS=Homo sapiens GN=COPB2 PE=1 SV=2 - [COPB2_HUMAN]	541.06
P60709	Actin, cytoplasmic 1 OS=Homo sapiens GN=ACTB PE=1 SV=1 - [ACTB_HUMAN]	523.49
P06733	Alpha-enolase OS=Homo sapiens GN=ENO1 PE=1 SV=2 - [ENOA_HUMAN]	506.97
P14625	Endoplasmic reticulum chaperone protein OS=Homo sapiens GN=HSP90B1 PE=1 SV=1 - [ENPL_HUMAN]	487.15
P68366	Tubulin alpha-4A chain OS=Homo sapiens GN=TUBA4A PE=1 SV=1 - [TBA4A_HUMAN]	487.14
Q71U36	Tubulin alpha-1A chain OS=Homo sapiens GN=TUBA1A PE=1 SV=1 - [TBA1A_HUMAN]	486.26
P05455	Lupus La protein OS=Homo sapiens GN=SSB PE=1 SV=2 - [LA_HUMAN]	465.37
P14314	Glucosidase 2 subunit beta OS=Homo sapiens GN=PRKCSH PE=1 SV=2 - [GLU2B_HUMAN]	433.44
Q9BUF5	Tubulin beta-6 chain OS=Homo sapiens GN=TUBB6 PE=1 SV=1 - [TBB6_HUMAN]	425.06
P25705	ATP synthase subunit alpha, mitochondrial OS=Homo sapiens GN=ATP5A1 PE=1 SV=1 - [ATPA_HUMAN]	408.35
Q9Y678	Coatomer subunit gamma-1 OS=Homo sapiens GN=COPG1 PE=1 SV=1 - [COPG1_HUMAN]	407.45
Q14697	Neutral alpha-glucosidase AB OS=Homo sapiens GN=GANAB PE=1 SV=3 - [GANAB_HUMAN]	406.11
P49411	Elongation factor Tu, mitochondrial OS=Homo sapiens GN=TUFM PE=1 SV=2 - [EFTU_HUMAN]	401.08
Q99733	Nucleosome assembly protein 1-like 4 OS=Homo sapiens GN=NAP1L4 PE=1 SV=1 - [NP1L4_HUMAN]	392.59
P08238	Heat shock protein HSP 90-beta OS=Homo sapiens GN=HSP90AB1 PE=1 SV=4 - [HS90B_HUMAN]	378.52
P48444	Coatomer subunit delta OS=Homo sapiens GN=ARCN1 PE=1 SV=1 - [COPD_HUMAN]	376.42
P52292	Importin subunit alpha-1 OS=Homo sapiens GN=KPNA2 PE=1 SV=1 - [IMA1_HUMAN]	349.11
P24534	Elongation factor 1-beta OS=Homo sapiens GN=EEF1B2 PE=1 SV=3 - [EF1B_HUMAN]	340.94
P38646	Stress-70 protein, mitochondrial OS=Homo sapiens GN=HSPA9 PE=1 SV=2 - [GRP75_HUMAN]	337.51
P07900	Heat shock protein HSP 90-alpha OS=Homo sapiens GN=HSP90AA1 PE=1 SV=5 - [HS90A_HUMAN]	311.22
P33993	DNA replication licensing factor MCM7 OS=Homo sapiens GN=MCM7 PE=1 SV=4 - [MCM7_HUMAN]	306.52

Accession	Description	Mascot
P02786	Transferrin receptor protein 1 OS=Homo sapiens GN=TFRC PE=1 SV=2 - [TFR1_HUMAN]	302.96
P35998	26S protease regulatory subunit 7 OS=Homo sapiens GN=PSMC2 PE=1 SV=3 - [PRS7_HUMAN]	296.87
P55209	Nucleosome assembly protein 1-like 1 OS=Homo sapiens GN=NAP1L1 PE=1 SV=1 - [NP1L1_HUMAN]	292.32
P27797	Calreticulin OS=Homo sapiens GN=CALR PE=1 SV=1 - [CALR_HUMAN]	271.02
P06748	Nucleophosmin OS=Homo sapiens GN=NPM1 PE=1 SV=2 - [NPM_HUMAN]	268.73
P63104	14-3-3 protein zeta/delta OS=Homo sapiens GN=YWHAZ PE=1 SV=1 - [1433Z_HUMAN]	264.06
P13489	Ribonuclease inhibitor OS=Homo sapiens GN=RNH1 PE=1 SV=2 - [RINI_HUMAN]	258.97
Q9H3U1	Protein unc-45 homolog A OS=Homo sapiens GN=UNC45A PE=1 SV=1 - [UN45A_HUMAN]	255.96
Q13200	26S proteasome non-ATPase regulatory subunit 2 OS=Homo sapiens GN=PSMD2 PE=1 SV=3 - [PSMD2_HUMAN]	255.04
Q9Y265	RuvB-like 1 OS=Homo sapiens GN=RUVBL1 PE=1 SV=1 - [RUVB1_HUMAN]	243.98
Q86VP6	Cullin-associated NEDD8-dissociated protein 1 OS=Homo sapiens GN=CAND1 PE=1 SV=2 - [CAND1_HUMAN]	241.09
Q8IYB7	DIS3-like exonuclease 2 OS=Homo sapiens GN=DIS3L2 PE=1 SV=4 - [DI3L2_HUMAN]	236.34
P55786	Puromycin-sensitive aminopeptidase OS=Homo sapiens GN=NPEPPS PE=1 SV=2 - [PSA_HUMAN]	230.5
P23396	40S ribosomal protein S3 OS=Homo sapiens GN=RPS3 PE=1 SV=2 - [RS3_HUMAN]	228.54
Q07020	60S ribosomal protein L18 OS=Homo sapiens GN=RPL18 PE=1 SV=2 - [RL18_HUMAN]	213.54
O00410	Importin-5 OS=Homo sapiens GN=IPO5 PE=1 SV=4 - [IPO5_HUMAN]	212.17
O00148	ATP-dependent RNA helicase DDX39A OS=Homo sapiens GN=DDX39A PE=1 SV=2 - [DX39A_HUMAN]	207.91
Q9Y4X5	E3 ubiquitin-protein ligase ARIH1 OS=Homo sapiens GN=ARIH1 PE=1 SV=2 - [ARI1_HUMAN]	203.5
Q00839	Heterogeneous nuclear ribonucleoprotein U OS=Homo sapiens GN=HNRNPU PE=1 SV=6 - [HNRPU_HUMAN]	202.94
P48449	Lanosterol synthase OS=Homo sapiens GN=LSS PE=1 SV=1 - [ERG7_HUMAN]	200.39
P47712	Cytosolic phospholipase A2 OS=Homo sapiens GN=PLA2G4A PE=1 SV=2 - [PA24A_HUMAN]	199.41
P67809	Nuclease-sensitive element-binding protein 1 OS=Homo sapiens GN=YBX1 PE=1 SV=3 - [YBOX1_HUMAN]	199.23
Q14974	Importin subunit beta-1 OS=Homo sapiens GN=KPNB1 PE=1 SV=2 - [IMB1_HUMAN]	193.35
P04264	Keratin, type II cytoskeletal 1 OS=Homo sapiens GN=KRT1 PE=1 SV=6 - [K2C1_HUMAN]	192.52
P62195	26S protease regulatory subunit 8 OS=Homo sapiens GN=PSMC5 PE=1 SV=1 - [PRS8_HUMAN]	191.03
P84098	60S ribosomal protein L19 OS=Homo sapiens GN=RPL19 PE=1 SV=1 - [RL19_HUMAN]	190.56
P30876	DNA-directed RNA polymerase II subunit RPB2 OS=Homo sapiens GN=POLR2B PE=1 SV=1 - [RPB2_HUMAN]	186.46
P62826	GTP-binding nuclear protein Ran OS=Homo sapiens GN=RAN PE=1 SV=3 - [RAN_HUMAN]	184.57

Accession	Description	Mascot
Q9BW61	DET1- and DDB1-associated protein 1 OS=Homo sapiens GN=DDA1 PE=1 SV=1 - [DDA1_HUMAN]	184.02
Q01813	ATP-dependent 6-phosphofructokinase, platelet type OS=Homo sapiens GN=PFBP PE=1 SV=2 - [PFBP_HUMAN]	182.64
O60884	DnaJ homolog subfamily A member 2 OS=Homo sapiens GN=DNAJA2 PE=1 SV=1 - [DNAJA2_HUMAN]	180.11
P10809	60 kDa heat shock protein, mitochondrial OS=Homo sapiens GN=HSPD1 PE=1 SV=2 - [CH60_HUMAN]	178.27
Q14204	Cytoplasmic dynein 1 heavy chain 1 OS=Homo sapiens GN=DYNC1H1 PE=1 SV=5 - [DYHC1_HUMAN]	170.64
P31946	14-3-3 protein beta/alpha OS=Homo sapiens GN=YWHAB PE=1 SV=3 - [1433B_HUMAN]	168.78
Q16531	DNA damage-binding protein 1 OS=Homo sapiens GN=DDB1 PE=1 SV=1 - [DDB1_HUMAN]	167.4
Q8IX15	Homeobox and leucine zipper protein Homez OS=Homo sapiens GN=HOMEZ PE=1 SV=2 - [HOMEZ_HUMAN]	167.33
P49327	Fatty acid synthase OS=Homo sapiens GN=FASN PE=1 SV=3 - [FAS_HUMAN]	164.37
Q01130	Serine/arginine-rich splicing factor 2 OS=Homo sapiens GN=SRSF2 PE=1 SV=4 - [SRSF2_HUMAN]	164.18
P31153	S-adenosylmethionine synthase isoform type-2 OS=Homo sapiens GN=MAT2A PE=1 SV=1 - [METK2_HUMAN]	155.37
Q9HAV4	Exportin-5 OS=Homo sapiens GN=XPO5 PE=1 SV=1 - [XPO5_HUMAN]	153.96
Q5TA31	E3 ubiquitin-protein ligase RNF187 OS=Homo sapiens GN=RNF187 PE=1 SV=2 - [RN187_HUMAN]	153.24
P17812	CTP synthase 1 OS=Homo sapiens GN=CTPS1 PE=1 SV=2 - [PYRG1_HUMAN]	152.16
P31689	DnaJ homolog subfamily A member 1 OS=Homo sapiens GN=DNAJA1 PE=1 SV=2 - [DNAJA1_HUMAN]	150.81
O00629	Importin subunit alpha-3 OS=Homo sapiens GN=KPNA4 PE=1 SV=1 - [IMA3_HUMAN]	147.29
P61923	Coatomer subunit zeta-1 OS=Homo sapiens GN=COPZ1 PE=1 SV=1 - [COPZ1_HUMAN]	144.22
P12270	Nucleoprotein TPR OS=Homo sapiens GN=TPR PE=1 SV=3 - [TPR_HUMAN]	142.18
P55060	Exportin-2 OS=Homo sapiens GN=CSE1L PE=1 SV=3 - [XPO2_HUMAN]	141
O95373	Importin-7 OS=Homo sapiens GN=IPO7 PE=1 SV=1 - [IPO7_HUMAN]	140.76
P17980	26S protease regulatory subunit 6A OS=Homo sapiens GN=PSMC3 PE=1 SV=3 - [PRS6A_HUMAN]	140.38
P27348	14-3-3 protein theta OS=Homo sapiens GN=YWHAQ PE=1 SV=1 - [1433T_HUMAN]	139.89
O14579	Coatomer subunit epsilon OS=Homo sapiens GN=COPE PE=1 SV=3 - [COPE_HUMAN]	136.25
Q9UIA9	Exportin-7 OS=Homo sapiens GN=XPO7 PE=1 SV=3 - [XPO7_HUMAN]	135.43
P26373	60S ribosomal protein L13 OS=Homo sapiens GN=RPL13 PE=1 SV=4 - [RL13_HUMAN]	135.39
P46779	60S ribosomal protein L28 OS=Homo sapiens GN=RPL28 PE=1 SV=3 - [RL28_HUMAN]	134.96
P68104	Elongation factor 1-alpha 1 OS=Homo sapiens GN=EEF1A1 PE=1 SV=1 - [EF1A1_HUMAN]	133.94
P62191	26S protease regulatory subunit 4 OS=Homo sapiens GN=PSMC1 PE=1 SV=1 - [PRS4_HUMAN]	131.53

Accession	Description	Mascot
P13639	Elongation factor 2 OS=Homo sapiens GN=EEF2 PE=1 SV=4 - [EF2_HUMAN]	131.18
P01891	HLA class I histocompatibility antigen, A-68 alpha chain OS=Homo sapiens GN=HLA-A PE=1 SV=4 - [1A68_HUMAN]	129.98
O60684	Importin subunit alpha-7 OS=Homo sapiens GN=KPNA6 PE=1 SV=1 - [IMA7_HUMAN]	128.09
P41091	Eukaryotic translation initiation factor 2 subunit 3 OS=Homo sapiens GN=EIF2S3 PE=1 SV=3 - [IF2G_HUMAN]	125.57
P53618	Coatomer subunit beta OS=Homo sapiens GN=COPB1 PE=1 SV=3 - [COPB_HUMAN]	125.01
P52294	Importin subunit alpha-5 OS=Homo sapiens GN=KPNA1 PE=1 SV=3 - [IMA5_HUMAN]	124.29
P62263	40S ribosomal protein S14 OS=Homo sapiens GN=RPS14 PE=1 SV=3 - [RS14_HUMAN]	124
Q99460	26S proteasome non-ATPase regulatory subunit 1 OS=Homo sapiens GN=PSMD1 PE=1 SV=2 - [PSMD1_HUMAN]	123.91
P63165	Small ubiquitin-related modifier 1 OS=Homo sapiens GN=SUMO1 PE=1 SV=1 - [SUMO1_HUMAN]	123.56
Q9BQA1	Methylosome protein 50 OS=Homo sapiens GN=WDR77 PE=1 SV=1 - [MEP50_HUMAN]	122.68
P42677	40S ribosomal protein S27 OS=Homo sapiens GN=RPS27 PE=1 SV=3 - [RS27_HUMAN]	120.25
P10155	60 kDa SS-A/Ro ribonucleoprotein OS=Homo sapiens GN=TROVE2 PE=1 SV=2 - [RO60_HUMAN]	119.32
P08134	Rho-related GTP-binding protein RhoC OS=Homo sapiens GN=RHOC PE=1 SV=1 - [RHOC_HUMAN]	119.07
P55084	Trifunctional enzyme subunit beta, mitochondrial OS=Homo sapiens GN=HADHB PE=1 SV=3 - [ECHB_HUMAN]	118.75
P04792	Heat shock protein beta-1 OS=Homo sapiens GN=HSPB1 PE=1 SV=2 - [HSPB1_HUMAN]	117.15
P00367	Glutamate dehydrogenase 1, mitochondrial OS=Homo sapiens GN=GLUD1 PE=1 SV=2 - [DHE3_HUMAN]	116.77
P35527	Keratin, type I cytoskeletal 9 OS=Homo sapiens GN=KRT9 PE=1 SV=3 - [K1C9_HUMAN]	116.19
P12004	Proliferating cell nuclear antigen OS=Homo sapiens GN=PCNA PE=1 SV=1 - [PCNA_HUMAN]	114.14
P78318	Immunoglobulin-binding protein 1 OS=Homo sapiens GN=IGBP1 PE=1 SV=1 - [IGBP1_HUMAN]	112.67
P61981	14-3-3 protein gamma OS=Homo sapiens GN=YWHAG PE=1 SV=2 - [1433G_HUMAN]	111.41
Q02543	60S ribosomal protein L18a OS=Homo sapiens GN=RPL18A PE=1 SV=2 - [RL18A_HUMAN]	108.93
Q13263	Transcription intermediary factor 1-beta OS=Homo sapiens GN=TRIM28 PE=1 SV=5 - [TIF1B_HUMAN]	105.94
P40939	Trifunctional enzyme subunit alpha, mitochondrial OS=Homo sapiens GN=HADHA PE=1 SV=2 - [ECHA_HUMAN]	104
P14324	Farnesyl pyrophosphate synthase OS=Homo sapiens GN=FDPS PE=1 SV=4 - [FPPS_HUMAN]	103.23
P60900	Proteasome subunit alpha type-6 OS=Homo sapiens GN=PSMA6 PE=1 SV=1 - [PSA6_HUMAN]	101.65
O00505	Importin subunit alpha-4 OS=Homo sapiens GN=KPNA3 PE=1 SV=2 - [IMA4_HUMAN]	101.12
P62306	Small nuclear ribonucleoprotein F OS=Homo sapiens GN=SNRPF PE=1 SV=1 - [RUXF_HUMAN]	101.12
P61586	Transforming protein RhoA OS=Homo sapiens GN=RHOA PE=1 SV=1 - [RHOA_HUMAN]	99.23

Accession	Description	Mascot
O60664	Perilipin-3 OS=Homo sapiens GN=PLIN3 PE=1 SV=3 - [PLIN3_HUMAN]	98.61
P25788	Proteasome subunit alpha type-3 OS=Homo sapiens GN=PSMA3 PE=1 SV=2 - [PSA3_HUMAN]	97.6
P11940	Polyadenylate-binding protein 1 OS=Homo sapiens GN=PABPC1 PE=1 SV=2 - [PABP1_HUMAN]	96.98
P39023	60S ribosomal protein L3 OS=Homo sapiens GN=RPL3 PE=1 SV=2 - [RL3_HUMAN]	96.83
P62316	Small nuclear ribonucleoprotein Sm D2 OS=Homo sapiens GN=SNRPD2 PE=1 SV=1 - [SMD2_HUMAN]	96.57
P35613	Basigin OS=Homo sapiens GN=BSG PE=1 SV=2 - [BASI_HUMAN]	95.44
Q5JVF3	PCI domain-containing protein 2 OS=Homo sapiens GN=PCID2 PE=1 SV=2 - [PCID2_HUMAN]	95.29
Q6IN85	Serine/threonine-protein phosphatase 4 regulatory subunit 3A OS=Homo sapiens GN=PPP4R3A PE=1 SV=1 - [P4R3A_HUMAN]	95.24
P42704	Leucine-rich PPR motif-containing protein, mitochondrial OS=Homo sapiens GN=LRPPRC PE=1 SV=3 - [LPPRC_HUMAN]	93.66
O60841	Eukaryotic translation initiation factor 5B OS=Homo sapiens GN=EIF5B PE=1 SV=4 - [IF2P_HUMAN]	93.54
O14744	Protein arginine N-methyltransferase 5 OS=Homo sapiens GN=PRMT5 PE=1 SV=4 - [ANM5_HUMAN]	93.09
P62491	Ras-related protein Rab-11A OS=Homo sapiens GN=RAB11A PE=1 SV=3 - [RB11A_HUMAN]	93.08
Q04917	14-3-3 protein eta OS=Homo sapiens GN=YWHAH PE=1 SV=4 - [1433F_HUMAN]	92.7
P49588	Alanine--tRNA ligase, cytoplasmic OS=Homo sapiens GN=AARS PE=1 SV=2 - [SYAC_HUMAN]	91.4
P38606	V-type proton ATPase catalytic subunit A OS=Homo sapiens GN=ATP6V1A PE=1 SV=2 - [VATA_HUMAN]	90.66
P36578	60S ribosomal protein L4 OS=Homo sapiens GN=RPL4 PE=1 SV=5 - [RL4_HUMAN]	89.68
Q9NVJ2	ADP-ribosylation factor-like protein 8B OS=Homo sapiens GN=ARL8B PE=1 SV=1 - [ARL8B_HUMAN]	89.48
P09661	U2 small nuclear ribonucleoprotein A' OS=Homo sapiens GN=SNRPA1 PE=1 SV=2 - [RU2A_HUMAN]	89.28
O95816	BAG family molecular chaperone regulator 2 OS=Homo sapiens GN=BAG2 PE=1 SV=1 - [BAG2_HUMAN]	89.09
P62424	60S ribosomal protein L7a OS=Homo sapiens GN=RPL7A PE=1 SV=2 - [RL7A_HUMAN]	88.53
P01111	GTPase NRas OS=Homo sapiens GN=NRAS PE=1 SV=1 - [RASN_HUMAN]	88.06
P14678	Small nuclear ribonucleoprotein-associated proteins B and B' OS=Homo sapiens GN=SNRPB PE=1 SV=2 - [RSMB_HUMAN]	87.63
Q15645	Pachytene checkpoint protein 2 homolog OS=Homo sapiens GN=TRIP13 PE=1 SV=2 - [PCH2_HUMAN]	87.37
P62269	40S ribosomal protein S18 OS=Homo sapiens GN=RPS18 PE=1 SV=3 - [RS18_HUMAN]	86.99
P62258	14-3-3 protein epsilon OS=Homo sapiens GN=YWHAE PE=1 SV=1 - [1433E_HUMAN]	86.31
Q99832	T-complex protein 1 subunit eta OS=Homo sapiens GN=CCT7 PE=1 SV=2 - [TCPH_HUMAN]	85.87
P43686	26S protease regulatory subunit 6B OS=Homo sapiens GN=PSMC4 PE=1 SV=2 - [PRS6B_HUMAN]	85.42

Accession	Description	Mascot
P61026	Ras-related protein Rab-10 OS=Homo sapiens GN=RAB10 PE=1 SV=1 - [RAB10_HUMAN]	85.29
P46783	40S ribosomal protein S10 OS=Homo sapiens GN=RPS10 PE=1 SV=1 - [RS10_HUMAN]	85.28
P63272	Transcription elongation factor SPT4 OS=Homo sapiens GN=SUPT4H1 PE=1 SV=1 - [SPT4H_HUMAN]	85.21
O00233	26S proteasome non-ATPase regulatory subunit 9 OS=Homo sapiens GN=PSMD9 PE=1 SV=3 - [PSMD9_HUMAN]	84.92
P25787	Proteasome subunit alpha type-2 OS=Homo sapiens GN=PSMA2 PE=1 SV=2 - [PSA2_HUMAN]	84.86
P61247	40S ribosomal protein S3a OS=Homo sapiens GN=RPS3A PE=1 SV=2 - [RS3A_HUMAN]	84.78
Q9P2R7	Succinyl-CoA ligase [ADP-forming] subunit beta, mitochondrial OS=Homo sapiens GN=SUCLA2 PE=1 SV=3 - [SUCB1_HUMAN]	84.58
P06576	ATP synthase subunit beta, mitochondrial OS=Homo sapiens GN=ATP5B PE=1 SV=3 - [ATPB_HUMAN]	84.23
P17858	ATP-dependent 6-phosphofructokinase, liver type OS=Homo sapiens GN=PFKL PE=1 SV=6 - [PFKAL_HUMAN]	83.62
Q15185	Prostaglandin E synthase 3 OS=Homo sapiens GN=PTGES3 PE=1 SV=1 - [TEBP_HUMAN]	83.51
Q5VYK3	Proteasome-associated protein ECM29 homolog OS=Homo sapiens GN=ECM29 PE=1 SV=2 - [ECM29_HUMAN]	83.24
P08237	ATP-dependent 6-phosphofructokinase, muscle type OS=Homo sapiens GN=PFKM PE=1 SV=2 - [PFKAM_HUMAN]	82.59
Q92616	Translational activator GCN1 OS=Homo sapiens GN=GCN1L1 PE=1 SV=6 - [GCN1L_HUMAN]	81.5
P46777	60S ribosomal protein L5 OS=Homo sapiens GN=RPL5 PE=1 SV=3 - [RL5_HUMAN]	81.46
Q06210	Glutamine--fructose-6-phosphate aminotransferase [isomerizing] 1 OS=Homo sapiens GN=GFPT1 PE=1 SV=3 - [GFPT1_HUMAN]	81.34
Q9H4A6	Golgi phosphoprotein 3 OS=Homo sapiens GN=GOLPH3 PE=1 SV=1 - [GOLP3_HUMAN]	81.31
Q8TEX9	Importin-4 OS=Homo sapiens GN=IPO4 PE=1 SV=2 - [IPO4_HUMAN]	80.48
Q96P70	Importin-9 OS=Homo sapiens GN=IPO9 PE=1 SV=3 - [IPO9_HUMAN]	80.04
P51570	Galactokinase OS=Homo sapiens GN=GALK1 PE=1 SV=1 - [GALK1_HUMAN]	79.61
O43242	26S proteasome non-ATPase regulatory subunit 3 OS=Homo sapiens GN=PSMD3 PE=1 SV=2 - [PSMD3_HUMAN]	79.5
P18754	Regulator of chromosome condensation OS=Homo sapiens GN=RCC1 PE=1 SV=1 - [RCC1_HUMAN]	79.24
Q969Z0	Protein TBRG4 OS=Homo sapiens GN=TBRG4 PE=1 SV=1 - [TBRG4_HUMAN]	78.63
Q9NZT2	Opioid growth factor receptor OS=Homo sapiens GN=OGFR PE=1 SV=3 - [OGFR_HUMAN]	78.32
Q9Y285	Phenylalanine--tRNA ligase alpha subunit OS=Homo sapiens GN=FARSA PE=1 SV=3 - [SYFA_HUMAN]	77.1
Q9BSD7	Cancer-related nucleoside-triphosphatase OS=Homo sapiens GN=NTPCR PE=1 SV=1 - [NTPCR_HUMAN]	76.97
Q9HDC9	Adipocyte plasma membrane-associated protein OS=Homo sapiens GN=APMAP PE=1 SV=2 - [APMAP_HUMAN]	75.9
Q92973	Transportin-1 OS=Homo sapiens GN=TNPO1 PE=1 SV=2 - [TNPO1_HUMAN]	75.81

Accession	Description	Mascot
O60547	GDP-mannose 4,6 dehydratase OS=Homo sapiens GN=GMDS PE=1 SV=1 - [GMDS_HUMAN]	75.09
Q01105	Protein SET OS=Homo sapiens GN=SET PE=1 SV=3 - [SET_HUMAN]	74.88
P05388	60S acidic ribosomal protein P0 OS=Homo sapiens GN=RPLP0 PE=1 SV=1 - [RLA0_HUMAN]	74.75
Q9NSE4	Isoleucine--tRNA ligase, mitochondrial OS=Homo sapiens GN=IARS2 PE=1 SV=2 - [SYIM_HUMAN]	73.84
Q13310	Polyadenylate-binding protein 4 OS=Homo sapiens GN=PABPC4 PE=1 SV=1 - [PABP4_HUMAN]	73.51
P61221	ATP-binding cassette sub-family E member 1 OS=Homo sapiens GN=ABCE1 PE=1 SV=1 - [ABCE1_HUMAN]	73.05
Q9BTW9	Tubulin-specific chaperone D OS=Homo sapiens GN=TBCD PE=1 SV=2 - [TBCD_HUMAN]	72.93
P46782	40S ribosomal protein S5 OS=Homo sapiens GN=RPS5 PE=1 SV=4 - [RS5_HUMAN]	72.91
Q9UBF2	Coatomer subunit gamma-2 OS=Homo sapiens GN=COPG2 PE=1 SV=1 - [COPG2_HUMAN]	71.55
P52597	Heterogeneous nuclear ribonucleoprotein F OS=Homo sapiens GN=HNRNPF PE=1 SV=3 - [HNRPF_HUMAN]	70.95
P34932	Heat shock 70 kDa protein 4 OS=Homo sapiens GN=HSPA4 PE=1 SV=4 - [HSP74_HUMAN]	70.74
Q2TB90	Putative hexokinase HKDC1 OS=Homo sapiens GN=HKDC1 PE=1 SV=3 - [HKDC1_HUMAN]	70.7
P62829	60S ribosomal protein L23 OS=Homo sapiens GN=RPL23 PE=1 SV=1 - [RL23_HUMAN]	70.61
Q9H814	Phosphorylated adapter RNA export protein OS=Homo sapiens GN=PHAX PE=1 SV=1 - [PHAX_HUMAN]	69.14
P25786	Proteasome subunit alpha type-1 OS=Homo sapiens GN=PSMA1 PE=1 SV=1 - [PSA1_HUMAN]	69.06
Q14203	Dynactin subunit 1 OS=Homo sapiens GN=DCTN1 PE=1 SV=3 - [DCTN1_HUMAN]	68.05
P51648	Fatty aldehyde dehydrogenase OS=Homo sapiens GN=ALDH3A2 PE=1 SV=1 - [AL3A2_HUMAN]	66.25
P60866	40S ribosomal protein S20 OS=Homo sapiens GN=RPS20 PE=1 SV=1 - [RS20_HUMAN]	65.92
P49593	Protein phosphatase 1F OS=Homo sapiens GN=PPM1F PE=1 SV=3 - [PPM1F_HUMAN]	65.03
O14732	Inositol monophosphatase 2 OS=Homo sapiens GN=IMPA2 PE=1 SV=1 - [IMPA2_HUMAN]	64.92
P08195	4F2 cell-surface antigen heavy chain OS=Homo sapiens GN=SLC3A2 PE=1 SV=3 - [4F2_HUMAN]	64.91
P41250	Glycine--tRNA ligase OS=Homo sapiens GN=GARS PE=1 SV=3 - [SYG_HUMAN]	64.54
P17655	Calpain-2 catalytic subunit OS=Homo sapiens GN=CAPN2 PE=1 SV=6 - [CAN2_HUMAN]	64.33
P63173	60S ribosomal protein L38 OS=Homo sapiens GN=RPL38 PE=1 SV=2 - [RL38_HUMAN]	64.1
P0CW18	Serine protease 56 OS=Homo sapiens GN=PRSS56 PE=1 SV=1 - [PRS56_HUMAN]	63.93
P61254	60S ribosomal protein L26 OS=Homo sapiens GN=RPL26 PE=1 SV=1 - [RL26_HUMAN]	63.88
P46459	Vesicle-fusing ATPase OS=Homo sapiens GN=NSF PE=1 SV=3 - [NSF_HUMAN]	63.86
P36404	ADP-ribosylation factor-like protein 2 OS=Homo sapiens GN=ARL2 PE=1 SV=4 - [ARL2_HUMAN]	63.39

Accession	Description	Mascot
P13645	Keratin, type I cytoskeletal 10 OS=Homo sapiens GN=KRT10 PE=1 SV=6 - [K1C10_HUMAN]	63.28
Q96EY4	Translation machinery-associated protein 16 OS=Homo sapiens GN=TMA16 PE=1 SV=2 - [TMA16_HUMAN]	62.58
O60313	Dynamin-like 120 kDa protein, mitochondrial OS=Homo sapiens GN=OPA1 PE=1 SV=3 - [OPA1_HUMAN]	62.51
P62280	40S ribosomal protein S11 OS=Homo sapiens GN=RPS11 PE=1 SV=3 - [RS11_HUMAN]	62.04
P52298	Nuclear cap-binding protein subunit 2 OS=Homo sapiens GN=NCBP2 PE=1 SV=1 - [NCBP2_HUMAN]	60.79
Q9BRK5	45 kDa calcium-binding protein OS=Homo sapiens GN=SDF4 PE=1 SV=1 - [CAB45_HUMAN]	60.73
Q13572	Inositol-tetrakisphosphate 1-kinase OS=Homo sapiens GN=ITPK1 PE=1 SV=2 - [ITPK1_HUMAN]	60.56
P35250	Replication factor C subunit 2 OS=Homo sapiens GN=RFC2 PE=1 SV=3 - [RFC2_HUMAN]	60.44
P49736	DNA replication licensing factor MCM2 OS=Homo sapiens GN=MCM2 PE=1 SV=4 - [MCM2_HUMAN]	60.32
P43358	Melanoma-associated antigen 4 OS=Homo sapiens GN=MAGEA4 PE=1 SV=2 - [MAGA4_HUMAN]	60.11
P12268	Inosine-5'-monophosphate dehydrogenase 2 OS=Homo sapiens GN=IMPDH2 PE=1 SV=2 - [IMDH2_HUMAN]	59.32
Q9P289	Serine/threonine-protein kinase 26 OS=Homo sapiens GN=STK26 PE=1 SV=2 - [STK26_HUMAN]	59.07
Q9HAV0	Guanine nucleotide-binding protein subunit beta-4 OS=Homo sapiens GN=GNB4 PE=1 SV=3 - [GBB4_HUMAN]	58.51
Q15393	Splicing factor 3B subunit 3 OS=Homo sapiens GN=SF3B3 PE=1 SV=4 - [SF3B3_HUMAN]	57.89
Q9BU61	NADH dehydrogenase [ubiquinone] 1 alpha subcomplex assembly factor 3 OS=Homo sapiens GN=NDUFAF3 PE=1 SV=1 - [NDUF3_HUMAN]	57.81
Q99436	Proteasome subunit beta type-7 OS=Homo sapiens GN=PSMB7 PE=1 SV=1 - [PSB7_HUMAN]	57.35
P61353	60S ribosomal protein L27 OS=Homo sapiens GN=RPL27 PE=1 SV=2 - [RL27_HUMAN]	57.32
O95831	Apoptosis-inducing factor 1, mitochondrial OS=Homo sapiens GN=AIFM1 PE=1 SV=1 - [AIFM1_HUMAN]	56.29
P27824	Calnexin OS=Homo sapiens GN=CANX PE=1 SV=2 - [CALX_HUMAN]	56.22
Q9Y305	Acyl-coenzyme A thioesterase 9, mitochondrial OS=Homo sapiens GN=ACOT9 PE=1 SV=2 - [ACOT9_HUMAN]	55.45
P50914	60S ribosomal protein L14 OS=Homo sapiens GN=RPL14 PE=1 SV=4 - [RL14_HUMAN]	55.41
P53803	DNA-directed RNA polymerases I, II, and III subunit RPABC4 OS=Homo sapiens GN=POLR2K PE=3 SV=1 - [RPAB4_HUMAN]	55.31
Q16790	Carbonic anhydrase 9 OS=Homo sapiens GN=CA9 PE=1 SV=2 - [CAH9_HUMAN]	55.3
Q99614	Tetratricopeptide repeat protein 1 OS=Homo sapiens GN=TTC1 PE=1 SV=1 - [TTC1_HUMAN]	55.19
Q9UG63	ATP-binding cassette sub-family F member 2 OS=Homo sapiens GN=ABCF2 PE=1 SV=2 - [ABCF2_HUMAN]	55.05
Q9Y4L1	Hypoxia up-regulated protein 1 OS=Homo sapiens GN=HYOU1 PE=1 SV=1 - [HYOU1_HUMAN]	54.76
Q9UNM6	26S proteasome non-ATPase regulatory subunit 13 OS=Homo sapiens GN=PSMD13 PE=1 SV=2 - [PSD13_HUMAN]	54.6

Accession	Description	Mascot
P14618	Pyruvate kinase PKM OS=Homo sapiens GN=PKM PE=1 SV=4 - [KPYM_HUMAN]	54.59
O60814	Histone H2B type 1-K OS=Homo sapiens GN=HIST1H2BK PE=1 SV=3 - [H2B1K_HUMAN]	54.41
P48643	T-complex protein 1 subunit epsilon OS=Homo sapiens GN=CCT5 PE=1 SV=1 - [TCPE_HUMAN]	53.88
P60842	Eukaryotic initiation factor 4A-I OS=Homo sapiens GN=EIF4A1 PE=1 SV=1 - [IF4A1_HUMAN]	53.84
P08579	U2 small nuclear ribonucleoprotein B'' OS=Homo sapiens GN=SNRPB2 PE=1 SV=1 - [RU2B_HUMAN]	53.54
P51153	Ras-related protein Rab-13 OS=Homo sapiens GN=RAB13 PE=1 SV=1 - [RAB13_HUMAN]	52.73
P61313	60S ribosomal protein L15 OS=Homo sapiens GN=RPL15 PE=1 SV=2 - [RL15_HUMAN]	52.73
Q9H2U1	ATP-dependent RNA helicase DHX36 OS=Homo sapiens GN=DHX36 PE=1 SV=2 - [DHX36_HUMAN]	52.28
Q7L8L6	FAST kinase domain-containing protein 5 OS=Homo sapiens GN=FASTKD5 PE=1 SV=1 - [FAKD5_HUMAN]	52.17
P31350	Ribonucleoside-diphosphate reductase subunit M2 OS=Homo sapiens GN=RRM2 PE=1 SV=1 - [RIR2_HUMAN]	51.94
Q9NUQ8	ATP-binding cassette sub-family F member 3 OS=Homo sapiens GN=ABCF3 PE=1 SV=2 - [ABCF3_HUMAN]	51.83
P62333	26S protease regulatory subunit 10B OS=Homo sapiens GN=PSMC6 PE=1 SV=1 - [PRS10_HUMAN]	51.79
O75436	Vacuolar protein sorting-associated protein 26A OS=Homo sapiens GN=VPS26A PE=1 SV=2 - [VP26A_HUMAN]	51.74
O75607	Nucleoplasmin-3 OS=Homo sapiens GN=NPM3 PE=1 SV=3 - [NPM3_HUMAN]	51.59
Q9Y3U8	60S ribosomal protein L36 OS=Homo sapiens GN=RPL36 PE=1 SV=3 - [RL36_HUMAN]	50.3
P60953	Cell division control protein 42 homolog OS=Homo sapiens GN=CDC42 PE=1 SV=2 - [CDC42_HUMAN]	49.53
P27708	CAD protein OS=Homo sapiens GN=CAD PE=1 SV=3 - [PYR1_HUMAN]	49.21
Q8N1F7	Nuclear pore complex protein Nup93 OS=Homo sapiens GN=NUP93 PE=1 SV=2 - [NUP93_HUMAN]	48.9
P53365	Arfaptin-2 OS=Homo sapiens GN=ARFIP2 PE=1 SV=1 - [ARFP2_HUMAN]	48.87
P04181	Ornithine aminotransferase, mitochondrial OS=Homo sapiens GN=OAT PE=1 SV=1 - [OAT_HUMAN]	48.75
P28072	Proteasome subunit beta type-6 OS=Homo sapiens GN=PSMB6 PE=1 SV=4 - [PSB6_HUMAN]	48.17
Q9HD40	O-phosphoserine-tRNA(Sec) selenium transferase OS=Homo sapiens GN=SEPSECS PE=1 SV=2 - [SPCS_HUMAN]	47.96
P11279	Lysosome-associated membrane glycoprotein 1 OS=Homo sapiens GN=LAMP1 PE=1 SV=3 - [LAMP1_HUMAN]	47.87
P50990	T-complex protein 1 subunit theta OS=Homo sapiens GN=CCT8 PE=1 SV=4 - [TCPQ_HUMAN]	47.71
O00231	26S proteasome non-ATPase regulatory subunit 11 OS=Homo sapiens GN=PSMD11 PE=1 SV=3 - [PSD11_HUMAN]	46.11
P62249	40S ribosomal protein S16 OS=Homo sapiens GN=RPS16 PE=1 SV=2 - [RS16_HUMAN]	45.94
Q9NR31	GTP-binding protein SAR1a OS=Homo sapiens GN=SAR1A PE=1 SV=1 - [SAR1A_HUMAN]	45.9
Q9H7Z7	Prostaglandin E synthase 2 OS=Homo sapiens GN=PTGES2 PE=1 SV=1 - [PGES2_HUMAN]	45.9

Accession	Description	Mascot
P19367	Hexokinase-1 OS=Homo sapiens GN=HK1 PE=1 SV=3 - [H XK1_HUMAN]	45.8
Q96D46	60S ribosomal export protein NMD3 OS=Homo sapiens GN=NMD3 PE=1 SV=1 - [NMD3_HUMAN]	44.84
O14980	Exportin-1 OS=Homo sapiens GN=XPO1 PE=1 SV=1 - [XPO1_HUMAN]	44.69
Q3ZCQ8	Mitochondrial import inner membrane translocase subunit TIM50 OS=Homo sapiens GN=TIMM50 PE=1 SV=2 - [TIM50_HUMAN]	44.23
P62277	40S ribosomal protein S13 OS=Homo sapiens GN=RPS13 PE=1 SV=2 - [RS13_HUMAN]	44.09
P43246	DNA mismatch repair protein Msh2 OS=Homo sapiens GN=MSH2 PE=1 SV=1 - [MSH2_HUMAN]	44.01
P62917	60S ribosomal protein L8 OS=Homo sapiens GN=RPL8 PE=1 SV=2 - [RL8_HUMAN]	43.82
Q02878	60S ribosomal protein L6 OS=Homo sapiens GN=RPL6 PE=1 SV=3 - [RL6_HUMAN]	43.67
O00487	26S proteasome non-ATPase regulatory subunit 14 OS=Homo sapiens GN=PSMD14 PE=1 SV=1 - [PSDE_HUMAN]	43.62
P62877	E3 ubiquitin-protein ligase RBX1 OS=Homo sapiens GN=RBX1 PE=1 SV=1 - [RBX1_HUMAN]	43.18
Q9H5X1	MIP18 family protein FAM96A OS=Homo sapiens GN=FAM96A PE=1 SV=1 - [FA96A_HUMAN]	42.79
O75489	NADH dehydrogenase [ubiquinone] iron-sulfur protein 3, mitochondrial OS=Homo sapiens GN=NDUFS3 PE=1 SV=1 - [NDUS3_HUMAN]	42.29
Q13619	Cullin-4A OS=Homo sapiens GN=CUL4A PE=1 SV=3 - [CUL4A_HUMAN]	42.19
Q9BZG1	Ras-related protein Rab-34 OS=Homo sapiens GN=RAB34 PE=1 SV=1 - [RAB34_HUMAN]	41.95
Q9BQ67	Glutamate-rich WD repeat-containing protein 1 OS=Homo sapiens GN=GRWD1 PE=1 SV=1 - [GRWD1_HUMAN]	41.87
Q15654	Thyroid receptor-interacting protein 6 OS=Homo sapiens GN=TRIP6 PE=1 SV=3 - [TRIP6_HUMAN]	41.7
Q04837	Single-stranded DNA-binding protein, mitochondrial OS=Homo sapiens GN=SSBP1 PE=1 SV=1 - [SSBP_HUMAN]	41.4
P62875	DNA-directed RNA polymerases I, II, and III subunit RPABC5 OS=Homo sapiens GN=POLR2L PE=1 SV=1 - [RPAB5_HUMAN]	41.24
P50502	Hsc70-interacting protein OS=Homo sapiens GN=ST13 PE=1 SV=2 - [F10A1_HUMAN]	40.35
Q15029	116 kDa U5 small nuclear ribonucleoprotein component OS=Homo sapiens GN=EFTUD2 PE=1 SV=1 - [U5S1_HUMAN]	39.91
P18124	60S ribosomal protein L7 OS=Homo sapiens GN=RPL7 PE=1 SV=1 - [RL7_HUMAN]	39.68
P19387	DNA-directed RNA polymerase II subunit RPB3 OS=Homo sapiens GN=POLR2C PE=1 SV=2 - [RPB3_HUMAN]	39.64
Q96NT1	Nucleosome assembly protein 1-like 5 OS=Homo sapiens GN=NAP1L5 PE=2 SV=1 - [NP1L5_HUMAN]	39.64
P50897	Palmitoyl-protein thioesterase 1 OS=Homo sapiens GN=PPT1 PE=1 SV=1 - [PPT1_HUMAN]	39.6
P37268	Squalene synthase OS=Homo sapiens GN=FDFT1 PE=1 SV=1 - [FDFT_HUMAN]	39.6
O43399	Tumor protein D54 OS=Homo sapiens GN=TPD52L2 PE=1 SV=2 - [TPD54_HUMAN]	39.29
Q1KMD3	Heterogeneous nuclear ribonucleoprotein U-like protein 2 OS=Homo sapiens GN=HNRNPUL2 PE=1 SV=1 - [HNRL2_HUMAN]	38.48

Accession	Description	Mascot
O15397	Importin-8 OS=Homo sapiens GN=IPO8 PE=1 SV=2 - [IPO8_HUMAN]	38.21
P25205	DNA replication licensing factor MCM3 OS=Homo sapiens GN=MCM3 PE=1 SV=3 - [MCM3_HUMAN]	38.12
Q13907	Isopentenyl-diphosphate Delta-isomerase 1 OS=Homo sapiens GN=IDI1 PE=1 SV=2 - [IDI1_HUMAN]	37.97
Q9UK73	Protein fem-1 homolog B OS=Homo sapiens GN=FEM1B PE=1 SV=1 - [FEM1B_HUMAN]	37.91
Q15365	Poly(rC)-binding protein 1 OS=Homo sapiens GN=PCBP1 PE=1 SV=2 - [PCBP1_HUMAN]	37.9
P18077	60S ribosomal protein L35a OS=Homo sapiens GN=RPL35A PE=1 SV=2 - [RL35A_HUMAN]	37.7
Q6NVV1	Putative 60S ribosomal protein L13a protein RPL13AP3 OS=Homo sapiens GN=RPL13AP3 PE=5 SV=1 - [R13P3_HUMAN]	37.61
P50213	Isocitrate dehydrogenase [NAD] subunit alpha, mitochondrial OS=Homo sapiens GN=IDH3A PE=1 SV=1 - [IDH3A_HUMAN]	37.54
Q53GA4	Pleckstrin homology-like domain family A member 2 OS=Homo sapiens GN=PHLDA2 PE=1 SV=2 - [PHLA2_HUMAN]	37.36
P52657	Transcription initiation factor IIA subunit 2 OS=Homo sapiens GN=GTF2A2 PE=1 SV=1 - [T2AG_HUMAN]	36.45
Q96BN8	Ubiquitin thioesterase otulin OS=Homo sapiens GN=OTULIN PE=1 SV=3 - [OTUL_HUMAN]	36.23
Q9H9P8	L-2-hydroxyglutarate dehydrogenase, mitochondrial OS=Homo sapiens GN=L2HGDH PE=1 SV=3 - [L2HDH_HUMAN]	36.22
P12110	Collagen alpha-2(VI) chain OS=Homo sapiens GN=COL6A2 PE=1 SV=4 - [CO6A2_HUMAN]	36.03
P27635	60S ribosomal protein L10 OS=Homo sapiens GN=RPL10 PE=1 SV=4 - [RL10_HUMAN]	36
Q9HCE1	Putative helicase MOV-10 OS=Homo sapiens GN=MOV10 PE=1 SV=2 - [MOV10_HUMAN]	35.94
P51149	Ras-related protein Rab-7a OS=Homo sapiens GN=RAB7A PE=1 SV=1 - [RAB7A_HUMAN]	35.88
P18085	ADP-ribosylation factor 4 OS=Homo sapiens GN=ARF4 PE=1 SV=3 - [ARF4_HUMAN]	35.64
Q96MC4	CEP295 N-terminal-like protein OS=Homo sapiens GN=CEP295NL PE=2 SV=1 - [C295L_HUMAN]	35.5
P11413	Glucose-6-phosphate 1-dehydrogenase OS=Homo sapiens GN=G6PD PE=1 SV=4 - [G6PD_HUMAN]	35.29
P84095	Rho-related GTP-binding protein RhoG OS=Homo sapiens GN=RHOG PE=1 SV=1 - [RHOG_HUMAN]	34.89
Q7Z4H3	HD domain-containing protein 2 OS=Homo sapiens GN=HDDC2 PE=1 SV=1 - [HDDC2_HUMAN]	34.75
Q6PIU2	Neutral cholesterol ester hydrolase 1 OS=Homo sapiens GN=NCEH1 PE=1 SV=3 - [NCEH1_HUMAN]	34.44
Q9NPQ8	Synembryn-A OS=Homo sapiens GN=RIC8A PE=1 SV=3 - [RIC8A_HUMAN]	34.34
P62753	40S ribosomal protein S6 OS=Homo sapiens GN=RPS6 PE=1 SV=1 - [RS6_HUMAN]	34.3
Q9NSD9	Phenylalanine--tRNA ligase beta subunit OS=Homo sapiens GN=FARSB PE=1 SV=3 - [SYFB_HUMAN]	33.86
Q07002	Cyclin-dependent kinase 18 OS=Homo sapiens GN=CDK18 PE=1 SV=3 - [CDK18_HUMAN]	33.65
P61978	Heterogeneous nuclear ribonucleoprotein K OS=Homo sapiens GN=HNRNPK PE=1 SV=1 - [HNRPK_HUMAN]	33.07

Accession	Description	Mascot
Q9BUJ2	Heterogeneous nuclear ribonucleoprotein U-like protein 1 OS=Homo sapiens GN=HNRNPUL1 PE=1 SV=2 - [HNRL1_HUMAN]	32.73
P21980	Protein-glutamine gamma-glutamyltransferase 2 OS=Homo sapiens GN=TGM2 PE=1 SV=2 - [TGM2_HUMAN]	32.51
Q16186	Proteasomal ubiquitin receptor ADRM1 OS=Homo sapiens GN=ADRM1 PE=1 SV=2 - [ADRM1_HUMAN]	32.5
P62906	60S ribosomal protein L10a OS=Homo sapiens GN=RPL10A PE=1 SV=2 - [RL10A_HUMAN]	32.32
Q8NF91	Nesprin-1 OS=Homo sapiens GN=SYNE1 PE=1 SV=4 - [SYNE1_HUMAN]	32.09
O43681	ATPase ASNA1 OS=Homo sapiens GN=ASNA1 PE=1 SV=2 - [ASNA_HUMAN]	32.06
P49902	Cytosolic purine 5'-nucleotidase OS=Homo sapiens GN=NT5C2 PE=1 SV=1 - [5NTC_HUMAN]	31.92
P13995	Bifunctional methylenetetrahydrofolate dehydrogenase/cyclohydrolase, mitochondrial OS=Homo sapiens GN=MTHFD2 PE=1 SV=2 - [MTDC_HUMAN]	31.82
P11177	Pyruvate dehydrogenase E1 component subunit beta, mitochondrial OS=Homo sapiens GN=PDHB PE=1 SV=3 - [ODPB_HUMAN]	31.48
P46781	40S ribosomal protein S9 OS=Homo sapiens GN=RPS9 PE=1 SV=3 - [RS9_HUMAN]	31.33
Q9Y2I1	Nischarin OS=Homo sapiens GN=NISCH PE=1 SV=3 - [NISCH_HUMAN]	31.31
P30153	Serine/threonine-protein phosphatase 2A 65 kDa regulatory subunit A alpha isoform OS=Homo sapiens GN=PPP2R1A PE=1 SV=4 - [2AAA_HUMAN]	31.22
P13637	Sodium/potassium-transporting ATPase subunit alpha-3 OS=Homo sapiens GN=ATP1A3 PE=1 SV=3 - [AT1A3_HUMAN]	31.17
P11172	Uridine 5'-monophosphate synthase OS=Homo sapiens GN=UMPS PE=1 SV=1 - [UMPS_HUMAN]	31.16
Q92598	Heat shock protein 105 kDa OS=Homo sapiens GN=HSPH1 PE=1 SV=1 - [HS105_HUMAN]	31.1
P61201	COP9 signalosome complex subunit 2 OS=Homo sapiens GN=COPS2 PE=1 SV=1 - [CSN2_HUMAN]	30.65
P23258	Tubulin gamma-1 chain OS=Homo sapiens GN=TUBG1 PE=1 SV=2 - [TBG1_HUMAN]	30.65
Q9NX14	NADH dehydrogenase [ubiquinone] 1 beta subcomplex subunit 11, mitochondrial OS=Homo sapiens GN=NDUFB11 PE=1 SV=1 - [NDUBB_HUMAN]	30.59
O75794	Cell division cycle protein 123 homolog OS=Homo sapiens GN=CDC123 PE=1 SV=1 - [CD123_HUMAN]	29.22
Q9P2R3	Rabankyrin-5 OS=Homo sapiens GN=ANKFY1 PE=1 SV=2 - [ANFY1_HUMAN]	28.97
O14818	Proteasome subunit alpha type-7 OS=Homo sapiens GN=PSMA7 PE=1 SV=1 - [PSA7_HUMAN]	28.88
O95757	Heat shock 70 kDa protein 4L OS=Homo sapiens GN=HSPA4L PE=1 SV=3 - [HS74L_HUMAN]	28.83
P48556	26S proteasome non-ATPase regulatory subunit 8 OS=Homo sapiens GN=PSMD8 PE=1 SV=2 - [PSMD8_HUMAN]	28.68
P51148	Ras-related protein Rab-5C OS=Homo sapiens GN=RAB5C PE=1 SV=2 - [RAB5C_HUMAN]	28.31
P20138	Myeloid cell surface antigen CD33 OS=Homo sapiens GN=CD33 PE=1 SV=2 - [CD33_HUMAN]	27.98

Accession	Description	Mascot
P04843	Dolichyl-diphosphooligosaccharide--protein glycosyltransferase subunit 1 OS=Homo sapiens GN=RPN1 PE=1 SV=1 - [RPN1_HUMAN]	27.68
Q9BW11	Max dimerization protein 3 OS=Homo sapiens GN=MXD3 PE=1 SV=1 - [MAD3_HUMAN]	27.54
Q96MM3	Zinc finger protein 42 homolog OS=Homo sapiens GN=ZFP42 PE=1 SV=2 - [ZFP42_HUMAN]	27.53
Q9Y3D0	Mitotic spindle-associated MMXD complex subunit MIP18 OS=Homo sapiens GN=FAM96B PE=1 SV=1 - [MIP18_HUMAN]	27.34
P31943	Heterogeneous nuclear ribonucleoprotein H OS=Homo sapiens GN=HNRNPH1 PE=1 SV=4 - [HNRH1_HUMAN]	26.92
P35813	Protein phosphatase 1A OS=Homo sapiens GN=PPM1A PE=1 SV=1 - [PPM1A_HUMAN]	26.67
O60232	Sjogren syndrome/scleroderma autoantigen 1 OS=Homo sapiens GN=SSSCA1 PE=1 SV=1 - [SSA27_HUMAN]	26.37
Q06828	Fibromodulin OS=Homo sapiens GN=FMOD PE=1 SV=2 - [FMOD_HUMAN]	26.22
P15880	40S ribosomal protein S2 OS=Homo sapiens GN=RPS2 PE=1 SV=2 - [RS2_HUMAN]	26.06
Q9BUK6	Protein misato homolog 1 OS=Homo sapiens GN=MSTO1 PE=1 SV=1 - [MSTO1_HUMAN]	26.06
P05067	Amyloid beta A4 protein OS=Homo sapiens GN=APP PE=1 SV=3 - [A4_HUMAN]	25.78
P0C0S5	Histone H2A.Z OS=Homo sapiens GN=H2AFZ PE=1 SV=2 - [H2AZ_HUMAN]	25.42
Q0P6H9	Transmembrane protein 62 OS=Homo sapiens GN=TMEM62 PE=1 SV=1 - [TMM62_HUMAN]	24.97
Q96QK1	Vacuolar protein sorting-associated protein 35 OS=Homo sapiens GN=VPS35 PE=1 SV=2 - [VPS35_HUMAN]	24.64
Q9NZR2	Low-density lipoprotein receptor-related protein 1B OS=Homo sapiens GN=LRP1B PE=1 SV=2 - [LRP1B_HUMAN]	24.31
P83731	60S ribosomal protein L24 OS=Homo sapiens GN=RPL24 PE=1 SV=1 - [RL24_HUMAN]	23.58
Q9NRG4	N-lysine methyltransferase SMYD2 OS=Homo sapiens GN=SMYD2 PE=1 SV=2 - [SMYD2_HUMAN]	22.79
Q13098	COP9 signalosome complex subunit 1 OS=Homo sapiens GN=GPS1 PE=1 SV=4 - [CSN1_HUMAN]	22.71
Q13131	5'-AMP-activated protein kinase catalytic subunit alpha-1 OS=Homo sapiens GN=PRKAA1 PE=1 SV=4 - [AAPK1_HUMAN]	22.71
Q9UNS2	COP9 signalosome complex subunit 3 OS=Homo sapiens GN=COPS3 PE=1 SV=3 - [CSN3_HUMAN]	22.04
Q13201	Multimerin-1 OS=Homo sapiens GN=MMRN1 PE=1 SV=3 - [MMRN1_HUMAN]	20.83
P05362	Intercellular adhesion molecule 1 OS=Homo sapiens GN=ICAM1 PE=1 SV=2 - [ICAM1_HUMAN]	20.5
P15170	Eukaryotic peptide chain release factor GTP-binding subunit ERF3A OS=Homo sapiens GN=GSPT1 PE=1 SV=1 - [ERF3A_HUMAN]	17.01
Q15386	Ubiquitin-protein ligase E3C OS=Homo sapiens GN=UBE3C PE=1 SV=3 - [UBE3C_HUMAN]	0

Appendix III

Mass spectrometry analysis results for activity 3

The most active fraction from the final ion exchange (Mono Q) chromatography step, fraction 29 (5.3.3.3.2) for activity 3, was analysed by mass spectrometry by Dr Deborah M Simpson (Centre for Proteasome Research, University of Liverpool) to identify candidate E3 ubiquitin ligases and/or chromatin remodellers. The full list of proteins identified is shown below in descending order of mascot score.

Accession	Description	Mascot
P67809	Nuclease-sensitive element-binding protein 1 OS=Homo sapiens GN=YBX1 PE=1 SV=3 - [YBOX1_HUMAN]	916.92
P16989	Y-box-binding protein 3 OS=Homo sapiens GN=YBX3 PE=1 SV=4 - [YBOX3_HUMAN]	458.57
P11940	Polyadenylate-binding protein 1 OS=Homo sapiens GN=PABPC1 PE=1 SV=2 - [PABP1_HUMAN]	395.36
P68363	Tubulin alpha-1B chain OS=Homo sapiens GN=TUBA1B PE=1 SV=1 - [TBA1B_HUMAN]	345.45
P04264	Keratin, type II cytoskeletal 1 OS=Homo sapiens GN=KRT1 PE=1 SV=6 - [K2C1_HUMAN]	322.05
Q9H2U1	ATP-dependent RNA helicase DHX36 OS=Homo sapiens GN=DHX36 PE=1 SV=2 - [DHX36_HUMAN]	319.59
P07437	Tubulin beta chain OS=Homo sapiens GN=TUBB PE=1 SV=2 - [TBB5_HUMAN]	293.16
P06733	Alpha-enolase OS=Homo sapiens GN=ENO1 PE=1 SV=2 - [ENOA_HUMAN]	286.25
P68371	Tubulin beta-4B chain OS=Homo sapiens GN=TUBB4B PE=1 SV=1 - [TBB4B_HUMAN]	285.62
P09132	Signal recognition particle 19 kDa protein OS=Homo sapiens GN=SRP19 PE=1 SV=3 - [SRP19_HUMAN]	263.72
Q13885	Tubulin beta-2A chain OS=Homo sapiens GN=TUBB2A PE=1 SV=1 - [TBB2A_HUMAN]	263.33
P11021	78 kDa glucose-regulated protein OS=Homo sapiens GN=HSPA5 PE=1 SV=2 - [GRP78_HUMAN]	262.34
P19338	Nucleolin OS=Homo sapiens GN=NCL PE=1 SV=3 - [NUCL_HUMAN]	252.54
P11142	Heat shock cognate 71 kDa protein OS=Homo sapiens GN=HSPA8 PE=1 SV=1 - [HSP7C_HUMAN]	222.02
P35527	Keratin, type I cytoskeletal 9 OS=Homo sapiens GN=KRT9 PE=1 SV=3 - [K1C9_HUMAN]	216.99
Q13310	Polyadenylate-binding protein 4 OS=Homo sapiens GN=PABPC4 PE=1 SV=1 - [PABP4_HUMAN]	213.52
P68366	Tubulin alpha-4A chain OS=Homo sapiens GN=TUBA4A PE=1 SV=1 - [TBA4A_HUMAN]	211.15

Accession	Description	Mascot
P60709	Actin, cytoplasmic 1 OS=Homo sapiens GN=ACTB PE=1 SV=1 - [ACTB_HUMAN]	192.57
O15355	Protein phosphatase 1G OS=Homo sapiens GN=PPM1G PE=1 SV=1 - [PPM1G_HUMAN]	155.14
P62805	Histone H4 OS=Homo sapiens GN=HIST1H4A PE=1 SV=2 - [H4_HUMAN]	155.1
P02786	Transferrin receptor protein 1 OS=Homo sapiens GN=TFRC PE=1 SV=2 - [TFR1_HUMAN]	137.95
Q9HCE1	Putative helicase MOV-10 OS=Homo sapiens GN=MOV10 PE=1 SV=2 - [MOV10_HUMAN]	125.83
P14314	Glucosidase 2 subunit beta OS=Homo sapiens GN=PRKCSH PE=1 SV=2 - [GLU2B_HUMAN]	118.94
P49411	Elongation factor Tu, mitochondrial OS=Homo sapiens GN=TUFM PE=1 SV=2 - [EFTU_HUMAN]	112.53
P62995	Transformer-2 protein homolog beta OS=Homo sapiens GN=TRA2B PE=1 SV=1 - [TRA2B_HUMAN]	108.24
P08238	Heat shock protein HSP 90-beta OS=Homo sapiens GN=HSP90AB1 PE=1 SV=4 - [HS90B_HUMAN]	107.79
P63104	14-3-3 protein zeta/delta OS=Homo sapiens GN=YWHAZ PE=1 SV=1 - [1433Z_HUMAN]	101.75
P25705	ATP synthase subunit alpha, mitochondrial OS=Homo sapiens GN=ATP5A1 PE=1 SV=1 - [ATPA_HUMAN]	96.86
P09661	U2 small nuclear ribonucleoprotein A' OS=Homo sapiens GN=SNRPA1 PE=1 SV=2 - [RU2A_HUMAN]	96.63
P08195	4F2 cell-surface antigen heavy chain OS=Homo sapiens GN=SLC3A2 PE=1 SV=3 - [4F2_HUMAN]	91.51
P62826	GTP-binding nuclear protein Ran OS=Homo sapiens GN=RAN PE=1 SV=3 - [RAN_HUMAN]	91.36
P38646	Stress-70 protein, mitochondrial OS=Homo sapiens GN=HSPA9 PE=1 SV=2 - [GRP75_HUMAN]	76.97
Q6PKG0	La-related protein 1 OS=Homo sapiens GN=LARP1 PE=1 SV=2 - [LARP1_HUMAN]	76.59
P14324	Farnesyl pyrophosphate synthase OS=Homo sapiens GN=FDPS PE=1 SV=4 - [FPPS_HUMAN]	76.3
P35908	Keratin, type II cytoskeletal 2 epidermal OS=Homo sapiens GN=KRT2 PE=1 SV=2 - [K22E_HUMAN]	75.98
Q99733	Nucleosome assembly protein 1-like 4 OS=Homo sapiens GN=NAP1L4 PE=1 SV=1 - [NP1L4_HUMAN]	72.75
P31327	Carbamoyl-phosphate synthase [ammonia], mitochondrial OS=Homo sapiens GN=CPS1 PE=1 SV=2 - [CPSM_HUMAN]	71.4
P14678	Small nuclear ribonucleoprotein-associated proteins B and B' OS=Homo sapiens GN=SNRPB PE=1 SV=2 - [RSMB_HUMAN]	70.18
P05455	Lupus La protein OS=Homo sapiens GN=SSB PE=1 SV=2 - [LA_HUMAN]	70.13
P62306	Small nuclear ribonucleoprotein F OS=Homo sapiens GN=SNRPF PE=1 SV=1 - [RUXF_HUMAN]	65.99
P08579	U2 small nuclear ribonucleoprotein B'' OS=Homo sapiens GN=SNRPB2 PE=1 SV=1 - [RU2B_HUMAN]	65.83
Q9BUJ2	Heterogeneous nuclear ribonucleoprotein U-like protein 1 OS=Homo sapiens GN=HNRNPUL1 PE=1 SV=2 - [HNRL1_HUMAN]	64.84
P49458	Signal recognition particle 9 kDa protein OS=Homo sapiens GN=SRP9 PE=1 SV=2 - [SRP09_HUMAN]	64.56
P17980	26S protease regulatory subunit 6A OS=Homo sapiens GN=PSMC3 PE=1 SV=3 - [PRS6A_HUMAN]	61.76
P62424	60S ribosomal protein L7a OS=Homo sapiens GN=RPL7A PE=1 SV=2 - [RL7A_HUMAN]	61.72

Accession	Description	Mascot
P01891	HLA class I histocompatibility antigen, A-68 alpha chain OS=Homo sapiens GN=HLA-A PE=1 SV=4 - [1A68_HUMAN]	61
P62316	Small nuclear ribonucleoprotein Sm D2 OS=Homo sapiens GN=SNRPD2 PE=1 SV=1 - [SMD2_HUMAN]	54.74
Q01813	ATP-dependent 6-phosphofructokinase, platelet type OS=Homo sapiens GN=PFBP PE=1 SV=2 - [PFBP_HUMAN]	53.67
P27824	Calnexin OS=Homo sapiens GN=CANX PE=1 SV=2 - [CALX_HUMAN]	50.44
Q7Z2W4	Zinc finger CCCH-type antiviral protein 1 OS=Homo sapiens GN=ZC3HAV1 PE=1 SV=3 - [ZC3HV_HUMAN]	49.93
P12111	Collagen alpha-3(VI) chain OS=Homo sapiens GN=COL6A3 PE=1 SV=5 - [COL6A3_HUMAN]	47.49
P29692	Elongation factor 1-delta OS=Homo sapiens GN=EEF1D PE=1 SV=5 - [EF1D_HUMAN]	46.14
P35052	Glypican-1 OS=Homo sapiens GN=GPC1 PE=1 SV=2 - [GPC1_HUMAN]	44.09
Q9P015	39S ribosomal protein L15, mitochondrial OS=Homo sapiens GN=MRPL15 PE=1 SV=1 - [RM15_HUMAN]	43.37
Q92900	Regulator of nonsense transcripts 1 OS=Homo sapiens GN=UPF1 PE=1 SV=2 - [RENT1_HUMAN]	43.3
A8MWD9	Putative small nuclear ribonucleoprotein G-like protein 15 OS=Homo sapiens GN=SNRPGP15 PE=5 SV=2 - [RUXGL_HUMAN]	43.07
P62195	26S protease regulatory subunit 8 OS=Homo sapiens GN=PSMC5 PE=1 SV=1 - [PRS8_HUMAN]	42.81
P68104	Elongation factor 1-alpha 1 OS=Homo sapiens GN=EEF1A1 PE=1 SV=1 - [EF1A1_HUMAN]	42.39
Q13200	26S proteasome non-ATPase regulatory subunit 2 OS=Homo sapiens GN=PSMD2 PE=1 SV=3 - [PSMD2_HUMAN]	41.53
P01889	HLA class I histocompatibility antigen, B-7 alpha chain OS=Homo sapiens GN=HLA-B PE=1 SV=3 - [1B07_HUMAN]	40.22
P52298	Nuclear cap-binding protein subunit 2 OS=Homo sapiens GN=NCBP2 PE=1 SV=1 - [NCBP2_HUMAN]	40.06
O00425	Insulin-like growth factor 2 mRNA-binding protein 3 OS=Homo sapiens GN=IGF2BP3 PE=1 SV=2 - [IF2B3_HUMAN]	30.95
P62241	40S ribosomal protein S8 OS=Homo sapiens GN=RPS8 PE=1 SV=2 - [RS8_HUMAN]	28.65
P62318	Small nuclear ribonucleoprotein Sm D3 OS=Homo sapiens GN=SNRPD3 PE=1 SV=1 - [SMD3_HUMAN]	28.53
P55060	Exportin-2 OS=Homo sapiens GN=CSE1L PE=1 SV=3 - [XPO2_HUMAN]	28.5
P37108	Signal recognition particle 14 kDa protein OS=Homo sapiens GN=SRP14 PE=1 SV=2 - [SRP14_HUMAN]	26.69
Q9BYD1	39S ribosomal protein L13, mitochondrial OS=Homo sapiens GN=MRPL13 PE=1 SV=1 - [RM13_HUMAN]	25.38
Q9Y623	Myosin-4 OS=Homo sapiens GN=MYH4 PE=1 SV=2 - [MYH4_HUMAN]	25.11
Q02878	60S ribosomal protein L6 OS=Homo sapiens GN=RPL6 PE=1 SV=3 - [RL6_HUMAN]	24.75
P62888	60S ribosomal protein L30 OS=Homo sapiens GN=RPL30 PE=1 SV=2 - [RL30_HUMAN]	24.43
P62906	60S ribosomal protein L10a OS=Homo sapiens GN=RPL10A PE=1 SV=2 - [RL10A_HUMAN]	23.38
P84098	60S ribosomal protein L19 OS=Homo sapiens GN=RPL19 PE=1 SV=1 - [RL19_HUMAN]	21.01
Q9H3U1	Protein unc-45 homolog A OS=Homo sapiens GN=UNC45A PE=1 SV=1 - [UN45A_HUMAN]	20.83

